Fall 12-2020

Evaluating the Most Common Modeling Methods of Rayleigh Damping and the Critical Damping Ratio Limitation Approach

Tunc Deniz Uludag
University of Nebraska-Lincoln, tuludag@unomaha.edu

EVALUATING THE MOST COMMON MODELING METHODS OF RAYLEIGH DAMPING AND THE CRITICAL DAMPING RATIO LIMITATION APPROACH

by

Tunc Deniz Uludag

A THESIS

Presented to the Faculty of

The Graduate College at the University of Nebraska

In Partial Fulfillment of Requirements

For the Degree of Master of Science

Major: Architectural Engineering

Under the Supervision of Professor Jay A. Puckett

Lincoln, Nebraska

December, 2020

EVALUATING THE MOST COMMON MODELING METHODS OF RAYLEIGH DAMPING AND THE CRITICAL DAMPING RATIO LIMITATION APPROACH

TUNC DENIZ ULUDAG, M.S.

University of Nebraska, 2020

Advisor: Jay A. Puckett

Performance-based design such as FEMA P-695 and ASCE 7 prescribe/limit damping ratios associated with dynamic nonlinear seismic analysis; however, the method for computing inherent damping is not prescriptive. The analyst in conjunction with the peer-review panel (FEMA P-695) or authority having jurisdiction (ASCE 7) must determine how damping is modeled. Depending upon the method, e.g., Rayleigh, simulations can result in significantly different responses even with the same assumed damping ratio. Note that over estimating damping will underestimate energy absorption by inelastic displacement, a non-conservative outcome.

FEMA P-695 non-linear time history analysis of 44 earthquakes was used for several Rayleigh methods to model four- and nine-story archetypes. The collapse margin ratios were obtained to assess the effect on collapse prediction. The results varied significantly depending upon the Rayleigh approach.

A new framework is proposed by limiting the energy dissipated by inherent damping, not using a damping ratio directly. This approach helps to ensure that the procedure (described by FEMA P-695, or ASCE 7) is prescriptive enough to prevent the unintended and non-conservative consequences and promote consistency of results. The approach is functional for time histories and are critical for determining the collapse margin ratio.

The new method provides similar collapse margin ratios invariant with the particularities of the Rayleigh method. This approach may provide code writing committees, and authorities having jurisdiction, a definitive method for consistently prescribing/limiting inherent damping energy as a percent of seismic energy input, thereby forcing the reminder of the energy dissipation into planned inelastic deformations. Although, the present work is limited to buckling restrained braced frames, the framework should work across various structural systems. The percentage associated with inherent damping will depend upon the structural system and is not addressed in the present work is left to experts in particulars for each system.

DEDICATION

To my family and dear friends whose love, support and sacrifice made it possible for me to pursue my dreams.

ACKNOWLEDGEMENT

I would like to express my sincere gratitude and appreciation to my advisor, Dr. Jay A. Puckett for his immense support, trust, motivation, leadership, and encouragement. I cannot thank him enough for the opportunities he provided me during my journey and his profound belief in my work. I would also like to thank Dr. Ece Erdogmus for her willingness to serve on my committee and provide me her assistance as well as helped me to start my journey at UNL.

I am particularly grateful to Dr. Patrick McManus, not only for his great guidance but also his valuable contributions and fruitful discussions. I would like to extend my thanks to Dr. Bobaru, Dr. Wittich and Dr. Kanyilmaz for their willingness to serve on my committee and provide their assistance. I am deeply indebted to Dr. Engin Aktas who inspired me to focus my career for his endless support and guidance.

Special thanks to the UNL Durham School of Architectural Engineering and Construction for providing help and support during Covid-19.

Without my parents, Erol Uludag and Aydanur Uludag, my sister Zeynep Simge Ozturk, and my niece, Nisan Ada Ozturk, this accomplishment would not have been possible and more meaningful. Special thanks to Deniz Ozturk whose love, kindness, and sacrifices have always been with me. Lastly, I would like to thank my dear friends, Talha Yildirim, Ben Christiansen, and Ahmet Kursad Sircan for always being there when I needed them.

TABLE OF CONTENT

LIST OF FIGURES

LIST OF TABLES

CHAPTER 1:

INTRODUCTION

Here, the chapter is divided into three parts: motivation and background, research goals and objectives, and scope and assumptions. And,

- fundamental background for structural dynamics, analysis, and seismic design,
- motivation of the present work,
- research goals and objectives, and
- limitations and assumptions

are provided.

1.1. Motivation and Background

Dynamic actions are the most challenging conditions for building structures these include winds, earthquakes, blasts, or vibration due to any source. Herein, dynamic actions are considered as only horizontal earthquake loading. During a seismic event, inertial forces due to the acceleration of masses are generated and the affected structures should be designed to resist the forces. Resisting the forces might be interpreted as a conversion of energy from seismic energy to internal energy. The conversion of the energy results in stresses, deformations, and displacements in the structural components. A structure might be designed to resist seismic actions within the elastic deformation range but this is typically uneconomical. Therefore, extensive research has been conducted and innovative solutions have been developed in order to find economical solutions to design structural components against seismic events. Performance-based or ductile-design concept is one of the economical solutions.

The idea of the design concept is absorbing energy through planned plastic deformation on the structural components. The plastic deformation is permanent and results in cumulative energy absorption on the system, also known as hysteresis energy dissipation. Thus, the portion of the seismic energy is dissipated by converting it to hysteresis energy and the rest of the seismic energy is dissipated by inherent damping. Inherent damping in building structures is occurred due to various sources but the most effective source of inherent damping might be accepted as internal frictions between connections, structural components, and non-structural components. Alternatively, representing the inherent damping in commercial software is difficult due to the consideration of computational-efficiency and nonlinearity. Because of difficulty, extensive research has been conducted and several modeling methods have been developed for the damping matrix in the inelastic response.

To model inherent damping, the Rayleigh approach is a typical mathematical model where the damping assumed as linear viscous damping. The Rayleigh damping provides a way to generate the damping matrix by using two coefficients associated with mass and stiffness. The coefficients are frequency-dependent. During an analysis, the frequencies at the current state must be calculated to regenerate the coefficients but this calculation is not recommended because of costly computation-time, also commercial software typically does not provide such an option. Additionally, the structural components that are allowed to undergo plastic deformation will exhibit varying different stiffnesses during a seismic event. Thus, stiffness at each current state must be calculated, however; the coefficients do not vary during the event so including the varying stiffness might result in unintended consequences. Therefore, several modeling methods for Rayleigh damping have been recommended.

The Federal Emergency Management Agency (FEMA) P-695 and ASCE 7 do not explain modeling inherent damping clearly and specifically in the inelastic response. Therefore, different modeling methods for Rayleigh damping continue to be used by researchers and structural engineers based upon judgment.

Herein, the contribution is to provide the evaluation for the most common Rayleigh modeling methods with respect to damping forces, energy dissipations, and assessment of the collapse risk, as well as to provide an approach to prevent the possible dissimilarity in the assessment.

1.2. Research Goals and Objectives

Herein, the primary research goals are to evaluate the methods developed for modeling of Rayleigh damping in structures designed by using performance-based criteria and to present an approach that prevents the possible dissimilarity in the assessment. Therefore, several different modeling methods were selected to expand the possible diversity of the results, and to be inclusive of different effects and used to demonstrate the importance of the modeling of the inherent damping.

Succinctly stated the following research objectives are to:

1. Evaluate the most common modeling methods of Rayleigh damping.

2. Observe how the collapse margin ratio is affected by the selection of the modeling methods.

3. Demonstrate the critical damping ratio limitation approach so as to prevent the unintended consequences of the selection of the modeling methods.

4. Recommend alternative procedures to address the limitations outlined.

1.3. Scope and Assumptions

Herein, the present work is limited in scope to:

1. Only horizontal earthquake loading was considered and the loading is limited to forty-four individual ground-motion records required by FEMA P-695. The records were provided by the web-based Pacific Earthquake Engineering Research Center ground-motion database (*PEER Ground Motion Database*) and were scaled with gravity *(g)* unit and the normalization factors determined by FEMA P-695.

2. Numerical analyses are limited to three different systems are; the SDOF system that consists of Buckling Restrained Brace (BRB) parts, four- and nine-story MDOF systems that are provided by (Kircher et al., 2010) and approved by the peer panel of FEMA P-695. These peer-reviewed BRB archetypes are used as an example of one kind of lateral system.

3. Rayleigh modeling methods are limited to seven and ten different methods for the SDOF and MDOF systems, respectively. The most common models were considered in order to involve the potential diversity of modeling.

4. The section sizes and material properties of the BRB elements are provided in the report where the MDOF systems presented, unlike the post-yield stiffness. Therefore, the post-yield stiffness ratio was determined as 2.5% with respect to (Black et al., 2002). Alternatively, BRB elements were modeled as plastic Wen link elements in SAP2000^{TM}.

5. Solely BRB elements were checked for strength and other structural elements were assumed to have sufficient capacity. Alternatively, the archetypes were checked for a

drift limit of 0.02%. Therefore, the collapse was controlled by strength of BRBs and story-drifts.

CHAPTER 2:

LITERATURE REVIEW

Here, the relevant literature is discussed as the following topics:

1. Fundamental overview of structural dynamics, seismic design, and steel structures,
2. Descriptions of energy dissipations in the inelastic response,
3. Current codes used to model inherent damping, and
4. Relevant researches that conducted on the modeling of the inherent damping in the inelastic response.

The chapter concludes by describing the terminologies used for the goals of the thesis and how the inherent damping is modeled in the inelastic response.

2.1. Structural Dynamics

Dynamic actions are the most challenging conditions for building structures, these include winds, earthquakes, blasts, or vibration due to any source. Here, dynamic actions are considered as only horizontal earthquake loading. The properties of interest included the equation of motion, natural frequency, and earthquake characteristics. For the further background of structural dynamics, see typically structural dynamics textbooks, e.g., (Chopra, 2012), (Rajasekaran, 2009), and (Thorby, 2008).

2.1.1. Equation of Motion: Earthquake Excitation

In seismic-prone regions, the most challenging problem that concerned by engineers is the response of structures due to the earthquake-induced motion. During a seismic event, the mass of the structure, and the ground are displaced relatively to each other. When these two

displacements are considered together, it is called the absolute displacement of the structure. At each instant of time the absolute displacement is calculated:

$$u^t(t) = u_g(t) + u(t) \tag{2.1}$$

where $u^t(t)$, $u_g(t)$, and $u(t)$ are respectively the absolute displacement, the displacement of the ground, and the relative displacement of the mass assigned. The one-story system is idealized by a Single-Degree-of-Freedom (SDOF) system and is subjected to earthquake excitation is shown in Figure 2.1.

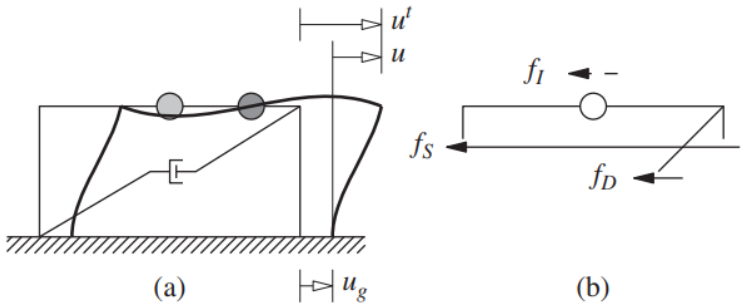

Figure 2.1: (a) Idealized one-story system, (b) Dynamic equilibrium (Chopra, 2012)

And the equation of dynamic equilibrium is

$$f_I + f_D + f_S = 0 \tag{2.2}$$

where f_I, f_D, and f_S are respectively the inertia force, the damping force, and stiffness force. Damping and stiffness forces are produced by structural deformation, which is obtained due to the relative motion between the ground and the mass assigned, however, the inertia force is related to absolute acceleration of the mass by

$$m\ddot{u}^t + c\dot{u} + f_S(u) = 0 \tag{2.3}$$

where $u(t)$, $\dot{u}(t)$, and $\ddot{u}(t)$ are the state variables that are described respectively by displacement, velocity, and acceleration. Substitution of Equation (2.1) and Equation (2.3) gives

$$m\ddot{u} + c\dot{u} + f_S(u) = -m\ddot{u}_g(t) \tag{2.4}$$

This is the equation of motion governing the relative displacement of SDOF structures that subjected to the earthquake excitation and is expressed as the combination of three components that are stiffness, damping, and mass.

The stiffness component refers to the deformation ability of a structural component to resist a force applied and it is expressed the force required by a unit deformation. Additionally, the structural components, which are allowed to undergo plastic deformation, exhibit two different stiffnesses, which are defined as initial and post-yield, during a seismic event. In Equation (2.4), the stiffness may vary with respect to each current state of the component. This nonlinear behavior is important in seismic design.

The damping component refers to a decay in the structural response due to the material and components mechanism. The damping is associated with energy lost that is not recoverable and it is typically dissipated as the heat loss. The phenomenon referred to as “inherent” or “structural” damping. Inherent damping could be considered due to various sources but the principal source of damping could be characterized as internal frictions between connections, structural components, and non-structural components.

The mass component refers to the consideration of the gravity with the weight of anything that specified dead and live, also known as gravity loads. These loads, are also static

loads, act on the structure vertically. In order to simplify calculations, the total weight for each floor is considered as lumped at each floor as demonstrated in Figure 2.1.

To demonstrate these components, the SDOF system that introduced in Figure 2.1 is idealized by using a mass-spring-damper system that is idealized as an external force is applied rather than earthquake excitation and the stiffness is represented in the figure is constant (elastic) rather than varying at the current state.

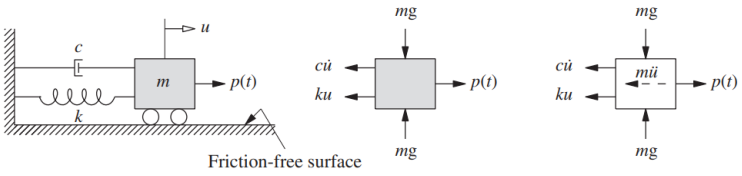

Figure 2.2: Mass-spring-damper system (Chopra, 2012)

The spring and damper are assumed to be massless and the mass is rigid. Also, the motion is assumed to be only in parallel to the base. The system that shown in Figure 2.2 is classified as a SDOF system because it is associated with a single mass component. For vertical structures, it is typically represented as the story-number of structures because the total mass at each story is assumed to be lumped at the floor. For MDOF systems and base acceleration, Equation (2.4) is modified to a matrix form as

$$[M]\begin{bmatrix}\ddot{u}_1\\ \cdot\\ \cdot\\ \ddot{u}_n\end{bmatrix}+[C]\begin{bmatrix}\dot{u}_1\\ \cdot\\ \cdot\\ \dot{u}_n\end{bmatrix}+[K]\begin{bmatrix}u_1\\ \cdot\\ \cdot\\ u_n\end{bmatrix}=-[M]\begin{bmatrix}\ddot{u}_{g1}(t)\\ \cdot\\ \cdot\\ \ddot{u}_{gn}(t)\end{bmatrix} \tag{2.5}$$

The system is expressed as the combination of three components which are the stiffness matrix, the damping matrix, and the mass matrix dotted with their state variables. In the general

sense, each of these matrices might vary with the current state. Herein the mass matrix is always considered constant. The stiffness matrix may vary at each current state due to the inelastic components. The damping matrix is described in Section 2.6. The mass matrix is often expressed as a diagonal matrix and developed by using the total mass assigned to each floor.

2.1.2. Dynamic Response

The dynamic response of structures could be interpreted as cyclic motions as swaying from side to side under seismic excitations. One cyclic motion duration is called the period and the period is expressed as the time that starts when the system is excited, and ends when the structure is back to its original position during free vibration. On the other hand, the number of cyclic motions in a second is called the natural frequency, which is expressed as cycles per second or Hertz (Hz). Under linear assumptions and neglecting damping, the natural frequency is a structural property because it exhibits the same property regardless of any external sources. The natural angular frequency is a function of the mass and stiffness of the structure and calculated by

$$\omega_n = \sqrt{\frac{k}{m}} \tag{2.6}$$

and the natural frequency is

$$f_n = \frac{\omega_n}{2\pi} \tag{2.7}$$

Here the damping ratio terms are neglected and removed because the small damping ratios do not have a significant effect on the natural frequency; herein solely small damping ratios were considered.

For harmonic excitation, the dynamic response of a lateral resisting system could be obtained different or equal to its static response, this depends on the ratio that determined with respect to the proportion of the excitation frequency and the natural frequency. The proportion is expressed as the dynamic amplification factor and it varies at each frequency ratio.

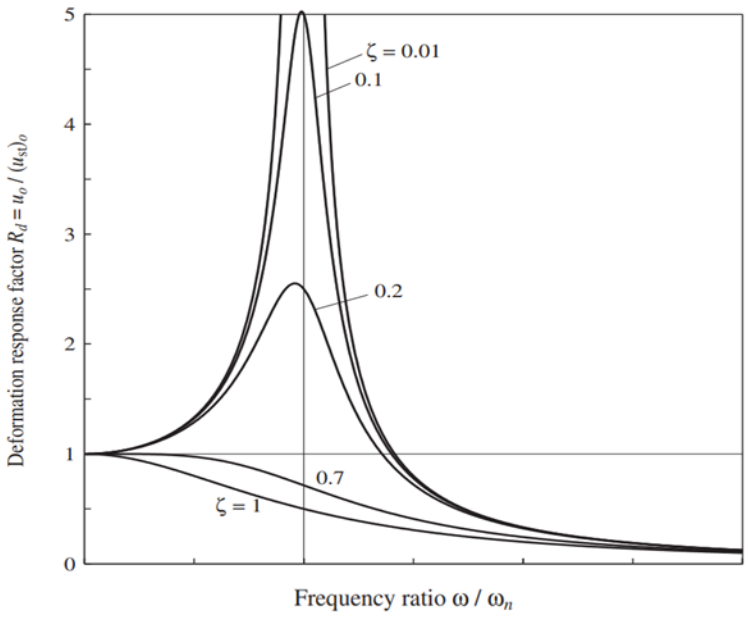

Figure 2.3: Dynamic amplification factor for different frequency ratios (Chopra, 2012)

In Figure 2.3, it is observed that the dynamic amplification factor is a function of the frequency ratio and the damping ratio and when the frequency ratio is equal to one, the dynamic amplification factor reaches its maximum value. However, when the frequency ratio is obtained as much lesser than one, the dynamic amplification factor is close to one which means the dynamic response is essentially the same as the static response. The relation between the dynamic response and the static response is shown in Figure 2.4.

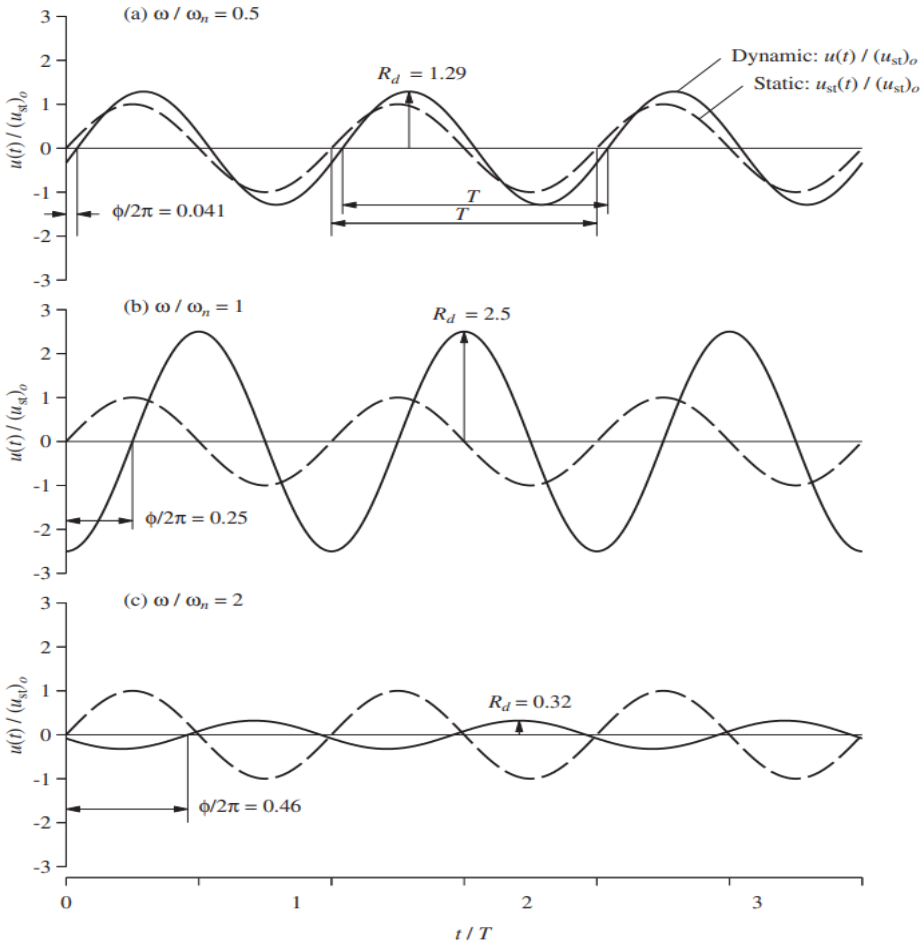

Figure 2.4: The relation between the dynamic and static response (Chopra, 2012)

When the dynamic response of the system is considered, not only stiffness but also different factors could be the dominant effect on the system response for the following cases:

1- When the frequency ratio is obtained as much lesser than one, the force is slowly varying and the dynamic amplification factor is slightly larger than one. In that case,

$$u_0 \simeq (u_{st})_0 = \frac{p_0}{k} \tag{2.8}$$

It means the amplitude of the dynamic response is controlled by the stiffness of the system. Therefore, adding more stiffness to the system has an influence on its response.

2- When the frequency ratio is obtained as much greater than one, the force is rapidly varying and the dynamic amplification factor is close to zero. In that case,

$$u_0 \simeq (u_{st})_0 \frac{\omega_n^2}{\omega^2} = \frac{p_0}{m\omega^2} \tag{2.9}$$

It means the amplitude of the dynamic response is controlled by the mass assigned to the system.

3- When the frequency ratio is obtained as close to one, the maximum dynamic amplification factor is obtained. In that case,

$$u_0 \simeq \frac{(u_{st})_0}{2\zeta} = \frac{p_0}{c\omega_n} \tag{2.10}$$

It means the response at resonance is limited by the damping component of the system; as damping goes to zero the response becomes infinite.

The cases that expressed above demonstrates that the dominant parameters that have impact influence on the dynamic response could be changes with respect to the frequency ratio obtained. Earthquake has a complex mix of harmonic loading characteristics and is discussed next.

2.1.3. Earthquake Excitation Characteristics

Earthquake excitations are one of the most challenging dynamic issues for structural design and the characteristics of ground motions should be well understood. The characteristics could be specified as peak ground acceleration, peak ground velocity, peak ground displacement, spectral characteristics, duration, etc. However, understanding the parameters described are useful for the intensity of ground motions and predicting the structural response (Tao et al.,

2019). The ground motions may be represented in time or frequency domains. The ground motion in the frequency domain could be determined by using several proposed methods that are the Fast Fourier transform, Hilbert transforms, generalized harmonic wavelets, etc. In the upper diagram and lower diagram in Figure 2.5, a ground motion record is represented in the time domain, and the frequency domain, respectively.

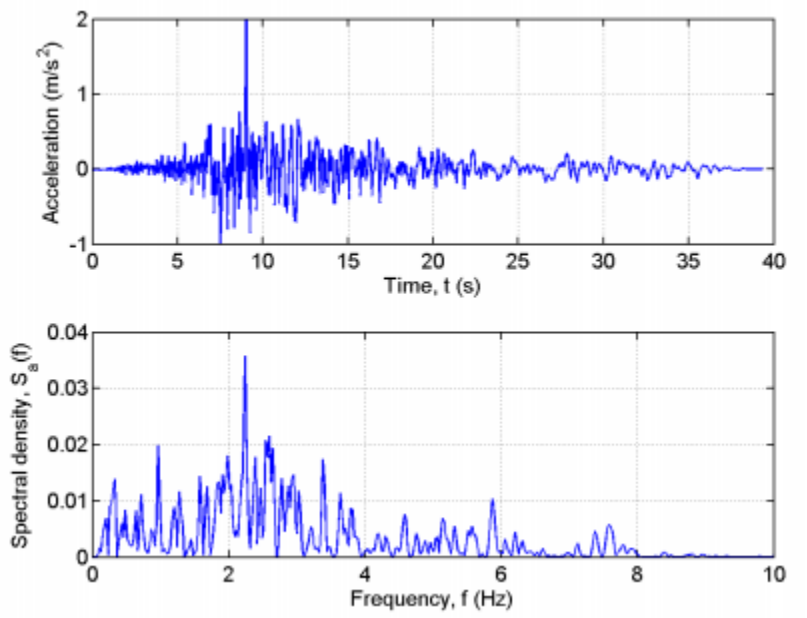

Figure 2.5: Typical horizontal ground motion accelerations (Strømmen, 2014)

Earthquake excitations are in general a complex because they are classified as stochastic which means it can only be predicted. Although it is multi-dimensional, it is often assumed that the structure is subjected to only horizontal ground acceleration for design purposes (Strømmen, 2014). It could be observed that it is a non-periodic, or stochastic transient process, so the frequency-domain approach may not be suitable because of the random base acceleration process. Additionally, frequency-domain technique often requires linear response, not typical of seismic modeling. Therefore, time-domain approaches are more suitable. However, the

frequency-domain record informs if dominant frequencies may align with natural frequencies of the structure, where the dynamic response is amplified as illustrated in Figure 2.3.

2.1.4. Equivalent Viscous Damping

Equivalent viscous damping, which is the simplest damping-form, could be used to represent inherent damping in the elastic structures because it is suitable for the equation of motion which governing differential is linear. Under harmonic force, equivalent viscous damping is considered based on the dynamic response at the frequency ratio that is obtained as equal to one. The damping ratio ζ_{eq} is calculated by

$$\zeta = \frac{1}{2}\frac{(u_{st})_0}{(u_0)_{\omega=\omega_n}} \tag{2.11}$$

At the resonance case, which the frequency ratio is obtained as equal to one, the damping ratio is accepted as the equivalent viscous damping because all energy-dissipating mechanisms are included. This is the simplest definition of the equivalent viscous damping. The most common method to determine the equivalent viscous damping is to equate the energy dissipated in a vibration cycle to an equivalent viscous system. Under the cyclic loading with displacement amplitude u_0, the force-displacement relation is demonstrated in Figure 2.6 (Chopra, 2012).

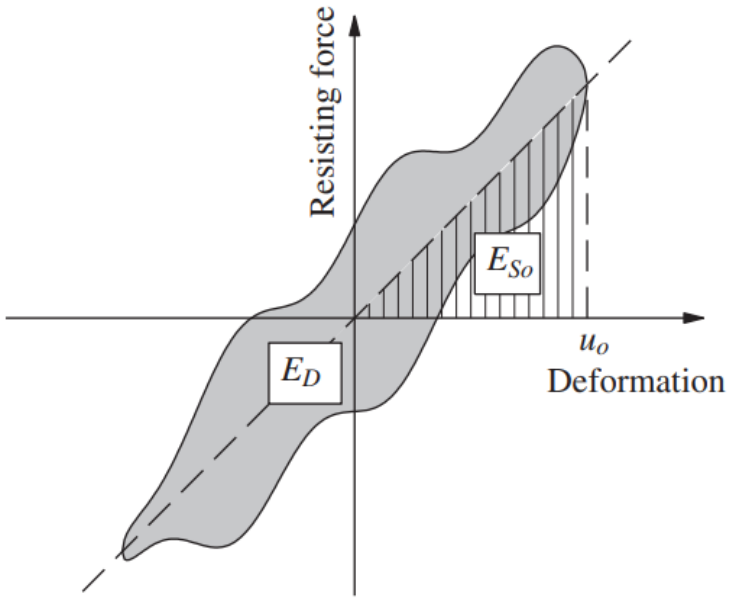

Figure 2.6: Energy dissipated E_D in a cycle of harmonic vibration (Chopra, 2012)

The area that enclosed by E_D represents the hysteresis loop and the energy dissipated in the actual structure and when this is equated the energy dissipated in viscous damping, the equivalent viscous damping could be calculated by

$$4\pi\zeta_{eq}\frac{\omega}{\omega_n}E_{So}=E_D \text{ or } \zeta_{eq}=\frac{1}{4\pi}\frac{1}{\omega/\omega_n}\frac{E_D}{E_{So}} \tag{2.12}$$

However, the energy dissipated in the actual structure, E_D, should be conducted at $\omega=\omega_n$. Thus, Equation (2.12) degenerates to

$$\zeta_{eq}=\frac{1}{4\pi}\frac{E_D}{E_{So}} \tag{2.13}$$

At the resonance case, the damping reaches the maximum effect on the dynamic response. Although the damping ratio ζ_{eq}, which is determined at the resonance case, does not provide the correct value for the other frequency ratios, it could be a sufficient approximation. The defining process of the equivalent viscous damping that described above is valid for the SDOF systems nevertheless it may be extended to MDOF systems. “An equivalent viscous damping ratio is assigned to each natural vibration mode of the system in such a way that the energy dissipated in viscous damping matches the actual energy dissipated in the system when the system vibrates in that mode at its natural frequency” (Chopra, 2012). On the other hand, all methods that described above is valid for linear systems. Likewise, equivalent viscous damping in inelastic systems has been modeled in some research studies; however, it is generally not a sufficient approach.

2.2. Seismic Design Overview

Seismic actions are among the most challenging conditions for building structures. A structure might be designed to resist seismic events within the elastic deformation range, however, this is typically uneconomical. Therefore, extensive research has been conducted and innovative solutions have been developed in order to find economical solutions. Performance-based-design or ductile design concept is one of the economical approaches.

Fundamental to seismic design is the concept by absorbing energy through planned plastic deformation on the select structural components. The plastic deformation is permanent and results in cumulative energy absorption, also known as hysteresis energy dissipation. Thus, the portion of the seismic energy is dissipated by converting it to hysteresis energy and ultimately heat loss.

2.3. Hysteresis Behavior

Numerous laboratory tests have been conducted to model the behavior of structures for seismic events. Because of the yielding of material under large excitations, hysteresis loops have been observed under oscillatory motion with a reversal of deformations, e.g., shown in Figure 2.7. Such behavior is typical of many kinds of component, e.g. bending, axial, torsion, and so forth. Herein, the discussion is limited to axial deformation as implemented in buckling restrained braces discussed in detail later.

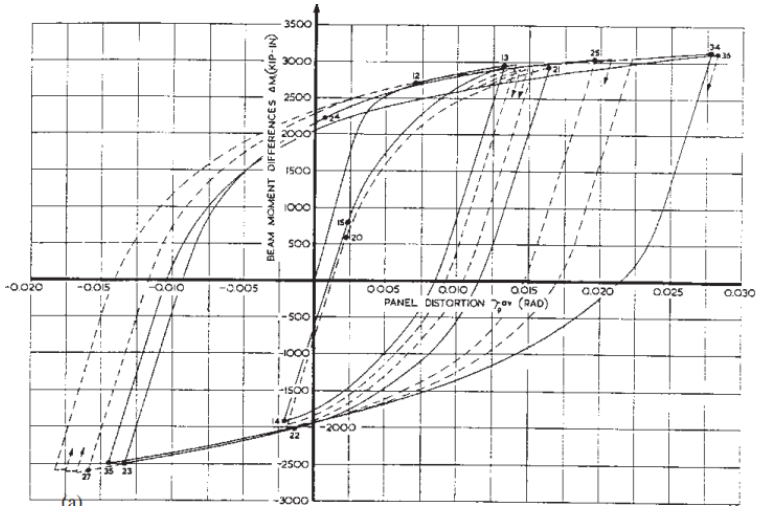

Figure 2.7: Hysteresis loops under cyclic loading (Chopra, 2012)

From mechanics, the energy-absorbing ability of a material is typically associated with the area within the stress-strain curve which is also known as toughness. Materials are defined into two categories as ductile and brittle materials based on the ability to absorb the energy. (Boresi & Schmidt, 2003). Ductile materials, e.g., steel can exhibit significant ductility when properly used in components, can provide a mechanism to absorb significant amount energy, again released to heat, that can provide structural safety for seismic loads that otherwise might not be possible. This energy dissipation is termed “hysteric” damping. Other mechanisms such as

friction might be considered in either term. Herein, the sum of the hysteric damping, and the inherent damping that is described next sections constitute the total energy dissipation, and therefore, is be equal to the energy input from the seismic event. The energy associated with elastic stiffness (potential) and mass (kinetic) typically just transfers back-and-forth during loading, not accumulated, and therefore, does not supply any absorption. Any other sources are considered minor.

2.3.1. Force - Deformation Relation

To observe the behavior of a structural element, force-deformation relation, which is recorded under several loading types in positive and negative directions, is used. The stress-strain relation of any material could be convertible to force-deformation relation by using cross-section and length of the element. The load is increased from its initial value to the rupture value of the element, however, the element response is not only affected by the magnitude but also the loading types, such as the rate of loading, monotonically loading, cycling loading, etc. (Boresi & Schmidt, 2003).

When the appropriate loading type is defined to model the oscillatory motion, hysteresis loops are generated under the reversal of deformations because of inelastic behavior. Forces and deformations result in back-and-forth based on loading at each time step. Next, the maximum forces on each deformation are determined in order to idealize the behavior, which is also known as the Backbone curve, shown in Figure 2.8.

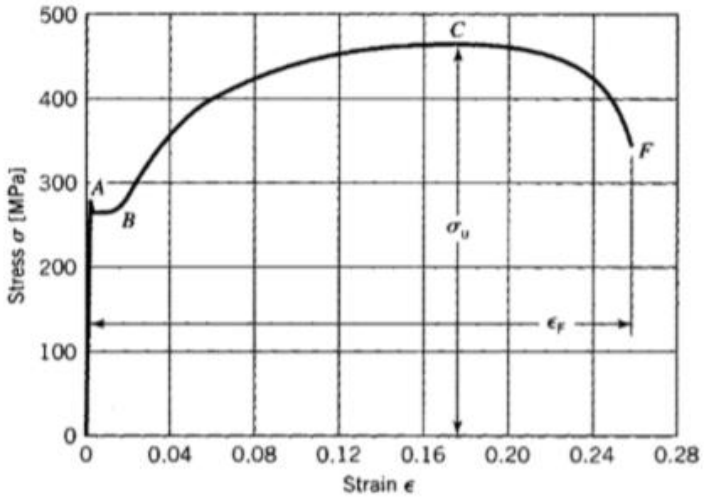

Figure 2.8: Typical Stress-strain diagram for structural steel (Boresi & Schmidt, 2003)

A, C, and F represent yield strength, ultimate strength, and fracture point respectively on the curve to characterize inelastic behavior. For different material types or specific structural elements, these points could be represented in different ways such as the kinematic hysteresis model, degrading hysteresis model, Takeda hysteresis model, pivot hysteresis model, concrete hysteresis model, isotropic hysteresis model, and BRB hardening hysteresis model. However, the backbone curve could be also simplified. The simplified curve is generated typically by two slopes that are initial and post-yield stiffness. Initial stiffness and post-yield stiffness are used to define behavior within the elastic range and the plastic range of the element, respectively (SAP2000, 2017, p. 200).

2.4. Steel Structures

Engineers often prefer to use structural steel due to its mechanical properties, availability in a variety of useful and practical shapes, economy, design simplicity, and ease and speed of construction. However, in order to achieve an adequately durable structure for its life-time, the steel structures are designed based upon requirements for safety, serviceability, and durability of

structures. In this section, types and limitations for steel structures were described. For the further background of steel structures, see typically steel structure textbooks, e.g., (Williams, 2011), (Dubina et al., 2012).

2.4.1. Limit States Design

So as to design an adequately durable structure for its life-time, the performance, and probability of failure of the structure should be considered, with this in mind, limit states design provides a framework that considers various limiting conditions. Thus, in a limit state framework, the inherent variability of loads, materials, construction practices, and approximations are included.

"A limit state is formally defined by the description of a condition for which a particular structural member or an entire structure fails to perform the function that is expected of it" (Dubina et al., 2012). For steel structures, four types of limit states are considered in which are ultimate limit state (ULS), serviceability limit state (SLS), fatigue limit state (FLS), accidental limit state (ALS). In specification-based design, engineers use prescriptive methods to determine loads and use those loads in an analytic to determine the demand on the components. Similarly, prescriptive methods are used to predict the resistance provided by the component to meet, or exceed, these demands.

In performance-based design, the ultimate limit state may be referred to as the collapse limit state and the load and resistance effects are predicted with more rigorous modeling. Herein, actual earthquake, time-histories are applied in SAP2000 that uses nonlinear dynamic analysis to predict the behavior and associated damage and/or collapse. Performance-based methods are becoming more commonplace in engineering practice for design and also the validation of new

devices for absorbing seismic energy. The Buckling Resisting Brace Frame (BRBF) uses such a device and is described next.

2.4.2. Buckling Resisting Brace Frame (BRBF)

The structures have two different resisting systems in order to resist the lateral and vertical loads which may or may not be combined. The vertical load resisting systems are designed so as to resist against gravity loads that specified as dead and live loads (Static) on the structures, however, this is not a difficult concern for the designers. The most challenging part of the design is defining the lateral load resisting system as load paths are more complex, and in the case of seismic loads, the loads are large. The most common types of lateral resisting systems are braced frames, rigid frames, and shear walls (AISC, 2010). The system selection might be a function of architectural constraint, type of loading, local construction practices, and so forth. Herein braced frames are considered.

Concentrically braced frames (CBF), buckling-restrained braced frames (BRBF), and eccentrically braced frames (EBF) which are the most common braced frame systems are demonstrated schematically as shown in Figure 2.9. Buckling-restrained Braced Frames (BRBF) are one of the innovative solutions that have been developed in order to find economical solutions to design the seismic load resisting system. (AISC 2016) In Figure 2.10, the isometric cutaway of an example buckling-restrained brace is shown in Figure 2.10.

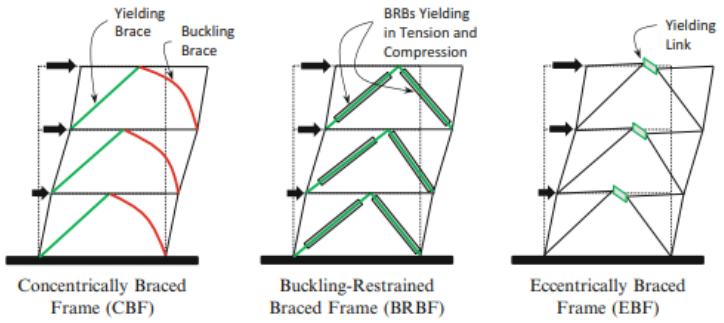

Figure 2.9: Types of steel braced frames (Marshall, 2021)

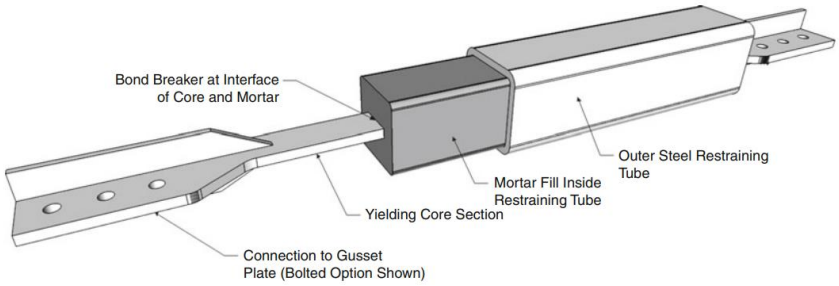

Figure 2.10: Isometric cutaway of buckling-restrained brace (Marshall, 2021)

It is an effective application for conventional braced frame systems so as to prevent buckling on the brace element, as well as, the brace element is reached its yield point before it is buckled. Additionally, it provides a similar strength in tension and compression. Typical hysteresis plots are shown in Figure 2.11.

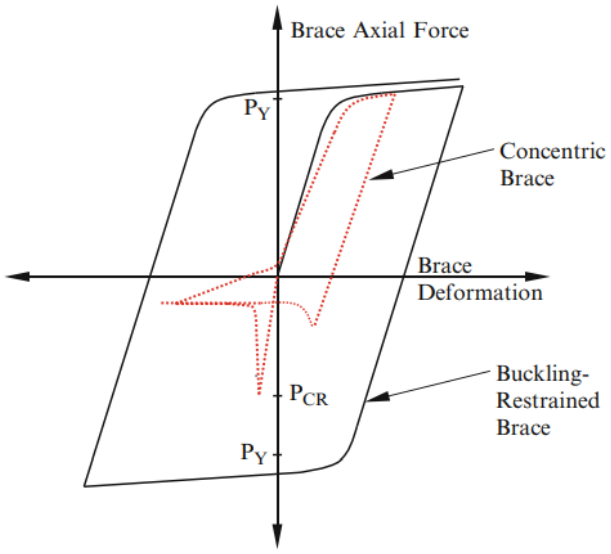

Figure 2.11: Typical hysteresis plot for buckling-restrained braces (Marshall, 2021)

As shown in Figure 2.11, BRBF exhibits significant ductility and when properly designed with the adjoining elements, the system can provide structural safety for seismic loads caused by severe earthquakes. The required properties, shown in Figure 2.12, are determined by testing.

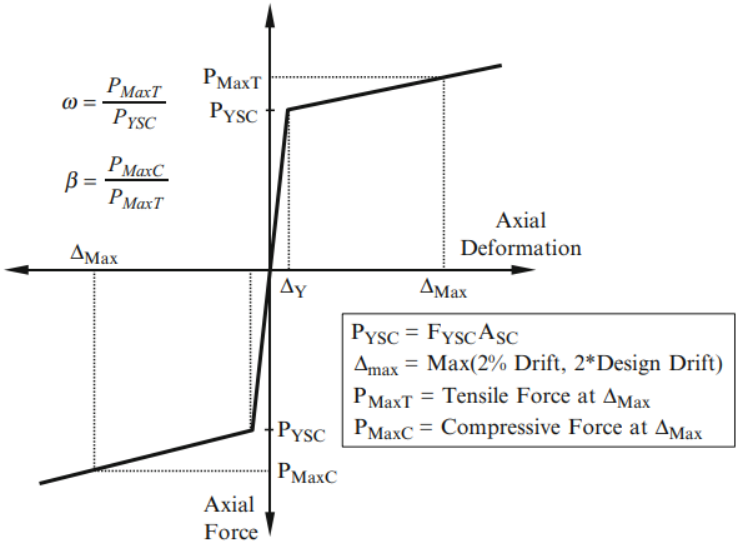

Figure 2.12: Determination of adjusted brace strength (Marshall, 2021)

In view of test data, these properties are observed, as well as, initial stiffness and post-yield stiffness might be defined so as to use the BRB model in the nonlinear analysis. However, testing alone will not establish acceptable behavior in the seismic structural system; the component test behavior must be combined with performance- and risk-based analysis to understand how the BRB will performance in typical structural frames. FEMA P-695 outlines this process.

2.5. FEMA P-695

Federal Emergency Management Agency (FEMA) describes a methodology that is recommended for use in seismic design so as to quantify building system performance and response parameters for use in seismic design. The performance and response parameters, Seismic Performance Factors (SPFs), are the response modification coefficient (*R* factor), the system overstrength factor (Ω_0), and deflection amplification factor (C_d). When a new seismic force resisting system is proposed, SPFs should be determined to use in seismic design process, with this in mind, a rational basis for establishing global SPFs is provided by the methodology (*Quantification of Building Seismic Performance Factors*, 2009).

2.5.1. Design Guide

A framework is provided by the Methodology in order to establish seismic performance factors (SPFs) based on probabilistic evaluation of collapse risk. The framework consists of a technical approach that involves nonlinear analysis techniques and uncertainties in ground motion, modeling, design, and test data. Key elements of the Methodology are illustrated in Figure 2.13.

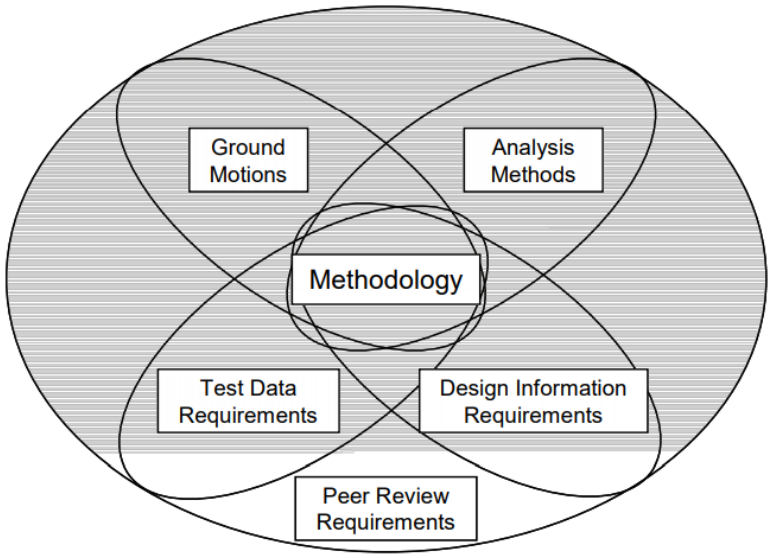

Figure 2.13: Key elements of the Methodology (*Quantification of Building Seismic Performance Factors*, 2009)

The characterizations of ground motion and analysis methods are fully defined in the Methodology as well as almost suitable to all seismic-force-resisting systems; however, the design information and the test data might not be applicable to each system, even non-existent for the new proposed systems. Therefore, the Methodology requires that the entire process to be reviewed by an independent review panel due to the complexity of analysis, the difficulty in modeling, and the lack of design information and test data. The entire process is illustrated schematically in Figure 2.14. This process will be explained in detail in later Sections.

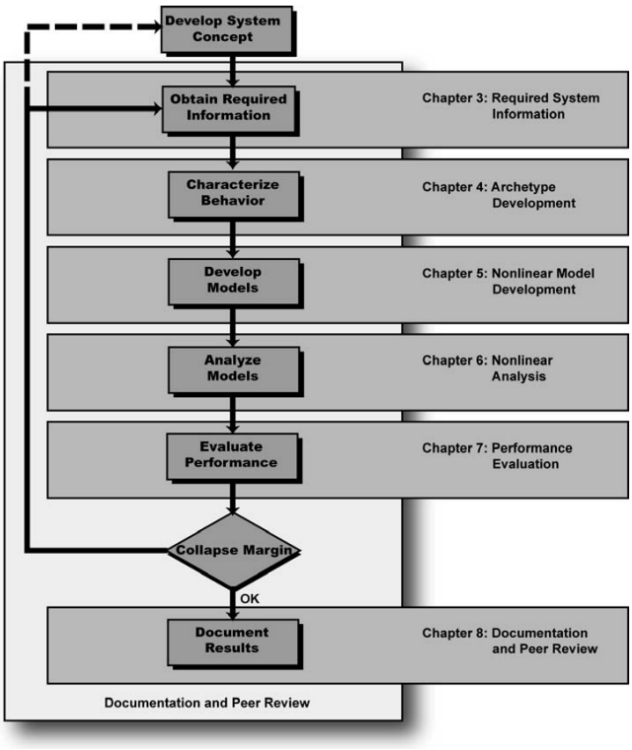

Figure 2.14: Process for documenting seismic performance factors (SPFs) (*Quantification of Building Seismic Performance Factors*, 2009)

2.5.2. Ground-Motion Records Sets

Two sets of ground motion records, which referred as the Far-Field and the Near-Field, are provided by the Methodology for nonlinear dynamic analysis in order to evaluate the collapse of the proposed systems, however, the Near-Field record set is not required. The Far-Field record set that consists of twenty-two component pairs of ground motions is referred "Far" due to its site location (10 km away from the fault rupture), as well as, the component pairs involve solely horizontal ground motions. The vertical components of ground motions are not considered as the primary collapse assessment for nonlinear dynamic analysis. Spectral accelerations (at 1-sec) for the component pairs that consist of *x* and *y* components of the earthquake records are demonstrated in Figure 2.15.

Table A-4D Summary of Factors Used to Normalize Recorded Ground Motions, and Parameters of Normalized Ground Motions for the Far-Field Record Set

ID No.	As-Recorded Parameters			Normaliz-ation Factor	Normalized Motions	
	1-Sec. Spec. Acc. (g)		PGVPEER (cm/s.)		PGA_{max} (g)	PGV_{max} (cm/s.)
	Comp. 1	Comp. 2				
1	1.02	0.94	57.2	0.65	0.34	41
2	0.38	0.63	44.8	0.83	0.40	38
3	0.72	1.16	59.2	0.63	0.52	39
4	0.35	0.37	34.1	1.09	0.37	46
5	0.26	0.48	28.4	1.31	0.46	43
6	0.24	0.23	36.7	1.01	0.39	43
7	0.31	0.29	36.0	1.03	0.53	39
8	0.33	0.23	33.9	1.10	0.26	42
9	0.43	0.61	54.1	0.69	0.25	41
10	0.11	0.11	27.4	1.36	0.30	54
11	0.50	0.33	37.7	0.99	0.24	51
12	0.20	0.36	32.4	1.15	0.48	49
13	0.46	0.28	34.2	1.09	0.58	38
14	0.27	0.38	42.3	0.88	0.49	39
15	0.35	0.54	47.3	0.79	0.40	43
16	0.31	0.25	42.8	0.87	0.31	40
17	0.33	0.34	31.7	1.17	0.53	42
18	0.54	0.39	45.4	0.82	0.45	36
19	0.49	0.95	90.7	0.41	0.18	47
20	0.30	0.43	38.8	0.96	0.49	38
21	0.25	0.15	17.8	2.10	0.44	40
22	0.25	0.30	25.9	1.44	0.50	44

Figure 2.15: Parameters of Normalized Ground Motions for the Far-Field Record Set (Quantification of Building Seismic Performance Factors, 2009)

Unwarranted variability between records was observed due to inherent differences such as site conditions, source type, or distance to source etc., however, the unwarranted variability could be prevented by multiplication of each record set with normalization factors that are defined based on their peak ground velocities as shown in Figure 2.15.

Alternatively, index archetypes are designed based on Seismic Design Category (SDC) B, C, or D criteria, and Maximum Considered Earthquake (MCE) spectral demand and response spectra as shown in Figure 2.16 and Figure 2.17, respectively, are used for the collapse evaluation. The spectral accelerations $S_{ms}(g)$ and $S_{m1}(g)$ are the short-period and one-second period values that provide the "anchor points" to define the curves shown in Figure 2.17. These values are derived with respect to site class D assuming five percent critical damping ratio.

Table 6-1 Summary of Maximum Considered Earthquake Spectral Accelerations And Transition Periods Used for Collapse Evaluation of Seismic Design Category D, C, and B Structure Archetypes, Respectively

Seismic Design Category		Maximum Considered Earthquake		Transition Period
Maximum	Minimum	S_{MS} (g)	S_{M1} (g)	T_s (sec.)
D		1.5	0.9	0.6
C	D	0.75	0.30	0.4
B	C	0.50	0.20	0.4
	B	0.25	0.10	0.4

Figure 2.16: MCE spectral accelerations (Quantification of Building Seismic Performance Factors, 2009)

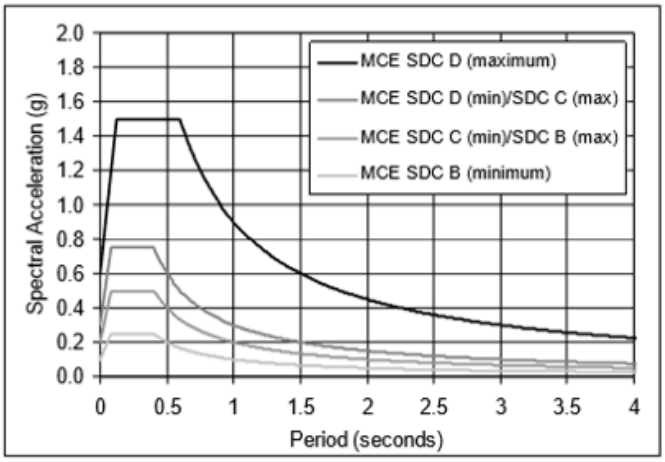

Figure 2.17: MCE response spectrum for each SDC (Quantification of Building Seismic Performance Factors, 2009)

However, the median values of the normalized Far-Field set do not align with the Maximum Considered Earthquake (MCE) spectral demand values; therefore, the normalized Far-Field record set is scaled to (MCE) demand. The scale factors and the medium spectrum scaled are provided in Figure 2.18 and Figure 2.19, respectively.

Table A-3 Median 5%-Damped Spectral Accelerations of Normalized Far-Field and Near-Field Record Sets and Scaling Factors for Anchoring the Normalized Far-Field Record Set to MCE Spectral Demand[1].

Period $T = C_u T_a$ (sec.)	Median Value of Normalized Record Set $\hat{S}_{NRT}$ (g)		Scaling Factors for Anchoring Far-Field Record Set to MCE Spectral Demand			
	Near-Field Set	Far-Field Set	SDC D_{max}	SDC C_{max} / SDC D_{min}	SDC B_{max} / SDC C_{min}	SDC B_{min}
0.25	0.936	0.779	1.93	0.96	0.64	0.32
0.3	1.020	0.775	1.94	0.97	0.65	0.32
0.35	0.939	0.761	1.97	0.99	0.66	0.33
0.4	0.901	0.748	2.00	1.00	0.67	0.33
0.45	0.886	0.749	2.00	0.89	0.59	0.30
0.5	0.855	0.736	2.04	0.82	0.54	0.27
0.6	0.833	0.602	2.49	0.83	0.55	0.28
0.7	0.805	0.537	2.40	0.80	0.53	0.27
0.8	0.739	0.449	2.50	0.83	0.56	0.28
0.9	0.633	0.399	2.50	0.83	0.56	0.28
1.0	0.571	0.348	2.59	0.86	0.58	0.29
1.2	0.476	0.301	2.49	0.83	0.55	0.28
1.4	0.404	0.256	2.51	0.84	0.56	0.28
1.6	0.356	0.208	2.70	0.90	0.60	0.30
1.8	0.319	0.168	2.98	0.99	0.66	0.33
2.0	0.284	0.148	3.05	1.02	0.68	0.34
2.2	0.258	0.133	3.08	1.03	0.68	0.34
2.4	0.230	0.118	3.18	1.06	0.71	0.35
2.6	0.210	0.106	3.28	1.09	0.73	0.36
2.8	0.190	0.091	3.53	1.18	0.79	0.39
3.0	0.172	0.080	3.75	1.25	0.83	0.42
3.5	0.132	0.063	4.10	1.37	0.91	0.46
4.0	0.104	0.052	4.29	1.43	0.95	0.48
4.5	0.086	0.046	4.34	1.45	0.96	0.48
5.0	0.072	0.041	4.43	1.48	0.98	0.49

Figure 2.18: Normalized Far-Field sets and scaling factors (Quantification of Building Seismic Performance Factors, 2009)

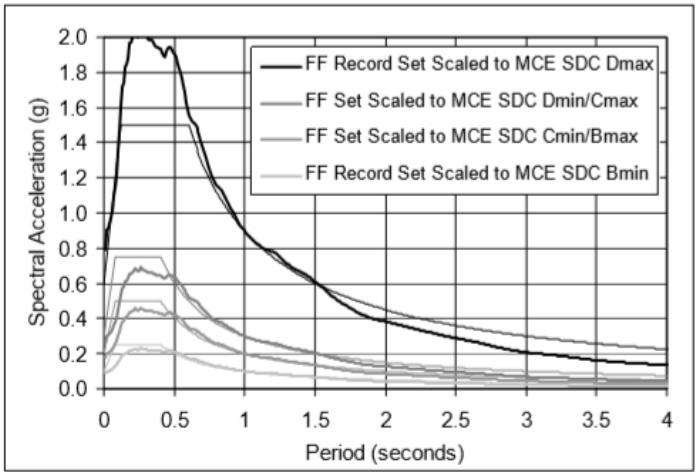

Figure 2.19: Median spectrum of the Far-Field record set (Quantification of Building Seismic Performance Factors, 2009)

2.5.3. Incremental Dynamic Analysis (IDA)

Structures that designed according to the limit states defined in Section 2.4.1 have to perform the sufficient strength and functionality under severe earthquake excitation. The primary consideration for structures designed to exhibit ductile behavior that does not exceed the permitted deformation under a severe earthquake. Therefore, the story-drift ratio for each story should not exceed the limit that is determined in the codes or else, it is accepted as the collapse. With this in mind, maximum story-drift ratios obtained by performing nonlinear dynamic analyses and are recorded to evaluate the collapse risk. Any ground motion record described in Section 2.5.2 may or may not cause the structure reach the collapse point determined by the story-drift ratio limitation because the records have different intensity and frequency contents that may not align with the natural frequencies of the considered structure. Therefore, FEMA P-695 requires to determine the median collapse intensity in order to evaluate the collapse risk. The median collapse intensity is determined by scaling the median spectral intensity, which is a suite to represent spectral intensities of ground-motion records, until one-half of the records resulted in the collapse and incremental dynamic analysis (IDA) process is performed to scale the intensities. In Figure 2.20, typical incremental dynamic analysis plot is illustrated.

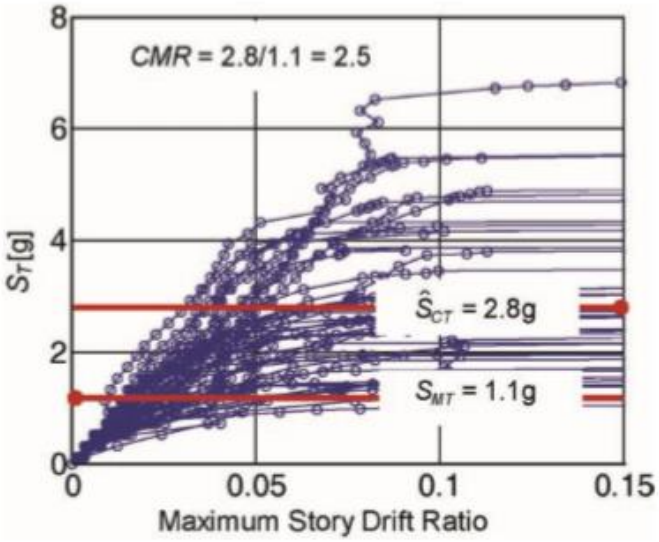

Figure 2.20: Incremental dynamic analysis response plot of spectral acceleration (Quantification of Building Seismic Performance Factors, 2009)

Here, $S_T(g)$ represents the spectral acceleration of the records. and it is a function of the fundamental periods, which are listed in Figure 2.18, because the spectral accelerations are determined by multiplying the scaling value by the median value of the normalized record set for the specified period. The intensity at the collapse point, S_{CT}, for each record is determined based on $S_T(g)$. Here, $\hat{S}_{CT}$ is the median collapse intensity for all records which means the median value of S_{CT} obtained from all records and S_{MT} is the spectral acceleration of the MCE hazard. However, FEMA P-695 provides two possible scaling options that are collectively or individually scaling. In Figure 2.20, the individually scaling option is illustrated, however, all records might be scaled collectively and $\hat{S}_{CT}$ is determined directly with respect to the scale factor that causes one-half of the records resulted in the collapse. Note that the terms, which are defined/mentioned here, are addressed in a detailed way in Section 3.9 also how the terms are obtained for the systems used are described in CHAPTER 4: under related sections.

2.5.4. Collapse Margin Ratio (CMR)

The considered structure is subjected to all scaled records in the Far-Field record set, that consists of forty-four individual records, is analyzed and the scaling target is to obtain two intensities that are specified as the MCE intensity, S_{MT}, and the median collapse intensity, $\hat{S}_{CT}$. The intensities are determined respectively based on the fundamental period of the structure and the lowest intensity at which one-half of the records cause collapse. A summary of intensities is illustrated using the collapse fragility curve, shown in Figure 2.21, which is a cumulative distribution curve and 0.5 represents the median point.

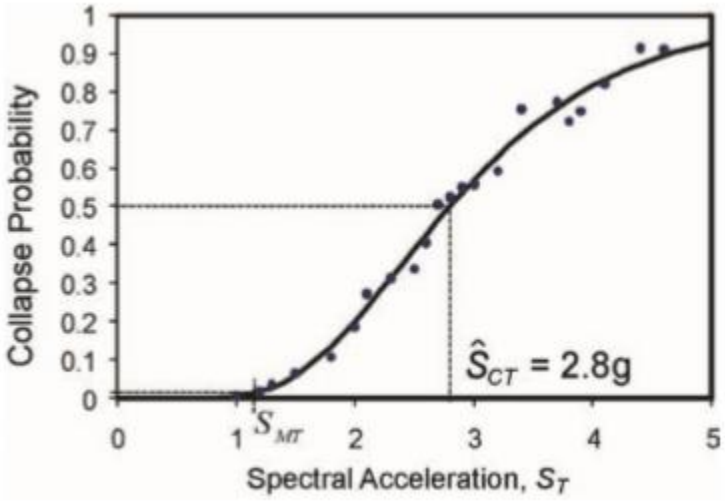

Figure 2.21: Collapse fragility curve, or cumulative distribution function (Quantification of Building Seismic Performance Factors, 2009)

Collapse Margin Ratio (CMR) is the primary parameter for the collapse assessment and it is determined based on the proportion of S_{MT} and $\hat{S}_{CT}$ intensities, shown in Equation (2.14).

$$CMR = \frac{\hat{S}_{CT}}{S_{MT}} \tag{2.14}$$

In short, CMR the multiplier on the MCE earthquake where fifty percent of the time a structure is expected to collapse if subjected to the forty-four seismic events per FEMA P-695.

2.6. Inherent Damping

Damping occurs with free vibration where the structural response decays with time and the energy is lost due to material and component mechanisms. This energy is not recoverable and is typically dissipated in heat loss. The phenomenon referred to as "inherent" damping. With forced vibration caused by wind and seismic events, the damping also provides energy dissipation that helps to decrease the structural response. Inherent damping might be considered due to various sources but the most principal source of damping might be characterized as internal frictions between connections, structural components, and non-structural components.

2.6.1. Identification

Structural engineers would like to have data on damping determined from the recorded responses of various structure types such as buildings, bridges, and dams. Damping is experimentally determined; testing is often expensive. A damping database provides structural engineers to estimate the damping ratios for analysis. On the other hand, accumulating the database is not easy because of a lack of budget and time progress so as to record sufficient response data. Therefore, defining the damping ratio with respect to the structure type is based on accumulated data and expert opinion. Example damping ratios are demonstrated in Figure 2.22. For background of damping ratio, see a typically structural dynamics textbook, e.g., (Chopra, 2012), (Strømmen, 2014), (Thorby, 2008), and (Rajasekaran, 2009).

Stress Level	Type and Condition of Structure	Damping Ratio (%)
Working stress, no more than about $\frac{1}{2}$ yield point	Welded steel, prestressed concrete, well-reinforced concrete (only slight cracking)	2–3
	Reinforced concrete with considerable cracking	3–5
	Bolted and/or riveted steel, wood structures with nailed or bolted joints	5–7
At or just below yield point	Welded steel, prestressed concrete (without complete loss in prestress)	5–7
	Prestressed concrete with no prestress left	7–10
	Reinforced concrete	7–10
	Bolted and/or riveted steel, wood structures with bolted joints	10–15
	Wood structures with nailed joints	15–20

Figure 2.22: Recommended damping values (Chopra, 2012)

The recommended damping ratios with respect to the material type used are listed in Figure 2.22 could be used but most building codes and performance-based standards typically use five percent.

2.6.2. Damping Matrix

Although inherent damping is characterized as nonlinear, amplitude-dependent, and varies during the response, it is often defined as a linear viscous model which is frequency-dependent and amplitude-independent. Linear viscous damping is determined mathematically by a selected damping ratio among the recommended ratios in Figure 2.22. In the analysis of linear and nonlinear systems, inherent damping is typically represented by the linear viscous model, and the classical damping matrix is developed for the systems (Charney et al., 2017b).(F. Charney et al., 2017a)

Classical damping matrix form provides MDOF systems to be analyzed independently by evaluating the system as a number of single degree-of-freedom systems. This is also called as the decoupling of the system (Charney et al., 2017b). One of the popular mathematical models is the Rayleigh damping matrix form which is linear viscous and maintains the orthogonality necessary to decouple for modal analysis.

2.6.3. Rayleigh Damping Matrix

A typical mathematical model for Rayleigh damping that assumes linear viscous damping where the damping forces are proportional to the structure's velocity. Rayleigh damping, is also classical damping matrix form, provides a way to generate the damping matrix by using two coefficients associated with mass and stiffness

$$c = a_0 m \text{ and } c = a_1 k \tag{2.15}$$

where *m* is the mass of the system, *k* is the stiffness of the system, and the constants a_0 and a_1 have units of sec^{-1} and sec, respectively shown in Equation (2.15), (Chopra, 2012). Damping matrix is developed by using these coefficients and the matrix developed is classical because of diagonality with respect to the model orthogonality properties. For MDOF systems, the representation of the model might be identified physically as shown in Figure 2.23. The discussion below follows (Chopra, 2012).

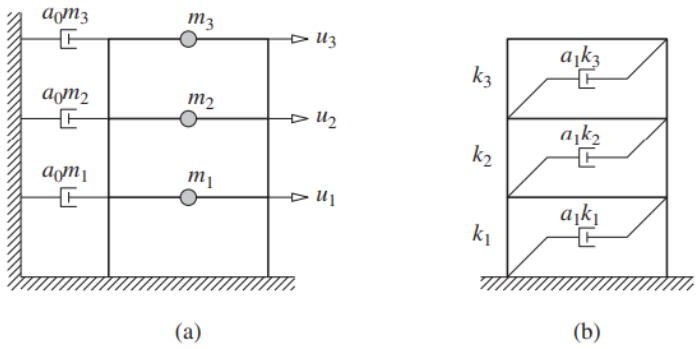

Figure 2.23: (a) Mass-proportional damping; (b) stiffness-proportional damping (Chopra, 2012)

Stiffness-proportional damping contribution might be interpreted as a physical phenomenon as an energy dissipation arising from deformations. Unlike stiffness-proportional damping contribution, mass-proportional damping contribution is difficult to describe as a physical phenomenon. The modal damping ratio for each system is used so as to determine the mass-proportional coefficient, a_0. The n^{th} mode generalized damping is shown in Equation (2.16),

$$c_n = a_0 M_n \tag{2.16}$$

where M_n is mass contribution to the n^{th} mode and the modal damping ratio related with mass-proportional damping is shown in Equation (2.17),

$$\zeta_n = \frac{a_0}{2}\frac{1}{\omega_n} \tag{2.17}$$

where ω_n is n^{th} mode natural frequency. In any one mode, a_0 could be determined by using Equation (2.18),

$$a_0 = 2\zeta_i\omega_i \tag{2.18}$$

where i represents i^{th} mode. Thus, the mass-proportional coefficient could be determined by

using Equation (2.18) in any mode. In a similar way, the modal damping ratio for each system is used to determine the stiffness-proportional coefficient, a_1 as shown in Equation (2.19),

$$c_n = a_1 \omega_n^2 M_n \text{ and } \zeta_n = \frac{a_1}{2} \omega_n \tag{2.19}$$

In any one mode, a_1 could be determined by using Equation (2.20),

$$a_1 = \frac{2\zeta_j}{\omega_j} \tag{2.20}$$

where j represents j^{th} mode. Thus, the stiffness-proportional coefficient could be determined by using Equation (2.20) in any mode. Rayleigh damping is calculated by using Equation (2.21) in order to develop the classical damping matrix,

$$c = a_0 m + a_1 k \tag{2.21}$$

Now, Equation (2.18) and Equation (2.20) is replaced in Rayleigh's Equation (2.22),

$$\zeta_n = \frac{a_0}{2} \frac{1}{\omega_n} + \frac{a_1}{2} \omega_n \tag{2.22}$$

The modal damping ratio for the n^{th} mode might be determined by using Equation (2.22) by specifying the modal damping ratios for any two modes. Then, Equation (2.22) is expressed in a matrix form as

$$\frac{1}{2} \begin{bmatrix} 1/\omega_i & \omega_i \\ 1/\omega_j & \omega_j \end{bmatrix} \begin{Bmatrix} a_0 \\ a_1 \end{Bmatrix} = \begin{Bmatrix} \zeta_i \\ \zeta_j \end{Bmatrix} \tag{2.23}$$

With the right-hand-side known, the coefficients a_0 and a_1 might be calculated by solving the two equations shown in Equation (2.23) and, if the damping ratios for the modes specified are the same the algebra simplifies to

$$a_0 = \zeta \frac{2\omega_i \omega_j}{\omega_i + \omega_j} \quad a_1 = \zeta \frac{2}{\omega_i + \omega_j} \tag{2.24}$$

Equation (2.24) is used to determine the coefficients a_0 and a_1 under the assumed constraint. The two modes specified with recommended damping ratios should be chosen reasonably in order to represent inherent damping or else unintended consequences could be observed. In Figure 2.24, modal damping ratios related to any two natural frequencies are plotted using Rayleigh's equation.

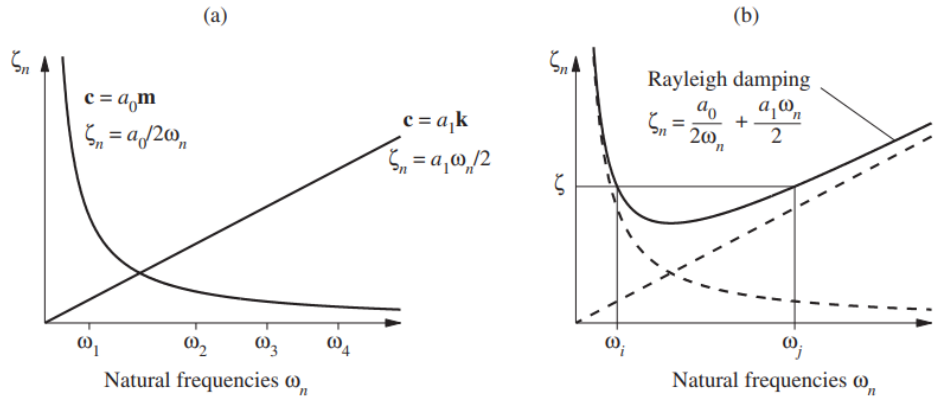

Figure 2.24: Variation of modal damping ratios: (a) mass-proportional damping and stiffness-proportional damping; (b) Rayleigh damping (Chopra, 2012)

The damping ratio by mass-proportional coefficient is inversely proportional to the natural frequency unlike the damping ratio by the stiffness-proportional coefficient and it could be easily interpreted that the coefficients are frequency-dependent.

2.6.4. Non-Linear Analysis by Using Rayleigh Damping

The structural components designed by performance-based-design criteria are allowed to undergo permitted plastic deformation and they exhibit varying different stiffnesses during a seismic event. Therefore, the stiffness used in Equation (2.21) must be calculated at the current state (time). Thus,

$$c = a_0 m + a_1 k(t) \tag{2.25}$$

where *t* represents time in a dynamic analysis and mass is assumed to be invariant with time. The damping matrix could be developed at each current state by using Equation (2.25), (Zareian & Medina, 2010). Additionally, the frequencies of the systems at the current state have to be calculated in order to determine the coefficients a_0 and a_1 shown in Equation (2.24). These natural frequencies obviously depend upon the current stiffness. Thus,

$$c = a_0(t) m + a_1(t) k(t) \tag{2.26}$$

The damping matrix might be developed at each time step by using Equation (2.26), (Zareian & Medina, 2010). Although varying stiffness and frequencies at each time step should be calculated so as to develop the damping matrix, this calculation is not recommended because calculating it is difficult and not computationally-efficient. Therefore, several modeling methods for Rayleigh damping have been recommended. For example, initial stiffness and tangent stiffness approaches are described according to the stiffness defined in Equation (2.21) in (Charney et al., 2017b) and (Zareian & Medina, 2010).

2.6.5. Literature Review

Previous research that has been conducted on the unintended consequences of the developing Rayleigh damping matrix in the inelastic systems is reviewed in this section. Hall (2006) conducted research on investigating the problems encountered from the use of Rayleigh damping. The research conducted resulted in a physical interpretation of the mass and stiffness-proportional parts of the damping matrix in order to evaluate the damping forces that are unrealistically large, and therefore non-conservative. He interprets the mass and stiffness proportional part of Rayleigh damping separately, the first one is that degrees of freedom of the structure are connected to external supports via linear viscous dampers that correspond physically to the mass-proportional part as well as this mechanism possibly not exist, nonetheless, the mass-proportional part is commonly included. The second one is that the degrees of freedom of a structure are interconnected via linear viscous dampers that correspond physically to the stiffness-proportional part. Again, see Figure 2.23.

In addition, the non-linearity mechanism due to yielding, cracking, sliding, and buckling limits the restoring forces so if the initial stiffness is used to develop the stiffness-proportion part in non-linear analysis, high forces might be observed. However, the restoring forces are limited actually, therefore, the high forces are unrealistic. Above all, he suggests eliminating the mass-proportional damping contribution and bound the stiffness-proportional damping contribution. Zareian and Medina (2010) performed research on investigating a practical method for proper modeling of structural damping in inelastic plane structural systems. The research performed resulted in a demonstration that the inelastic dynamic response is exhibited unrealistic damping forces when the stiffness proportional part of the damping matrix is defined based on the initial stiffness, and, the forces become unrealistically high when the nonlinearity and damping ratio

increase. Additionally, the forces cause an overestimation (and non-conservative) of the energy dissipation capacity of the system due to inherent damping energy dissipation is increased. Chopra and McKenna (2016) conducted research on investigating modeling viscous damping in nonlinear response. Their investigation concluded four points based on their recommendations, interpretations and comparisons in order to evaluate the unintended consequences of modeling damping in inelastic response. First, Rayleigh damping could be caused spurious damping forces in the inelastic response, unlike the forces disappear in the elastic response. Second, they recommend using the superposition of modal damping matrices to develop the damping matrix because of eliminating the spurious damping forces irrespectively from the number of modes included or values assigned to modal damping ratios. Third, they demonstrated that the inelastic response could be greatly affected based on how the damping is defined, to demonstrate it, they presented the response for three different damping models that are Rayleigh damping based on initial stiffness, Rayleigh damping using tangent stiffness, and superposition of modal damping matrices, nonetheless, they observed that the results are much improved when Rayleigh damping based on tangent stiffness model is used. Lastly, they do not recommend Rayleigh damping based on the tangent stiffness model because of two contradicts that are lack of a physical basis and has conceptual implications that are troubling - due to hysteresis in damping force-velocity relationship and negative tangent stiffness slope because of gravity loads. Lu and Morris (2017) performed research on investigating assessment of three viscous damping methods for nonlinear time-history analysis. The research performed resulted in a comparison between the results from three different damping modeling, as a conclusion, the modal damping method is with the advantage of controlling on the modal damping ratios for each mode of the structure (This effect might be intentional to help improve the FEMA P-695 validation of a new device, or

unintentional by not understanding the important of the damping method selected). However, the modal damping method is not useful for the non-linear direct-integration analysis, as well as, the modal damping method uses the initial modal properties of the structure, so, more damping might be observed in the inelastic modes. And, they also concluded that using the tangent stiffness method does not produce spurious damping forces that are the major concern for the initial stiffness method.

Charney and Garcia (2017) conducted research on modeling inherent damping in nonlinear dynamic analysis. The research performed resulted in an assessment of four different modeling methods that are full initial stiffness, partial initial stiffness, full tangent stiffness, and partial tangent stiffness. They proposed two basic approaches that are full tangent stiffness, and partial initial stiffness in order to eliminate unrealistic damping forces that are observed when full initial stiffness is used. First approach, full tangent stiffness is deemed flawed due to the probability of negative tangent stiffness, as well as, it is conceptually flawed because of hysteresis loops that are developed in the damping force versus velocity relationships of the yielding elements. Second approach, Partial Initial Stiffness could produce unrealistic damping forces when changes in geometry are accounted for by using the corotational transformation, therefore, it is not recommended to use when the collapse analysis is performed. However, they recommended that partial initial stiffness is used, when it is used, the geometric stiffness should not be included as part of the damping matrix. Their conclusion was that a new approach is needed.

Carr and Puthanpurayil (2017) performed research on investigating damping models for inelastic time-history analyses. The research performed also mentions the same unintended consequences of the modeling damping by using Rayleigh damping and they proposed a new

approach that prevents the untoward effects by formulating Rayleigh damping at an elemental level. This approach is presented with two different damping models are: Elemental Rayleigh and Elemental Wilson-Penzien. It attempts to reflect the overall system nonlinearity in the damping matrix.

2.6.6. Inherent Damping Definition by FEMA

FEMA provides guidance and some warning regarding the assignment of a damping ratio(s). However, they leave the selection largely to the analyst in collaboration/approval of the peer-review panel.

> "For nonlinear dynamic analyses, equivalent viscous damping is typically assumed to be in the range of 2% to 5% of critical damping for the first few vibration modes that tend to dominate the response. Care should be taken to ensure that added viscous damping does not increase beyond acceptable levels as the model yields. The appropriate amount of damping, and strategies to incorporate it in the assessment, should be confirmed with the peer review panel." (*Quantification of Building Seismic Performance Factors*, 2009).

Given the large number of possible damping devices, materials, and deployment in different lateral systems with different geometries (archetypes), over prescription is likely of something as "simple" as damping seems unnecessary. However, as outlined in the previous literature damping is complex and likely may not be modeled properly with a simplistic ratio. In fact, even with the same ratio and different methods within analysis can lead to different and non-conservative results. This is a fundamental premise of the present work.

2.6.7. Inherent Damping Definition by ASCE 7

ASCE 7 outlines in Section 16.3.5 that outlines performance-based a maximum damping ratio that can be used for inelastic time-history analysis. Again, there are no details about how to use this ratio in modeling software.

> "Hysteretic energy dissipation of structural members shall be modeled directly. Additional inherent damping not associated with inelastic behavior of elements shall be modeled appropriate to the structure type and shall not exceed %2.5 equivalent viscous damping in the significant modes of response." (American Society of Civil Engineers., 2017).

2.6.8. Summary

This chapter introduces the basics of structural dynamics for SDOF and MDOF systems including damping and excitation due to ground accelerations associated with seismic events. The typical linear assumptions are not applicable for most seismic design that use a performance-based approach with nonlinear time-history analysis. Complexity associate with how to model damping in these cases is significant and the correct approach is unobvious. Moreover, procedures required in FEMA P-695 and ASCE 7 are nonspecific about how damping should be modeled. Numerous research reports are cited that outline these difficulties and the need for a better approach.

The state of the art at this time, combined with specifications, allow for different approach regarding damping to be used that can yield significantly different results with the same damping ratio, e.g., five percent. The presence work attempts to address this important issue.

CHAPTER 3:

METHODOLOGY

This chapter describes an overview of the Rayleigh modeling methods evaluated, analysis procedures used for SDOF and MDOF systems.

3.1. Description of Rayleigh Damping Modeling Methods

Extensive research has been conducted and several modeling methods have been developed for the damping matrix in the inelastic response. Because, in a non-linear time-history analysis software, the developing damping matrix is difficult due the consideration of computational-efficiency and nonlinearity. Therefore, often assumed is a linear viscous damping model that is frequency-dependent as described in Section 2.6.

Under large excitations, the stiffness of the structure, which designed by performance-based to resist seismic events, varies at each current state. Because, the select structural components that are allowed to undergo planned plastic deformation, the structural system exhibits varying different stiffnesses during a seismic event. Additionally, the frequencies of the structure at each time step may have to be calculated but this calculation is not recommended because of costly computation-time. Commercial software typically does not provide such an option.

The stiffnesses and frequencies are varied at each current state, however, it is not easy to compute them at each time step in order to find the mass and stiffness-proportional coefficients because this requires the solution of the general eigenvalue problem for each state. Therefore, several modeling methods for the Rayleigh concept have been recommended. The modeling methods that are recommended in literature are: initial stiffness, tangent stiffness, mass-proportional coefficient only, and elastic elements only (F. Charney et al., 2017). Herein, initial

stiffness and tangent stiffness are termed as approaches A and B, respectively. These approaches are expressed in Equation (2.21) and (2.25), respectively. Nevertheless, mass only and elastic elements only (with mass) are termed as approaches C and D, respectively and are addressed in Section 3.4. Because of approach that might be used, unintended forces, unrealistic responses, and non-physical behaviors may be observed.

These approaches described above have been tested by using the first and second frequency mostly. Because these frequencies are typically considered as the dominant. However, most building codes and performance-based standards do not prescribe the dominant frequencies clearly and specifically. Herein, the first few vibration modes that tend to dominate the response were considered as the dominant frequencies. Therefore, the combination of the Rayleigh modeling methods with different dominant frequencies was generated in order to evaluate the possible modeling methods that could be used and observe how the collapse margin ratio (CMR) is affected by selection of a particular method.

For MDOF systems, ten different modeling methods have been selected to expand the diversity of the results and to be inclusive of different effects. These methods demonstrate the importance of the selection on inherent damping procedures. However, it is not possible to generate ten different modeling methods for SDOF systems. Because they have only one natural frequency and one mode shape. Therefore, seven different modeling methods were generated for the SDOF as listed in Table 3.1. Later, the MDOF systems are addressed.

Table 3.1: The Rayleigh damping modeling methods for the SDOF system

Study	Approach	Stiffness Options	1st Frequency	2nd Frequency	Mass Coefficient	Stiffness Coefficient
1	A	Initial Stiffness	Elastic	Elastic	0.4236	0.0059
2	B	Tangent Stiffness	Elastic	Elastic	0.4236	0.0059
3	C	Mass Only	Elastic	Elastic	0.4236	-
4	A	Initial Stiffness	Post-Yield	Post-Yield	0.0791	0.0316
5	B	Tangent Stiffness	Post-Yield	Post-Yield	0.0791	0.0316
6	B	Tangent Stiffness	Elastic	Post-Yield	0.1333	0.0100
7	D	Elastic Elements	Elastic	Elastic	0.4236	0.0059

Four different approaches are possible for SDOF systems but they have only one natural frequency so the same natural frequency was used for some modeling methods and the post-yield frequency was also considered as a dominant frequency in order to expand the possible diversity of the results. The mass and stiffness coefficients were calculated by using the first and second natural frequencies that are listed above and five percent damping ratio is used throughout. Five percent is often used and is prescribed in FEMA P-695.

MDOF systems have several modes and natural frequencies, unlike SDOF systems. Thus, the first few dominant vibration modes, which are the first, second, and third, and the approaches described are combined thus ten different modeling methods were generated as listed in Table 3.2. Similarly, the mass and stiffness coefficients were calculated by using the first and second frequencies listed and five percent damping ratio for all modes, also, the coefficients determined are constant at each time step.

Table 3.2: The Rayleigh damping modeling methods for the MDOF systems

Study	Approach	Stiffness options	1st Frequency	2nd Frequency	Mass Coefficient	Stiffness Coefficient
1	A	Initial Stiffness	1st frequency	2nd frequency	0.4047	0.0047
2	B	Tangent Stiffness	1st frequency	2nd frequency	0.4047	0.0047
3	C	Mass Only	1st frequency	2nd frequency	0.4047	-
4	D	Elastic Elements	1st frequency	2nd frequency	0.4047	0.0047
5	A	Initial Stiffness	1st frequency	3rd frequency	0.4496	0.0032
6	B	Tangent Stiffness	1st frequency	3rd frequency	0.4496	0.0032
7	D	Elastic Elements	1st frequency	3rd frequency	0.4496	0.0032
8	A	Initial Stiffness	2nd frequency	3rd frequency	0.9797	0.0024
9	B	Tangent Stiffness	2nd frequency	3rd frequency	0.9797	0.0024
10	D	Elastic Elements	2nd frequency	3rd frequency	0.9797	0.0024

3.2. Modeling of Rayleigh Damping for Nonlinear Analysis using SAP2000™

SAP2000™ is a software package from Computer and Structures, Inc. for structural analysis and design. The software is a fully integrated system for modeling, analyzing, designing, and optimizing structures. The discussion here follows (SAP2000, 2017).

3.2.1. Damping Forms

In dynamic analysis, inherent damping might be specified as a material-based. Material-based damping is a property of the material so it is used for all load cases. Three different

options to model damping by the material-based are available in SAP2000™. These options are illustrated in Figure 3.1.

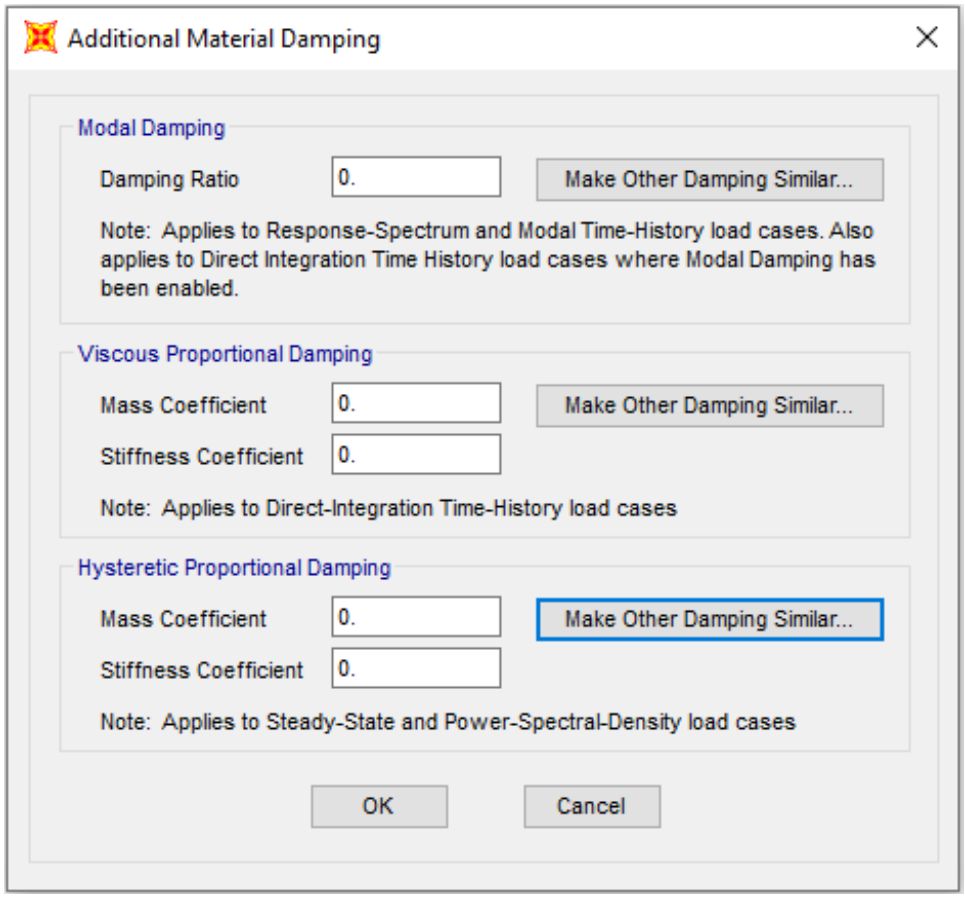

Figure 3.1: Additional material damping form (SAP2000, 2017)

The modal damping option is stiffness weighted and it is used for only the response-spectrum and the modal time-history analysis, not in the nonlinear analysis. For the viscous-proportional and hysteretic-proportional damping options, only the initial stiffness option exists for the nonlinear elements. Thus, the additional material damping form does not provide control on stiffness options. Besides, the material-based damping does not have effect on link elements. Herein, inelastic elements were defined as link elements.

Another way to model the damping is the load case-based damping form is illustrated in Figure 3.2. The damping is modeled as a full damping matrix in this form so as to allow decoupling between the modes, unlike the modal damping. This might be used for the direct-integration time-history analysis.

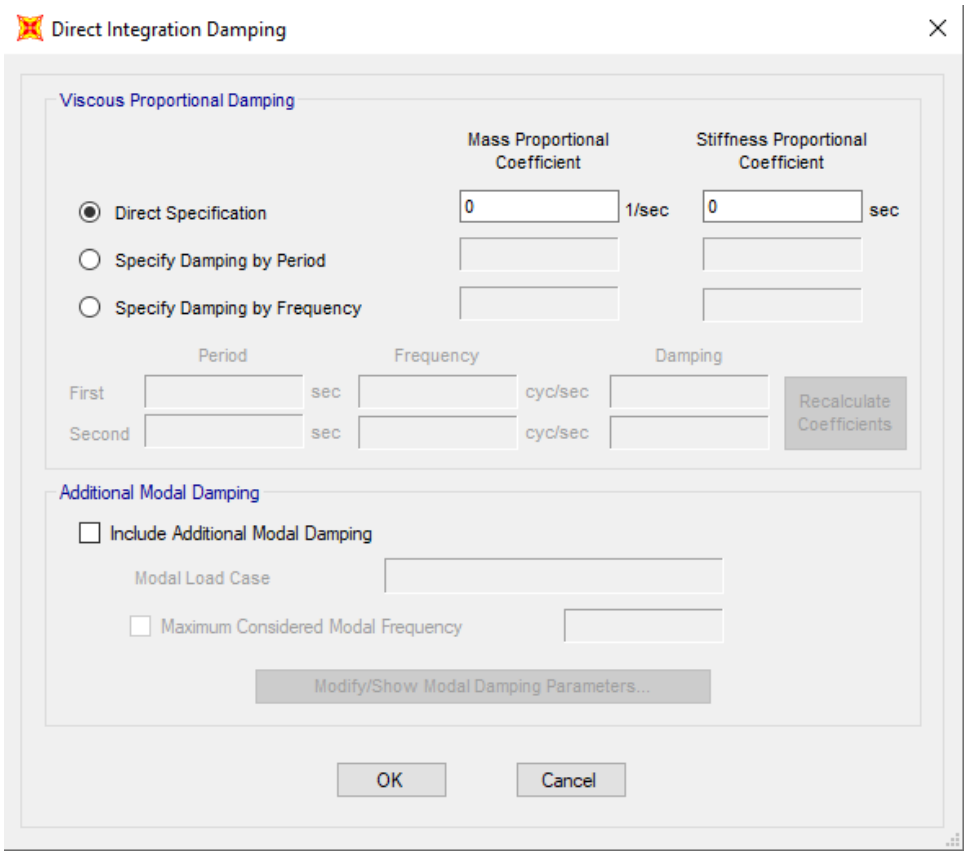

Figure 3.2: Dynamic load case damping form (SAP2000, 2017)

In the viscous-proportional damping form, the damping matrix is developed by scaling the stiffness matrix and the mass matrix by the coefficients as expressed in Equation (2.21). The coefficients are defined in three different ways. They might be specified directly by using the direct specification option. Alternatively, they might be computed by using the specify damping by periods or frequencies options after critical modal damping ratios at any two frequencies, or periods are specified.

3.2.2. Link/Support Property Data Form

Different Rayleigh modeling methods described in section 3.1 provides the possible diversity with respect to stiffness options and natural frequencies. Although Equation (2.12) is described for the damping matrix with respect to varying stiffness and frequency, SAP2000™ does not provide the equation. However, it provides a way to define the varying stiffness at the current state described in Equation (2.25) by using link/support property data as illustrated in Figure 3.3.

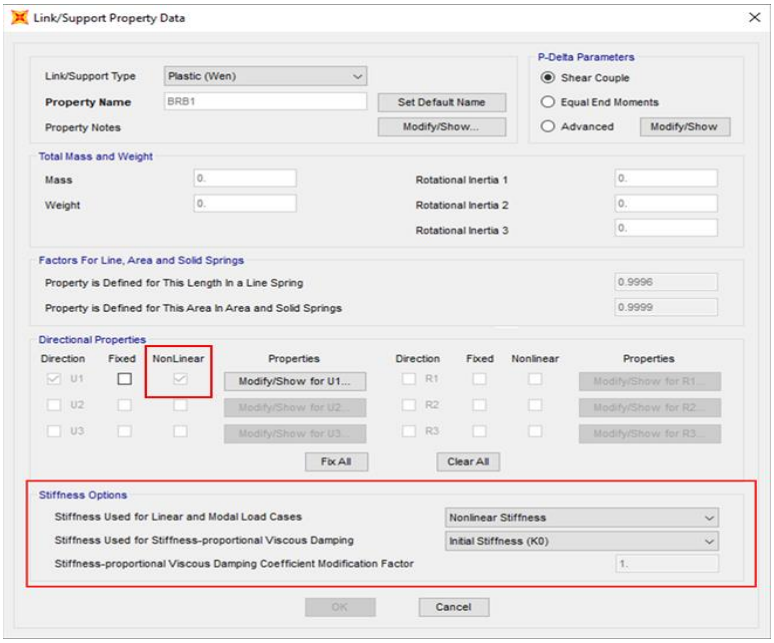

Figure 3.3: Stiffness options for analysis (SAP2000, 2017)

For the non-linear analysis, the link/support property data option provides two different ways are; “Stiffness Used for Stiffness-proportional Viscous Damping” and “Stiffness-proportional Viscous Damping Coefficient Modification Factor”. Initial stiffness, tangent stiffness, and only elastic elements approaches are defined by using these ways and the other approach is provided by eliminating the stiffness-proportional coefficient in the load case form

that is illustrated in Figure 3.2. Thus, all approaches described are defined in SAP2000^{TM}. The details of the stiffness options and the coefficients used are provided in Figure A.5.

3.3. Modeling of the SDOF System

Here, the modeling of the SDOF system selected to evaluate the influence of the Rayleigh modeling methods on damping force, inherent energy dissipation, displacement results, and damping-velocity relation is described. The SDOF system has two different spring elements are: brace (elastic) and fuse (inelastic) elements shown in Figure A.2 and Figure 3.4, respectively. Here, the spring elements represent a BRB element. As might be observed from Figure 2.10, a BRB element consists of several elements e.g. a gusset plate that connects to larger section that tapers to the core (yielding) section. The confining tube provides buckling restraint; however, to not significant participate directly in the BRB stiffness. Therefore, herein the part designed to exhibit planned deformation is referred to as inelastic element, or fuse and other parts are referred to as elastic element or brace element. Thus, the SDOF system has two static DOFs and single dynamic DOF because of terms that are associated with degrees of freedom that are assigned mass or stiffness.

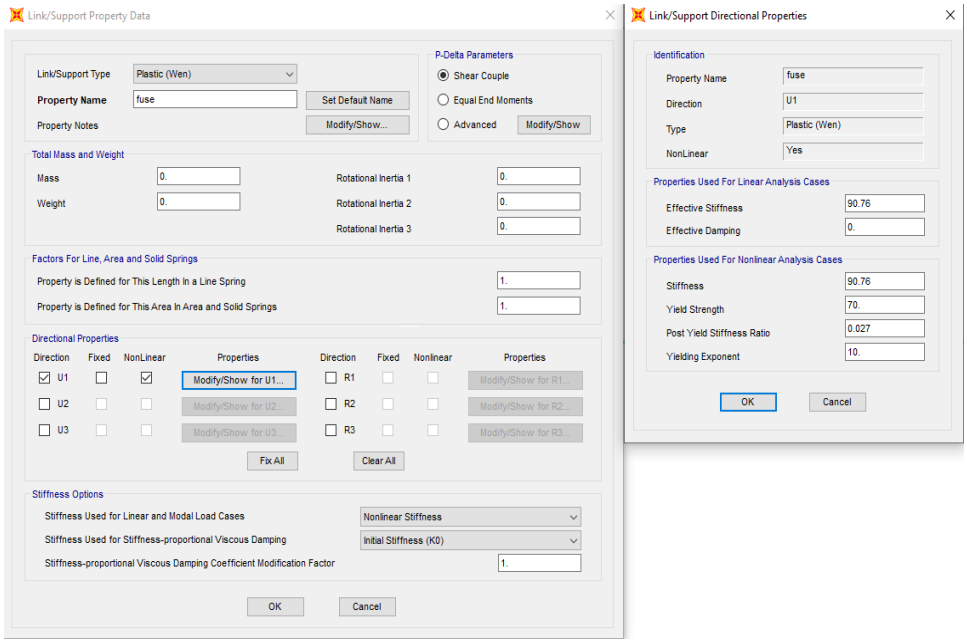

Figure 3.4: Modeling of fuse element (SAP2000, 2017)

The Plastic (Wen) link element was selected in order to model the inelastic behavior of the fuse element. The link element provides users to control the sharpness of the yielding transition and the simplified backbone curve described in Section 2.3.1 by using two different slopes are; initial and post-yield stiffness. The Wen model and the solution methodology is based upon a kinematic strain hardening model as shown in Figure 3.5. The Primary parameters are in the initial stiffness *k*, post-yield stiffness ratio, and exp a coefficient that determine the sharpness between the initial- and post-yield slope (SAP2000, 2017).

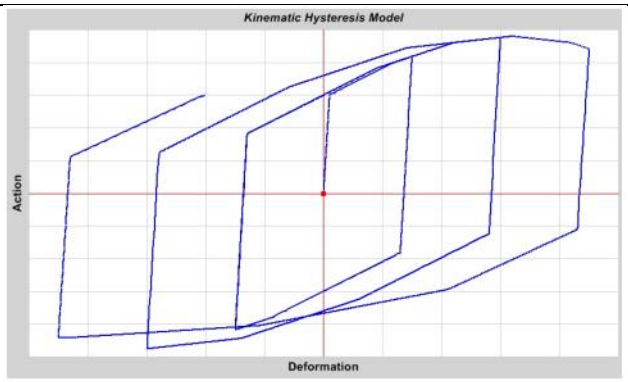

a. The kinematic hysteresis model under increasing cyclic load

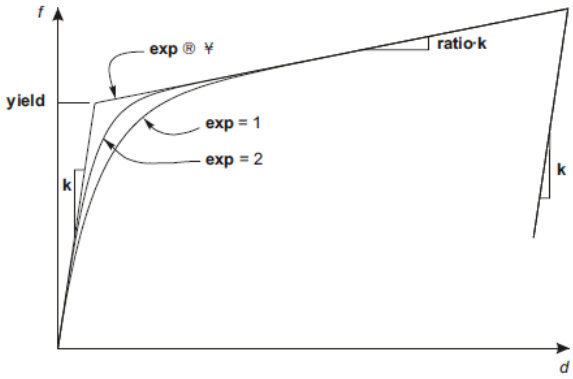

b. Plastic Wen model

Figure 3.5: The Wen and kinematic hysteresis model (SAP2000, 2017)

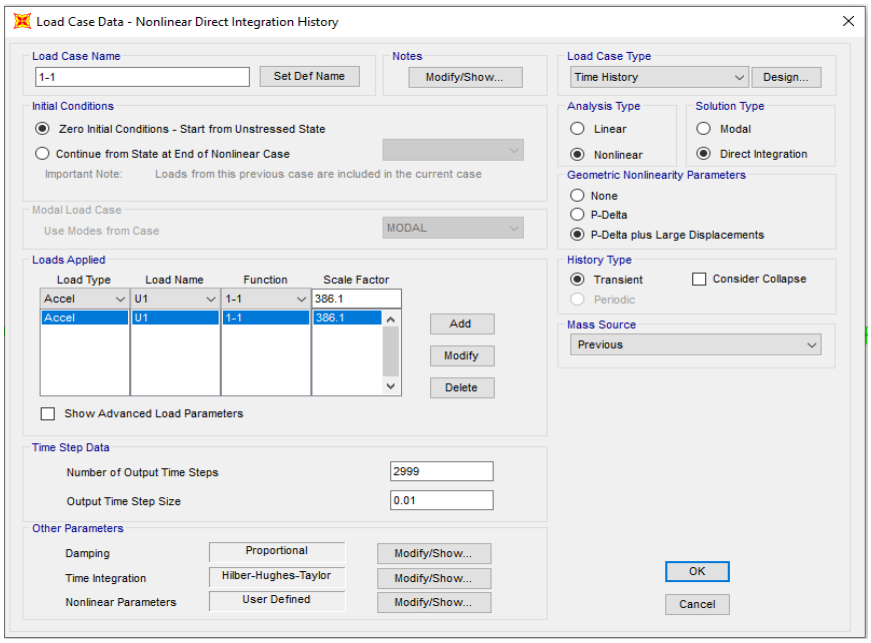

Figure 3.6: Modeling time-history ID:1-1 load case (SAP2000, 2017)

The SDOF system was modeled considering both the geometric and material nonlinearity. The material nonlinearity was included using the nonlinear option that is indicated inside the red rectangular box in Figure 3.3 and the geometric nonlinearity was considered in the load case definition by including “P-delta plus Large Displacements” shown in Figure 3.6. The time-history function and its properties are illustrated in Section 3.7. And, the SDOF system is illustrated in Figure 3.7.

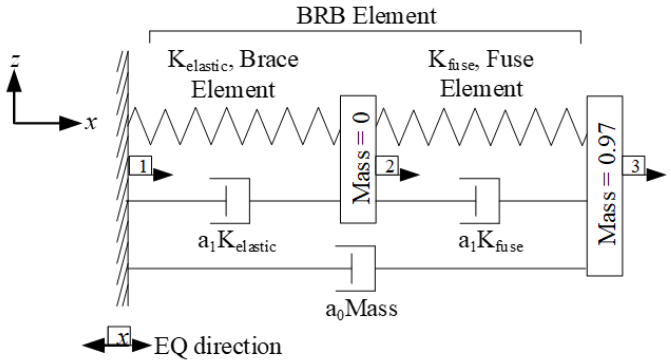

Figure 3.7: The SDOF system

The SAP2000™ model that involves the system properties, restraints and the mass is demonstrated in Figure A.1 and the modeling methods listed in Table 3.1 are illustrated in Figure A.5.

3.3.1. Modeling of Rayleigh Damping Methods

The SDOF system described in Section 3.3 has two static DOFs and single dynamic DOF with respect to terms that are associated with degrees of freedom that are assigned mass and stiffness. The Rayleigh concept described in Section 3.4 is a Static DOF Damping so the damping matrix is developed by using each node that has stiffness assigned (physically realistic). However, it requires two frequencies in order to determine the mass and stiffness-proportional parts of the damping matrix. However, the system has only one natural frequency so the same natural frequency was used for both the first and second frequencies. In Figure 3.8, the first method listed in Table 3.1 was modeled in SAP2000™.

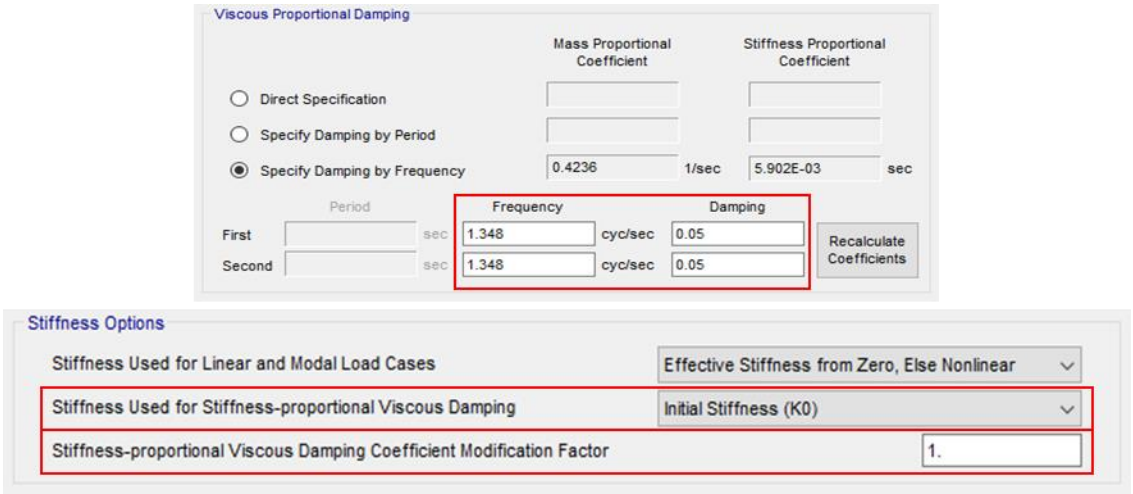

Figure 3.8: The natural frequencies and stiffness options for the first method

Here, the stiffness options described in Section 3.2.2 are illustrated for the inelastic element (fuse or core in a BRB). However, the stiffness-proportional viscous damping coefficient modification

factor was set to one for both fuse and brace elements in order to add stiffness contributions. The same natural frequency and the damping ratio were used so as to determine the coefficients using the option; “Specify damping by frequency”. In addition, the post-yield frequency was used as the second dominant frequency for some of modeling methods listed in Table 3.1. Therefore, each method that is determined to expand the potential diversity of the assessment was modeled using different properties, and the stiffness options and the damping coefficients defined for each study are illustrated in Appendix A.1, in Figure A.5.

3.4. Static DOF Damping

The damping matrix might be developed using two different approaches with respect to terms that are associated with degrees of freedom. The approaches are called as Dynamic DOF Damping, which involves the terms only associated with those degrees of freedom that are assigned mass, and Static DOF Damping, which involves the terms associated with all degrees of freedom that are assigned stiffness (Charney et al., 2017).

The modal damping and Rayleigh damping described in Section 2.6.5 are the most common two concepts in order to model inherent damping in the inelastic response. The modal damping is specified as Dynamic DOF damping and the Rayleigh damping is referred to as Static DOF damping. Here, the Rayleigh concept was checked in order to observe that it is the Static DOF damping. Therefore, the SDOF system shown in Figure 3.7 is idealized as shown in Figure 3.9.

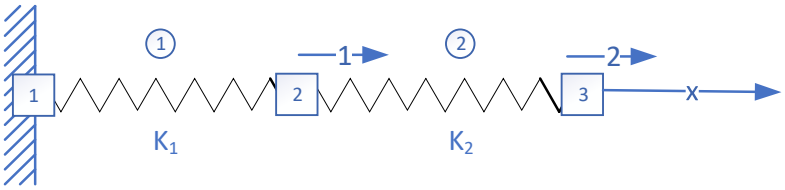

Figure 3.9: The simplified-SDOF system

Here, each node, the structural elements, and the displacements are represented with numbers inside the rectangular boxes, numbers inside the circles, and numbers in the arrows, respectively. And, K_1 and K_2 represent the stiffness of the structural elements. Additionally, the system motion was restrained in x-direction. With all in mind, the stiffness matrix of the structural elements is determined by

$$\text{For Element 1: } \begin{Bmatrix} f_{1x} \\ f_{2x} \end{Bmatrix} = \begin{bmatrix} K_1 & -K_1 \\ -K_1 & K_1 \end{bmatrix} \begin{Bmatrix} u_1 \\ u_2 \end{Bmatrix}$$
$$\text{For Element 2: } \begin{Bmatrix} f_{2x} \\ f_{3x} \end{Bmatrix} = \begin{bmatrix} K_2 & -K_2 \\ -K_2 & K_2 \end{bmatrix} \begin{Bmatrix} u_2 \\ u_3 \end{Bmatrix} \tag{3.1}$$

However, the first node is restrained in the x-direction so, it was neglected from the equation and when two matrices are added

$$\begin{Bmatrix} F_{2x} \\ F_{3x} \end{Bmatrix} = \begin{bmatrix} K_1 + K_2 & -K_2 \\ -K_2 & K_2 \end{bmatrix} \begin{Bmatrix} u_2 \\ u_3 \end{Bmatrix} \tag{3.2}$$

The system stiffness matrix was obtained. Thus, the Rayleigh damping or the Static DOF damping is expressed by

$$C_{Rayleigh} = a_0 \begin{bmatrix} 0 & 0 \\ 0 & M_3 \end{bmatrix} + a_1 \begin{bmatrix} K_1 + K_2 & -K_2 \\ -K_2 & K_2 \end{bmatrix} \tag{3.3}$$

Here, the stiffness-proportional part represents the damping contribution, which obtained from each structural element and connection, and it is physically realistic because this is deemed as one of the inherent damping sources. Unlike the stiffness part, the mass-proportional part is identified as a virtual dashpot, which is located between the degree of freedom and virtual external support, so it is not physically realistic but a mathematical nicety.

The SDOF system was performed four times by using different factors that are called stiffness-proportional viscous damping coefficient modification factor shown in Figure 3.10. The maximum displacements that obtained for each analysis were recorded in order to compare the results, by comparison, it was aimed to observe how the individual structural elements affect the damping contribution.

Figure 3.10: Stiffness-proportional coefficient modification factor

Firstly, it was analyzed without damping property which means the critical damping ratio defined as zero. And, this analysis was specified as the reference analysis. Next, five percent critical damping ratio was assigned to the system, however, the stiffness contribution was eliminated by defining the factor as zero (Approach C). As shown in Figure 3.11, the first and second analysis results are obtained differently due to the contribution provided by the mass-proportional part of the damping matrix.

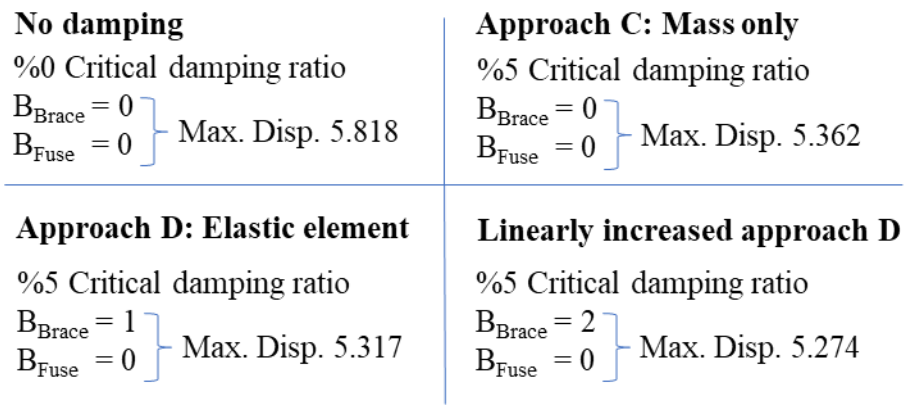

Figure 3.11: The maximum displacement results for each analysis

B_{Brace} and B_{Fuse} represent the coefficient modification factors for the brace element (elastic element), which is referred to as K_1 in Equation (3.3), and the inelastic element, which is referred to as K_2 in Equation (3.3), respectively. As shown in Figure 3.11, the results of third and fourth analyses indicates that the Rayleigh concept is a Static DOF Damping. Because, the stiffness-proportional part was defined only for the elastic element (Approach C) and the decrease in the displacement was obtained. This indicates that the Rayleigh concept includes the contributions for each node in the system.

3.5. Comparison of SAP2000™ and NONLIN Models

NONLIN is a software that designed for structural dynamics and earthquake engineering subjects, however, it is specifically designed as a teaching tool for graduate classes and it is useful because of highly interactive, graphically intensive, and user friendly (Charney & Barngrover, 2012). Here, the SDOF system described in Section 3.3 was modeled in both SAP2000™ and NONLIN and the results were compared.

In NONLIN, it is not allowed to define two static degrees of freedom for an SDOF, which means, the stiffness matrix expressed in Equation (3.2) is not useful. As a remedy, the effective stiffness was calculated by

$$K_{effective} = \left[\frac{K_1}{K_1 K_2} + \frac{K_2}{K_2 K_1} \right]^{-1} \tag{3.4}$$

Here, K_1 and K_2 represent the stiffness respectively for the brace and fuse elements. Additionally, the geometric nonlinearity was not included in both, however, the geometric nonlinearity was included for the rest of the work herein. The other properties described in Section 3.3 were defined as the same for both. Besides, the same ground motion record was imported in NONLIN. The NONLIN model is demonstrated in Figure 3.12.

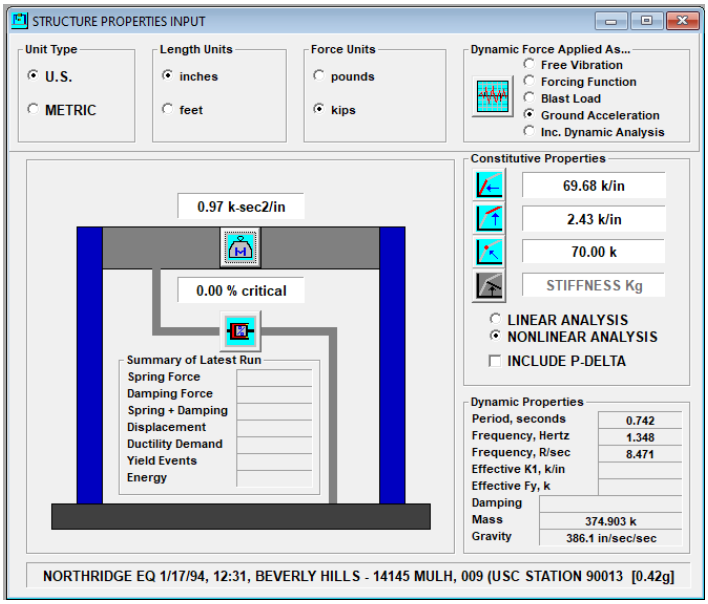

Figure 3.12: NONLIN model for the SDOF system

Here, it is observed that the dynamic properties were obtained as the same for both models. Next, when the analyses were completed, the forces that generated in the springs and the displacements that obtained at each node were plotted in order to compare the dynamic response of each system. In Figure 3.13, the hysteresis loops that obtained from each model are shown.

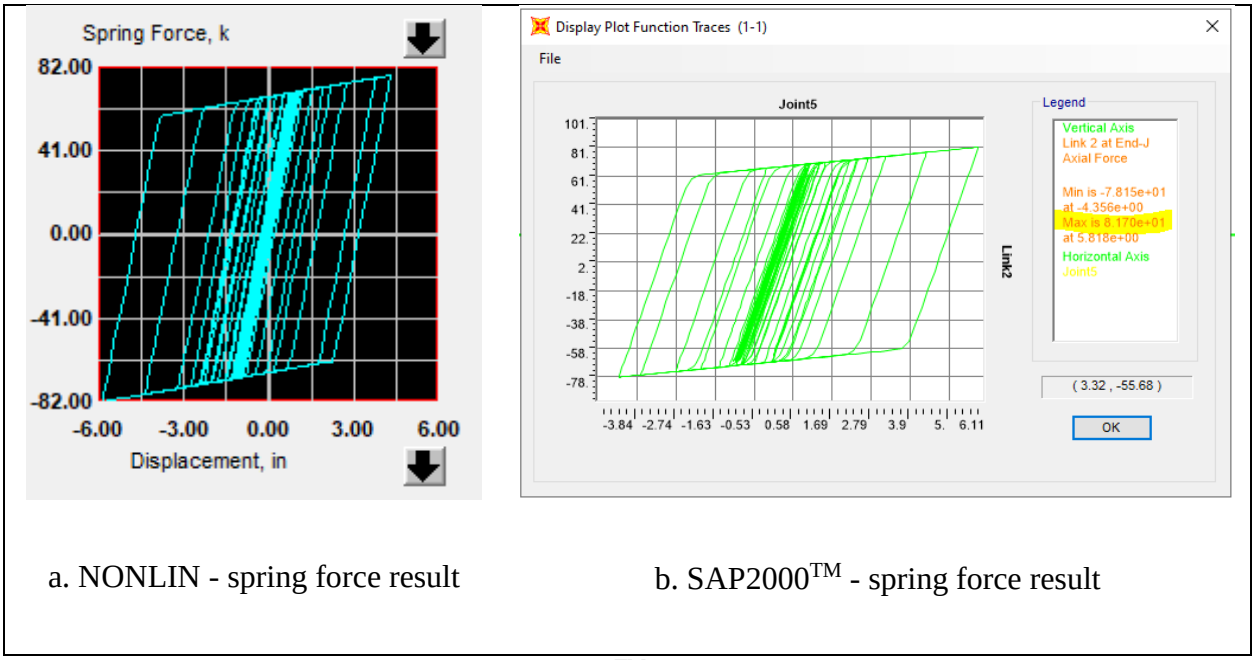

a. NONLIN - spring force result

b. SAP2000^{TM} - spring force result

Figure 3.13: Comparison of SAP2000^{TM} and NONLIN based on spring forces

The small negligble difference are likely due the integration methods for the time-history analysis. Other results compared are illustrated in Appendix A.1, in Figure A.3, and Figure A.4.

The results that described above were obtained based on the dynamic response of the SDOF without damping property, however, the present work was conducted in order to evaluate the modeling methods for inherent damping. Therefore, the five percent critical damping ratio was assigned to the models and the models were analyzed again. Similarly, the results were obtained but the difference was slightly increased because NONLIN uses the dynamic DOF damping to develop a damping matrix, unlike the Rayleigh concept used in SAP2000^{TM}.

3.6. SAP2000^{TM} - Application Programming Interface (API)

The CSI Application Programming Interface (API) is provided by SAP2000^{TM} to users in order to allow them to automate many of the processes performed, and to customize the analysis and design results. The API is a powerful tool due to providing a way to export or import data

with other programs (Computers and structures INC., 2020). Herein, the MATLAB programming language was used to access SAP2000^{TM} through the API.

The energy analysis, the assessment of the collapse risk, and evaluating the different modeling methods require that numerous nonlinear analyses are performed because the system or several systems might be set repeatedly with small changes in order to evaluate the foregoing and the results obtained must be recorded. The advantages described by automation by using the API thus are:

1. Recording data, plotting data, and setting the models were automatically performed by the MATLAB algorithms,

2. Considerable time was saved,

3. An advantage was obtained graphically by using the MATLAB graphics power, and

4. The analysis and design results were customized using the API and the plots demanded for the assessment were provided.

Herein, the code that consists of the MATLAB algorithms was not shared completely because of numerous rows involved; however, the required parts were demonstrated in the sections. For the further background of the API process, see CSI API document, (Computers and structures INC., 2020).

3.7. Fast Fourier Transform (FFT) for the Forty-four Time-History Records

The forty-four individual ground-motion records that required by FEMA P-695 were downloaded and deployed with a tool that is provided by the web-based Pacific Earthquake Engineering Research Center ground-motion database (*PEER Ground Motion Database*). The

records are in time-domain, gravity *(g)* unit, and not scaled with normalization factors described in Section 2.5.2. The records in time-domain are more suitable for design purposes as described in Section 2.1.3; however, the records were transformed into frequency-domain to observe the frequencies with the most energy. The Fast Fourier Transform (FFT) method was used to obtain the records in frequency-domain.

A combination of SAP2000™ and MATLAB was used in order to transform the records that in time-domain. Because the records in time-domain were already imported into SAP2000™, therefore, the time and acceleration values for each record were available in MATLAB, as shown in Figure 3.14.

```
%% function plots
timevalues=zeros(20000,44);
values=zeros(20000,44);
MyTimee=zeros(20000,44);
Valuee=zeros(20000,44);
for j=1:44
Func = NET.explicitCast(SapModel.Func,'SAP2000v1.cFunction');
FuncTH = NET.explicitCast(Func.FuncTH,'SAP2000v1.cFunctionTH');

 NumberItems = 0;
 MyTime = NET.createArray('System.Double',2);
 Value = NET.createArray('System.Double',2);


[ret, NumberItems, MyTimee, Valuee] = Func.GetValues(EQ(j), NumberItems, MyTime, Value);
stepnumber=Estep(ceil(j/2));
for i=1:stepnumber
    timevalues(i,j) = MyTimee(i);
    values(i,j) = Valuee(i);
end
```

Figure 3.14: The cutaway of getting values from SAP2000™ to MATLAB

After the values were imported into MATLAB, the acceleration data in the time-domain, the number of samples, sampling interval, sampling frequency, and Nyquist frequency were determined in order to perform frequency analysis. Next, these parameters were normalized by using the "FTT" function of MATLAB to obtain the Fourier Transform of data and the FTT of each ground-motion record are illustrated in Appendix A.2. However, the ground-motion

records, which are mostly used in the present work, are illustrated separately in time-domain and frequency-domain in Figure 3.15, Figure 3.16, and Figure 3.17.

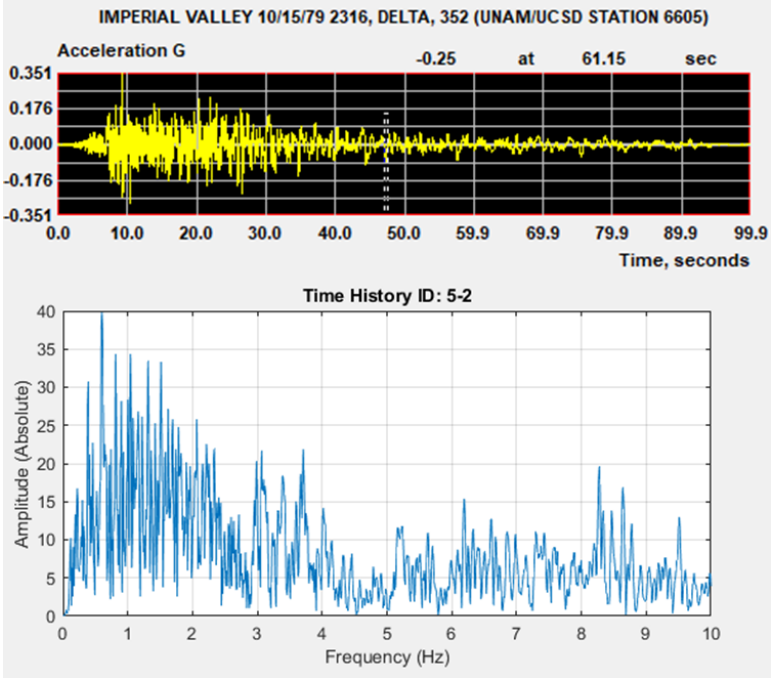

Figure 3.15: Acceleration and FFT plots for time-history ID: 5-2

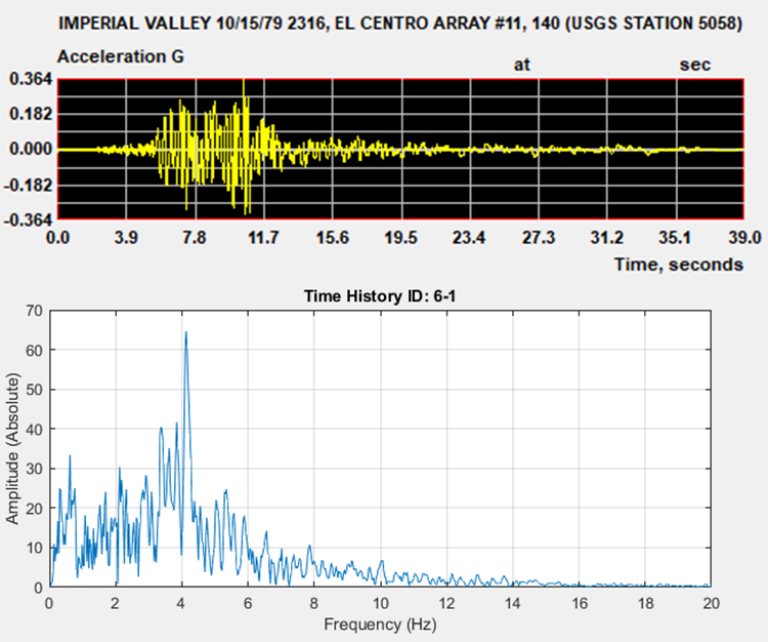

Figure 3.16: Acceleration and FFT plots for time-history ID: 6-1

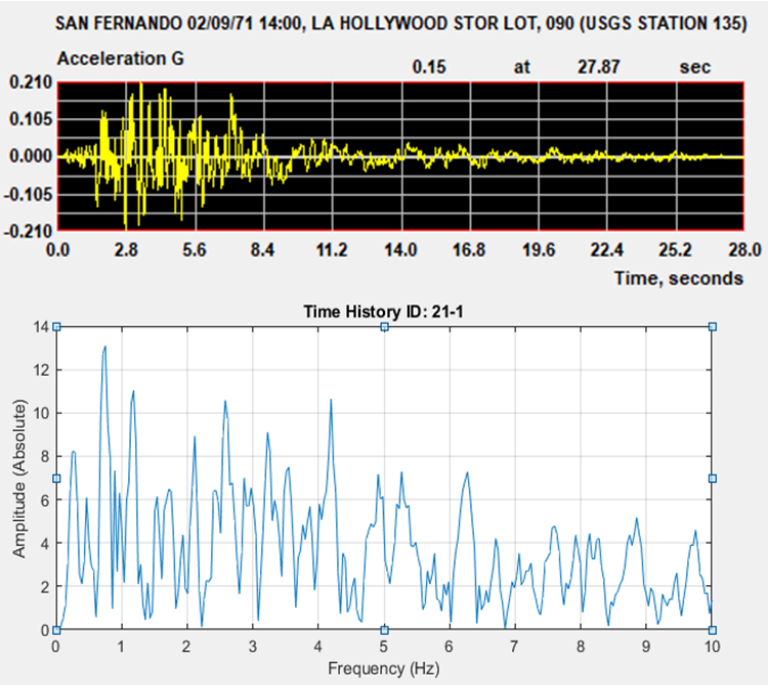

Figure 3.17: Acceleration and FFT plots for time-history ID: 21-1

3.8. Energy Dissipations

The idea of the ductile design concept described in Section 2.2 is absorbing the seismic energy imparted through planned plastic deformation in the select structural components, also called the internal energy principle. The plastic deformation is planned and it results in cumulative energy absorption described as the hysteresis energy dissipation on the inelastic system in Section 2.3. Thus, the input energy is dissipated by converting it to hysteresis energy and inherent damping energy. Here, the energy terms are defined by integrating the equation of motion of the inelastic systems, described in Section 2.1.1. For the further background of dissipated energy, see the structural dynamics textbook, (Chopra, 2012).

Equation (2.4) is integrated as follows

$$\int_0^u m\ddot{u}(t)\partial u + \int_0^u c\dot{u}(t)\partial u + \int_0^u f_s(u)\partial u = -\int_0^u m\ddot{u}_g(t)\partial u \tag{3.5}$$

the seismic energy imparted or the input energy is the term on the right side of the equation

$$E_I(t) = -\int_0^u m\ddot{u}_g(t)\partial u \tag{3.6}$$

The other term, which is associated with mass and located on the left side of Equation (3.5), is the kinetic energy thus the kinetic energy

$$E_K(t) = \int_0^u m\ddot{u}(t)\partial u = \int_0^{\dot{u}} m\dot{u}(t)\partial\dot{u} = \frac{m\dot{u}^2}{2} \tag{3.7}$$

The second term, which is associated with damping and located on the left side of Equation (3.5), is the inherent damping energy described in Section 2.6 thus the inherent damping energy is

$$E_D(t) = \int_0^u f_D(t)\partial u = \int_0^u c\dot{u}(t)\partial u \tag{3.8}$$

the third term, which is associated with stiffness and located on the left side of Equation (3.5), is the hysteresis energy described in Section 2.3 and the elastic energy should be subtracted because it is recoverable, thus, the hysteresis energy

$$E_H(t) = E_Y(t) - E_E(t) = \int_0^u f_s(u)\partial u - \frac{\left[f_s(t)\right]^2}{2k} \tag{3.9}$$

however, the hysteresis and inherent energy dissipation equations could be expressed by rewriting the integrals with respect to time

$$\begin{aligned} E_D(t) &= \int_0^t c\left[\dot{u}(t)\right]^2 \partial t \\ E_Y(t) &= \int_0^t \dot{u} f_s(u)\partial t \end{aligned} \tag{3.10}$$

the foregoing energy analysis is used for a system and typical results are illustrated in Figure 3.18.

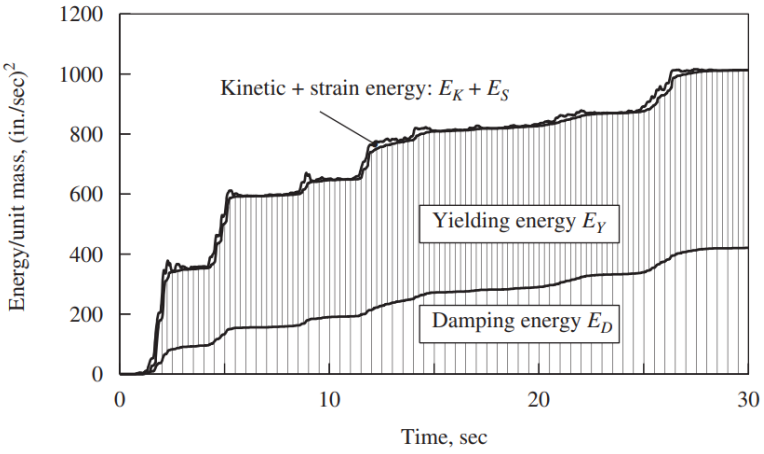

Figure 3.18: Time variation of energy dissipations (Chopra, 2012)

A combination of SAP2000™ and MATLAB was used in order to determine the input, hysteresis, and damping energy that obtained in the dynamic response of the SDOF system that subjected to the ground motion records. When the system analysis is completed, results of the joints and structural elements for each record were exported from SAP2000™ to MATLAB by using the API, in which the exporting process is illustrated in Appendix A.3 in Figure A.10 and Figure A.11. Thus, the parameters that used in the energy analysis were provided so the input, hysteresis, and inherent damping energy were determined using the functions that defined in MATLAB, shown in Figure 3.19.

```
%Kinetic energy

Ek=(Mass/2)*ResultVl(2:stepnumber+1,1).^2;
figure
plot(time,Ek)
xlabel('Time (s)')
ylabel('Kinetic Energy (Kips-in/s)')
title('Kinetic Energy vs Time')
```

```
%Elastic Energy

Es=(1/(2*initialstiffness))*(LinkForce(2:stepnumber+1,1).^2);
figure
plot(time,Es)
xlabel('Time (s)')
ylabel('Elastic Energy (Kips-in/s)')
title('Elastic Energy vs Time')
```

```
%Input energy

for i=2:stepnumber
    j=0.01*i;
    ingI(i)=trapz([0.01:0.01:j],-g*Mass.*values(1:i,1).*ResultVl(1:i,1));
end

figure
plot(time,ingI-Ek')
xlabel('Time (s)')
ylabel('Input Energy (Kips-in/s)')
title('Input Energy vs Time')
```

```
%Hysteresis energy

for i=2:stepnumber
    j=0.01*i;
    ingH(i)=trapz([0.01:0.01:j],LinkForce(1:i,2).*ResultVl(1:i,1));
end
figure
plot(time,ingH-Es')
xlabel('Time (s)')
ylabel('Energy Dissipation (Kips-in/s)')
title('Hysteresis Energy vs Time')
```

```
%Damping energy

for i=2:stepnumber
    j=0.01*i;
    ingD(i)=trapz([0.01:0.01:j],MassC*(ResultVl(1:i,1).^2)-Dampingforce3(1:i).*ResultVl(1:i,3));
end
plot(time,ingD)
xlabel('Time (s)')
ylabel('Energy Dissipation (Kips-in/s)')
title('Inherent Damping Energy vs Time')
```

Figure 3.19: The energy analysis for the SDOF system

Here, the energy analysis for the SDOF system is described and the same process was repeated for the MDOF systems. However, for MDOF systems, the energy terms are determined by integrating the equation of motion expressed in Equation (2.5).

3.9. Incremental Dynamic Analysis (IDA)

The assessment of the collapse risk that described by FEMA is performed using Incremental Dynamic Analysis (IDA) described in Section 2.5.3. However, the IDA progress involves numerous dynamic analyses, which are required to be performed for a single system. Because the forty-four ground-motion records described in Section 2.5.2 are scaled several times and the system that subjected to each scaled record is analyzed separately for each scale factor. Here, the IDA progress for the MDOF systems is described and it must be noted that the progress was automated using the API described in Section 3.6.

Firstly, the forty-four individual ground-motion records, which are required to be performed (by FEMA P-695), were downloaded from a tool that is provided by the web-based

Pacific Earthquake Engineering Research Center ground motion database (*PEER Ground Motion Database*). Next, the records were imported into MATLAB. However, the records are in time-domain, gravity *(g)* unit, and not normalized so they were not scaled with the normalization factors described in Section 2.5.2. In Figure 3.20, the progress, in which the records are scaled with the gravity unit, the normalization factors, and the scale factors, is illustrated.

```
scalee=[1.7:0.1:1.9];

for jj=1:3

LoadCases = NET.explicitCast(SapModel.LoadCases,'SAP2000v1.cLoadCases');
DirHistNonLinear = NET.explicitCast(LoadCases.DirHistNonlinear,'SAP2000v1.cCaseDirectHistoryNonlinear');
DirHistNonlinear = NET.explicitCast(LoadCases.DirHistNonlinear,'SAP2000v1.cCaseDirectHistoryNonlinear');
      LoadType=NET.createArray('System.String',6);
      LoadName=NET.createArray('System.String',6);
      Func=NET.createArray('System.String',6);
      CSys=NET.createArray('System.String',6);

      for i=1:44
          ii=ceil(i/2);
      ret = DirHistNonlinear.SetCase(EQ(i));
      ret = DirHistNonlinear.SetDampProportional(EQ(i), 1, 0, 0,0,0,0,0);
      ret = DirHistNonlinear.SetGeometricNonlinearity(EQ(i), 2);
      LoadType(1) = 'Accel';
      LoadName(1) = 'U1';
      Func(1) = EQ(i);
      g=386.09;
      SF(1) = g*NormalizationFactor(ii)*scalee(jj);
      TF(1) = 1;
      AT(1) = 0;
      CSys(1) = 'Global';
      Ang(1) = 0;
      ret = DirHistNonlinear.SetLoads(EQ(i), 1, LoadType, LoadName, Func, SF, TF, AT, CSys, Ang);
      ret = DirHistNonlinear.SetTimeStep(EQ(i), Estep(ii), Etime(ii));
      ret = DirHistNonlinear.SetDampProportional(EQ(i), 1, 0.2051, 0, 0, 0, 0, 0);
      end
```

Figure 3.20: The scaling progress for the ground-motion records

Here, the progress, which is defining the dynamic nonlinear loading case that described as nonlinear direct-time integration time history case by SAP2000^{TM}, is shown and the scale factor term is referred to as “SF” that provides the scaling of the ground-motion records. The scale factor term consists of three multiplications that are the gravity unit, the normalization factor, and the scale factor, respectively. The gravity unit is constant and the normalization factors are defined by FEMA P-695 (see Figure 2.15), however, the scale factors are user-defined in order to obtain the collapse point of the system. Therefore, a trial-error approach is needed for defining the scale factors and when a scaling range was defined, the progress was automatically performed by the MATLAB code employing the API.

The system that subjected to scaled records was analyzed separately for each scale factor and the maximum displacements were recorded in order to compare with the story-drift limitation described in Section 2.4.1. The systems were deemed collapsed when the maximum displacement recorded was obtained higher than the displacement that is defined with respect to the limitation. Thus, the progress was repeated until the scale factor, which causes that one-half of the ground motion records resulted in the collapse, was obtained.

The other terms illustrated in Figure 3.20 supply defining the ground motion properties, the ground motion direction, the geometric nonlinearity, and the damping property. The short portion of the code is illustrated here but the code involves opening the software, modeling the system, importing all ground motion records, all information to analyze the system, and exporting results from SAP2000^{TM} to MATLAB. However, the code was not presented completely because it consists of numerous rows.

3.10. Modeling of MDOF systems

Here, the modeling of the MDOF systems, which were selected to evaluate the influence of the Rayleigh modeling methods, is described. The MDOF systems were selected from the report that involves the evaluation of the FEMA P-695 methodology, (Kircher et al., 2010).

3.10.1. Evaluation of the FEMA P-695 Methodology

Evaluation of the FEMA P-695 Methodology for Quantification of Building Seismic Performance Factors presents several systems that designed based on FEMA P-695 Methodology and it summarizes findings and conclusions of the systems presented. Additionally, recommendations for improvement and further study are provided in the report (Kircher et al., 2010).

3.10.2. Archetype Selections, Configurations and Design

It is not possible to evaluate all configurations for a proposed system due to numerous configurations exist for structures, therefore, the FEMA P-695 framework requires several configurations, which are deemed sufficient enough to involve the potential diversity of the structure types, in order to evaluate a proposed system. Nevertheless, the proposed system that designed based on each configuration is represented as an archetype and independent peer review panel of the archetypes are required by FEMA P-695.

Although a proposed system and the archetype configurations are required to be performed for the assessment of the collapse risk, herein, an innovative seismic resisting system was not proposed so the archetype configurations were not designed. Therefore, two MDOF systems (archetypes), which were approved by the peer panel of FEMA P-695, were selected from the report shown in Figure 3.21 and the fundamental periods for the systems selected are demonstrated in the same figure.

The fundamental period of a building is determined based on a function of the lateral resisting system type, the building height, and the seismic design category and it is described in ASCE 7 - 16 (American Society of Civil Engineers., 2017).

Table 7-1 Building Height and Period for Buckling-Restrained Brace Frame Archetypes

Building Height		Building Period (sec.)			
Stories	h_n (ft.)	D_{max}	D_{min}/C_{max}	C_{min}/B_{max}	B_{min}
1	13	0.29	0.31	0.33	0.35
2	26	0.48	0.52	0.56	0.59
3	39	0.66	0.70	0.76	0.80
4	52	0.81	0.87	0.95	0.99
6	78	1.10	1.18	1.28	1.34
9	117	1.49	1.60	1.74	1.81
12	156	1.85	1.99	2.16	2.25
18	234	2.51	2.69	2.93	3.05

Figure 3.21: Archetypes for Buckling-Restrained Brace Frames (Kircher et al., 2010)

After the fundamental period of a building is calculated, S_{MT} value described in Section 2.5.3 is the spectral acceleration at the fundamental period and it is determined by using the median value and the scale factor for anchoring that demonstrated in Figure 2.18. The spectral accelerations, which are obtained according to fundamental periods of each archetype selected are demonstrated Figure 3.22.

Table 7-6 Buckling-Restrained Braced Frame Archetype Design Properties for Phase II Performance Evaluation

Archetype ID Number	No. of Stories	Key Archetype Design Parameters						
		Analysis Procedure	Seismic Design Criteria					$S_{MT}(T)$ (g)
			SDC	R	T (sec)	T_1 (sec)	V/W (g)	
Performance Group PG-10, SDC D_{max}, Long-Period								
4S-LB-15BDmax	4	RSA	D_{max}	8	0.81	1.15	0.078	1.11
6S-LB-15B-Dmax	6	RSA	D_{max}	8	1.10	1.68	0.058	0.816
9S-LB-15B-Dmax	9	RSA	D_{max}	8	1.49	2.35	0.047	0.602
12S-LB-15B-Dmax	12	RSA	D_{max}	8	1.85	2.78	0.037	0.485
18S-LB-15B-Dmax	18	RSA	D_{max}	8	2.51	3.96	0.037	0.358
Performance Group PG-12, SDC D_{min}, Long-Period								
2S-LB-15B-Dmin	2	RSA	D_{min}	8	0.52	0.86	0.063	0.579
3S-LB-15B-Dmin	3	RSA	D_{min}	8	0.70	1.25	0.063	0.427
4S-LB-15B-Dmin	4	RSA	D_{min}	8	0.87	1.71	0.063	0.344
6S-LB-15B-Dmin	6	RSA	D_{min}	8	1.18	2.61	0.019	0.254
9S-LB-15B-Dmin	9	RSA	D_{min}	8	1.60	3.93	0.019	0.187
12S-LB-15B-Dmin	12	RSA	D_{min}	8	1.99	5.38	0.019	0.151
18S-LB-15B-Dmin	18	RSA	D_{min}	8	2.69	9.07	0.019	0.111

Figure 3.22: Design properties for select archetypes (Kircher et al., 2010)

Here, the archetype design parameters for the four-story and the nine-story MDOF systems are illustrated. These parameters are seismic design categories, dynamic amplification factors, fundamental periods, the period that corresponding to the lowest frequency at which deformation occurs, and base shear coefficient that normalized with the total weight, respectively. The archetypes selected were designed based on different seismic design categories and their first mode periods are different. In addition, the difference is observed from their dynamic responses that resulted in different S_{MT} value. The methodology requires to generate performance groups that consists of several criteria in order to involve the potential diversity of the building types. Thus, the archetypes are designed based on the performance groups that specify their basic configuration, design load level, the period domain. The performance group for the archetypes selected are demonstrated in Figure 3.23.

Table 7-2 Performance Groups for Evaluation of Buckling-Restrained Braced Frame Archetypes

Performance Group Summary					
Group No.	Grouping Criteria				Number of Archetypes[1]
	Basic Configuration	Design Load Level		Period Domain	
		Gravity	Seismic		
PG-1	ZZ-Diagonal Bracing 15-Foot Bays	Typical	SDC D_{max}	Short	3
PG-2				Long	5
PG-3			SDC D_{min}	Short	3[1]
PG-4				Long	7
PG-5	ZZ-Diagonal Bracing 25-Foot Bays	Typical	SDC D_{max}	Short	3
PG-6				Long	5
PG-7			SDC D_{min}	Short	3[1]
PG-8				Long	7
PG-9	LB-Diagonal Bracing 15-Foot Bays	Typical	SDC D_{max}	Short	3
PG-10				Long	5
PG-11			SDC D_{min}	Short	3[1]
PG-12				Long	7

Figure 3.23: Performance group list for select archetypes (Kircher et al., 2010)

Here, the basic configuration criterion specifies the lateral resisting system type for each performance group. The archetypes selected have the same configuration and gravity load level so the same frame dimensions and the building plan are used as shown in Figure 3.24.

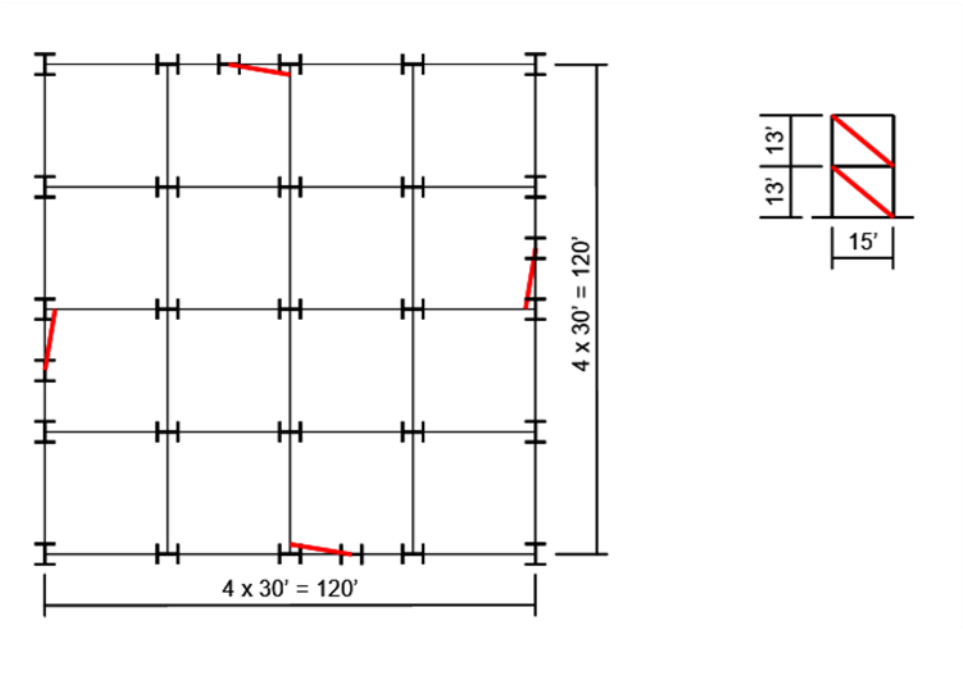

Figure 3.24: The plan view of select archetypes (Kircher et al., 2010)

After the foregoing descriptions, the total gravity load that acting on the archetypes was determined and it is used to determine the base shear that obtained on the system because of the seismic loading defined based on the seismic design category. The gravity load calculation is illustrated in Appendix A.4, in Figure A.12. However, the material properties and member sizes for the frame are provided by the report so nonlinear static analyses were not performed. The material properties, wide flange member sizes and BRB areas are provided in Figure 3.25, Figure 3.26, and Figure 3.27, respectively.

Table E-1 Structural Materials for BRBF Archetypes

Steel Section	Material Properties
W sections	ASTM A992 F_y=50 ksi; F_u=65 ksi
BRB Steel Core	ASTM A36 or JIS G3136 SN 400B with supplemental yield requirements: F_{ysc}=42 ksi

Figure 3.25: Material properties (Kircher et al., 2010)

Table E-5 Member Sizes for Buckling-Restrained Braced Frame Performance Group PG-10

Story	Brace Area (in^2)	Column Size	Beam Size
Archetype ID No. 4S-LB-15B-Dmax			
4	5.0	W14x74	W21x50
3	7.0	W14x82	W21x62
2	9.0	W14x132	W21x73
1	10.0	W14x145	W21x73

Figure 3.26: Member sizes for the four-story MDOF system (Kircher et al., 2010)

Table E-6 Member Sizes for Buckling-Restrained Braced Frame Performance Group PG-12

Story	Brace Area (in^2)	Column Size	Beam Size
Archetype ID No. 9S-LB-15B-Dmin			
9	3.0	W14x74	W18x35
8	3.0	W14x74	W21x50
7	3.0	W14x74	W21x50
6	3.0	W14x132	W21x50
5	4.0	W14x132	W21x50
4	4.0	W14x132	W21x62
3	6.0	W14x159	W21x62
2	6.0	W14x159	W21x62
1	6.0	W14x176	W21x62

Figure 3.27: Member sizes for the nine-story MDOF system (Kircher et al., 2010)

3.10.3. BRB Properties

Buckling-restrained Braced Frames (BRBF) described in Section 2.4.2 are presented as an innovative solution that has been developed to find economical solutions of designing the seismic load resisting system. The properties shown in Figure 2.12 for the new proposed BRB should be observed by testing it in order to determine the adjusted strength. However, in the report, a new BRB is not proposed so, the properties of a BRB that tested before were used. Nevertheless, the section sizes and material properties of the BRB elements are presented in the report thus the initial stiffness and yielding force are determined, unlike the post-yield stiffness property.

The post-yield stiffness ratio is a primary property in order to perform the nonlinear dynamic analysis and it was not presented in the report. Therefore, a literature review has been conducted to find a typical value for the ratio, it is observed that the typical range is two to five percent, based upon the report (Kersting et al., 2016). Thus, the post-yield stiffness ratio was determined as 2.5% with respect to the book (Black et al., 2002). Additionally, the fracture point of the BRB was not presented in the report as well as not required, because the story-drift limitation described in Section 2.4.1 controls the collapse (Kersting et al., 2016).

The Plastic link element (Wen Link) was preferred to model the inelastic behavior of the BRB in SAP2000. The link element provides users to control the sharpness of the yielding transition and it uses the simplified backbone curve described in Section 2.3.1 thus the inelastic behavior is modeled by using two different slopes which are initial and post-yield stiffness ratios. In Figure 3.28, the link properties of the BRB element in the first story of the four-story MDOF system are illustrated.

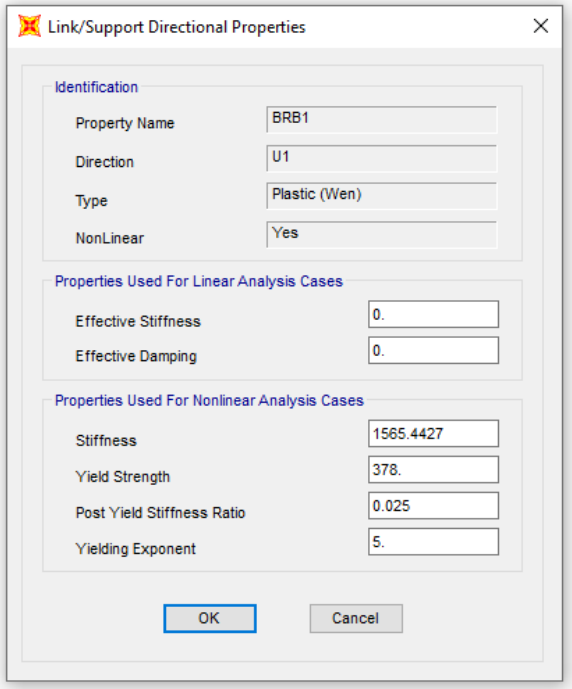

Figure 3.28: The four-story MDOF system - BRB properties for first story

Here, the properties used for the nonlinear analysis are shown, the yield exponent term supplies users to control the sharpness of the yielding transition. It was defined as five for all BRB elements in order to obtain a sharp transition. Nevertheless, other BRB models are illustrated in Appendix A.4, in Figure A.13 and Figure A.14.

3.10.4. SAP2000^{TM} Model

Here, SAP2000^{TM} models of the MDOF systems depicted in the foregoing are sketched also the required constraints, loading details, and element releases are explained. The structural framing consists of two different resisting systems to resist vertical and lateral loads. However, the methodology suggests designing each archetype as a gravity column and a frame in order to represent the vertical load resisting systems and the lateral load resisting systems, respectively, and, the suggestion is deemed sufficient with respect to express the behavior. Therefore, the MDOF systems were modeled as shown in Figure 3.29 and Figure A.15.

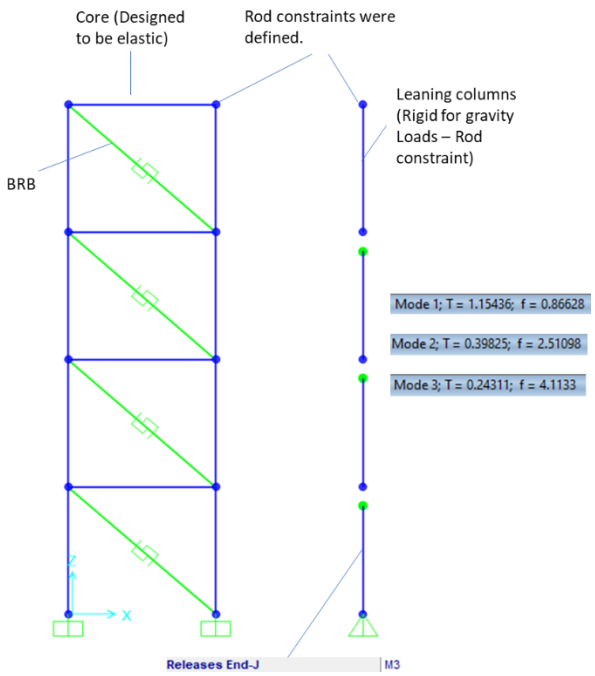

Figure 3.29: SAP2000^{TM} model for the four-story MDOF system

Here, it is observed that the same constraints and element releases were applied to the systems. The lateral loads are transmitted to the resisting system through diaphragms, however, based on the suggestion, the diaphragms are not modeled in the nonlinear analysis. Therefore, rod constraints are defined in order to represent the diaphragm behavior in between the BRB frame and the gravity column that represents the gravity frame for each floor. Thus, it was supplied that the two-node on each floor are displaced together. The element releases were applied to each gravity column because their contributions to the lateral load resisting system were neglected in the report. Also, the external support for the gravity columns was defined as a pin restraint, in which it does not contribute resisting against the rotation. Top-end for each gravity column was released for the rotation thus the lateral resisting contributions of the gravity columns were eliminated. The archetypes have the same gravity load level and the building plan. Therefore, the gravity loads demonstrated in Figure A.12 were applied to each floor for both

archetypes. The gravity loads were applied to gravity columns on each floor because the gravity column represents all columns on the floor. Thus, the BRB frames were designed to carry solely their own weight.

CHAPTER 4:

NUMERICAL RESULTS

Here, the chapter is divided into three parts: analysis results for the SDOF system, analysis results for the MDOF systems, and the critical damping ratio limitation approach.

In the first part, the SDOF system described in Section 3.3 was analyzed by using the API in order to observe the influence of the Rayleigh modeling methods on the

- damping force,
- damping-velocity relation,
- inherent energy dissipation,
- displacement results, and
- energy dissipation mechanism

at both the system and element levels are discussed.

In the second part, the MDOF systems described in Section 3.10 were analyzed to observe the influence of the Rayleigh modeling methods of all items listed in the first part, including in addition the assessment of the collapse risk considering IDA, and collapse margin ratios (CMRs).

In the third part, a new inherent damping energy limitation is described. Here, the MDOF systems, which Rayleigh methods modified based on the approach, were analyzed to observe the influence of the approach on the assessment of the collapse risk. The numerical results for IDA and CMRs are discussed, as well as, an example application is presented.

4.1. Analysis Results for the SDOF System

In this section, the structural element forces, damping forces, displacements, and energy results of the SDOF systems, which are computed separately for each Rayleigh modeling method, are discussed. The modeling details for the SDOF systems are described in Section 3.3. Regardless, the SDOF system is described in detail in Figure 4.1 where the link elements are used to model the BRB, mass, damping, and excitation. The BRB modeled in two parts; brace (elastic) and fuse (inelastic) elements and only one mass is present and the system is excited with time history ID: 1-1 as shown in Figure 3.6.

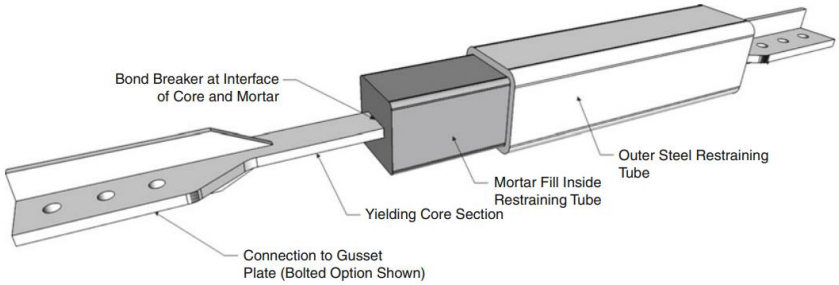

a. Isometric cutaway of buckling-restrained brace (Marshall, 2021)

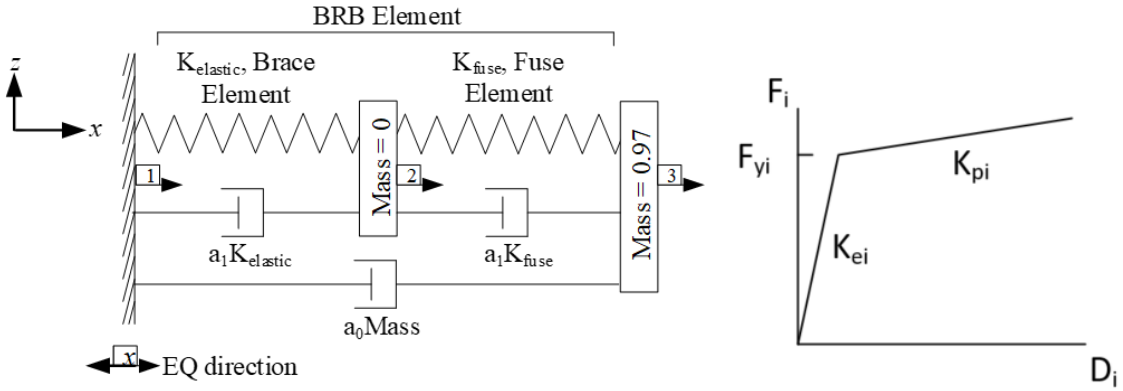

b. The SDOF system and the simplified-backbone curve

Figure 4.1: Details of the SDOF system

Alternatively, as described earlier, seven methods used to model inherent damping have influences on the response of the system, which is subjected to the FEMA P-695 time-history ID: 1-1, are listed Table 4.1. In addition, to illustrate how the parameters are determined in order to develop the damping matrix, Table 4.2 is presented.

Table 4.1: Rayleigh damping modeling methods for the SDOF system

Study	**Approach**	**Stiffness Options**	**Damping ratio**	**1st Frequency (sec^{-1})**	**2nd Frequency (sec^{-1})**	**Mass Coeff. (sec^{-1})**	**Stiffness Coeff. (sec)**
1	A (2.6.3)	Initial Stiffness	5%	1.348	1.348	0.4236	0.0059
2	B (2.6.3)	Tangent Stiffness	5%	1.348	1.348	0.4236	0.0059
3	C (3.4)	Mass Only	5%	1.348	1.348	0.4236	-
4	A (2.6.3)	Initial Stiffness	5%	0.252	0.252	0.0791	0.0316
5	B (2.6.3)	Tangent Stiffness	5%	0.252	0.252	0.0791	0.0316
6	B (2.6.3)	Tangent Stiffness	5%	1.348	0.252	0.1333	0.0100
7	D (3.4)	Elastic Elements	5%	1.348	1.348	0.4236	0.0059

Table 4.2: Parameters to develop the damping matrix for each method

Study	**$K_{elastic}$, Kip/in**	**K_{fuse}, Kip/in (initial)**	**K_{fuse}, Kip/in (post-yield)**	**Mass Kip-sec^2/in**	**$a_1K_{elastic}$, Kip-sec/in**	**a_1K_{fuse}, Kip-sec/in**	**a_0Mass, Kip-sec/in**
1	300	90.76	-	0.97	1.770	0.535	0.411
2	300	90.76	2.45	0.97	1.770	Varies	0.411
3	300	90.76	2.45	0.97	-	-	0.411
4	300	90.76	-	0.97	9.480	2.868	0.077
5	300	90.76	2.45	0.97	9.480	Varies	0.077
6	300	90.76	2.45	0.97	3.000	Varies	0.129
7	300	-	-	0.97	1.770	-	0.411

The SAP2000™ model that involves the system properties, restraints and mass is demonstrated

in Figure A.1 and the modeling methods listed in Table 4.1 are illustrated in Figure A.5. Additionally, note that each Rayleigh modeling method is referred to as the study numbers in the figures.

4.1.1. Influence of Modeling Methods on Damping Force

The Rayleigh concept assumes damping forces are proportional to the velocity and damping matrix developed by the velocity at the current state. Two coefficients described in Section 2.6.3 are proportional to the mass and stiffness as illustrated in Table 4.1 and Table 4.2. Although the coefficients, which are defined with respect to the system properties, may vary at each current state, the coefficients do not vary during the analysis. The damping matrix is developed based upon Equation (3.3) for each static node. In addition, the link elements were used to model different behavior under large excitations as shown in Figure 4.2 and Figure 4.3. The process is described as:

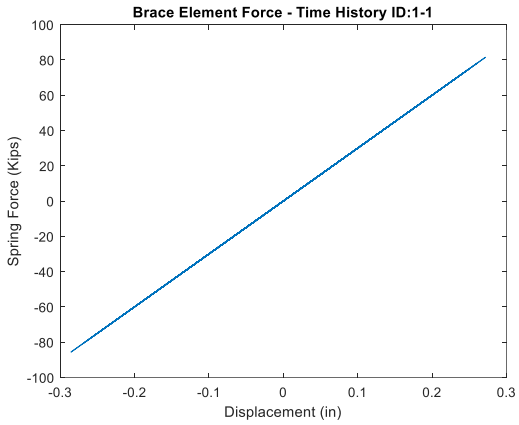

Figure 4.2: The SDOF system - Force vs disp. plot of the brace (elastic portion) for the first method

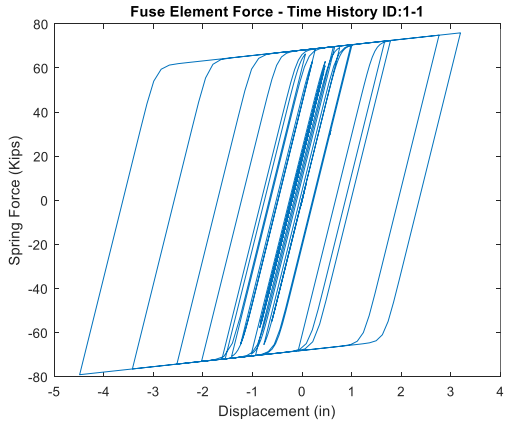

Figure 4.3: The SDOF system - Force vs disp. plot of the fuse (inelastic portion) for the first method

1. Develop the damping matrix

Here, to illustrate how the damping matrix is developed, the first method is used thus the stiffness option of the fuse element is selected as the initial-stiffness and is used regardless of the stiffness at the current state. Nevertheless, the damping force is calculated by multiplying Equation (3.3) with the velocity as shown below

$$C_{Rayleigh}\dot{u}(t) = a_0\begin{bmatrix}0 & 0\\ 0 & M_3\end{bmatrix}\begin{bmatrix}\dot{u}_2(t)\\ \dot{u}_3(t)\end{bmatrix} + a_1\begin{bmatrix}K_1+K_2 & -K_2\\ -K_2 & K_2\end{bmatrix}\begin{bmatrix}\dot{u}_2(t)\\ \dot{u}_3(t)\end{bmatrix} \tag{4.1}$$

Here, K_1 and K_2, which represent the stiffnesses of the brace and fuse elements, respectively. The initial stiffness of the fuse element is largely different from its post-yield stiffness so when the transition from initial to post-yield stiffness (yielding) occurs, its stiffness is considerably decreased. It is observed from Equation (4.1) that there is no mass-proportional damping contribution at node two. The SDOF system, which was analyzed using the first

method, was analyzed and the results are provided in Figure 4.4. The post-yield stiffness is included where the tangent stiffness approach is used.

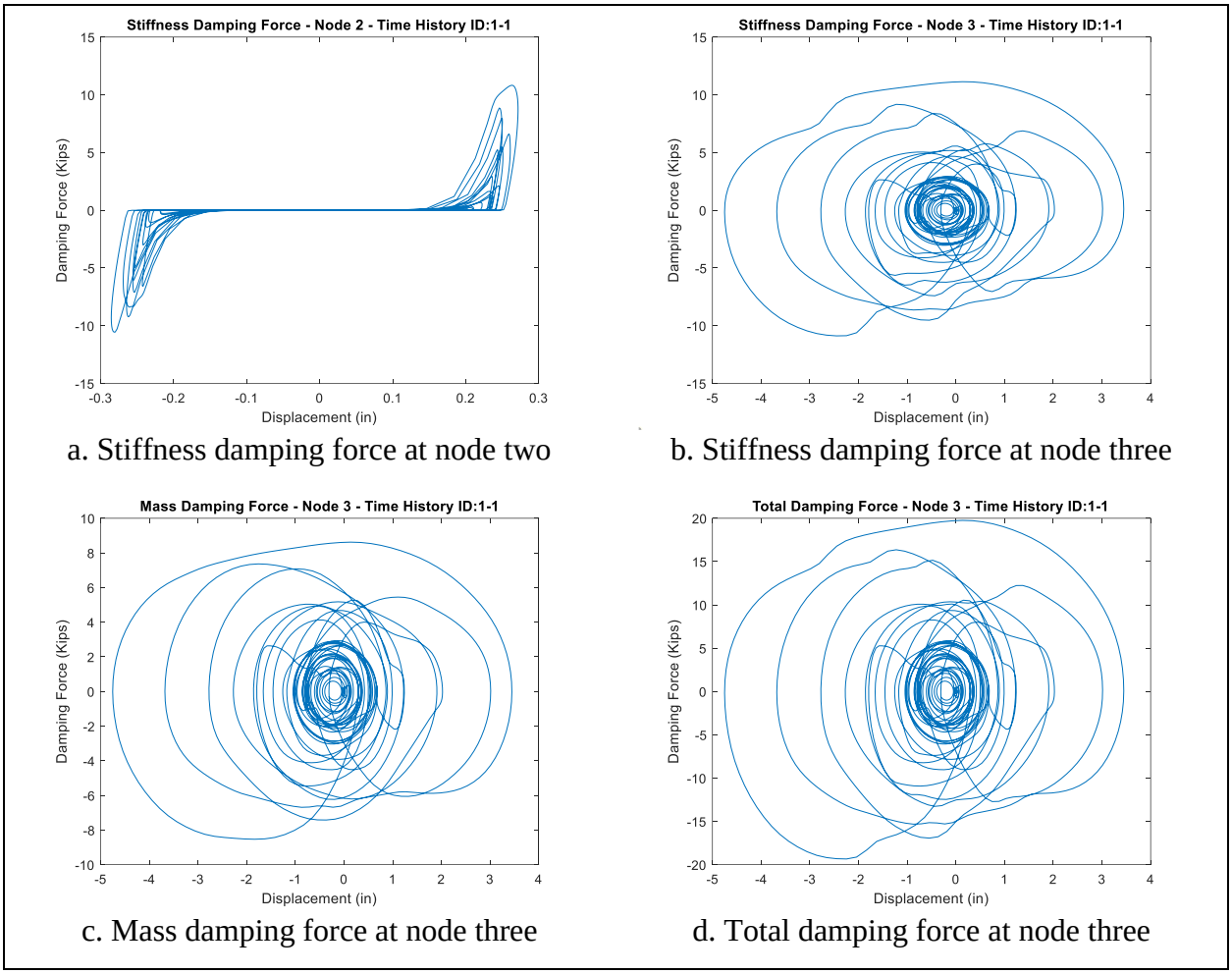

a. Stiffness damping force at node two

b. Stiffness damping force at node three

c. Mass damping force at node three

d. Total damping force at node three

Figure 4.4: The SDOF system - Damping force plots for the first method

The mass and stiffness-proportional coefficients are a function of the natural frequencies, which are defined with respect to the initial properties, and the damping ratios that are determined as five percent. For illustration, for the first and fourth methods, the stiffnesses for the damping matrix were included in the same way but different natural frequencies were defined to determine the coefficients and it is observed that the methods were caused obtaining significantly different damping forces.

2. Compare the methods

There are many details for each of the methods used. To accommodate discussion, the stiffness and mass proportional damping contributions are demonstrated separately for each node and the plots for other methods are demonstrated in Appendix B.1. Each modeling method is discussed below.

In the first method, Approach A caused obtaining the largest damping. In the second method, Approach B was used to account for the varying stiffness of the inelastic element and is included by determining K_2 but it is observed that the damping effect is significantly decreased. In the third (Approach C) and seventh methods (Approach D), the stiffness damping contributions of the fuse element were eliminated so the spurious damping forces were not obtained and the coefficients do not have to be regenerated at each current state. Similar results were obtained because the stiffness damping contributions at node two were not significant. Regardless, the third method is not recommended because the mass-proportional part is referred to as that DOFs were connected to external supports via a linear viscous damper but this mechanism possibly not exist, and not a physical phenomenon.

3. Observe the damping force-velocity relation

The velocity is another variable to determine the damping force. For the first method, the plots, which involve the stiffness and mass damping forces, are demonstrated in Figure 4.5 as one example. The plots for other methods are demonstrated in Appendix B.2.

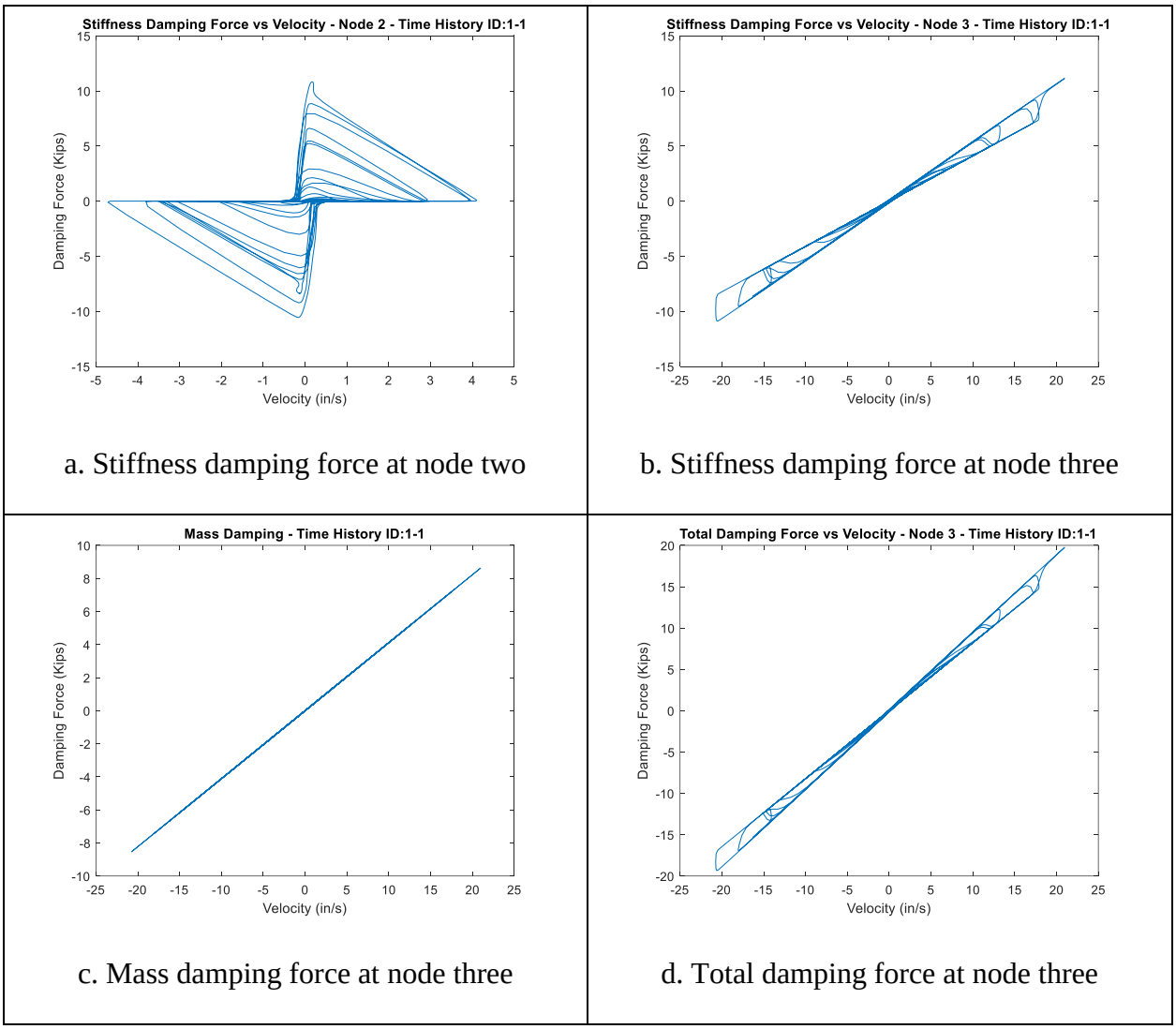

a. Stiffness damping force at node two

b. Stiffness damping force at node three

c. Mass damping force at node three

d. Total damping force at node three

Figure 4.5: The SDOF system - Damping force vs velocity plots for the first method

The mass-proportional contributions were obtained linearly for all methods because the mass-proportional coefficient and the contribution is a function of the velocity just at node three. In the first method, although the stiffness values and the stiffness-proportional coefficient were not varied, the stiffness-proportional contributions were obtained nonlinearly because of the velocity values at each node. However, for the seventh method, the stiffness-proportional contribution is obtained linearly because the contribution of the fuse element was eliminated.

Lastly, it is observed that the damping forces that are determined using the Rayleigh mathematical model are proportional to the velocity, how the stiffness is included, and the coefficients. The crux of the analysis is described next where energy dissipation is computed and compared.

4.1.2. Influence of Modeling Methods on the Energy Dissipations

The seismic energy imparted (input energy) is dissipated through the internal energy principle and energy loss. Absorbing the seismic energy through planned plastic deformation on the select structural components is referred to as the internal energy principle and the plastic deformation results in cumulative energy absorption, which is described as the hysteresis energy dissipation in Section 2.3. The energy loss, which is the other dissipation phenomenon, is referred to as inherent damping energy dissipation that results in irrecoverable heat loss (typically) due to material and component mechanism. Thus, the input energy is absorbed through the hysteresis and inherent damping energy dissipations.

The energy-absorbing ability is typically associated with the area within the force-displacement curve which is also known as toughness so the hysteresis and inherent damping energy dissipations are a function of forces that are the element and damping forces, respectively. Nevertheless, the hysteresis and inherent damping energy dissipations are additive and must balance the energy input due to the seismic event. The SDOF systems were analyzed and the input energy, and the energy dissipations were determined by integrating the equations expressed in section 3.8. In this section, the energy plots for the first method are demonstrated in Figure 4.6 for the first method. The energy plots for other methods are demonstrated in Appendix B.3.

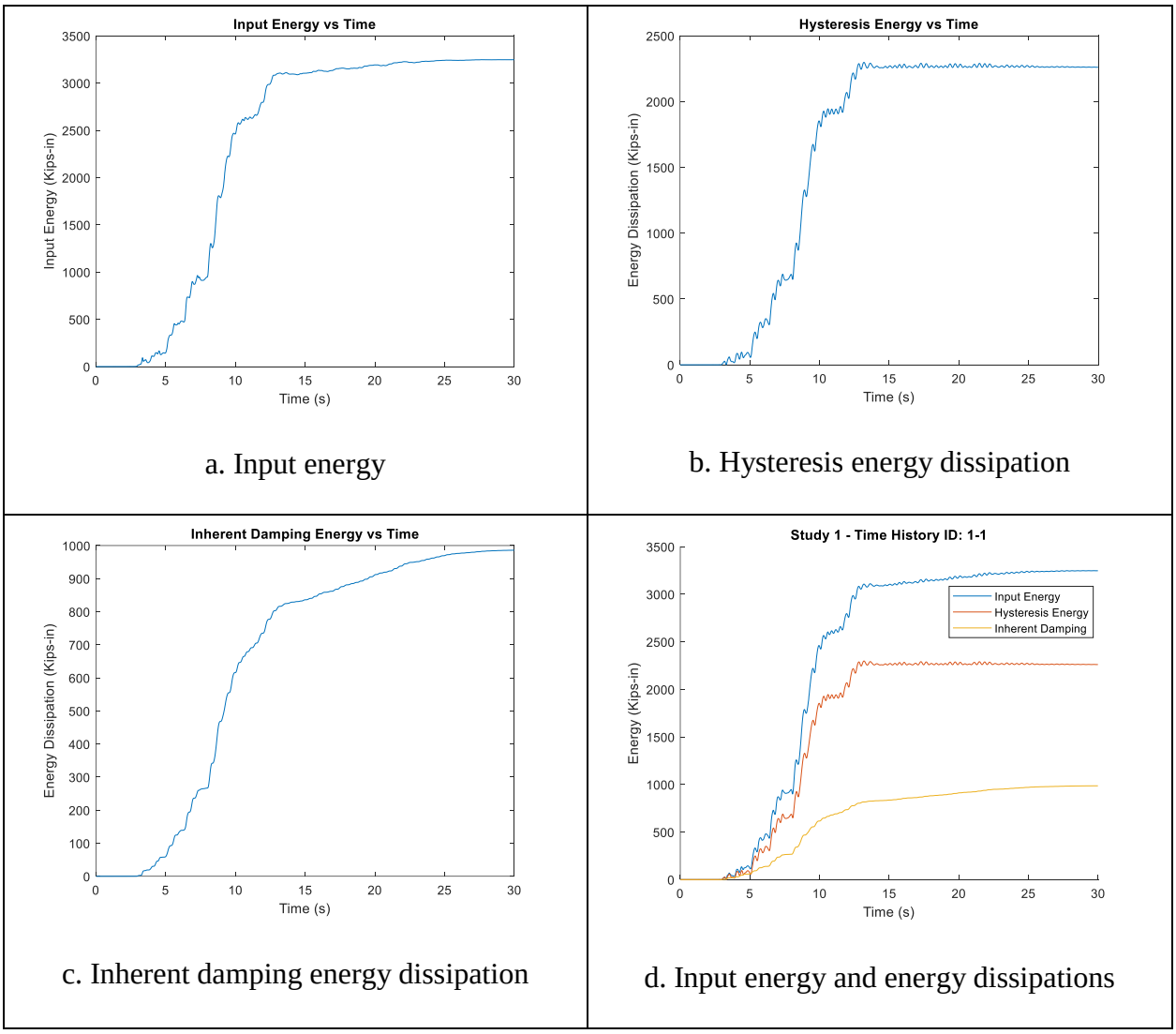

a. Input energy

b. Hysteresis energy dissipation

c. Inherent damping energy dissipation

d. Input energy and energy dissipations

Figure 4.6: The SDOF system - Energy plots for the first method

Here, the kinetic energy of the system and the elastic energy of the structural elements were eliminated from the input energy and hysteresis energy, respectively because they are conserved. Nevertheless, the input energy was obtained based on the acceleration of the mass, and the hysteresis and inherent damping energy dissipations were obtained with respect to the deformations that are associated with the element forces and damping forces, respectively.

It is observed that the fuse element exhibited elastic behavior early during time history, after which the seismic input increases and the fuse response is inelastic and hysteric energy in

absorbed. Later in the time history, the seismic demands decrease and the response is linear so no more hysteresis energy was cumulated. In each Rayleigh modeling method, the use of different stiffness options and the coefficients resulted in the dissimilarity of the inherent damping energy dissipations and the normalized values of the energy dissipations are illustrated as a percentage of the input energy in Figure 4.7.

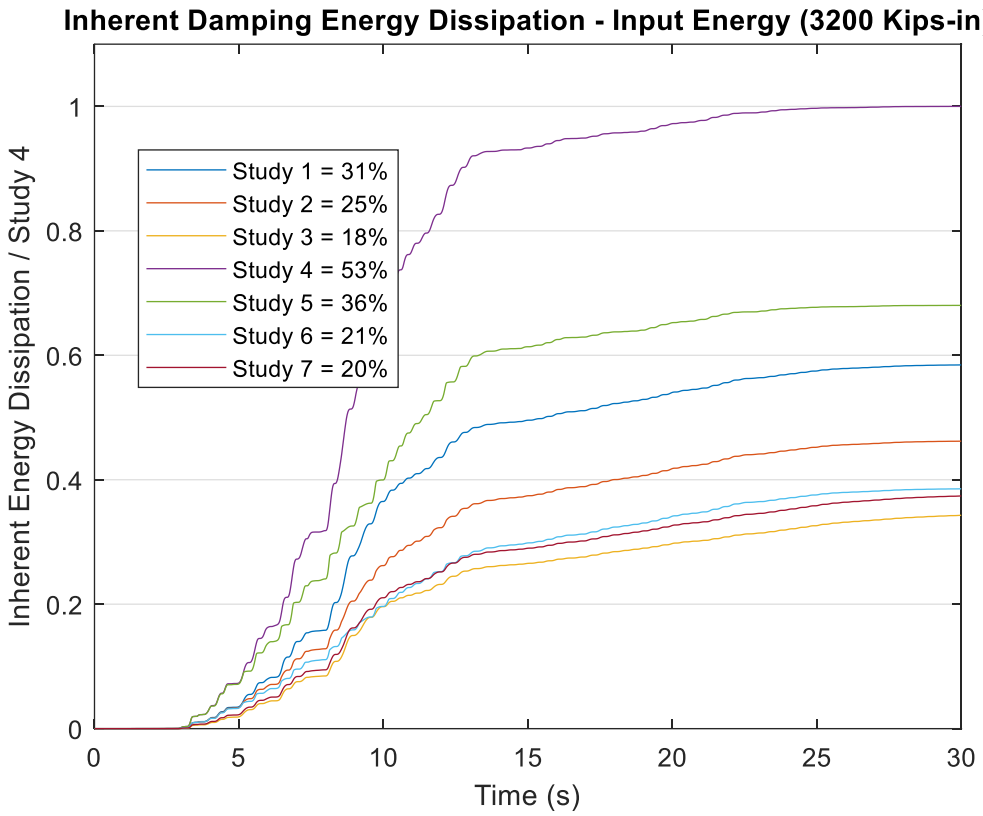

Figure 4.7: The SDOF system - TH ID: 1-1 - Normalized damping energy dissipations

Here, the dissimilarity of the inherent damping energy dissipations is observed and obviously this resulted in the variation in the response. For instance, when the first and second methods were compared, the first method resulted in the higher inherent damping energy dissipation thus smaller response was obtained; however, in the second method, higher deformation, which

brought fourth higher hysteresis energy dissipation. Regardless, it is also observed that the result for the fourth method was non-conservative from a design perspective.

In conclusion, it is observed that in each Rayleigh modeling method, the damping matrix was developed differently due to the use of different stiffness options and the coefficients. This resulted in the dissimilarity in the damping forces. Also, different responses were obtained because of the dissimilarity, therefore also, the hysteresis behavior of the inelastic element and the energy dissipations were obtained differently for each method. This is illustrated for the FEMA P-695 time-history suite in the next section.

4.1.3. Influence of Modeling Methods on the Response

It is deemed as a collapse or failure based on the limit state conditions when the fuse element or brace element reaches the capacity or else, fails to perform the function that is expected of it. There are four types of limit state conditions described in Section 2.4.1; however, the BRB frame is designed based on the collapse limit state which controls the response. Under large excitations, the fracture may not be observed on any structural elements but the response is reached to the allowable deformation limit, which is defined in order to control the geometric nonlinearity in the system. Therefore, the assessment of the collapse risk of the BRB frame is performed with respect to the deformation limits, also known as the story-drift limitations.

In the previous numerical results, it was concluded that each method caused the system to result in different responses, and this is interpreted as each method might be resulted in a different assessment of collapse risk. Therefore, to observe the influence of modeling methods on displacement results, the SDOF systems were subjected to the forty-four individual ground motion-records selected by FEMA. However, firstly, the records were scaled by gravity (g) unit

and the normalization factors described in Section 2.5.2. Secondly, the systems were analyzed and the displacement results for each method are demonstrated in Figure 4.8.

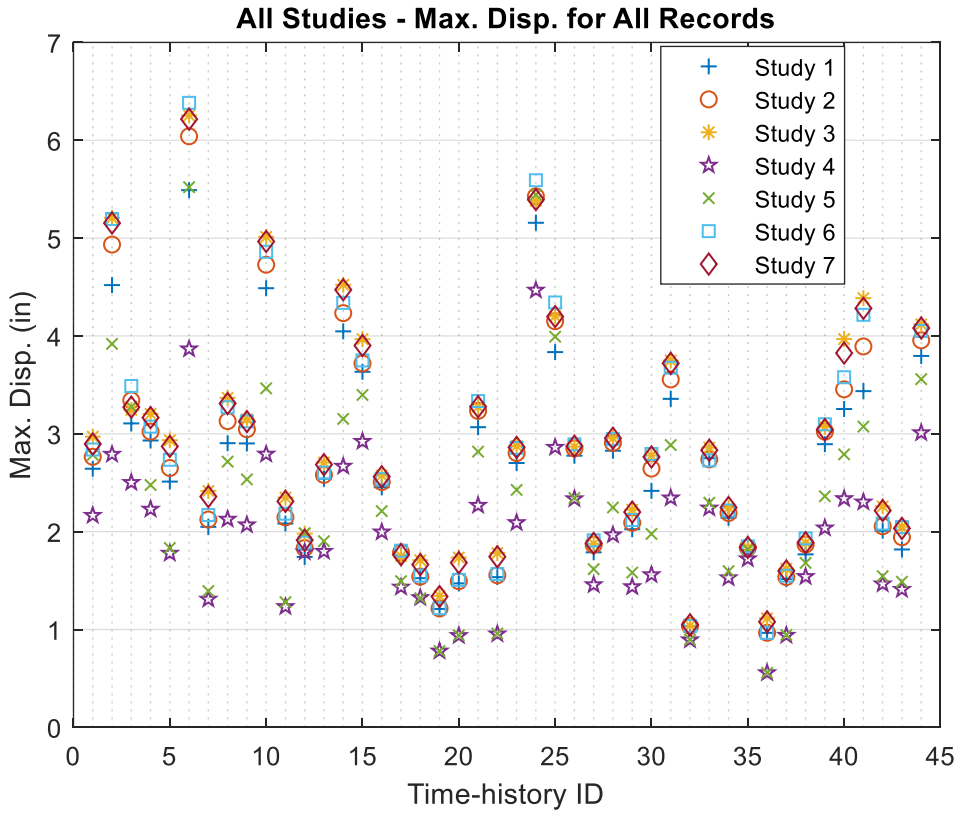

Figure 4.8: The SDOF system - Max. displacements for all studies

Here, it is observed that each ground-motion record (time-history) caused different responses as they are selected by FEMA specifically to involve the possible diversity of earthquake characteristics. Nevertheless, although some records resulted in large deformations, others were not, hence for each record, different plastic ranges in the fuse element were obtained. Therefore, the hysteresis energy dissipations were obtained differently due to the variation in the energy-absorbing ability that depends on the area within the force-displacement curve.

The differences resulted in the variation of the energy rates because the hysteresis and inherent damping energy dissipations are proportional to each other. However, when the large plastic range or the high amount of hysteresis energy dissipation was obtained, the variation in the damping forces was obtained obviously because of the complexity and large nonlinearity range. Consequently, the six records that caused the largest displacements were selected and the results were normalized and are demonstrated in Figure 4.9.

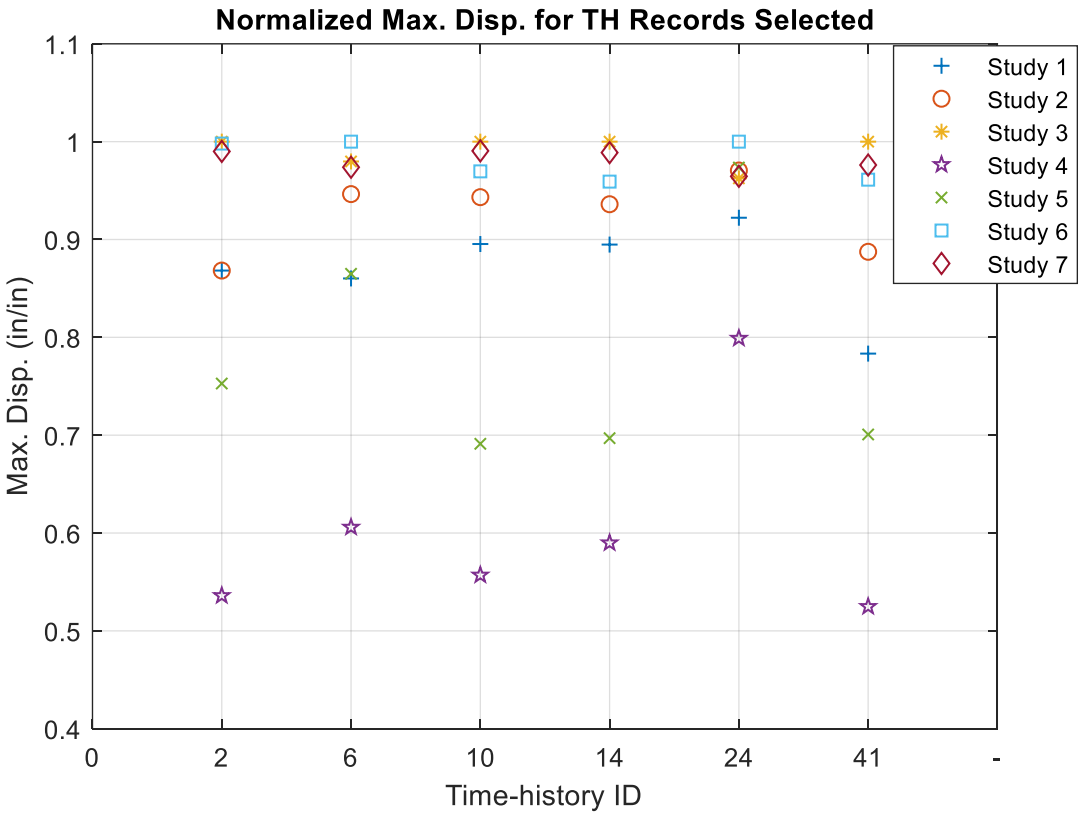

Figure 4.9: The SDOF system - Normalized max. displacements for all methods

To select the records, the records in frequency-domain were reviewed and for each record, the frequencies with the most energy were compared with the natural frequencies because the different responses were mainly occasioned due to the dynamic amplification factors. The factors are determined with respect to the frequency ratios that are proportion between the

system and the ground-motion records frequencies. Hence, the records were selected based on the comparison and the displacement results from Figure 4.8.

In Figure 4.9, it is obviously, and importantly, observed that each Rayleigh modeling method resulted in different responses. However, none of the methods are the exact representation of the inherent damping due to the assumptions so the methods were occasioned to higher or lesser displacements than it is. Alternatively, the methods have an influence on the displacement results in both ways positively or negatively with respect to how the damping matrix is developed. However, non-conservative performance results were obtained from the systems that modeled using the fourth and fifth methods, in which the different coefficients were determined due to the different natural frequencies defined. Therefore, the natural frequencies must be decided carefully, or else the decision might be controlled by FEMA P-695.

In summary, the SDOF analyses clearly indicated that significant differences in the response are obtained for the same five percent damping ratio and these differences are due to the assumptions associated with modeling of inherent damping. Because the SDOF is a simple representation of a single story (or mode), the present analysis does not tell the entire story and the analysis is rigor is increased to MDOF systems.

4.2. Analysis Results for the MDOF Systems

The assessment of the collapse risk that is proposed by the FEMA P-695 is determined based on the collapse margin ratios (CMRs) that described in Section 2.5.4. Nevertheless, CMRs are determined with respect to strength and story-drift limitations. Based on the SDOF results that were obtained here, it was concluded that an MDOF system (or archetype) must be evaluated according to the FEMA P-695 process in order to observe the influence of the Rayleigh modeling methods on the assessment of the collapse risk. Because, in FEMA P-695,

the method for the modeling of the inherent damping is not described clearly as expressed in Section 2.6.6 and here it was concluded that this would lead to different ratios.

To observe that the influence of the Rayleigh modeling methods on the inherent energy dissipation, the drift ratio results, and the assessment of the collapse risk, the MDOF systems described in Section 3.10 were analyzed using the API. Also, the collapse margin ratio (CMR) results, which were obtained from the IDA, are discussed. Similarly, each Rayleigh modeling method are referred to as the study numbers in figures and tables.

4.2.1. Influence of Modeling Methods on Energy Dissipation

In the foregoing sections, it is observed that the damping matrix is developed differently with respect to the use of different stiffness options and the coefficients. Hence, the damping forces, which were obtained differently for each method, resulted in a variation in the response and the variation caused in the different energy rates. To observe the influence of the Rayleigh modeling methods on the assessment of the collapse risk, ten Rayleigh modeling methods described in Section 3.1 were determined with respect to the natural frequencies and the way that stiffness included. Here, the four-story MDOF systems (archetype), which were designed separately for each Rayleigh modeling method, are evaluated based on the inherent damping energy dissipations.

The MDOF system described in Section 3.10 consists of two different resisting systems to resist vertical and lateral loadings; however, the vertical load resisting system was modeled as leaning columns that represent all columns at each story as illustrated in Figure 3.29. The lateral load resisting system consists of four BRB elements that are located separately at each story and the system was designed to exhibit inelastic behavior in only the BRB element. Therefore, under large excitations, the hysteresis energy dissipations were obtained only in BRB elements. The

mass of each floor was assigned to the leaning columns thus in each story, the system has three static DOFs and single dynamic DOF. However, the damping matrix is developed with respect to the Rayleigh concept so stiffness-proportional damping contributions of each node are involved.

The four-story MDOF systems were analyzed to obtain the input energy and the energy dissipations that were calculated by integrating the equations expressed in section 3.8. Here, the energy plots for the first method are demonstrated in Figure 4.10 as one example.

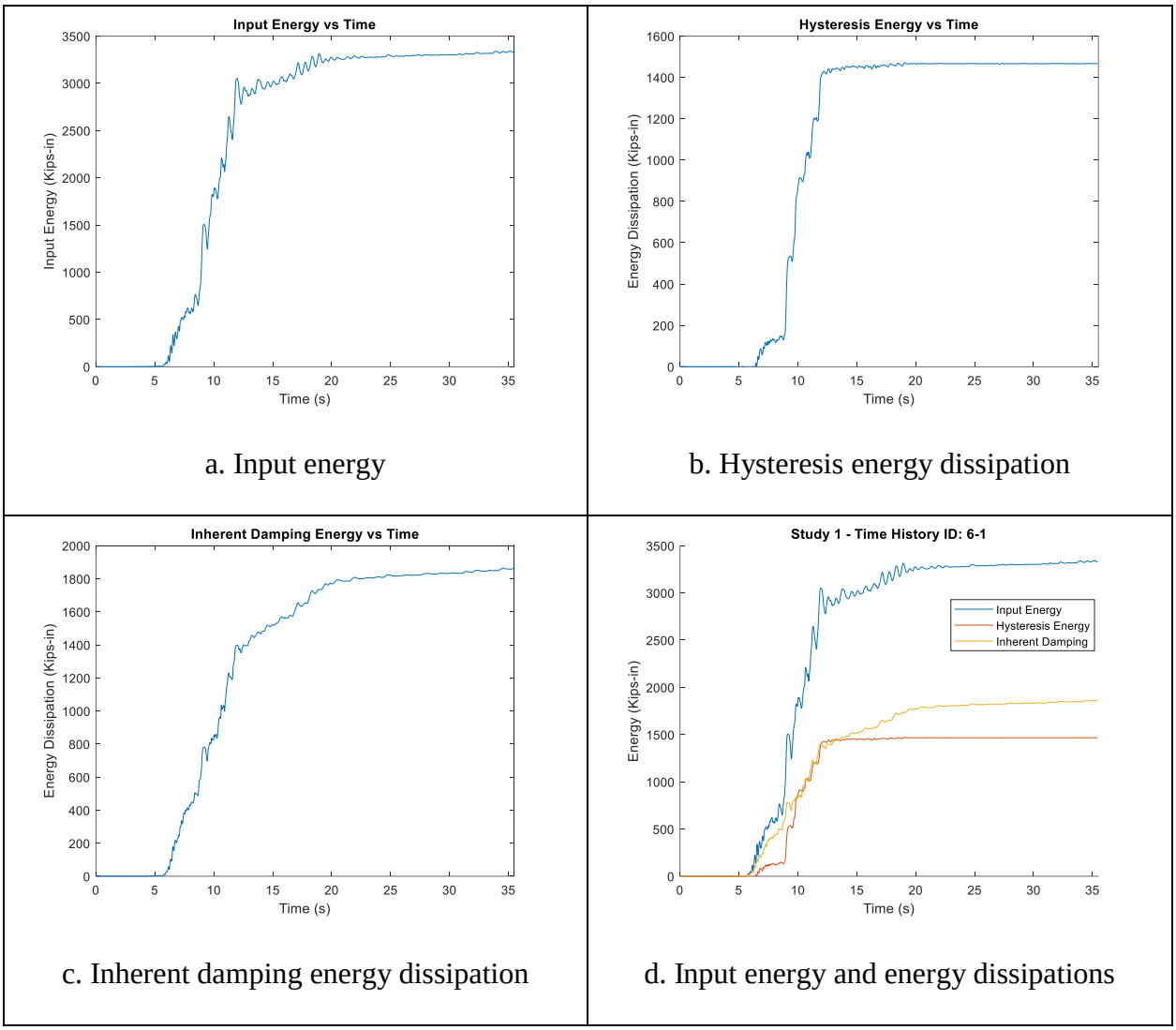

a. Input energy

b. Hysteresis energy dissipation

c. Inherent damping energy dissipation

d. Input energy and energy dissipations

Figure 4.10: The four-story MDOF system - Energy plots for the first method

Note that, the energy plots for the other methods are illustrated in Appendix C.1. Here, the energies that are not cumulative, the kinetic energies that are obtained due to each mass assigned, and the elastic energies that are obtained from structural elements were eliminated from the input energy and hysteresis energy, respectively. Nevertheless, the total input energy was obtained by adding energies that were determined separately at each story due to the acceleration of the mass assigned.

The total hysteresis energy dissipation was obtained by adding energy dissipations that were obtained separately from BRBs. The hysteresis energy was obtained by using the internal energy principle, in which the inelastic deformations that were obtained associated with the BRB forces were used. However, the total inherent damping energy was obtained by adding energies that were obtained separately from each node on floors with respect to the area associated with the damping force-deformation curves.

In Figure 4.10, it is observed that during high accelerations, the BRBs exhibited inelastic behavior and at other time, e.g., late in the time history, the solely elastic behavior so no more hysteresis energy was cumulated. Hence, the input energy, which is equal to the summation of the hysteresis and inherent damping energy dissipations. Because, unlike the hysteresis energy, the inherent damping energy-absorbing ability is obtained under both elastic and plastic response. When the results were compared, it is observed that the use of different stiffness options and the coefficients resulted in the dissimilarity of the inherent damping energy dissipations. Hence, to observe the dissimilarity clearly, the values of the inherent damping energy dissipations were normalized and are demonstrated as a percentage of the input energy in Figure 4.11.

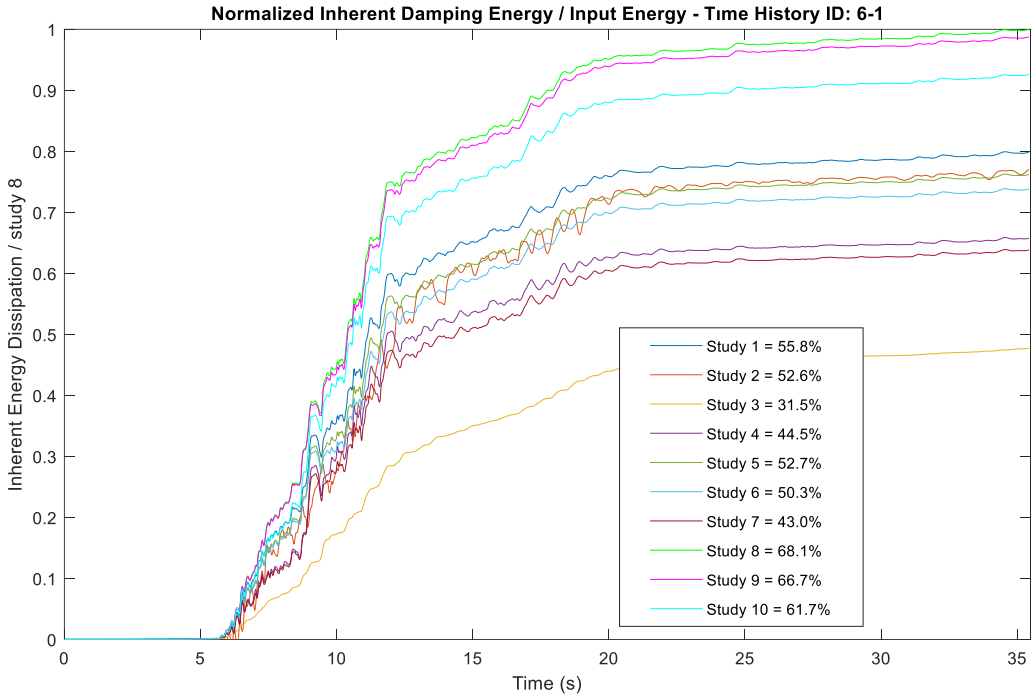

Figure 4.11: The four-story MDOF system - Normalized damping energy dissipations

Here, it is obviously observed that the methods caused different inherent damping energy dissipations even though all are based upon a five percent damping ratio. And, as the response is a function of the energy-absorbing ability, the different dissipations resulted in a variation in the response. For instance, as a comparison of the eight and third methods, the eight method caused the system to result in smaller responses, unlike the third method, however, higher hysteresis energy dissipations were obtained in the third method because of higher deformations.

In the last three methods, the natural frequencies were selected as the second and third frequencies to determine the mass and stiffness-proportional coefficients and this resulted in excessive damping forces that are caused the high amount of energy dissipation. Also, the third method, which eliminates the stiffness contribution of the inherent damping, resulted in the

lowest damping forces. Hence, non-conservative performance results were obtained from the last three methods and the third method.

As a summary, it is observed that in each Rayleigh modeling method, the damping matrix is developed differently due to the use of different stiffness options and the natural frequencies and this resulted in different inherent damping energy dissipations. Also, the variation of the response was obtained due to different energy dissipation results thus the hysteresis behavior of the BRBs, and the energy dissipation rates were obtained differently for each method. The damping method, although not clearly prescribed in FEMA P-695 or ASCE 7 is critical and must be carefully understood. In the next section, the analysis is expanded to assess the criticality of the assumed method to the risk of collapse in a seismic event as determined by FEMA's P-695.

4.2.2. Influence of Modeling Methods on the Assessment of Collapse Risk

Under large excitations, it is expected that the systems must perform sufficient strength and functionality. However, the inelastic systems are primarily designed to exhibit ductile behavior that does not exceed the planned deformation and when it exceeds the planned limit, the system is deemed as collapsed with respect to the collapse limit state. The fracture may or may not be observed in any structural elements therefore the systems are checked based on the excessive forces (strength) and displacements (story-drifts). Therefore, the systems are primarily designed not to reach the excessive forces and displacements.

FEMA P-695 provides a procedure for proposed or existing systems, in which the assessment of the collapse risk is performed with respect to strength and story-drifts. For each system, FEMA P-695 requires determining the collapse margin ratio (CMR) that is a function of S_{MT} and $\hat{S}_{CT}$ values that are the spectral acceleration at the specified period and the intensity at

the collapse point, respectively. The values are determined by performing the Incremental Dynamic Analysis (IDA) described in Section 3.9, in which the intensities of the ground motions are scaled collectively until the system reaches the collapse point. Here, CMR results that were obtained on MDOF systems are discussed.

Firstly, the scale factors were determined for the MDOF systems and the systems that were subjected to the scaled forty-four individual ground-motion records were analyzed. Hence, to find the scale factor at which one-half of the records cause collapse, the forces and displacements were compared with fracture point of BRBs and the displacement that is calculated by using the story-drift limit.

The allowable maximum displacement was determined as 3.12 inches which correspond to two percent of the story height; however, it was multiplied with Over-strength factor that is defined as 2.5 thus the story-drift limit was defined as five percent. Here, for the first method, the results are demonstrated in Figure 4.12. Also, the results for other methods are illustrated in Appendix C.2 and Appendix C.3 separately for each MDOF system.

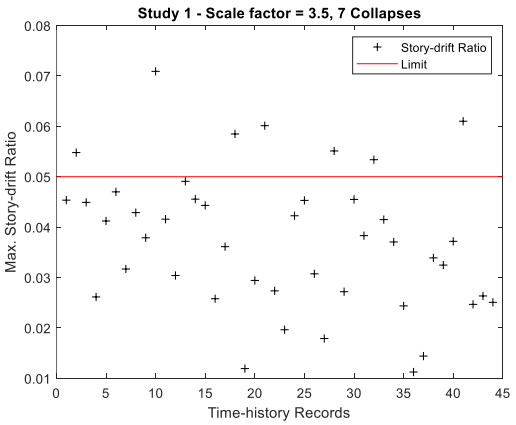

a. The four-story - Scale factor = 3.5

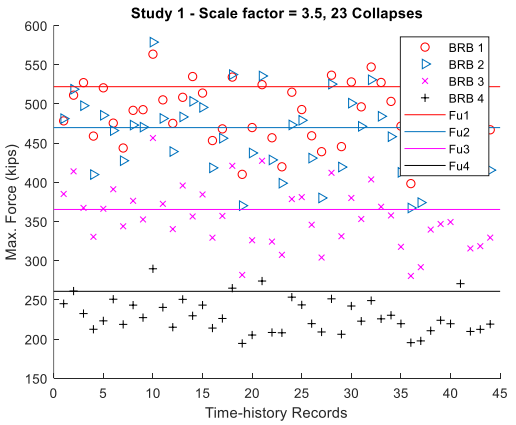

b. The four-story - Scale factor = 3.5

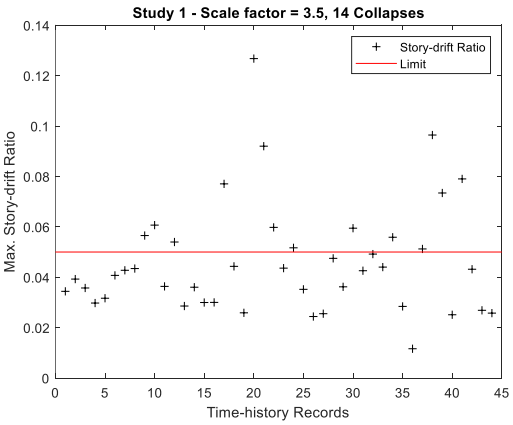

c. The nine-story - Scale factor = 3.5

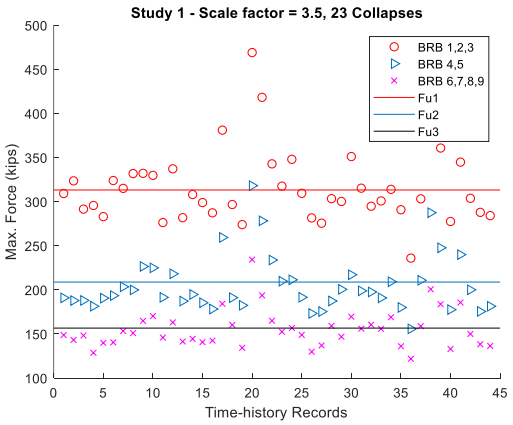

d. The nine-story - Scale factor = 3.5

Figure 4.12: The MDOF systems - Selected IDA results for the first method

As expressed before, the ground-motion records were selected by FEMA specifically to involve the possible diversity of the earthquake characteristics. Hence, here it is observed that different responses were obtained because of the dynamic amplification factors that are determined according to the frequency ratios. Therefore, different inelastic deformation ranges in BRBs were obtained and the hysteresis energy dissipations were obtained differently due to the variation in the energy-absorbing ability.

In each record, the differences in the responses and hysteresis energy dissipations caused the variation of the energy rates because the hysteresis and inherent damping energy dissipations are proportional to each other. However, when the large inelastic deformation range or the high amount of hysteresis energy dissipation was obtained, the variation in the damping forces due to the Rayleigh modeling methods was obtained obviously because of the complexity.

The scale factor range in order to perform IDA must be selected carefully so as to supply a significant reduction in the computation time. Here, the scale factors (in tenths) were determined as close as enough to the precise factor (in hundredths) because of the computation

time. Therefore, some of the scale factors were selected based on 23 or 24 collapses because of the range in tenths. The results are listed in Table 4.3 and Table 4.4 for each MDOF system, respectively.

Table 4.3: The four-story MDOF system - Collapse margin ratios

Study	**Approach**	**Stiffness Options**	**1st Frequency**	**2nd Frequency**	**S_{MT} (g)**	**Scale factor**	**S_{CT} (g)**	**CMR**
1	A	Initial Stiffness	1st frequency	2nd frequency	1.11	3.50	1.549	1.40
2	B	Tangent Stiffness	1st frequency	2nd frequency	1.11	3.30	1.460	1.32
3	C	Mass Only	1st frequency	2nd frequency	1.11	3.20	1.416	1.28
4	D	Elastic Elements	1st frequency	2nd frequency	1.11	3.20	1.416	1.28
5	A	Initial Stiffness	1st frequency	3rd frequency	1.11	3.50	1.549	1.40
6	B	Tangent Stiffness	1st frequency	3rd frequency	1.11	3.30	1.460	1.32
7	D	Elastic Elements	1st frequency	3rd frequency	1.11	3.20	1.416	1.28
8	A	Initial Stiffness	2nd frequency	3rd frequency	1.11	3.90	1.726	1.55
9	B	Tangent Stiffness	2nd frequency	3rd frequency	1.11	3.80	1.682	1.52
10	D	Elastic Elements	2nd frequency	3rd frequency	1.11	3.70	1.637	1.48

Table 4.4: The nine-story MDOF system - Collapse margin ratios

Study	Approach	Stiffness Options	1st Frequency	2nd Frequency	S_{MT} (g)	Scale factor	S_{CT} (g)	CMR
1	A	Initial Stiffness	1st frequency	2nd frequency	0.187	3.50	0.728	3.89
2	B	Tangent Stiffness	1st frequency	2nd frequency	0.187	3.20	0.666	3.56
3	C	Mass Only	1st frequency	2nd frequency	0.187	3.00	0.624	3.34
4	D	Elastic Elements	1st frequency	2nd frequency	0.187	3.20	0.666	3.56
5	A	Initial Stiffness	1st frequency	3rd frequency	0.187	3.30	0.686	3.67
6	B	Tangent Stiffness	1st frequency	3rd frequency	0.187	3.20	0.666	3.56
7	D	Elastic Elements	1st frequency	3rd frequency	0.187	3.10	0.645	3.45
8	A	Initial Stiffness	2nd frequency	3rd frequency	0.187	3.60	0.749	4.00
9	B	Tangent Stiffness	2nd frequency	3rd frequency	0.187	3.40	0.707	3.78
10	D	Elastic Elements	2nd frequency	3rd frequency	0.187	3.40	0.707	3.78

Here, $\hat{S}_{CT}$ values, which is the intensity at the collapse point, were determined by multiplying the median values of the normalized record (shown in Figure 2.18) by the scale factors determined. Nevertheless, the S_{MT} values are demonstrated in Figure 3.22. Lastly, CMRs were determined by dividing the $\hat{S}_{CT}$ value by the S_{MT} value and the results are listed in Table 4.3 and Table 4.4 for each MDOF system, respectively.

For each Rayleigh modeling method, the stiffness options and the natural frequencies are listed in the tables. Here, it should be reminded that the methods that are listed were determined to involve the most possible ones. However, the Rayleigh concept might be involved using

another approach that may cause non-conservative results, in which as it is observed in the SDOF system when the post-yield frequency defined as the dominant frequency.

Lastly, it is observed that in CMRs, approximately 20% difference might be obtained due to the use of different Rayleigh modeling methods. Thus, for a new proposed system or an existing system, the assessment of the collapse risk may result in an untrustworthy evaluation with respect to how the damping matrix is developed. Because in FEMA P-695, the procedure described for the modeling of inherent damping is not prescriptive enough to prevent the difference observed. Therefore, as a conclusion of the evaluation, it is recommended that modeling of inherent damping must be carefully considered.

4.3. The Critical Damping Ratio Limitation Approach

In the foregoing sections, the different Rayleigh modeling methods are evaluated based on the influence on the damping forces, energy dissipation rates, and the assessment of collapse risk. And, it is observed that the response was obtained differently due to developing the damping matrix differently with respect to the natural frequencies defined and how the stiffness is included. Therefore, CMR was obtained differently for each method.

The results demonstrate the importance of carefully consider or a more prescriptive method to modeling inherent damping for the inelastic systems. However, in FEMA P-695, the description for the modeling of the inherent damping does not clearly express a method for developing the damping matrix. Hence, the inherent damping is modeled in several different ways, which are resulted in the dissimilarity of CMR so the evaluation of a new proposed system or an existing system might be an untrustworthy assessment due to the way that damping matrix is developed.

None of the methods discussed herein is exact modeling method of the Rayleigh concept because it is not computational-efficient to include varying coefficients at each current state, therefore also, each method was occasioned to unintended consequences described in Section 2.6.6. From the previous results, it is concluded that another limitation is required to prevent the unintended consequences of the select modeling methods. Here, a new approach was proposed in order to achieve similar collapse margin ratios for the Rayleigh modeling methods used as regardless of how the damping matrix is developed.

In the approach, the critical damping ratio defined by FEMA P-695 is varied based on the limitation on the inherent damping energy dissipation to prevent the dissimilarity of CMRs. Hence, the approach allows to use any Rayleigh modeling method preferred with respect to unintended consequences because the energy dissipated is controlled by the limitation defined. In the present work, to apply the approach, the maximum energy dissipation limit was determined with respect to the energy results that are obtained from each method. However, in the future work, the limitation might be provided for each structure type by FEMA and/or ASCE 7 based upon their judgment, and experiences.

4.3.1. The Approach Procedure

Each ground-motion record causes the system results in different dynamic responses because of the potential diversity of the ground-motion characteristics, which is occasioned to obtain different dynamic amplification factors. Because of the different responses, the variation in the inelastic behavior or the plastic deformation range is obtained thus the energy dissipation rates are also observed differently. And, as expressed before, the influence of the Rayleigh modeling methods is more significantly noticed when large deformations are obtained. Therefore, firstly, the MDOF systems that subjected to the forty-four ground-motion records

were analyzed in order to pick the record that caused the maximum deformation for each system. The analysis results are demonstrated in Figure 4.13 and Figure 4.14 for each system, respectively.

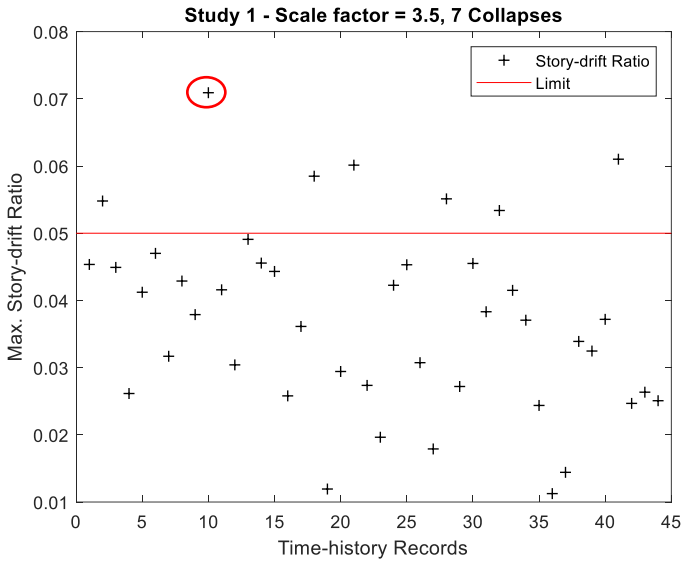

Figure 4.13: The four-story MDOF system - Displacement results for all records

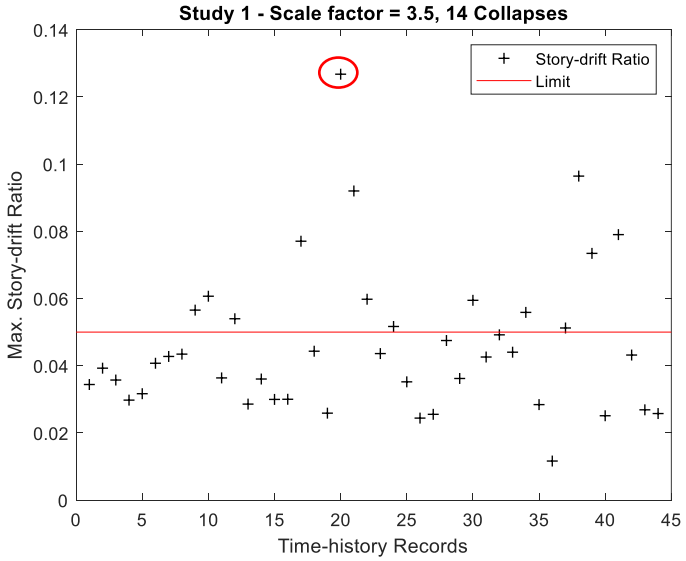

Figure 4.14: The nine-story MDOF system - Displacement results for all records

Here, the records that caused the maximum deformation was indicated for each MDOF system, respectively. For each modeling method, the analyses of the MDOF systems that subjected to the records indicated were performed in order to observe the percentage that expresses the rate of the amount of energy dissipated by the inherent damping. The percentages were determined by dividing the amount of the inherent damping energy by the total seismic energy imparted and among the percentages, the minimum one was indicated as a limitation that controls the maximum energy dissipated. However, the process for determining the limitation might not be required in the future, if FEMA P-695 and/or ASCE 7 provide the limitation based upon their judgment and experiences. Regardless, the percentages are listed in Table 4.5 and Table 4.6 for each MDOF system, respectively.

Table 4.5: The four-story MDOF system - Modified-critical damping ratios

Critical damping ratio limitation by using time-history ID: 5-2					
Study	**Input Energy / Percentage (%)**	**Inherent Energy Dissipation / Percentage (%)**	**Hysteretic Energy Dissipation / Percentage (%)**	**New Damping Ratio / Percentage (%)**	**New Inherent Energy Dissipation / Percentage (%)**
1	100	45.4	54.6	2.97	31.2
2	100	42.0	58.0	3.32	31.2
3	100	31.2	68.8	5.00	31.2
4	100	37.9	62.1	3.86	31.2
5	100	43.9	56.1	3.13	31.2
6	100	41.5	58.5	3.39	31.2
7	100	38.4	61.6	3.80	31.2
8	100	61.6	38.4	1.77	31.2
9	100	60.2	39.8	1.84	31.2
10	100	58.7	41.1	1.94	31.2

Table 4.6: The nine-story MDOF system - Modified-critical damping ratios

Critical damping ratio limitation by using time-history ID: 10-2					
Study	**Input Energy / Percentage (%)**	**Inherent Energy Dissipation / Percentage (%)**	**Hysteretic Energy Dissipation / Percentage (%)**	**New Damping Ratio / Percentage (%)**	**New Inherent Energy Dissipation / Percentage (%)**
1	100	31.1	68.9	2.93	22.1
2	100	26.2	73.8	3.88	22.1
3	100	22.1	77.9	5.00	22.1
4	100	25.3	74.7	4.09	22.1
5	100	29.6	70.4	3.19	22.1
6	100	26.4	73.6	3.81	22.1
7	100	25.8	74.2	3.96	22.1
8	100	45.8	54.2	1.50	22.1
9	100	44.1	55.9	1.61	22.1
10	100	43.7	56.3	1.63	22.1

Here, the maximum energy dissipation limit was determined as 31.2% and 22.1% of the seismic energy imparted for the four-story and nine-story MDOF systems, respectively. However, Rayleigh modeling methods were caused the system to result in different energy rates. Therefore, for each method that resulted in more energy dissipation than the limit, the critical damping ratio was modified in order to control the variation in the energy rates or prevent the non-conservative results.

In the Rayleigh concept, the damping matrix is developed with respect to the stiffness and mass-proportional coefficients that are a function of the natural frequencies and the critical damping ratios. With this in mind, the approach provides preventing to obtain more energy absorption than it is by modifying the critical damping ratio for each method. Based on the approach, the MDOF systems, which subjected to the records indicated, might be simulated several times in order to find a new critical damping ratio, which supplies less energy dissipation

than the limit. After each analysis is performed, the energy percentage is determined and compared with the limit. Based on the comparison, the critical damping ratio might be decreased and the process is repeated until the energy percentage is obtained under the limit.

Although any ratio that supplies less energy than the limit might be used, here in all methods, the critical damping ratio was set as to obtain exactly the maximum energy dissipation limit in order to evaluate the influence of the approach on CMRs. The maximum energy dissipation limit was determined as 31.2% and 22.1% of the seismic energy imparted for the four-story and nine-story MDOF systems, respectively. For instance, for the first method, the four-story MDOF was analyzed several times to observe the exactly 31.2% inherent energy dissipation rate and the energy rate was observed, when the critical damping ratio was set as 2.97%. The damping ratios that are modified for all methods are listed in Table 4.5 and Table 4.6 for each MDOF system, respectively.

4.3.2. Influence of the Approach on Collapse Margin Ratio

Firstly, the critical damping ratios, which were defined with respect to the maximum energy dissipation limit, were defined into the dynamic load case form illustrated in Figure 3.2 thus the mass and stiffness-proportional coefficients were regenerated for each method. Next, IDA was performed, in which the modified-systems subjected to the scaled forty-four individual ground-motion records were analyzed. Nevertheless, the maximum forces in BRBs and displacements were compared with the fracture points and displacement determined with respect to the story-drift limit in order to find the scale factor that causes the one-half of the records resulted in exceed strength capacity or story-drift limit.

Similarly, the allowable maximum displacement was determined as 3.12 inches which correspond to two percent of the story height; however, it was multiplied with Over-strength

factor that is defined as 2.5 thus the story-drift limit was defined as five percent. Here, for the modified-first, the results are demonstrated in Figure 4.15. The results for the other methods are illustrated in Appendix D.1 for each MDOF system.

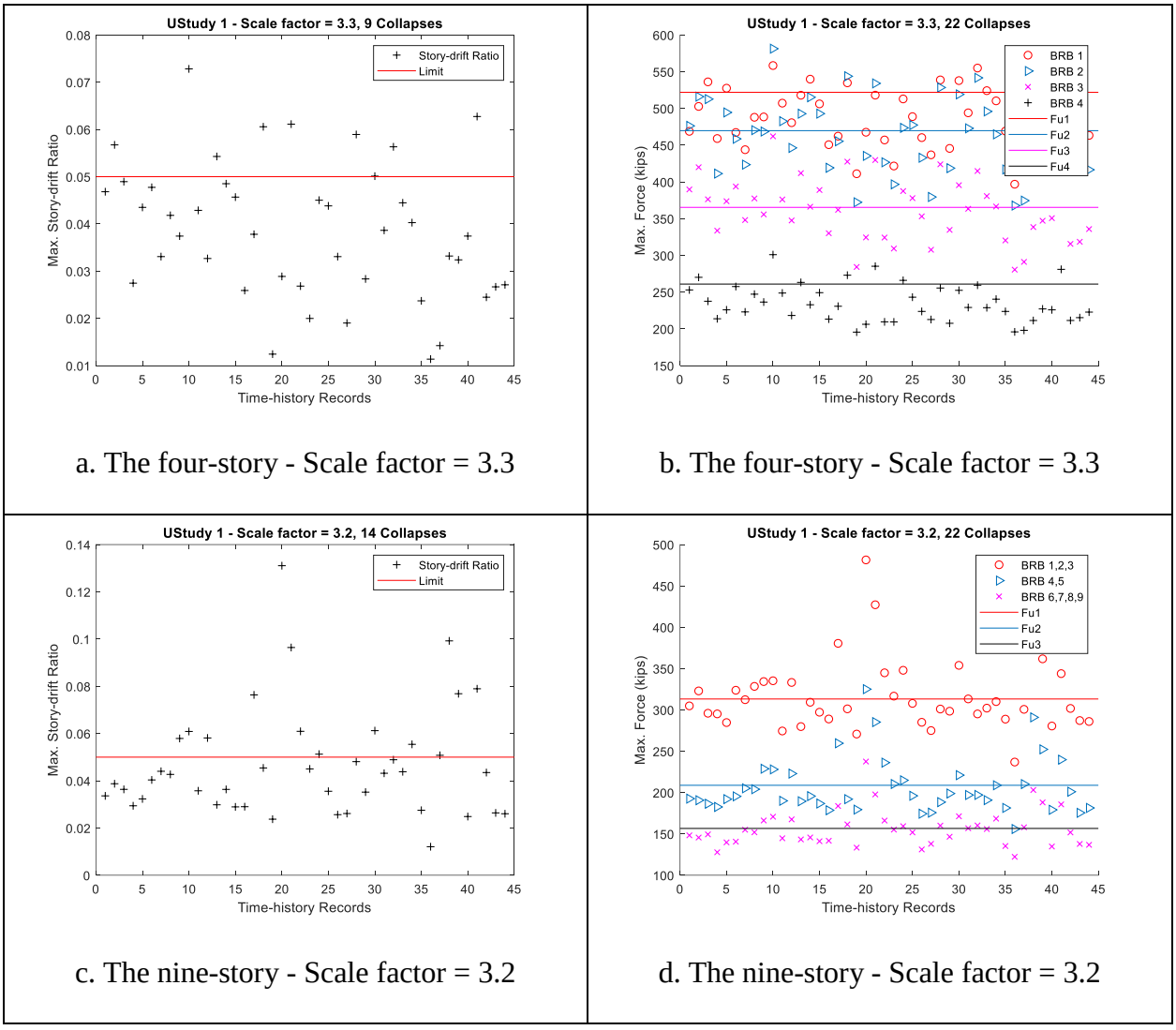

a. The four-story - Scale factor = 3.3

b. The four-story - Scale factor = 3.3

c. The nine-story - Scale factor = 3.2

d. The nine-story - Scale factor = 3.2

Figure 4.15: The MDOF systems - Updated IDA results for the first method

The scale factor range to perform IDA were selected carefully so as to supply a significant reduction in the computation time. Here, the scale factors (in tenths) were determined as close as enough to the precise factor (in hundredths) because of the computation time and the results are listed in Table 4.7 and Table 4.8 for each MDOF system, respectively.

Similarly, $\hat{S}_{CT}$ value, which is the intensity at the collapse point, was determined by multiplying the median value of the normalized record set (shown in Figure 2.18) by the scale factor determined. Nevertheless, the S_{MT} values are demonstrated in Figure 3.22. Lastly, for each method, CMR was determined by dividing the $\hat{S}_{CT}$ value by the S_{MT} value and the results are listed in Table 4.7 and Table 4.8 for each MDOF system, respectively.

Table 4.7: The four-story MDOF system - Updated collapse margin ratios

Study	**Approach**	**Stiffness Options**	**1st Frequency**	**2nd Frequency**	**S_{MT} (g)**	**New Scale factor**	**S_{CT} (g)**	**CMR**
1	A	Initial Stiffness	1st frequency	2nd frequency	1.11	3.30	1.460	1.32
2	B	Tangent Stiffness	1st frequency	2nd frequency	1.11	3.10	1.372	1.24
3	C	Mass Only	1st frequency	2nd frequency	1.11	3.20	1.416	1.28
4	D	Elastic Elements	1st frequency	2nd frequency	1.11	3.20	1.416	1.28
5	A	Initial Stiffness	1st frequency	3rd frequency	1.11	3.30	1.460	1.32
6	B	Tangent Stiffness	1st frequency	3rd frequency	1.11	3.10	1.372	1.24
7	D	Elastic Elements	1st frequency	3rd frequency	1.11	3.20	1.416	1.28
8	A	Initial Stiffness	2nd frequency	3rd frequency	1.11	3.20	1.416	1.28
9	B	Tangent Stiffness	2nd frequency	3rd frequency	1.11	3.20	1.416	1.28
10	D	Elastic Elements	2nd frequency	3rd frequency	1.11	3.20	1.416	1.28

Table 4.8: The nine-story MDOF system - Updated collapse margin ratios

Study	**Approach**	**Stiffness Options**	**1st Frequency**	**2nd Frequency**	**S_{MT} (g)**	**New Scale factor**	**S_{CT} (g)**	**CMR**
1	A	Initial Stiffness	1st frequency	2nd frequency	0.187	3.20	0.666	3.56
2	B	Tangent Stiffness	1st frequency	2nd frequency	0.187	3.10	0.645	3.45
3	C	Mass Only	1st frequency	2nd frequency	0.187	3.00	0.624	3.34
4	D	Elastic Elements	1st frequency	2nd frequency	0.187	3.10	0.645	3.45
5	A	Initial Stiffness	1st frequency	3rd frequency	0.187	3.10	0.645	3.45
6	B	Tangent Stiffness	1st frequency	3rd frequency	0.187	3.10	0.645	3.45
7	D	Elastic Elements	1st frequency	3rd frequency	0.187	3.00	0.624	3.34
8	A	Initial Stiffness	2nd frequency	3rd frequency	0.187	3.00	0.624	3.34
9	B	Tangent Stiffness	2nd frequency	3rd frequency	0.187	3.00	0.624	3.34
10	D	Elastic Elements	2nd frequency	3rd frequency	0.187	3.00	0.624	3.34

As a result, it is observed that the 20% difference, which is obtained on CMRs due to the use of different Rayleigh modeling methods, was decreased to approximately three to four percent because of the critical damping ratio limitation applied on each method. In addition, here it is observed that none of the methods resulted in over ratio than it is expected due to the control on the energy dissipation. Thus, this might be interpreted that for a new proposed system or an existing system, the assessment of the collapse risk results in a reliable evaluation now because of the approach.

The approach provides a limitation that prevents the unintended and non-conservative results so the damping matrix is developed using any natural frequencies, which determined

based on the system properties, or any stiffness options selected. In a conclusion, the approach is recommended to FEMA P-695 and ASCE 7 so they may expand their procedure in order to make it prescriptive enough to prevent unintended and non-conservative consequences.

4.3.3. An Example Application of the Approach

Here to show the process for determining a new critical damping ratio, the approach was applied to the nine-story MDOF system. Besides, it should be noticed that the approach was not applied by the peer review panel of FEMA P-695 so the maximum energy dissipation limit was not defined by them. Alternatively, the limit must be defined in order to apply the approach, therefore, it is deemed that the maximum energy dissipation limit is determined as 22.1% for the type of the MDOF system described here. The first method that is illustrated in Table 3.2 was preferred to model the inherent damping. Regardless, the whole process was performed by using the SAP2000^{TM}, therefore, the example application of the approach is discussed here with respect to the SAP2000^{TM}.

Firstly, the MDOF system that subjected to the forty-four ground-motion records were analyzed in order to pick the record that caused the maximum displacement. The analysis results are demonstrated in Figure 4.14 and the record is indicated as time history ID: 10-2. Next, the MDOF system that subjected to the record was analyzed in order to observe the percentage that expresses the rate of the amount of energy dissipated by the inherent damping. After the analysis, the plots for the amount of the inherent damping energy dissipation (damping energy), and the total seismic energy imparted (input energy) were obtained easily from the display option in SAP2000^{TM} and are demonstrated in Figure 4.16. The percentage, which is illustrated in Table 4.6, was obtained as 31.1% by dividing the amount of the damping energy (3430 kips-in) by the amount of the input energy (11030 kips-in).

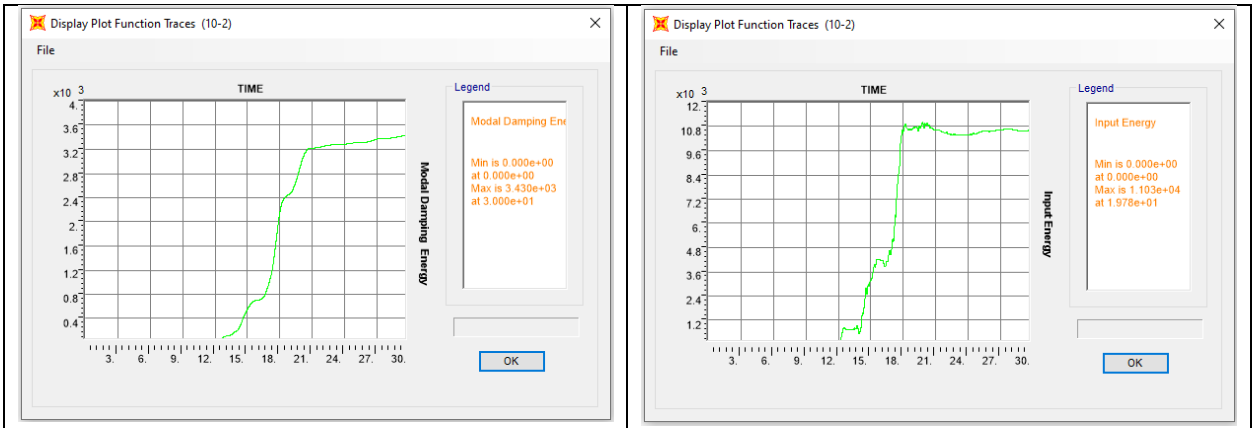

a. The damping energy

b. The input energy

Figure 4.16: Energy results of the nine-story MDOF system subjected to TH ID: 10-2

Here, it is observed that the percentage obtained is exceeded the maximum energy dissipation limit that is defined as 22.1%. Therefore, five percent critical damping ratio was modified to four percent in order to obtain less energy than the limit and new ratio was defined into the dynamic load case form that is illustrated in Figure 3.2 thus the mass and stiffness-proportional coefficients were regenerated for the first method. Next, the modified-MDOF system was analyzed and the percentage was determined as 27.1%. However, it is still exceeded the limit, therefore, the same process was repeated by using the critical damping ratios that were modified as 3.1% and 2.93% and the percentages were obtained as 22.3% and 22.1%, respectively. Thus, the new critical damping ratio was determined as 2.93% with respect to the limitation defined.

CHAPTER 5:

CONCLUSIONS AND FUTURE WORK

Here, succinct summary of the present work, observations, interpretation of the numerical results, conclusions and recommendations are discussed.

5.1. Summary

The present work might be summarized in three parts: numerical analysis of the SDOF system, numerical analysis of the MDOF systems, and the application of the energy limitation approach. Note that, herein SAP2000^{TM} was used to perform analysis and its Open Application Programming Interface (OAPI) was utilized as a combination of SAP2000^{TM} and MATLAB to use the graphical power of MATLAB.

In the first part, the methods listed in Table 3.1 were modeled on the SDOF system described in Section 3.3 and the system was analyzed in order to observe the stiffness and mass contributions separately in the damping matrix, as well as to evaluate energy dissipations. And, it is observed that in each Rayleigh modeling method, the damping matrix was developed differently due to the use of different stiffness options and the coefficients. Similarly, the hysteresis behaviors and energy dissipations were obtained differently for each method. Next, the forty-four time-history records required by the FEMA P-695 were applied to the SDOF system and the maximum displacements obtained were evaluated. And, the evaluation clearly indicates that significant differences in the response are obtained for the same five percent damping ratio.

In the second part, the four- and nine-story Buckling Resisting Brace Frame (BRBF) archetypes provided by the report (Kircher et al., 2010) and approved by the peer panel of FEMA P-695 were utilized to evaluate the methods listed in Table 3.2. To be inclusive of different effects, the archetypes were carefully selected based on their frequency, story numbers, and

Seismic Design Category (SDC). First, the four-story MDOF system subjected to the selected time-history record was analyzed and seismic energy imparted (input energy), hysteresis energy dissipation, and inherent damping energy dissipation results for each method were compared. And, it is observed that significant differences in the response were obtained due to different energy dissipation results thus the hysteresis behaviors and energy dissipation rates were obtained differently for each method. Next, to observe how the collapse margin ratio (defined by FEMA P-695) affected due to use of different methods, the MDOF systems subjected to the forty-four time-history records were analyzed and different collapse margin ratios were obtained for each method. And, this demonstrates the importance of carefully consider and/or a more prescriptive method to modeling damping.

The results obtained in the second part indicate that another limitation is required to prevent the unintended consequences of the selection of the modeling methods. Herein, a new approach is provided as varying the critical damping ratio based on limiting energy dissipated by inherent damping to prevent the issue explained above. By using the approach, it is aimed to achieve a similar collapse margin ratio regardless of the method preferred.

In the third part, the MDOF systems were simulated with the forty-four time-history records in order to pick the time-history record that causes the maximum displacement. First, for each method, the systems were simulated with the time-history record picked to determine the percentage which is calculated by dividing the inherent damping energy dissipation to the input energy. Next, among the percentages, the minimum one was accepted as a limit so any modeling method that resulted in more inherent damping energy dissipation than the limit needs to be modified by varying the critical damping ratio. Therefore, the systems were simulated several times in order to obtain a new critical damping ratio that supplies less energy dissipation than the

limit and the ratios were modified for each method. Lastly, the incremental dynamic analyses were performed on the systems modeled with respect to the modified-ratios and it is observed that the approach provides to obtain similar collapse margin ratios regardless of the method used.

5.2. Conclusions and Recommendations

The overall goals of the present work as stated in Chapter 1 are; to evaluate the methods developed for modeling of Rayleigh damping in structures designed by using performance-based criteria and to present an approach that prevents the possible dissimilarity in the assessment.

The following conclusions are drawn for each of the objectives:

1. The first objective was accomplished by evaluating the most common modeling methods of Rayleigh damping and is discussed below.
    - First, it is observed that the damping forces determined using the Rayleigh mathematical model are proportional to the velocity, how the stiffness is included, and the coefficients. Therefore, in each Rayleigh modeling method, the damping matrix was developed differently due to the use of different stiffness approaches and the coefficients and this resulted in significant differences in damping forces that cause to obtain different responses.
    - Next, to describe the crux of the analysis, energy dissipations were computed and compared and it is observed that the hysteresis behaviors and the energy dissipations were obtained differently for each method.
    - Lastly, because the previous numerical results are interpreted that the methods might be resulted in a different assessment of the collapse risk, IDA progress was performed and the numerical results of the SDOF system clearly indicate that significant differences in the response are obtained due to different

modeling methods (with the same five percent damping ratio). However, the analysis does not tell the entire story so it is rigor is increased to MDOF systems to evaluate CMRs.

2. The second objective was accomplished by performing IDA for the MDOF systems to observe how the collapse margin ratio is affected by the selection of the modeling methods and is discussed below.
    - First, to observe how the methods affect the response of MDOF systems, energy dissipations were computed and compared. And, it is observed that in each Rayleigh modeling method, the damping matrix is developed differently due to the use of different stiffness approaches and the natural frequencies and this resulted in different inherent damping energy dissipations. Because of the different energy dissipations, significant differences in the response were obtained thus the hysteresis behavior of the BRBs and the energy dissipation rates were obtained differently for each method.
    - Second, because of the significant differences obtained, the analysis was expanded to assess the criticality of the assumed method for the risk of collapse in a seismic event as determined by FEMA P-695. And, it is observed that in CMRs, approximately 20% difference might be obtained due to the use of different Rayleigh modeling methods. This might be interpreted that for a new proposed system or an existing system, the assessment of the collapse risk may result in an untrustworthy evaluation with respect to how the damping matrix is developed.

3. The third objective was accomplished by applying the critical damping ratio limitation approach to each method in order to prevent the unintended consequences. And, it is observed that the limitation provided by the approach prevents the unintended and non-conservative results thus the damping matrix might be developed using any natural frequencies or any stiffness approach selected.
4. To accomplish the fourth objective following recommendations and conclusions are presented.
    - First, the evaluation of the modeling methods indicated that the procedure for the modeling of inherent damping described in FEMA P-695 is not prescriptive enough to prevent obtaining the significant differences in the response. Because, presently, FEMA P-695 only specifies five percent, but is mute on the manner in how this value is used and it is left to the peer-review committee to review and approve. Therefore, as a conclusion of the evaluation, it is recommended that modeling of inherent damping must be carefully considered, or else a more prescriptive method might be presented in FEMA P-695.
    - Second, herein, the numerical results indicate that the approach provides to achieve similar CMR for each method. Therefore, for each structure type, a limitation of the maximum energy dissipated by inherent damping might be provided by FEMA P-695, and ASCE 7 based upon their judgment and experiences. Thus, inherent damping might be modeled with any Rayleigh method that utilize a critical damping ratio that supplies less energy dissipation than the limit defined. As a result, the approach is recommended to

FEMA P-695 and ASCE 7 to prevent unintended consequences of different modeling methods.

5.3. Implications

The new approach may provide code writing committees, and authorities having jurisdiction, a definitive method for consistently prescribing/limiting inherent damping energy as a percent of seismic energy input, thereby forcing the remainder of the energy dissipation into planned inelastic deformations. This provides similar collapse margin ratios invariant with the particularities of the Rayleigh method.

REFERENCES

AISC, A. (2010). AISC 341-10, seismic provisions for structural steel buildings. *Chicago, IL: American Institute of Steel Construction*.

American Society of Civil Engineers. (2017). *Minimum design loads and associated criteria for buildings and other structures: ASCE/SEI 7-16.* Published by American Society of Civil Engineers.

Black, C., Aiken, I. D., & Makris, N. (2002). *Component testing, stability analysis, and characterization of buckling-restrained unbonded braces (TM).* Pacific Earthquake Engineering Research Center.

Boresi, A. P., & Schmidt, R. J. (2003). *Advanced mechanics of materials* (6th ed). John Wiley & Sons.

Carr, A. J., Puthanpurayil, A. M., Lavan, O., & Dhakal, R. P. (2017). *DAMPING MODELS FOR INELASTIC TIME-HISTORY ANALYSES-A PROPOSED MODELLING APPROACH*. 11.

Charney, F. A., & Barngrover, B. (2012). *NONLIN: Software for Earthquake Engineering Education*. 1–12. https://doi.org/10.1061/40700(2004)177

Charney, F., Lopez-Garcia, D., Hardyniec, A., & Ugalde, D. (2017). *MODELING INHERENT DAMPING IN NONLINEAR DYNAMIC ANALYSIS*. 12.

Charney, Lopez-Garcia, D., Hardyniec, A., & Ugalde, D. (2017). *MODELING INHERENT DAMPING IN NONLINEAR DYNAMIC ANALYSIS*. 12.

Chopra, A. K. (2012). *Dynamics of Structures* (4 edition). Pearson.

Chopra, A. K., & McKenna, F. (2016). Modeling viscous damping in nonlinear response history analysis of buildings for earthquake excitation. *Earthquake Engineering & Structural Dynamics*, *45*(2), 193–211. https://doi.org/10.1002/eqe.2622

Computers and structures INC. (2020). *CSi OAPI Documentation.* Berkeley , California, USA.

Dubina, D., Ungureanu, V., & Landolfo, R. (2012). Design of cold-formed steel structures. *Eurocode*, *3*, 1–3.

Hall, J. F. (2006). Problems encountered from the use (or misuse) of Rayleigh damping. *Earthquake Engineering & Structural Dynamics*, *35*(5), 525–545. https://doi.org/10.1002/eqe.541

Kersting, R. A., Fahnestock, L. A., & Lopez, W. A. (2016). *Seismic design of steel buckling-restrained braced frames: A guide for practicing engineers* (NIST GCR 15-917-34; p. NIST GCR 15-917-34). National Institute of Standards and Technology. https://doi.org/10.6028/NIST.GCR.15-917-34

Kircher, C., Deierlein, G., Hooper, J., Krawinkler, H., Mahin, S., Shing, B., & Wallace, J. (2010). *Evaluation of the FEMA P-695 Methodology for Quantification of Building Seismic Performance Factors*. https://www.nist.gov/publications/evaluation-fema-p-695-methodology-quantification-building-seismic-performance-factors

Lu, Y., & Morris, G. R. (2017). *ASSESSMENT OF THREE VISCOUS DAMPING METHODS FOR NONLINEAR HISTORY ANALYSIS: RAYLEIGH WITH INITIAL STIFFNESS, RAYLEIGH WITH TANGENT STIFFNESS, AND MODAL*. 12.

Marshall, J. D. (2021). Buckling-Restrained Braces and Their Implementation in Structural Design of Steel Buildings. In M. Beer, I. A. Kougioumtzoglou, E. Patelli, & I. S.-K. Au

(Eds.), *Encyclopedia of Earthquake Engineering* (pp. 1–11). Springer Berlin Heidelberg. https://doi.org/10.1007/978-3-642-36197-5_313-1

PEER Ground Motion Database—PEER Center. (n.d.). Retrieved September 8, 2020, from https://ngawest2.berkeley.edu/

Quantification of Building Seismic Performance Factors. (2009). U.S. Department of Homeland Security, FEMA.

Rajasekaran, S. (2009). *Structural dynamics of earthquake engineering: Theory and application using MATHEMATICA and MATLAB*. Elsevier.

SAP2000, C. (2017). Integrated finite element analysis and design of structures. *Computers and Structures*.

Strømmen, E. N. (2014). *Structural dynamics*. Springer.

Tao, D., Lin, J., & Lu, Z. (2019). Time-Frequency Energy Distribution of Ground Motion and Its Effect on the Dynamic Response of Nonlinear Structures. *Sustainability*, *11*(3), 702.

Thorby, D. (2008). *Structural dynamics and vibration in practice: An engineering handbook*. Butterworth-Heinemann.

Williams, A. (2011). *Steel Structures Design ASD/LRFD*. McGraw-Hill.

Zareian, F., & Medina, R. A. (2010). A practical method for proper modeling of structural damping in inelastic plane structural systems. *Computers & Structures*, *88*(1), 45–53. https://doi.org/10.1016/j.compstruc.2009.08.001

APPENDIX A: METHODOLOGY

Here, the appendix is divided into four parts; modeling of Rayleigh damping for nonlinear analysis using SAP2000^{TM}, Fast Fourier Transform for the forty-four time-history record, the MATLAB code for SAP2000^{TM} - API, and modeling of the MDOF systems. And,

- the details of the stiffness options and the coefficients used,
- modeling of the Rayleigh methods in SAP2000^{TM},
- FTT of each ground-motion record,
- some portion of the MATLAB code for SAP2000^{TM} - API, and
- details for modeling of the MDOF systems

are provided.

A.1. Modeling of Rayleigh Damping for Nonlinear Analysis using SAP2000™

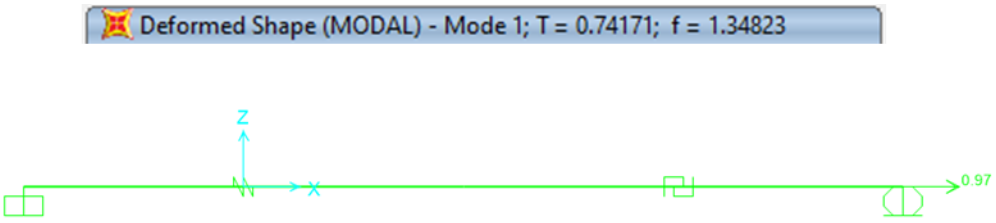

Figure A.1: SAP2000™ model for the SDOF system

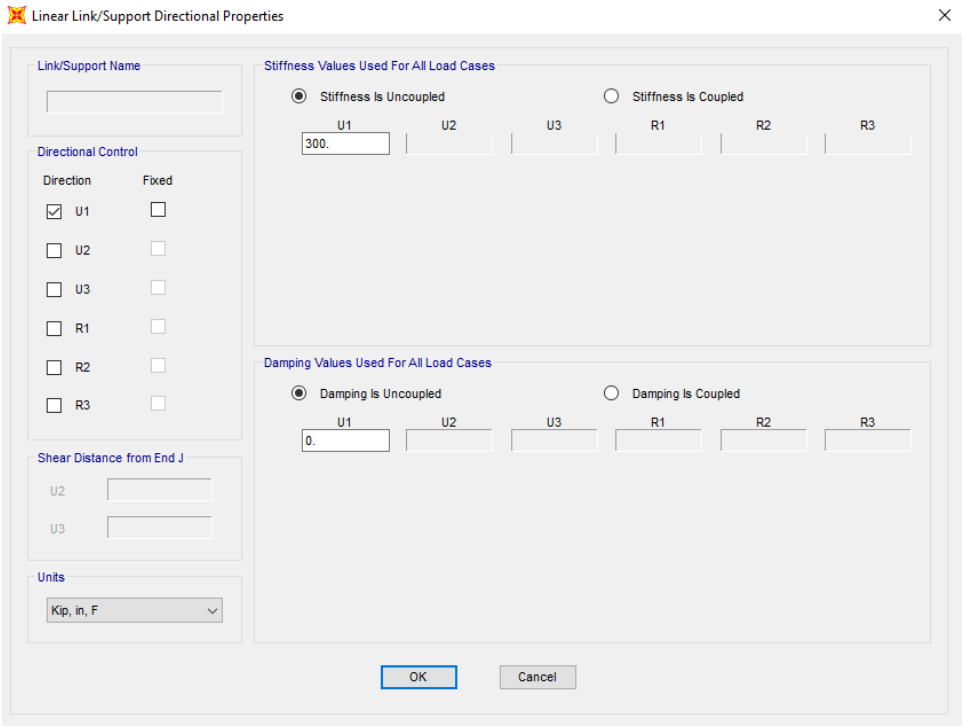

Figure A.2: Modeling of brace element (SAP2000, 2017)

```
------------------
ANALYSIS TYPE = NONLINEAR

STRUCTURAL PROPERTIES AS INPUT
Initial Stiffness                    69.680 k/in
Strain Hardening Stiffness            2.430 k/in
Structure Yield Strength             70.000 k
Yield Displacement                    1.005 in

Structural Weight                   374.903 k
Structural Damping                    0.000 % Critical

STRUCTURAL PROPERTIES DERIVED FROM INPUT:
Structure Mass (Mass Units)           0.971 k-sec2/in
Structure Circular Frequency          8.471 radians/sec
Structure Cyclic Frequency            1.348 Hertz
Structure Period of Vibration         0.742 seconds
Structural Damping Constant           0.000 k-sec/in

FORCING FUNCTION PROPERTIES:
Title       NORTHRIDGE EQ 1/17/94, 12:31, BEVERLY HILLS - 14145 MULH, 009 (USC STATION
90013
Absolute Maximum Value                0.416
Number of Data Points                  2999
Digitization Timestep                 0.010 seconds
Analytical Timestep                  0.0004 seconds

SUMMARY OF RESPONSE MAXIMA:
Maximum Inertial Force              188.1174 k
Maximum Damping Force                 0.0000 k
Maximum Spring Force                81.8553 k
Maximum Damping + Spring Force      81.8490 k
Maximum Total Force (D+S+I)         155.8783 k
Maximum Computed Displacement         5.8833 in
Maximum Computed Velocity           25.7579 in/sec
Maximum Computed Acceleration       193.7357 in/sec2
Number of Yield Excursions               44
Displacement Ductility Demand         5.8564
```

Figure A.3: NONLIN results for the SDOF system

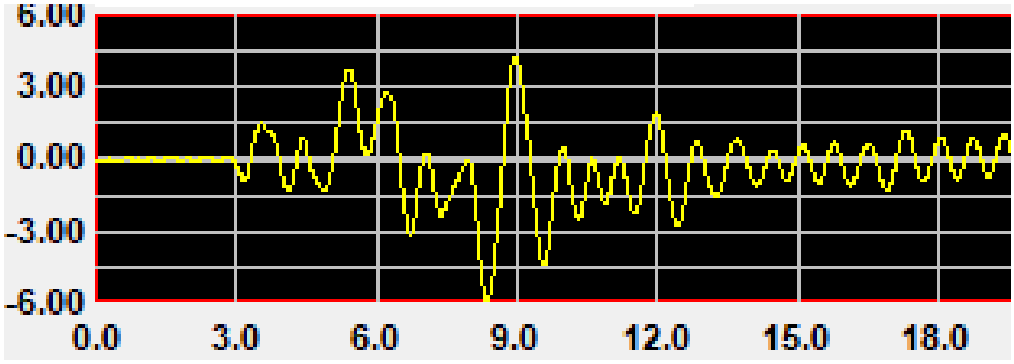

a. NONLIN - displacements result

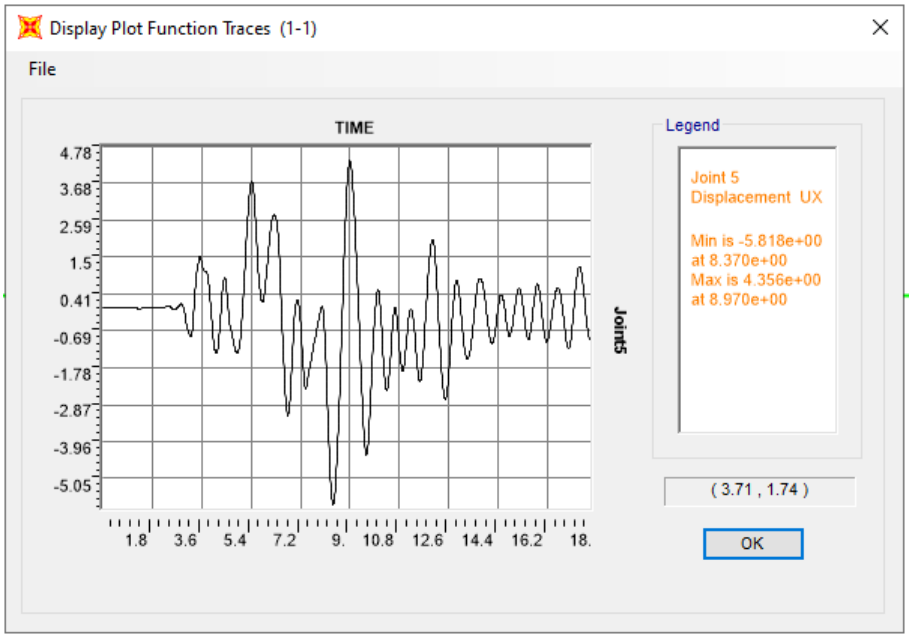

b. SAP2000™ - displacements result

Figure A.4: Comparison of SAP2000™ and NONLIN based on displacement results

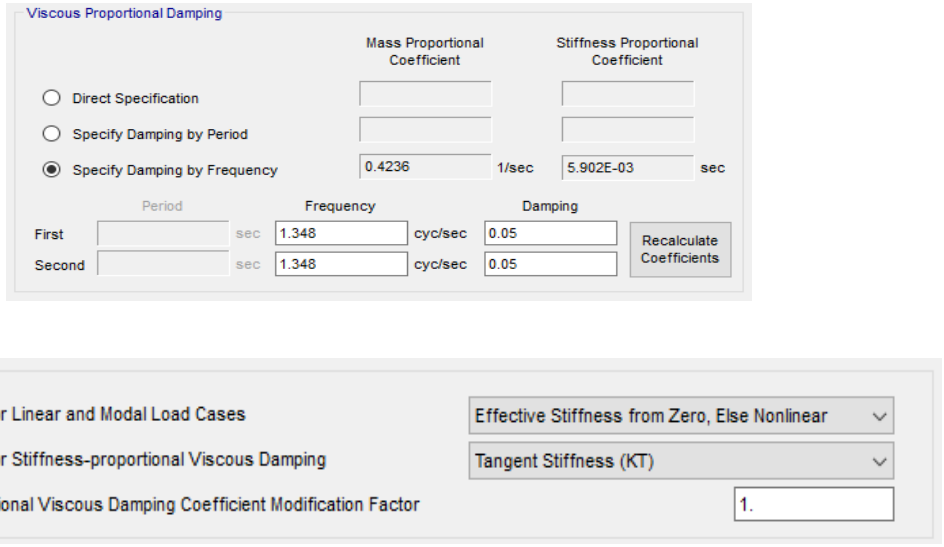

a. The dominant frequencies and stiffness options for the second method

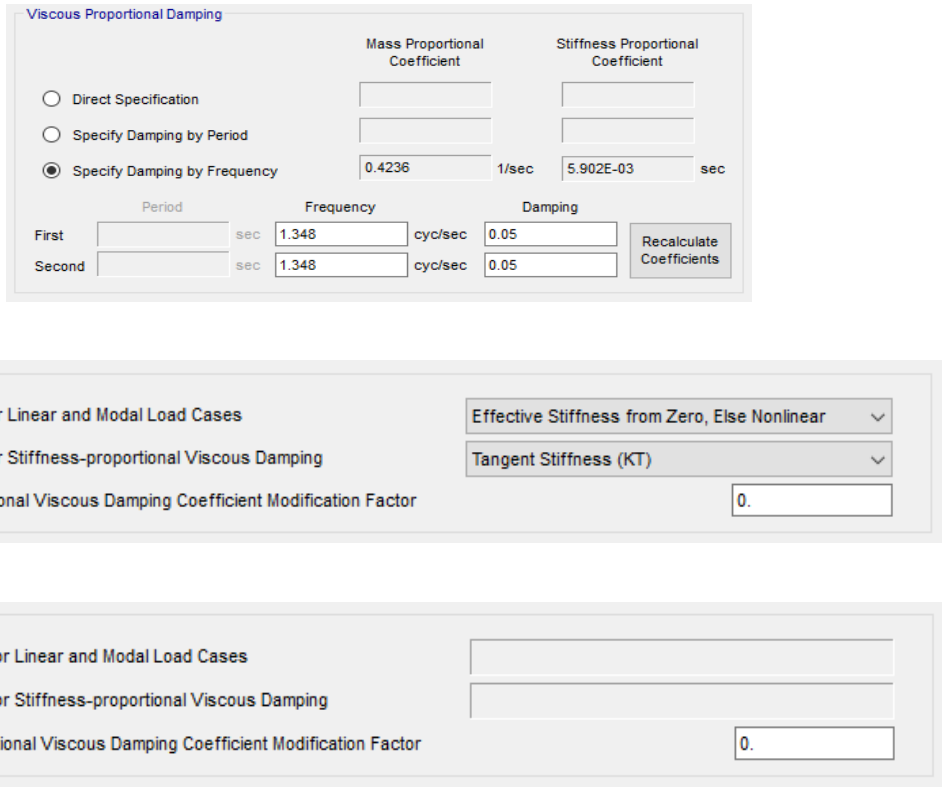

b. The dominant frequencies and stiffness options for the third method

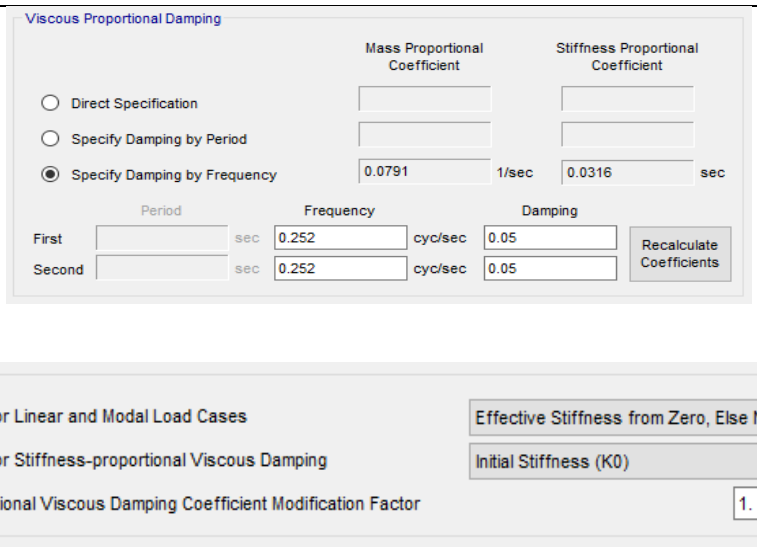

c. The dominant frequencies and stiffness options for the fourth method

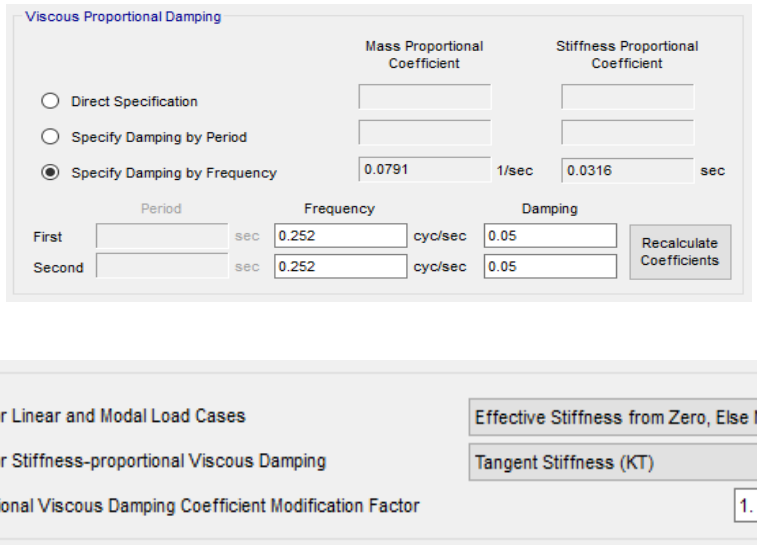

d. The dominant frequencies and stiffness options for the fifth method

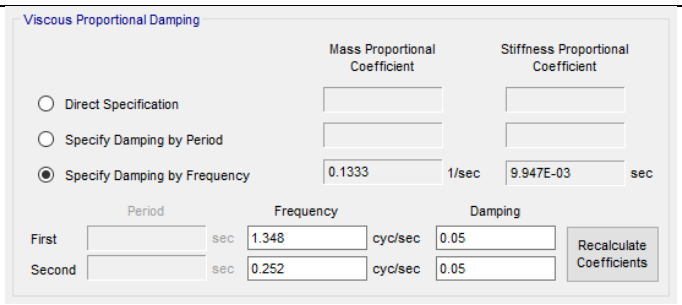

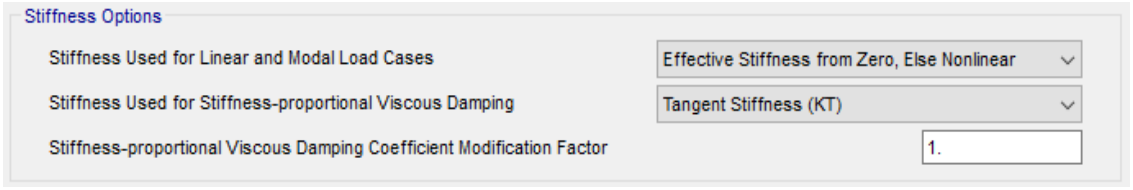

e. The dominant frequencies and stiffness options for the sixth method

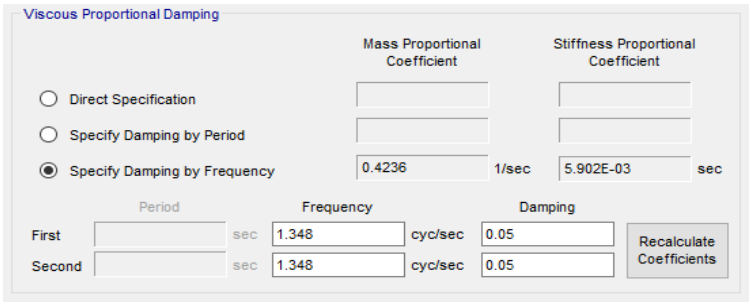

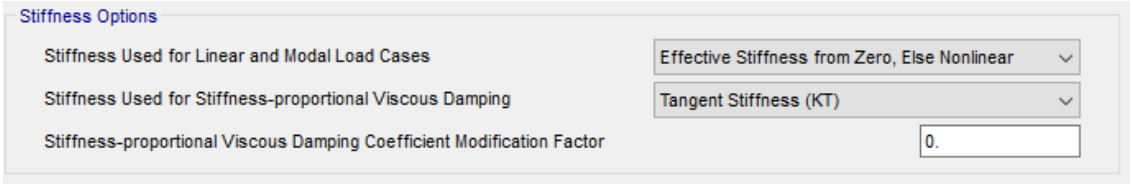

f. The dominant frequencies and stiffness options for the seventh method

Figure A.5: Modeling of the Rayleigh damping methods

A.2. Fast Fourier Transform for the Forty-four Time-History Records

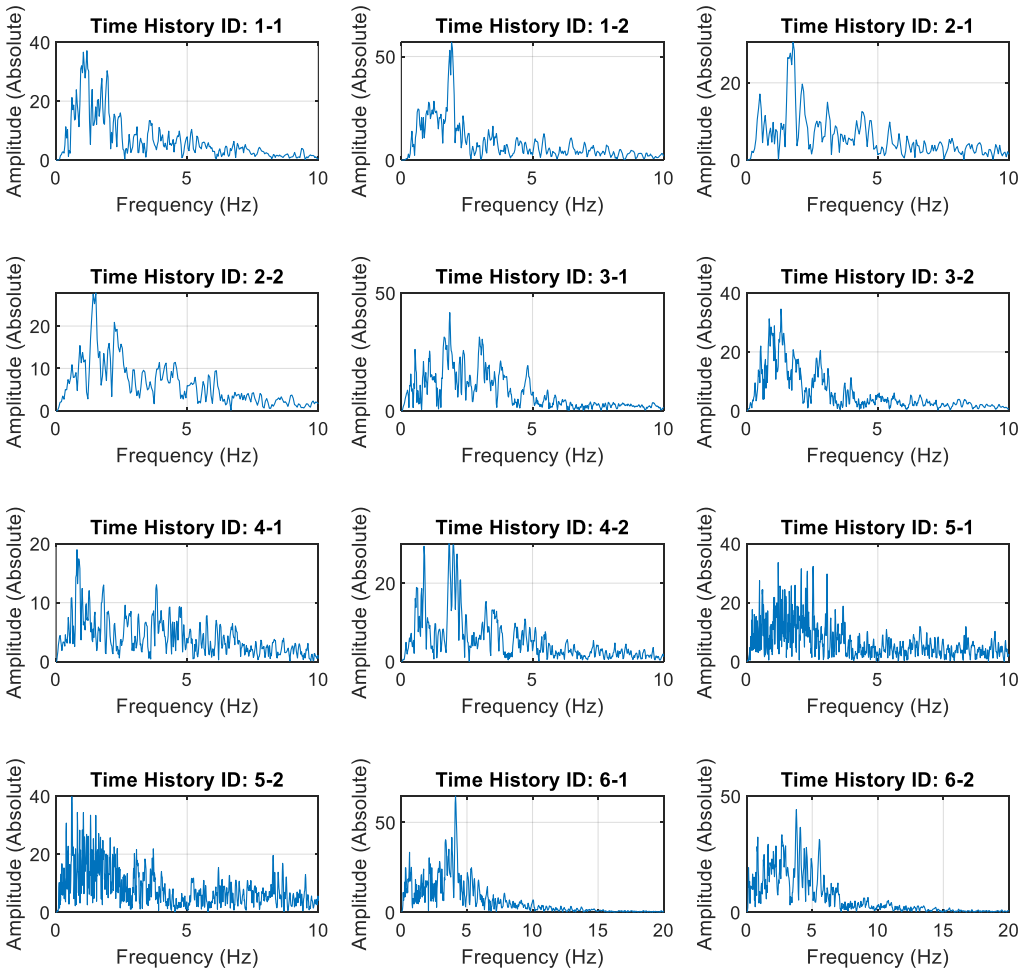

Figure A.6: Fast Fourier Transform for time-history records ID: 1 to 6

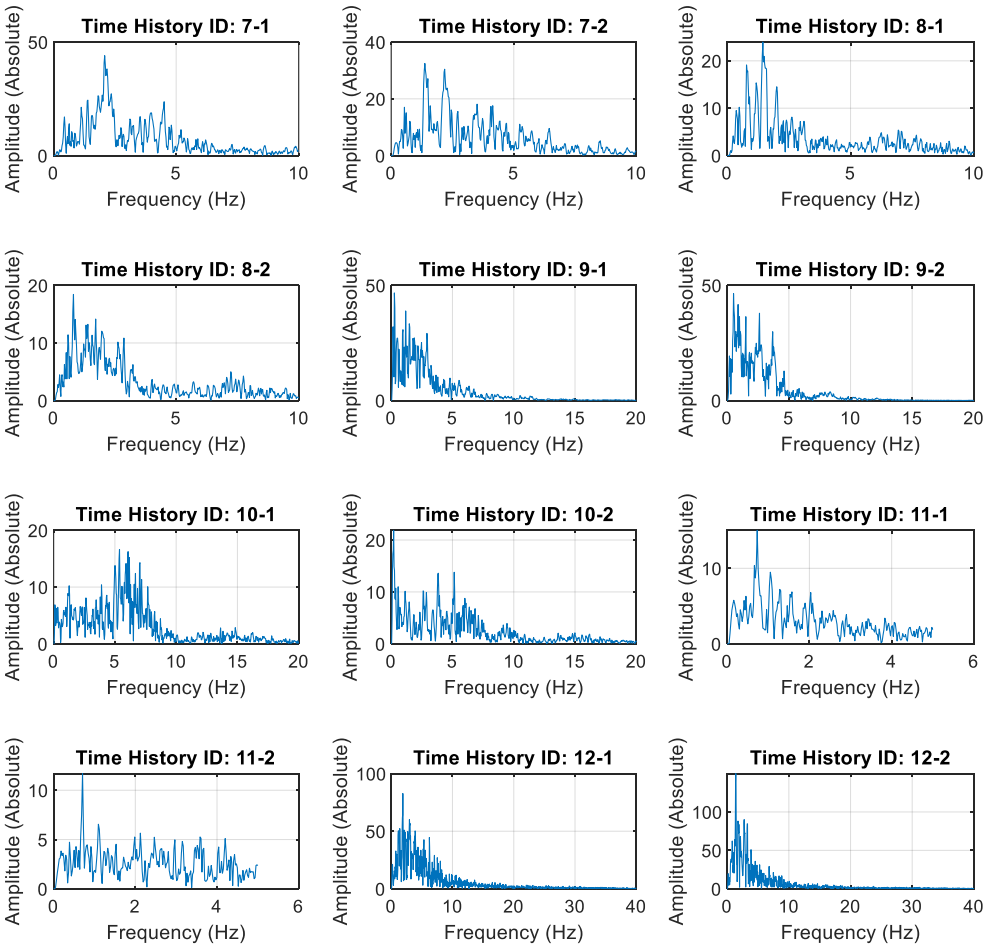

Figure A.7: Fast Fourier Transform for time-history records ID: 7 to 12

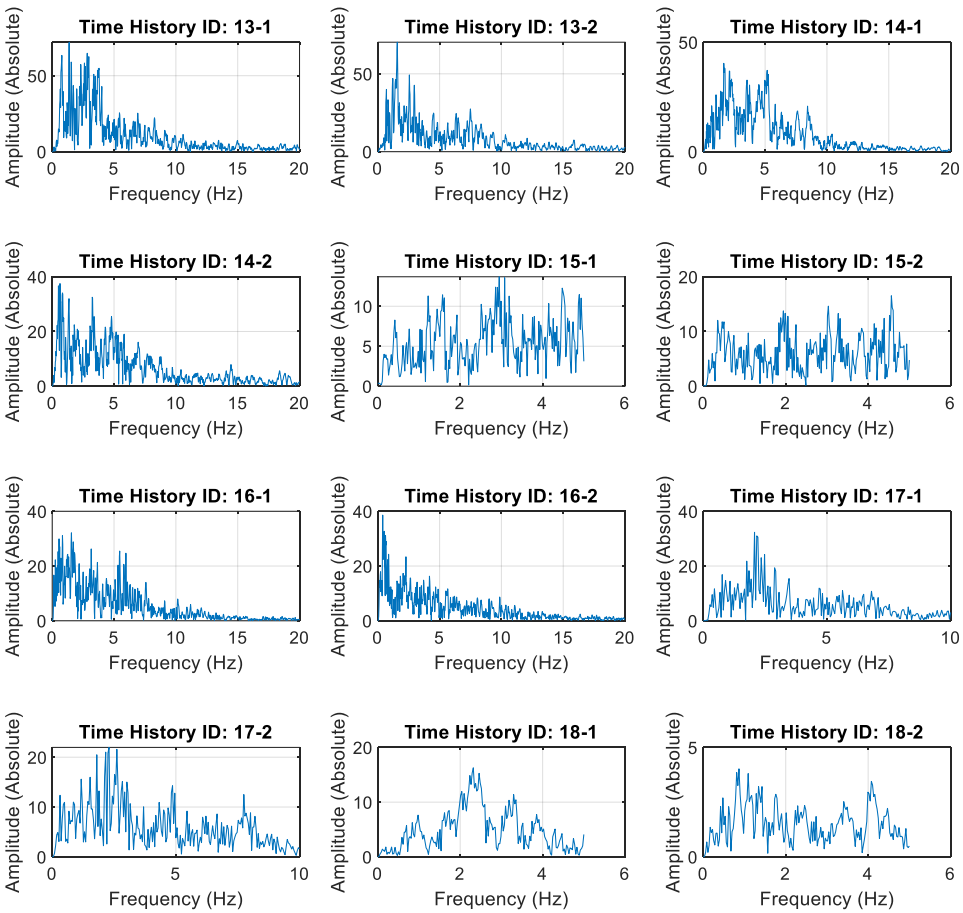

Figure A.8: Fast Fourier Transform for time-history records ID: 13 to 18

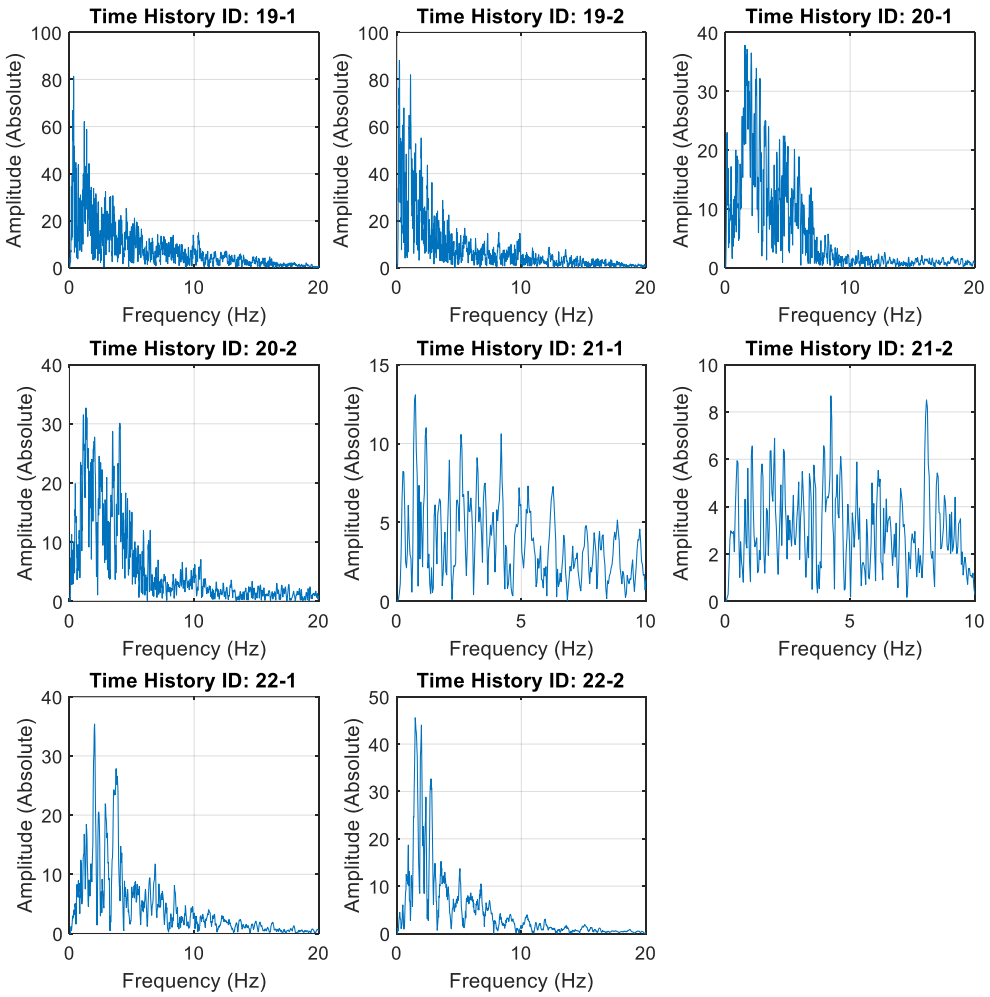

Figure A.9: Fast Fourier Transform for time-history records ID: 19 to 22

A.3. The MATLAB code for SAP2000™ - API

```
%Joint results

 for b=1:44

  ret = AnalysisResultsSetup.DeselectAllCasesAndCombosForOutput;

  ret = AnalysisResultsSetup.SetCaseSelectedForOutput(EQ(b));

  ret = AnalysisResultsSetup.SetOptionDirectHist(2);

  ResultU1=zeros(Estep(ceil(b/2))+1,44);
  ResultF1=zeros(Estep(ceil(b/2))+1,44);
% Joint Disp.
JointID = NET.createArray('System.String',44);
JointID(1) = '5';
JointID(2) = '1';
JointID(3) = '4';

for k=1:3
[ret, NumberResults, Obj, Elm, ACase, StepType, StepNum, U1, U2, U3, R1, ...
    R2, R3] = AnalysisResults.JointDispl(JointID(k), SAP2000v1.eItemTypeElm.ObjectElm, ...
NumberResults, Obj, Elm, ACase, StepType, StepNum, U1, U2, U3, R1, R2, R3);
[ret, NumberResults, Obj, Elm, LoadCase, StepType, StepNum, F1, F2, F3, M1, ...
    M2, M3] = AnalysisResults.JointReact(JointID(k), SAP2000v1.eItemTypeElm.ObjectElm, ...
NumberResults, Obj, Elm, LoadCase, StepType, StepNum, F1, F2, F3, M1, M2, M3);
[ret, NumberResults, Obj, Elm, LoadCase, StepType, StepNum, V1, V2, V3, RR1, ...
    RR2, RR3] = AnalysisResults.JointVel(JointID(k), SAP2000v1.eItemTypeElm.ObjectElm, ...
NumberResults, Obj, Elm, LoadCase, StepType, StepNum, U1, U2, U3, R1, R2, R3);
for i=1:Estep(ceil(b/2))+1
    ResultU1(i,k) = U1(i);
    ResultF1(i,k) = F1(i);
    ResultV1(i,k) = V1(i);
end
end
end
```

Figure A.10: SAP2000™ - API - Exporting joint results

```
%Spring element results

for c=1:44

 ret = AnalysisResultsSetup.DeselectAllCasesAndCombosForOutput;

 ret = AnalysisResultsSetup.SetCaseSelectedForOutput(EQ(c));

 ret = AnalysisResultsSetup.SetOptionDirectHist(2);

    LinkDeformation=zeros(Estep(c)+1,44);
    LinkForce=zeros(Estep(ceil(c/2))+1,44);


LinkID = NET.createArray('System.String',44);
LinkID(1)='1';
LinkID(2)='2';


for l=1:2
[ret, NumberResults, Obj, Elm, PointElm, LoadCase, StepType, StepNum, P, V2, V3, T, ...
    M2, M3] = AnalysisResults.LinkForce(LinkID(l), SAP2000v1.eItemTypeElm.ObjectElm, ...
NumberResults, Obj, Elm, PointElm, LoadCase, StepType, StepNum, P, V2, V3, T, M2, M3);
[ret, NumberResults, Obj, Elm, LoadCase, StepType, StepNum, U1, U2, U3, R1, ...
    R2, R3] = AnalysisResults.LinkDeformation(LinkID(l), SAP2000v1.eItemTypeElm.ObjectElm, ...
NumberResults, Obj, Elm, LoadCase, StepType, StepNum, U1, U2, U3, R1, R2, R3);
z=1;
for i=1:Estep(ceil(c/2))+1
    LinkDeformation(i,l) = U1(i);
    LinkForce(i,l) = P(z);
    z=z+2;
end
end
end
```

Figure A.11: SAP2000™ - API - Exporting spring elements results

A.4. Modeling of the MDOF Systems

Floor Level Dead Load		
Seismic Floor weight (mass):	85	psf
Length of bay:	120	ft
Width of bay:	60	ft
Area:	7200	ft^2
Dead Weight:	612	kip

a. Floor level dead load

Roof Level Dead Load		
Seismic Floor weight (mass):	67	psf
Length of bay:	120	ft
Width of bay:	60	ft
Area assigned:	7200	ft^2
Dead weight:	482.4	kip

b. Roof level dead load

Floor Level Live Load		
Seismic Floor weight (mass):	50	psf
Length of bay:	120	ft
Width of bay:	60	ft
Area:	7200	ft^2
Live weight:	360	kip

c. Floor level live load

Roof Level live Load		
Seismic Floor weight (mass):	20	psf
Length of bay:	120	ft
Width of bay:	60	ft
Area assigned:	7200	ft^2
Dead weight:	144	kip

d. Floor level live load

Figure A.12: Design loading for the MDOF systems

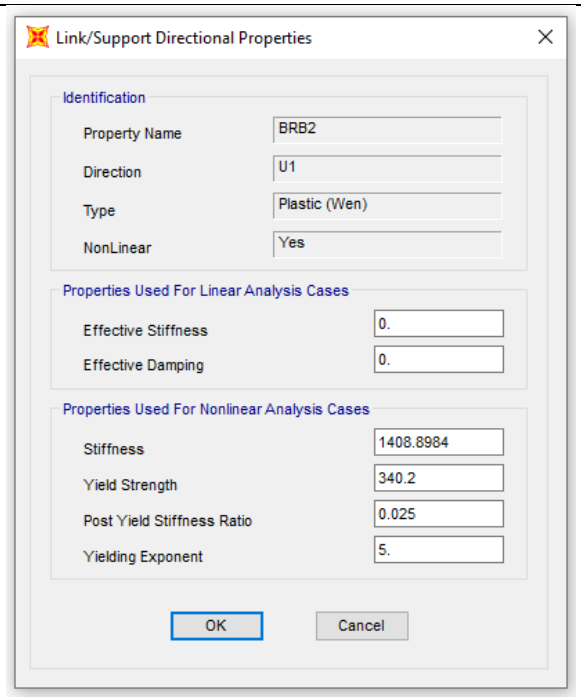

a. BRB properties for second story

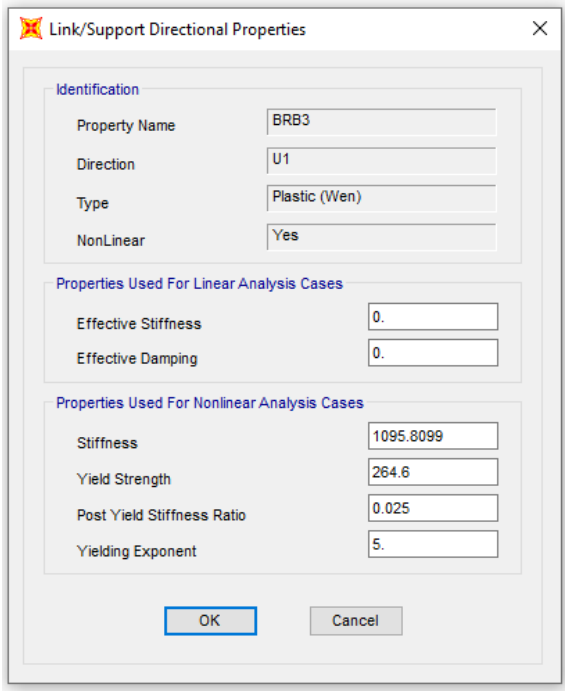

b. BRB properties for third story

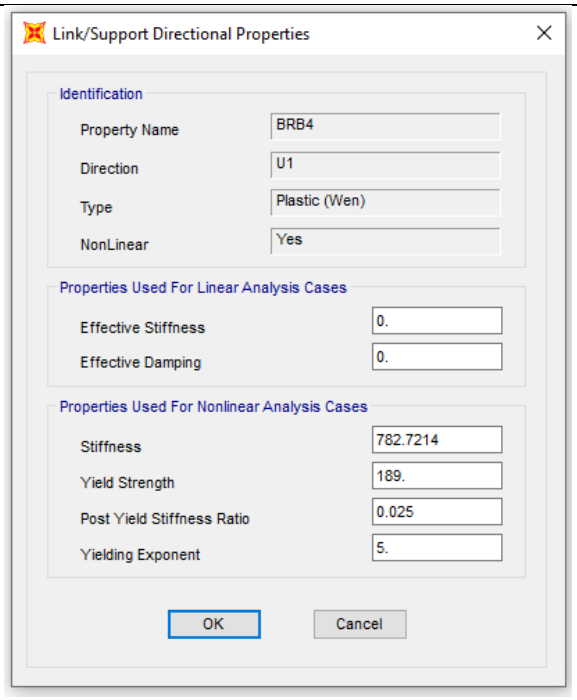

c. BRB properties for fourth story

Figure A.13: The four-story MDOF system - BRB properties

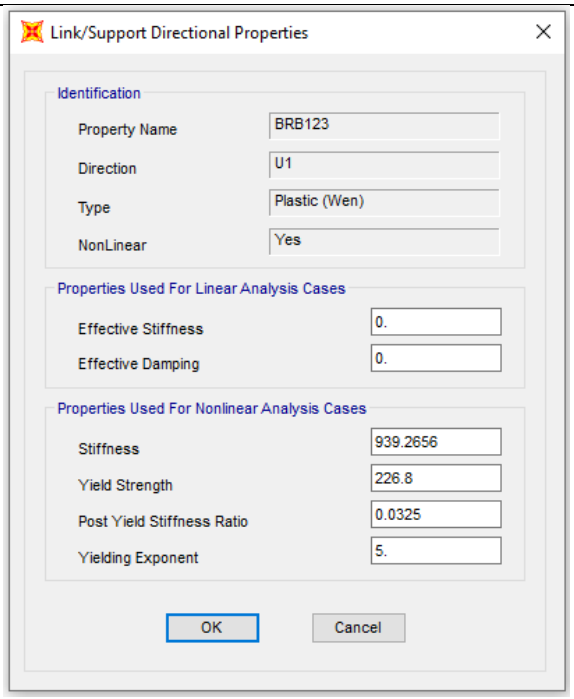

a. BRB properties for first, second, and third stories

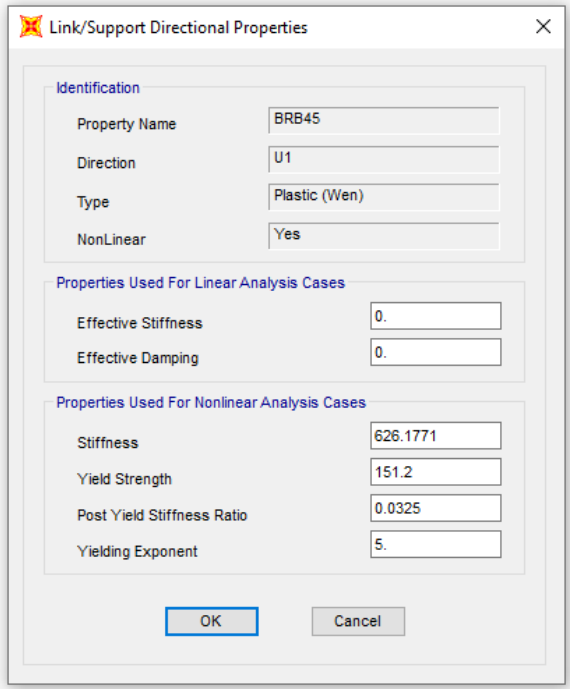

b. BRB properties for fourth and fifth stories

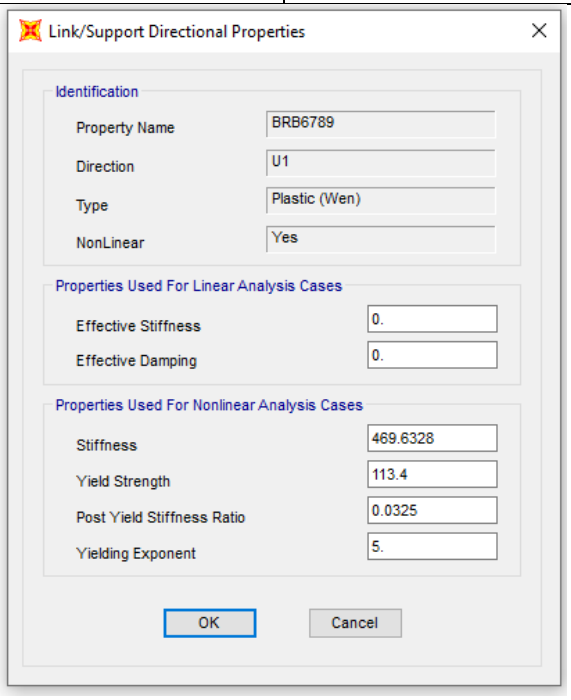

c. BRB properties for sixth, seventh, eighth, and ninth stories

Figure A.14: The nine-story MDOF system - BRB properties

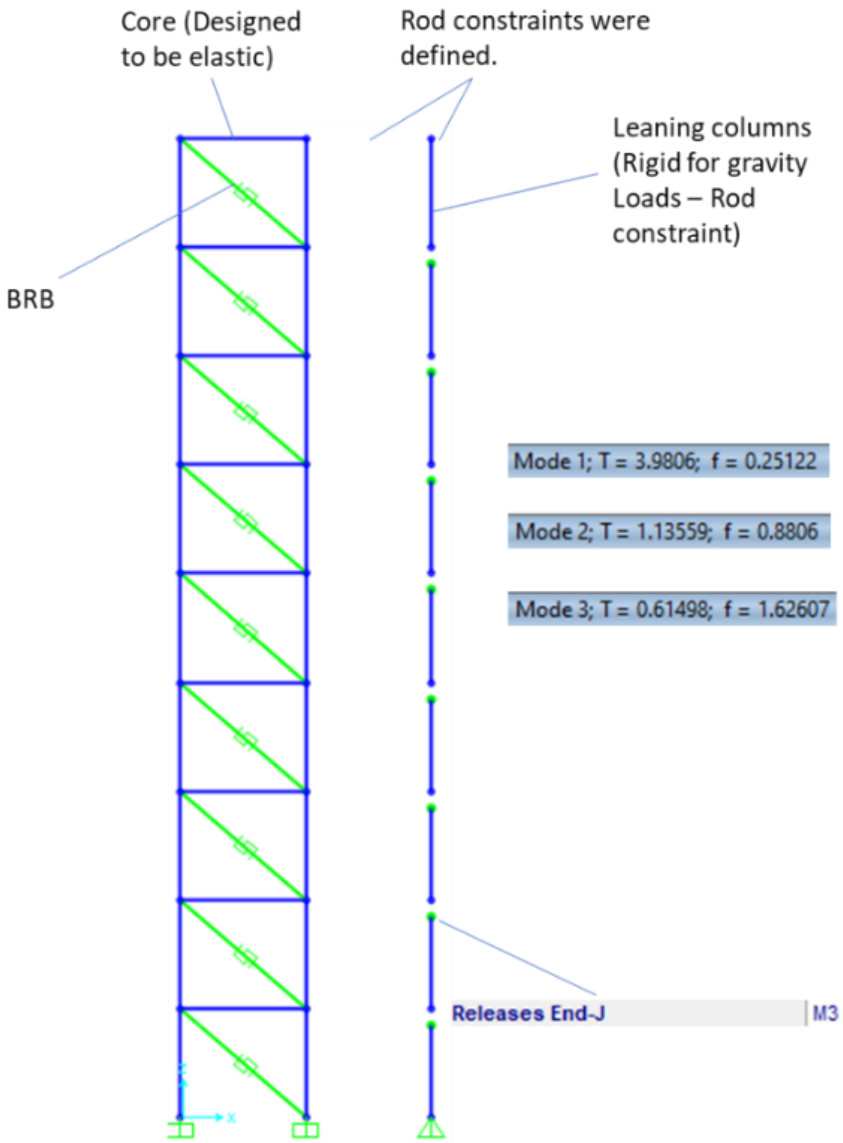

Figure A.15: SAP2000^{TM} model for the nine-story MDOF system

APPENDIX B: THE SDOF SYSTEM

Here, the appendix is divided into three parts; influence of modeling methods on damping force, damping force-velocity relation, and influence of modeling methods on inherent damping energy dissipation. And,

- spring force, damping force, and base shear plots,
- damping force versus velocity plots, and
- input energy, hysteresis energy dissipation, and inherent damping energy dissipation plots

are provided for each Rayleigh modeling method.

B.1. Influence of Modeling Methods on Damping Force

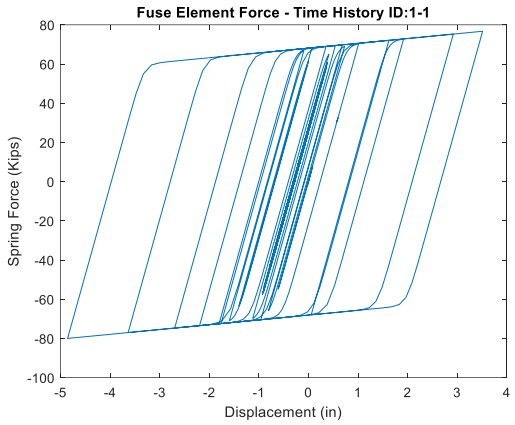

a. Force vs disp. plot of the fuse element

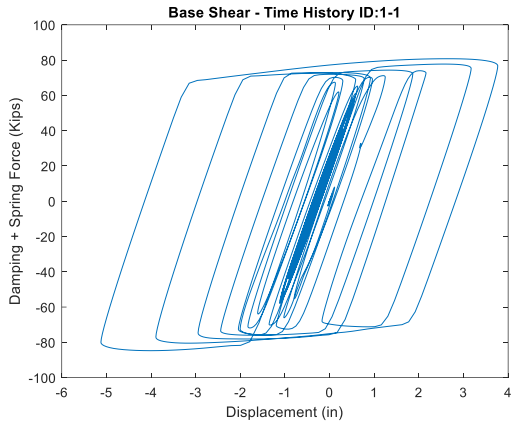

b. Base shear

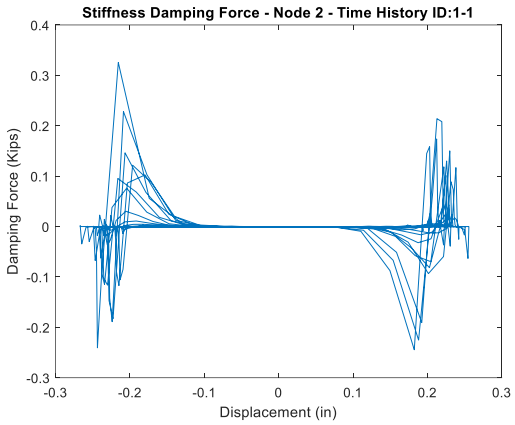

c. Stiffness damping force at node two

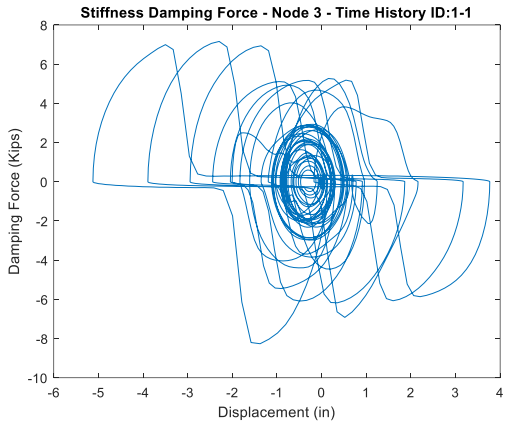

d. Stiffness damping force at node three

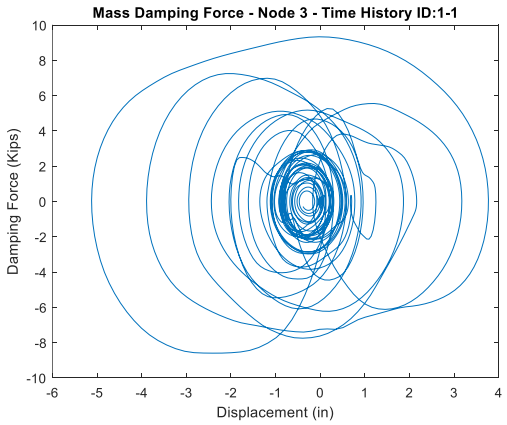

e. Mass damping force at node three

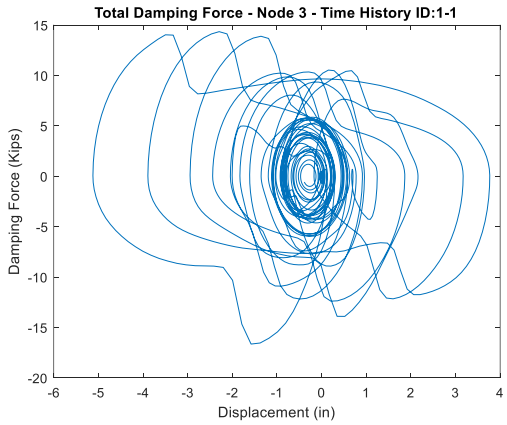

f. Total damping force at node three

Figure B.1: The SDOF system - Force plots for the second method

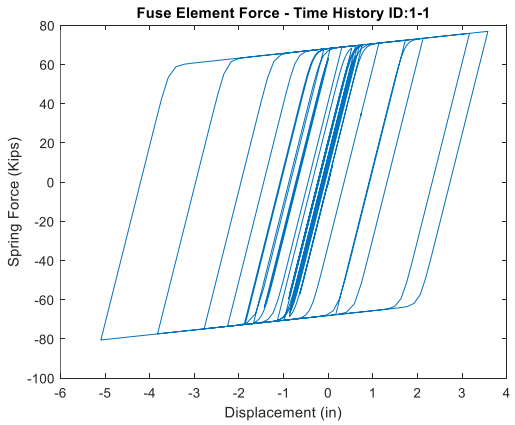

a. Force vs disp. plot of the fuse element

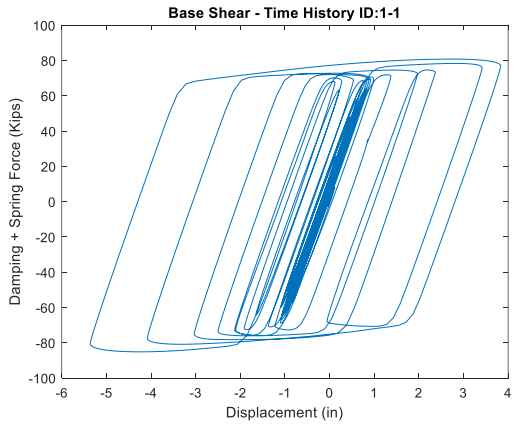

b. Base shear

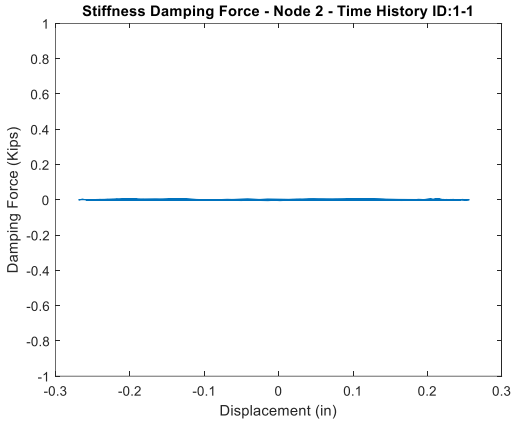

c. Stiffness damping force at node two

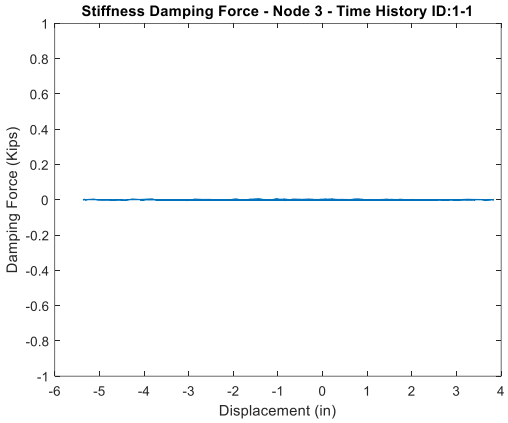

d. Stiffness damping force at node two

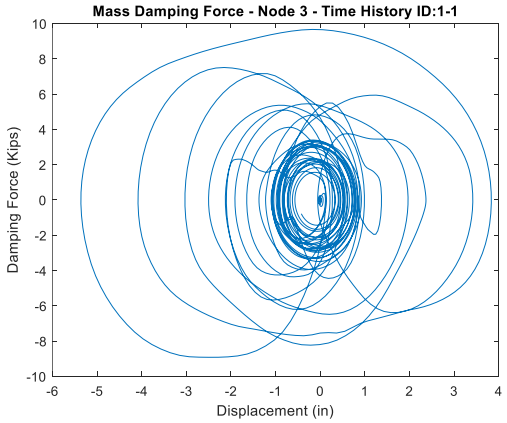

e. Mass Damping force at node three

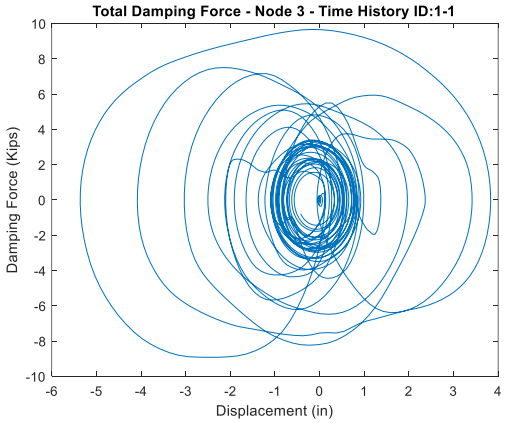

f. Total Damping force at node three

Figure B.2: The SDOF system - Force plots for the third method

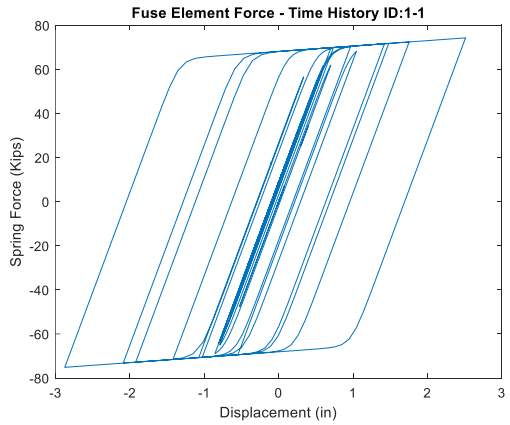

a. Force vs disp. plot of the fuse element

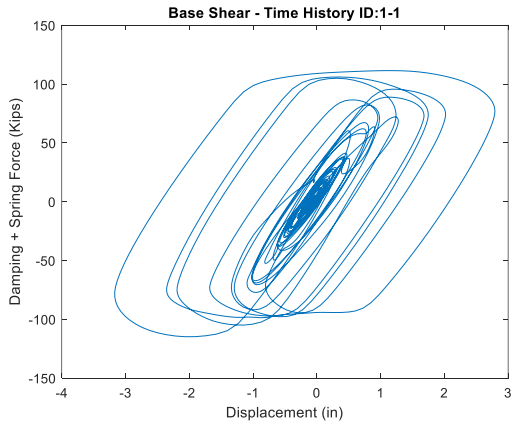

b. Base shear

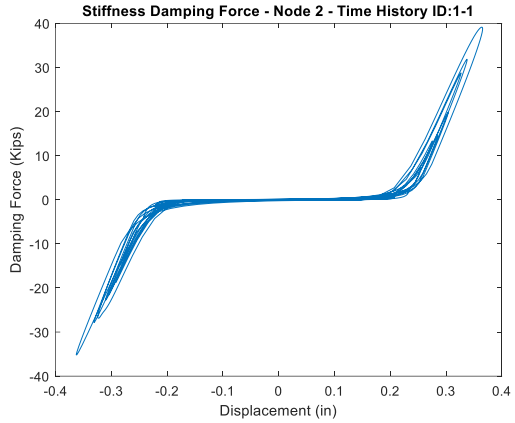

c. Stiffness damping force at node two

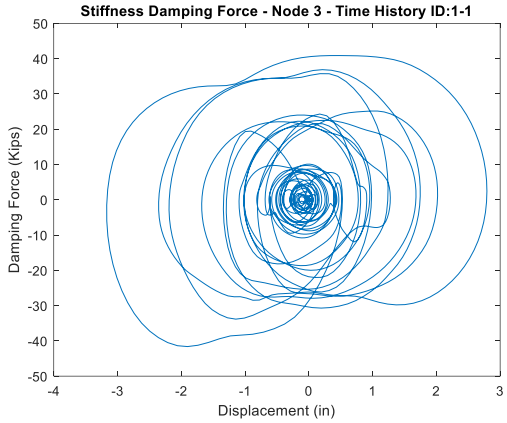

d. Stiffness damping force at node three

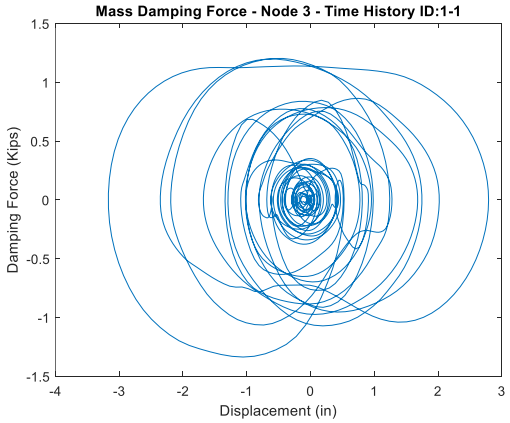

e. Mass damping force at node three

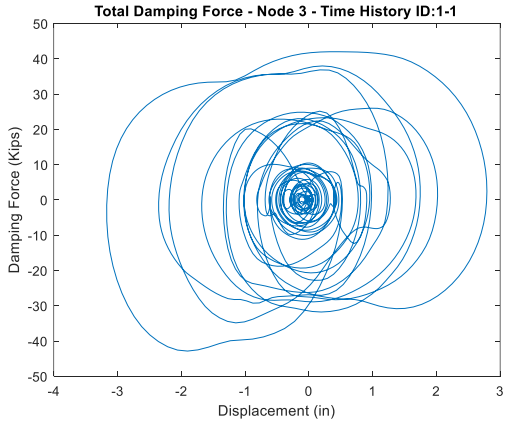

f. Total damping force at node three

Figure B.3: The SDOF system - Force plots for the fourth method

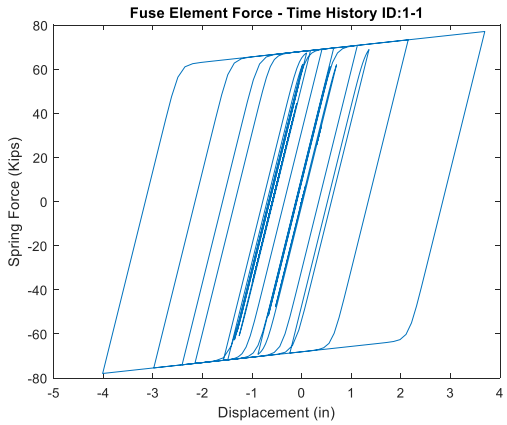

a. Force vs disp. plot of the fuse element

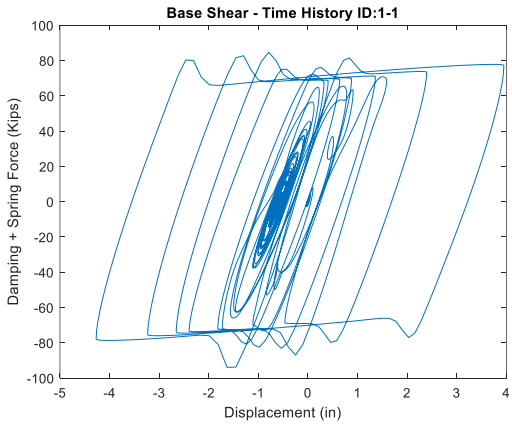

b. Base shear

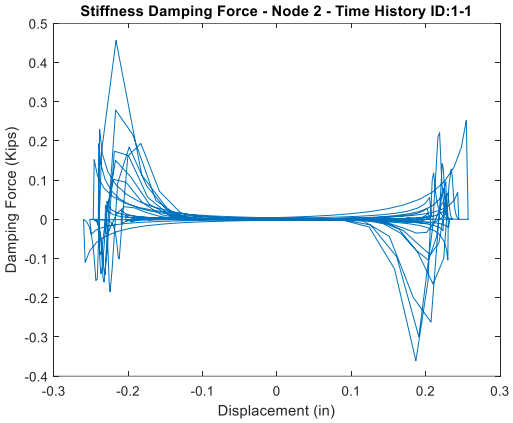

c. Stiffness damping force at node two

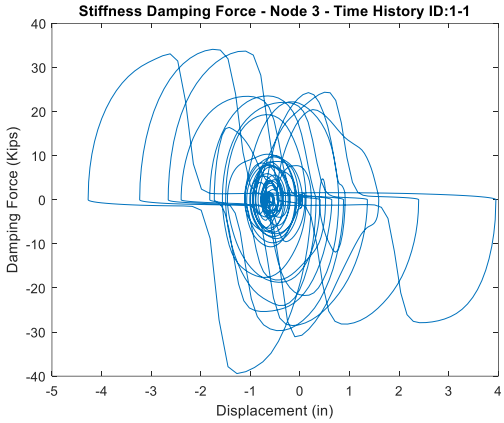

d. Stiffness damping force at node three

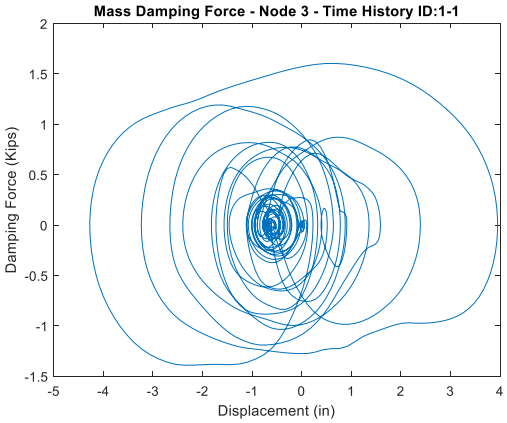

e. Mass damping force at node three

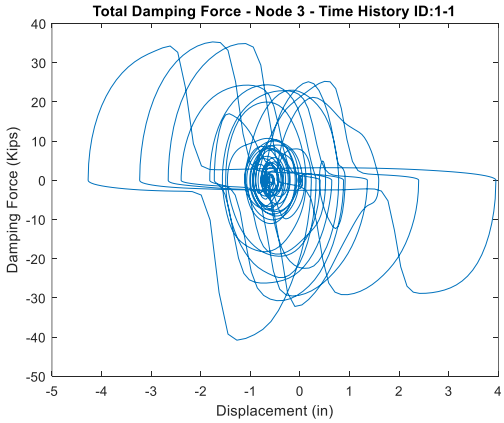

f. Total damping force at node three

Figure B.4: The SDOF system - Force plots for the fifth method

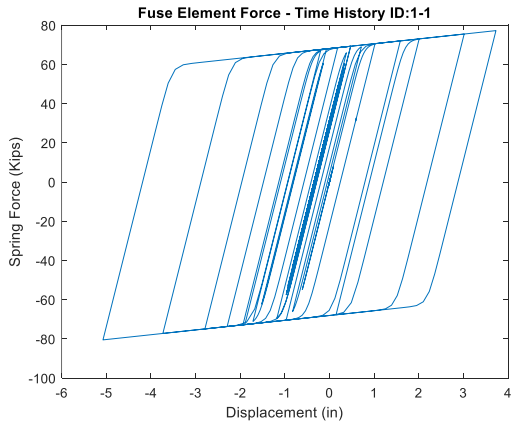

a. Force vs disp. plot of the fuse element

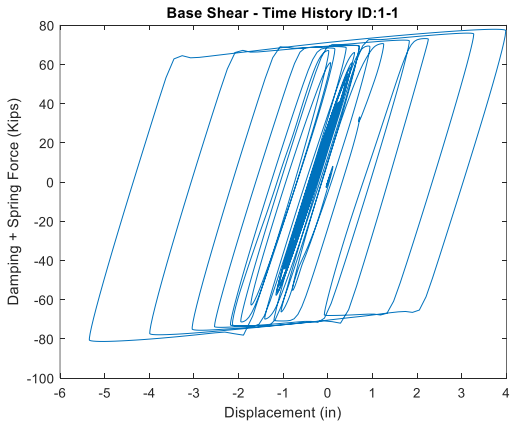

b. Base shear

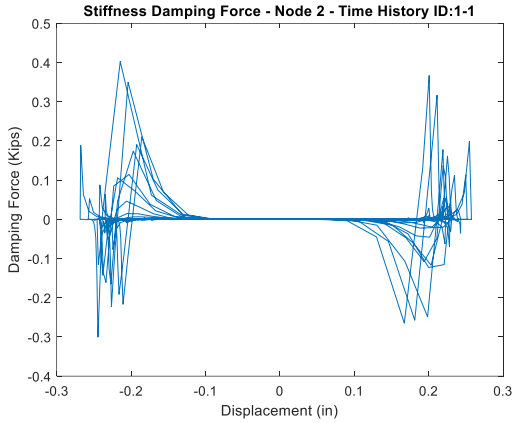

c. Stiffness damping force at node two

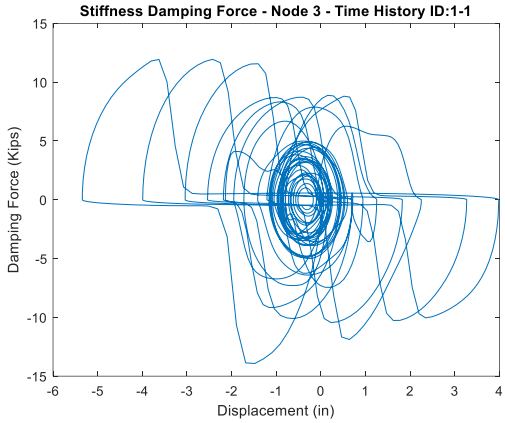

d. Stiffness damping force at node three

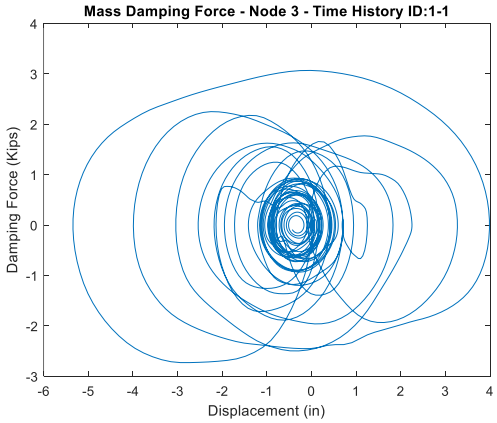

e. Mass damping force at node three

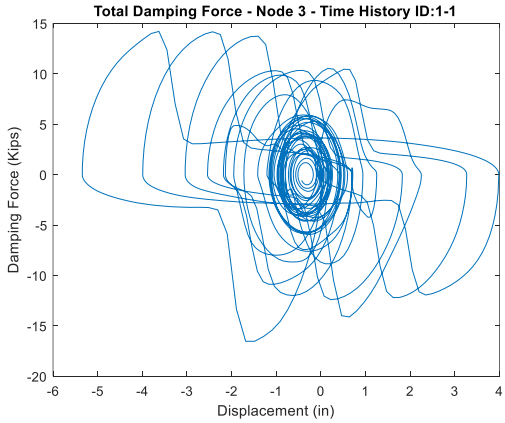

f. Total damping force at node three

Figure B.5: The SDOF system - Force plots for the sixth method

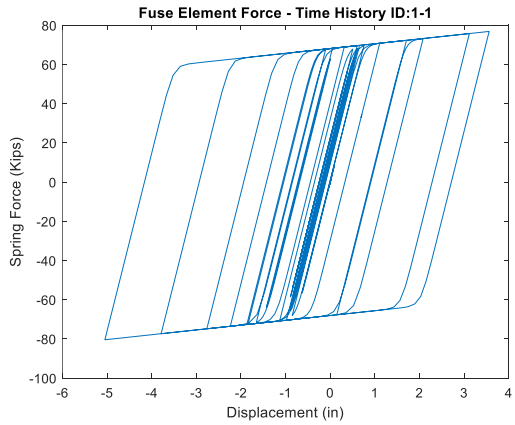

a. Force vs disp. plot of the fuse element

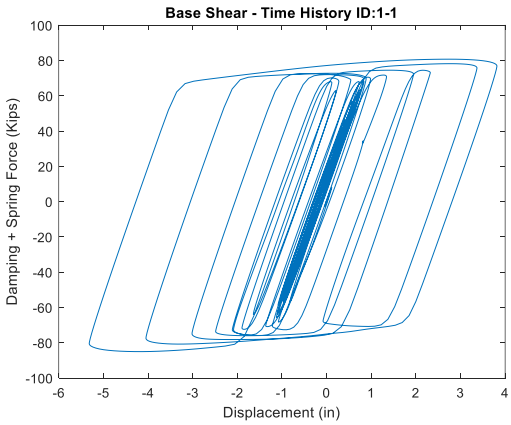

b. Base shear

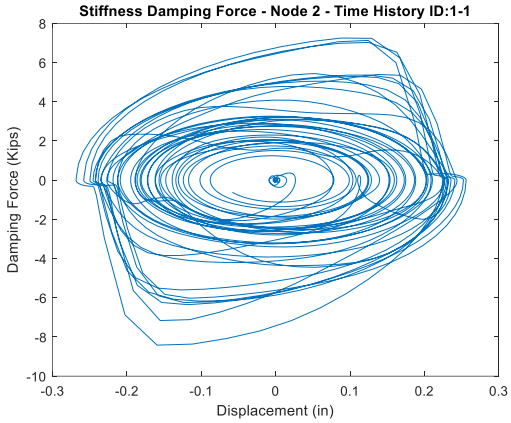

c. Stiffness damping force at node two

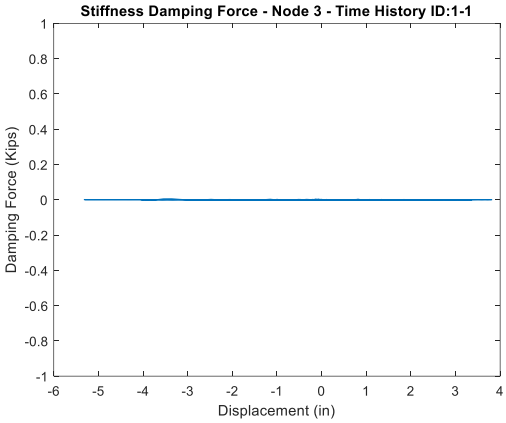

d. Stiffness damping force at node three

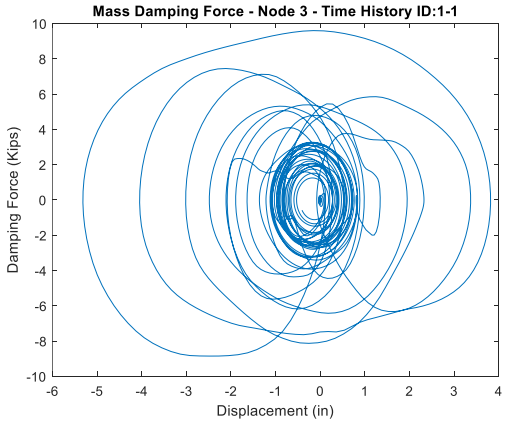

e. Mass damping force at node three

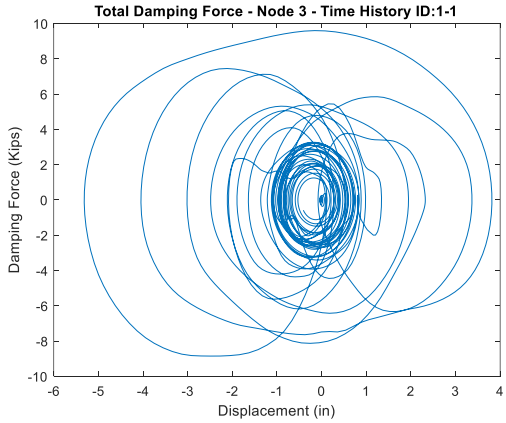

f. Total damping force at node three

Figure B.6: The SDOF system - Force plots for the seventh method

B.2. Damping Force - Velocity Relation

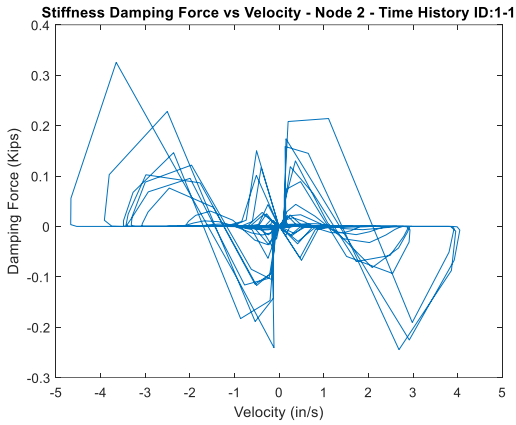

a. Stiffness damping force at node two

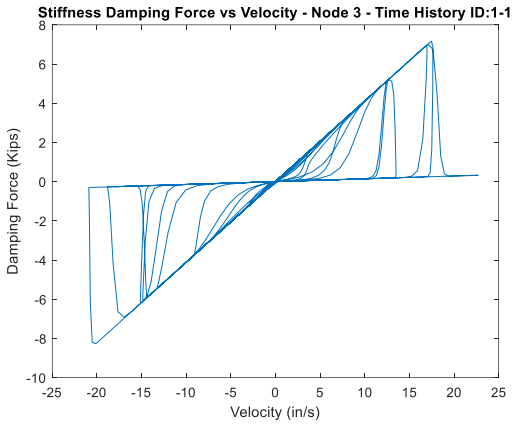

b. Stiffness damping force at node three

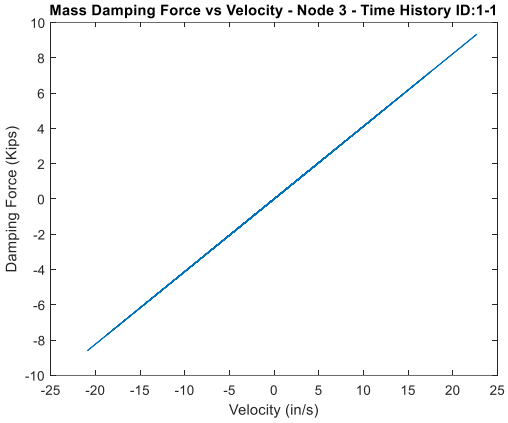

c. Mass damping force at node three

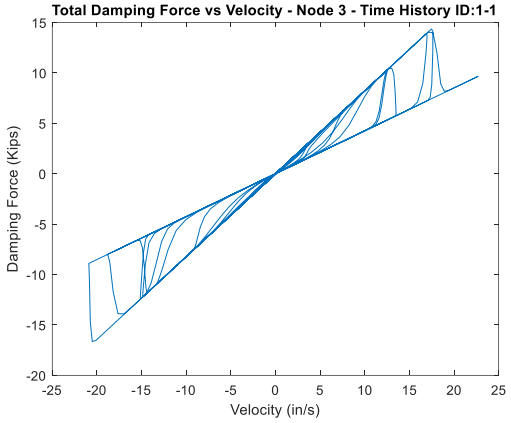

d. Total damping force at node three

Figure B.7: The SDOF system - Damp. force vs velocity plots for the second method

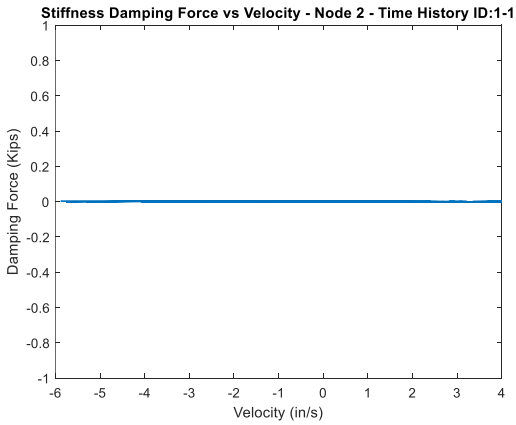

a. Stiffness damping force at node two

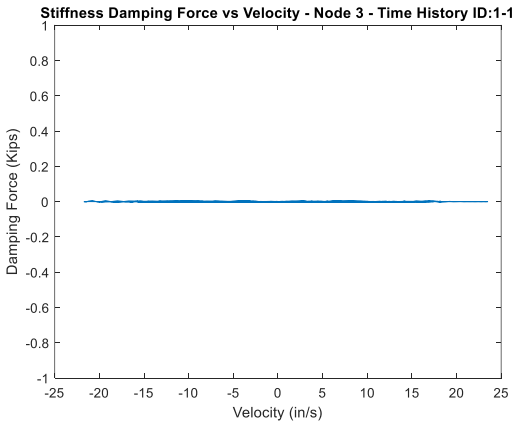

b. Stiffness damping force at node three

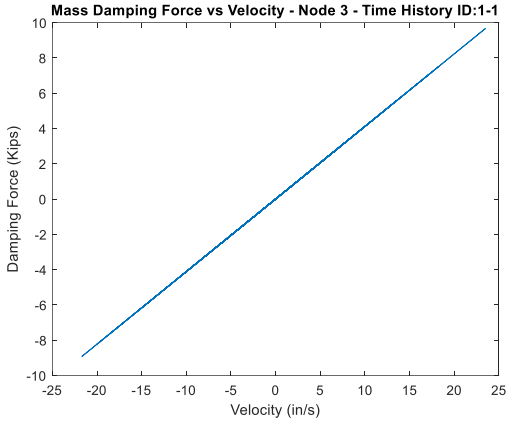

c. Mass damping force at node three

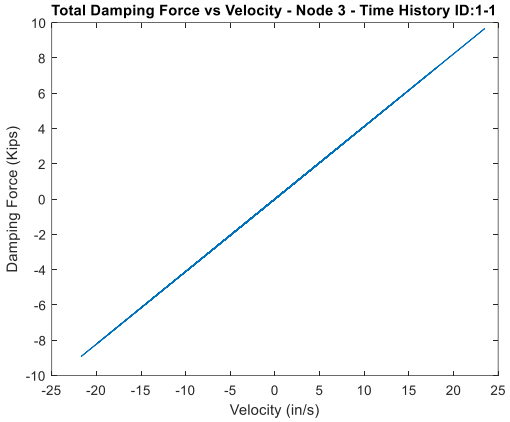

d. Total damping force at node three

Figure B.8: The SDOF system - Damp. force vs velocity plots for the third method

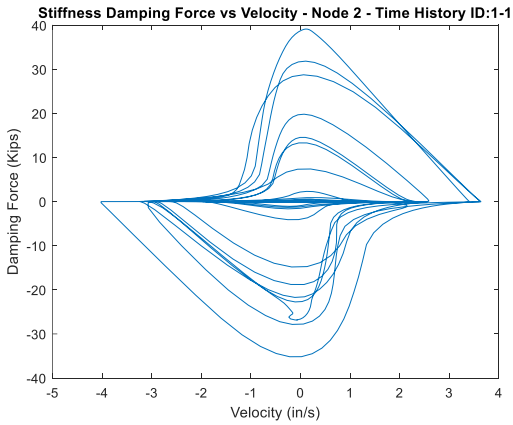

a. Stiffness damping force at node two

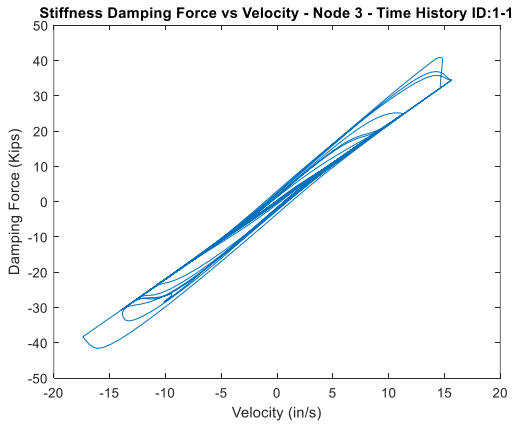

b. Stiffness damping force at node three

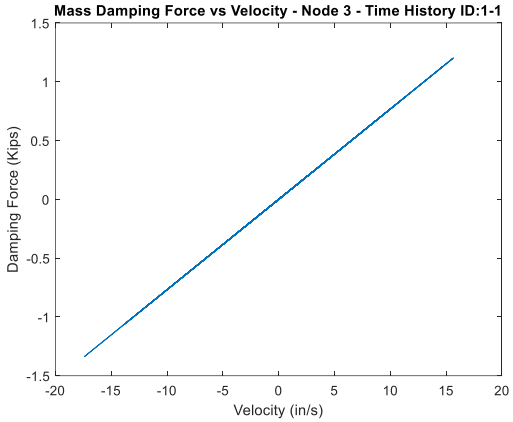

c. Mass damping force at node three

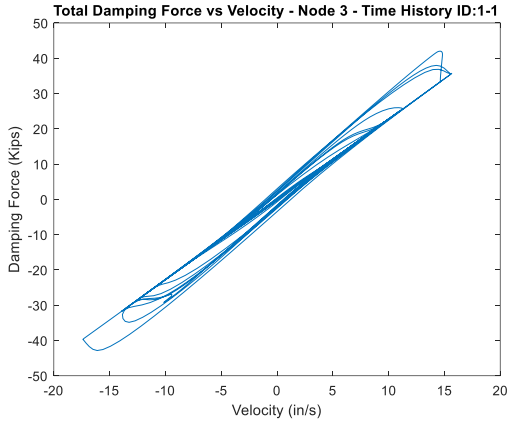

d. Total damping force at node three

Figure B.9: The SDOF system - Damp. force vs velocity plots for the fourth method

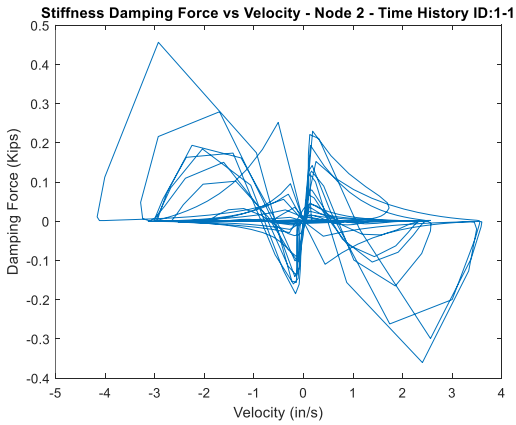

a. Stiffness damping force at node two

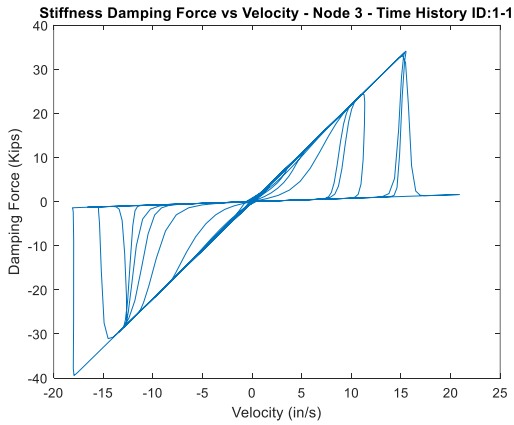

b. Stiffness damping force at node three

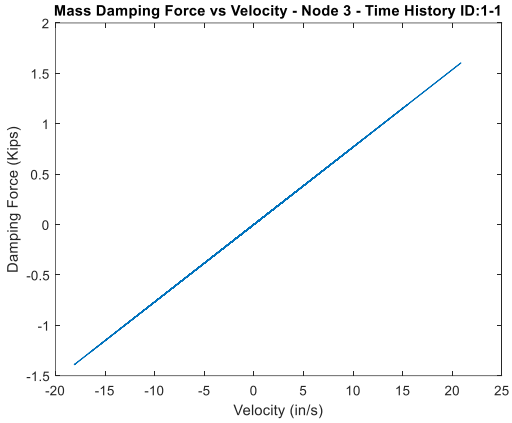

c. Mass damping force at node three

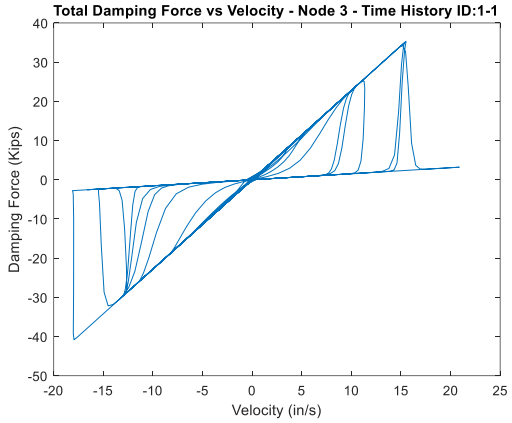

d. Total damping force at node three

Figure B.10: The SDOF system - Damp. force vs velocity plots for the fifth method

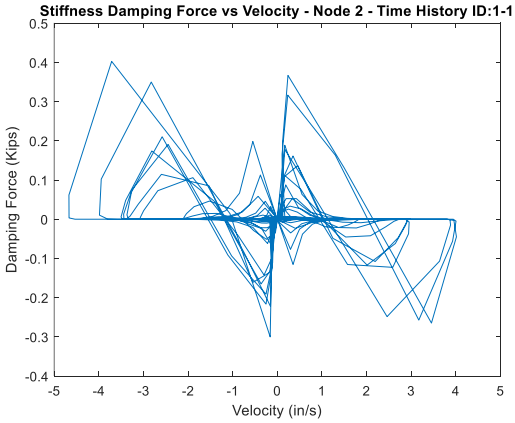

a. Stiffness damping force at node two

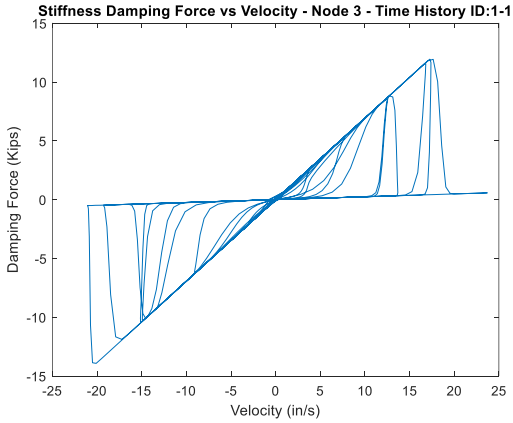

b. Stiffness damping force at node three

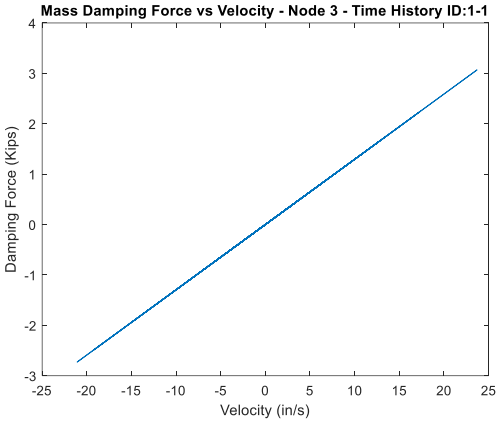

c. Mass damping force at node three

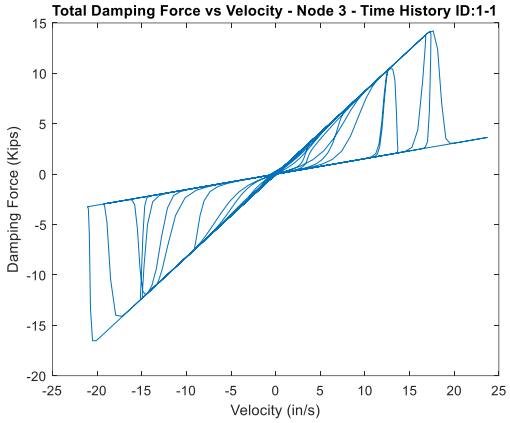

d. Total damping force at node three

Figure B.11: The SDOF system - Damp. force vs velocity plots for the sixth method

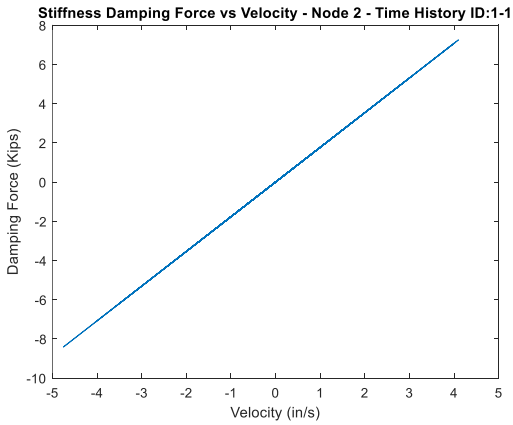

a. Stiffness damping force at node two

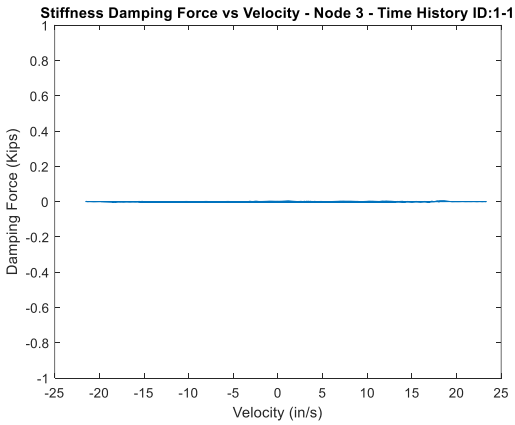

b. Stiffness damping force at node three

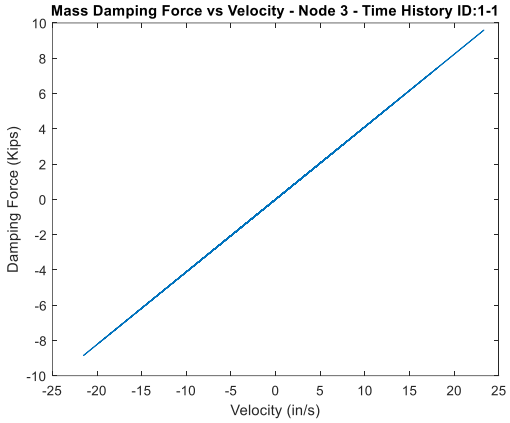

c. Mass damping force at node three

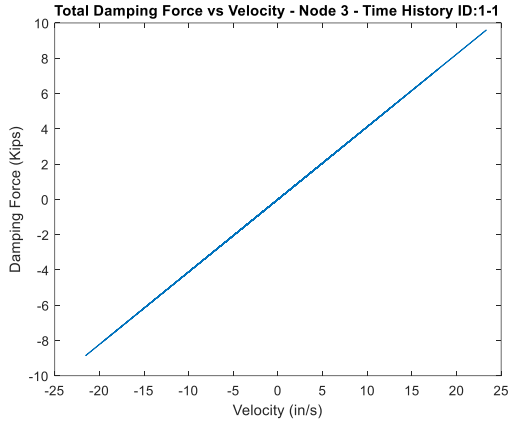

d. Total damping force at node three

Figure B.12: The SDOF system - Damp. force vs velocity plot for the seventh method

B.3. Influence of Modeling Methods on Inherent Damping Energy Dissipation

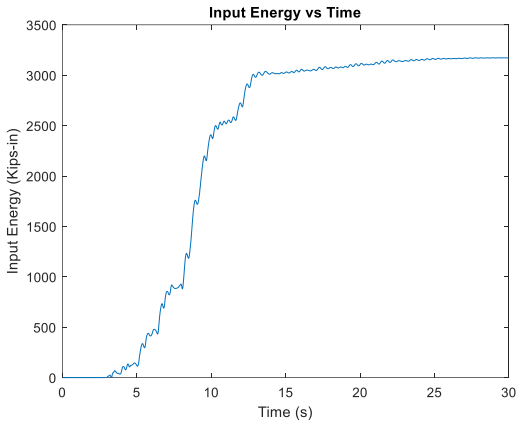

a. Input energy

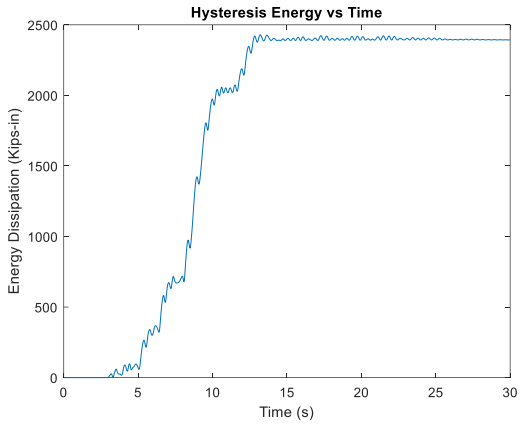

b. Hysteresis energy dissipation

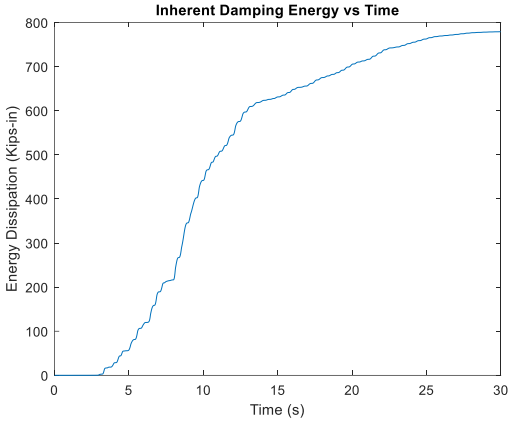

c. Inherent damping energy dissipation

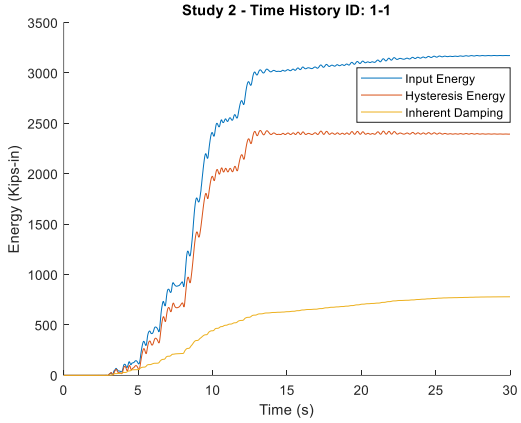

d. Input energy and energy dissipations

Figure B.13: The SDOF system - Energy plots for the second method

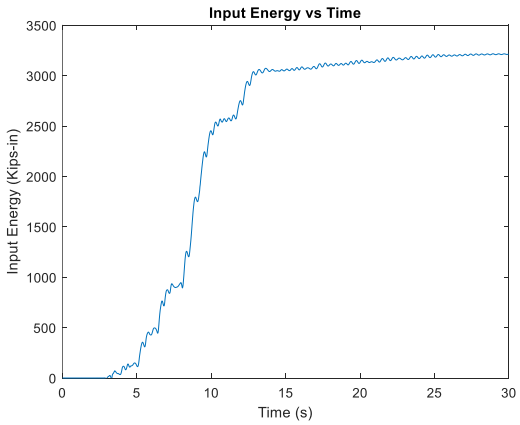

a. Input energy

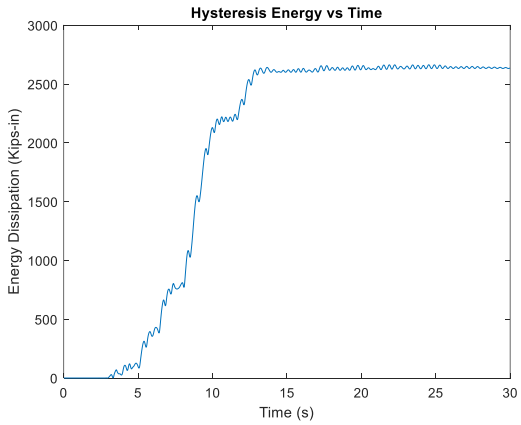

b. Hysteresis energy dissipation

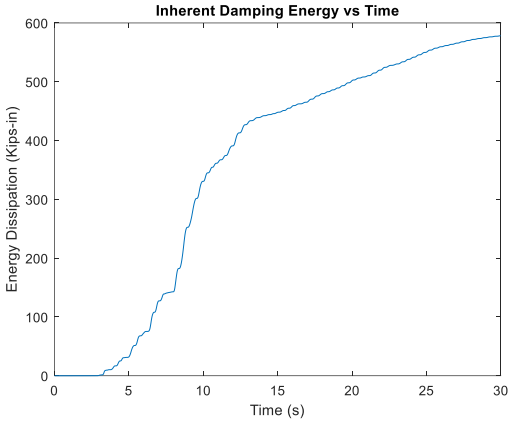

c. Inherent damping energy dissipation

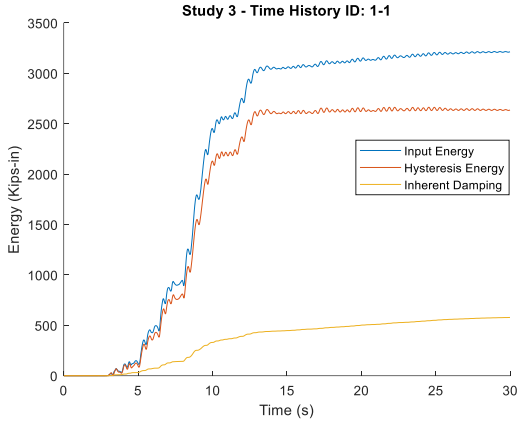

d. Input energy and energy dissipations

Figure B.14: The SDOF system - Energy plots for the third method

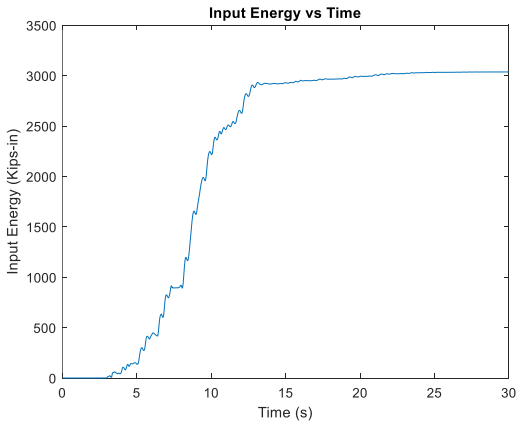

a. Input energy

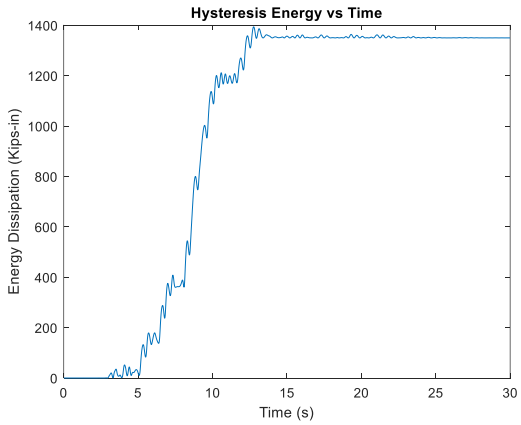

b. Hysteresis energy dissipation

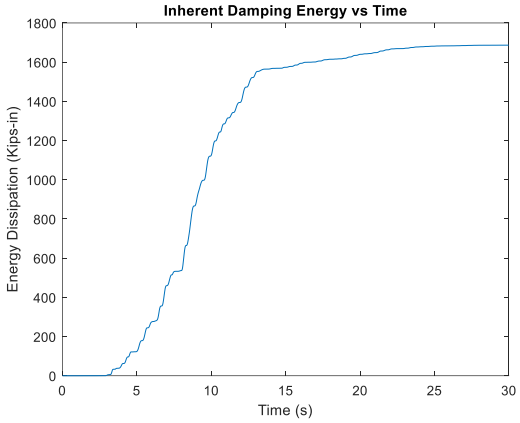

c. Inherent damping energy dissipation

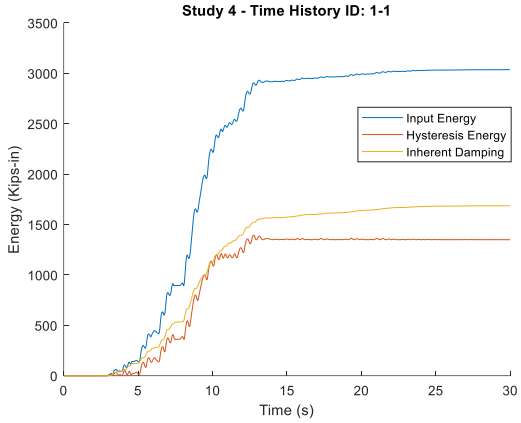

d. Input energy and energy dissipations

Figure B.15: The SDOF system - Energy plots for the fourth method

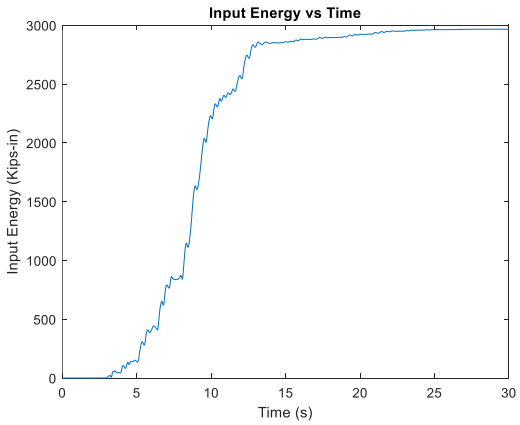

a. Input energy

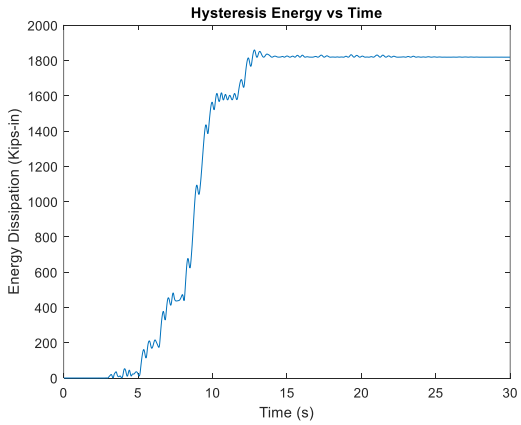

b. Hysteresis energy dissipation

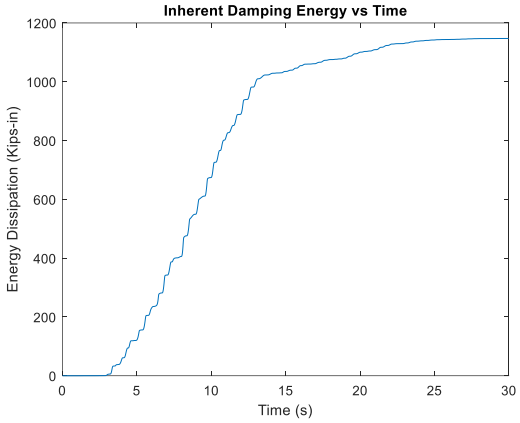

c. Inherent damping energy dissipation

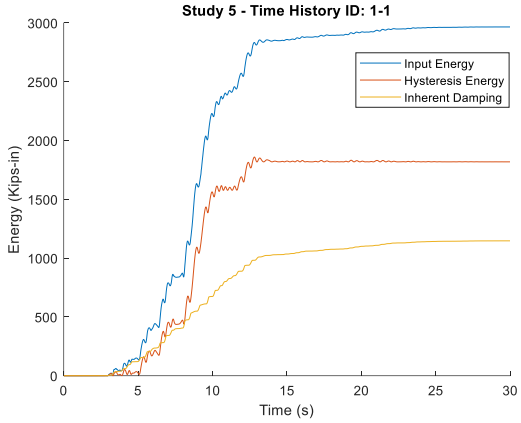

d. Input energy and energy dissipations

Figure B.16: The SDOF system - Energy plots for the fifth method

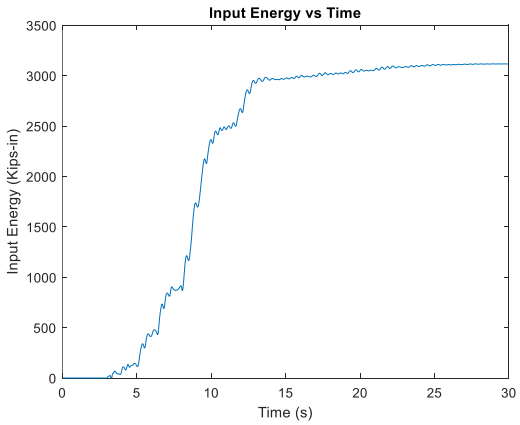

a. Input energy

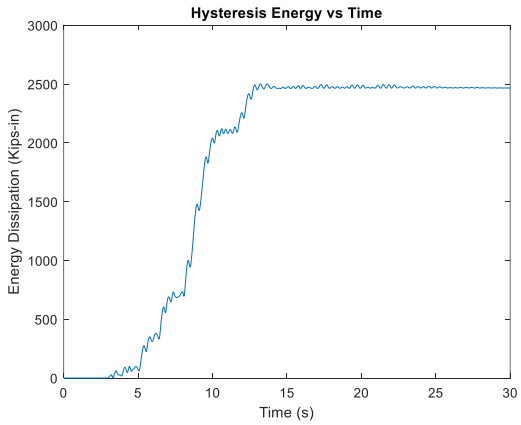

b. Hysteresis energy dissipation

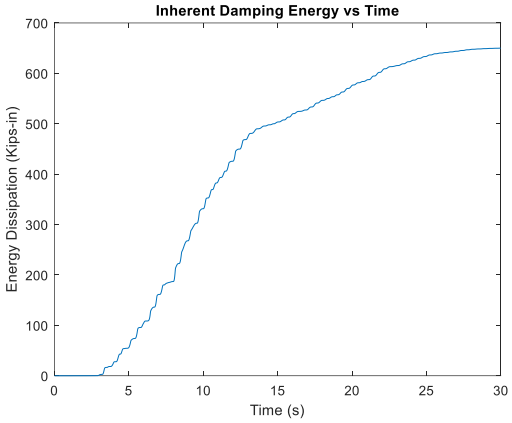

c. Inherent damping energy dissipation

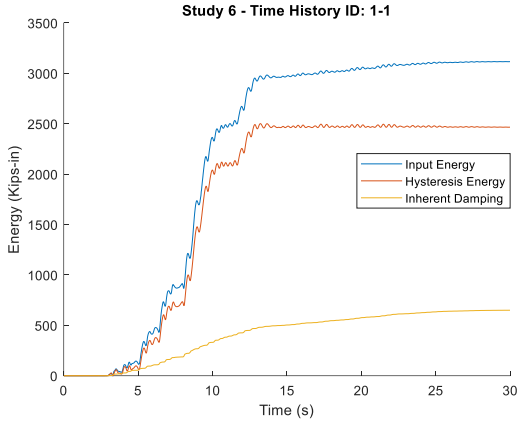

d. Input energy and energy dissipations

Figure B.17: The SDOF system - Energy plots for the sixth method

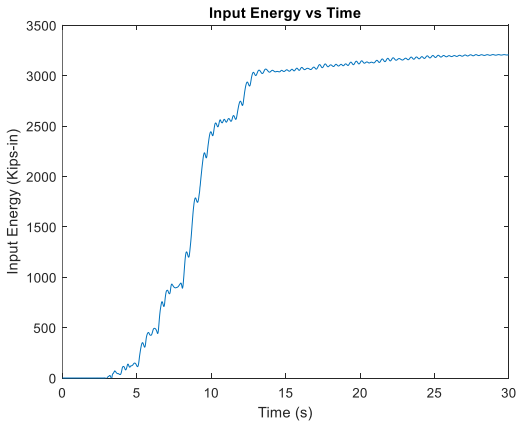

a. Input energy

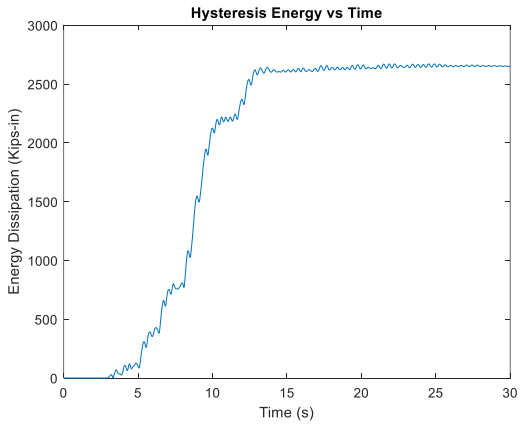

b. Hysteresis energy dissipation

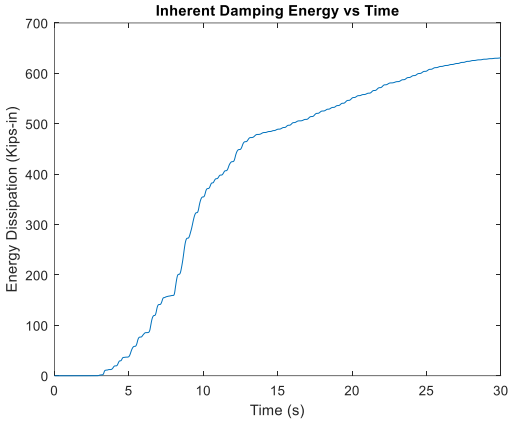

c. Inherent damping energy dissipation

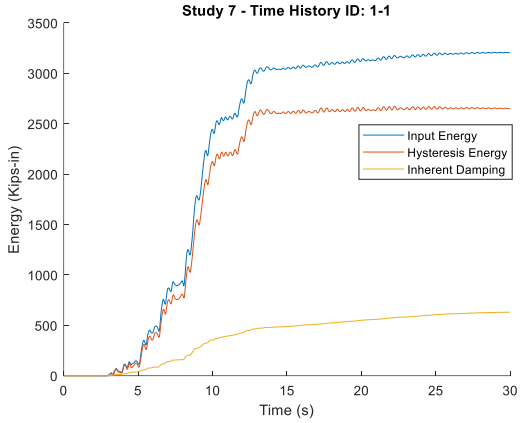

d. Input energy and energy dissipations

Figure B.18: The SDOF system - Energy plots for the seventh method

APPENDIX C: THE MDOF SYSTEMS

Here, the appendix is divided into three parts; influence of modeling methods on energy dissipation, influence of modeling methods on IDA Results for the four-story MDOF system, and influence of modeling methods on IDA Results for the nine-story MDOF system. And,

- input energy, hysteresis energy dissipation, and inherent damping energy dissipation plots
- IDA results for the four-story MDOF system, and
- IDA results for the nine-story MDOF system

are provided for each Rayleigh modeling method.

C.1. Influence of Modeling Methods on Energy Dissipation

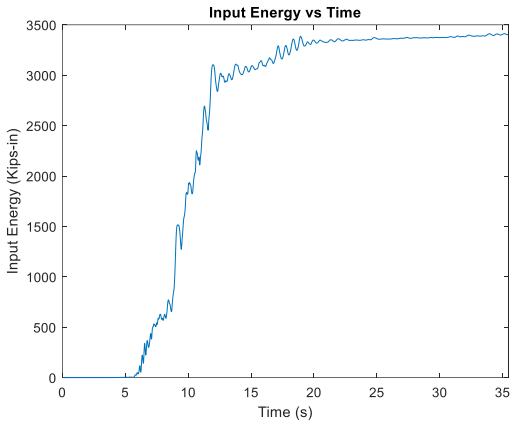

a. Input energy

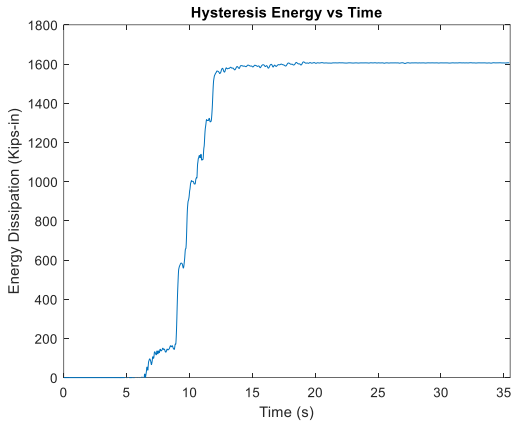

b. Hysteresis energy dissipation

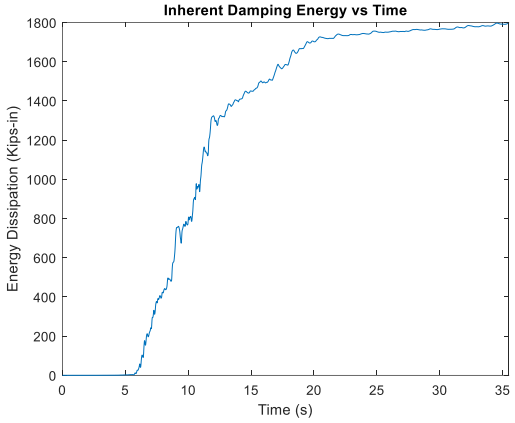

c. Inherent damping energy dissipation

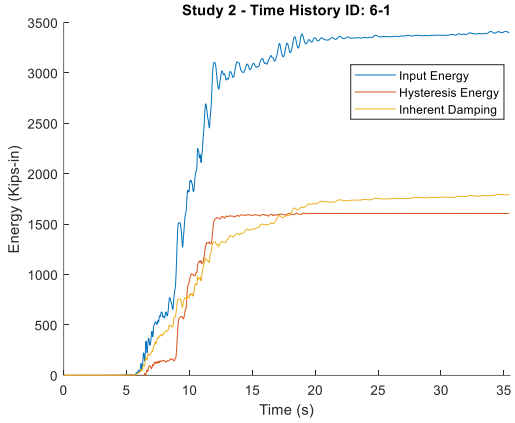

d. Input energy and energy dissipations

Figure C.1: The four-story MDOF system - Energy plots for the second method

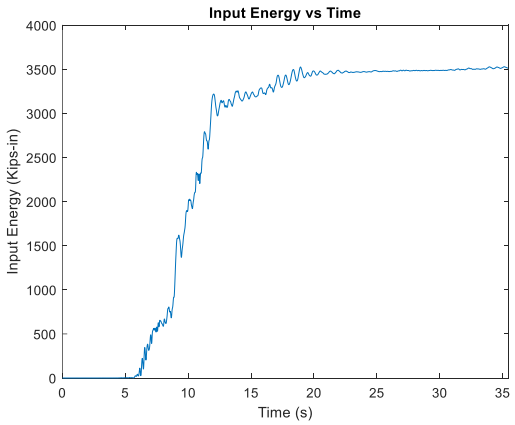

a. Input energy

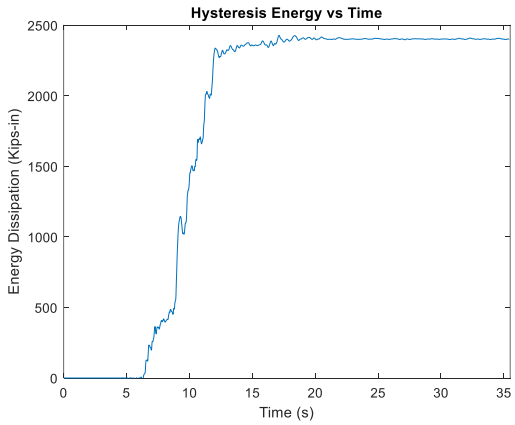

b. Hysteresis energy dissipation

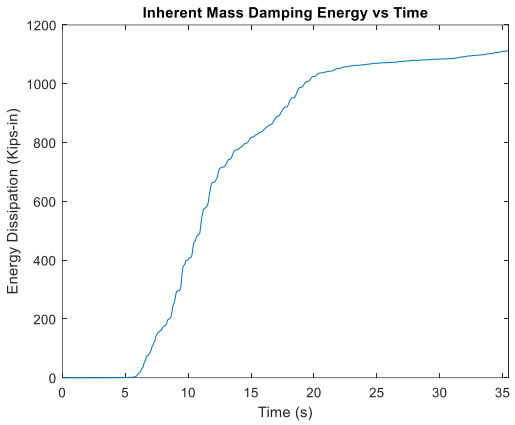

c. Inherent damping energy dissipation

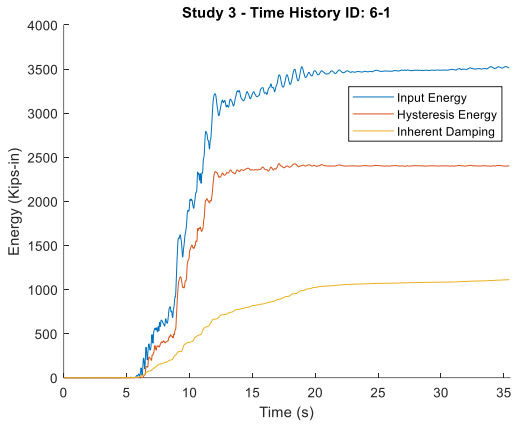

d. Input energy and energy dissipations

Figure C.2: The four-story MDOF system - Energy plots for the third method

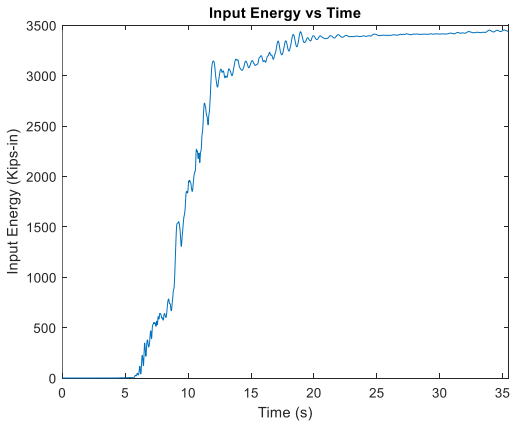

a. Input energy

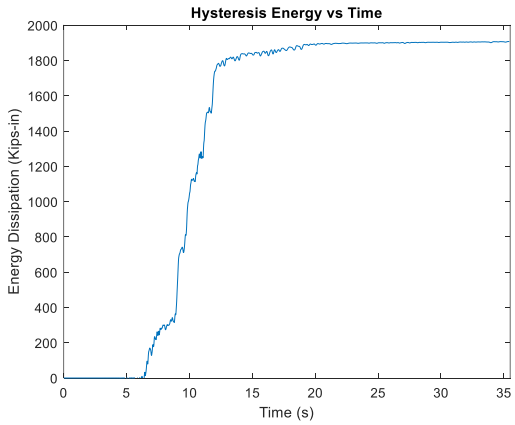

b. Hysteresis energy dissipation

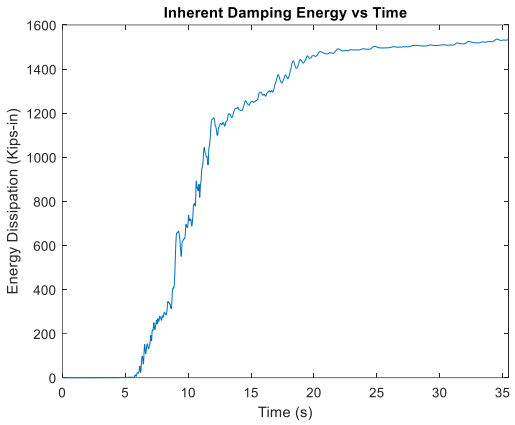

c. Inherent damping energy dissipation

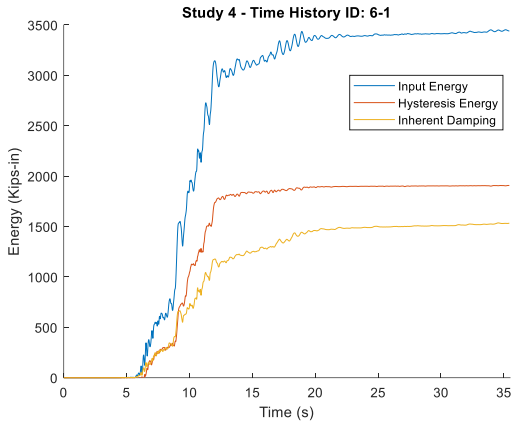

d. Input energy and energy dissipations

Figure C.3: The four-story MDOF system - Energy plots for the fourth method

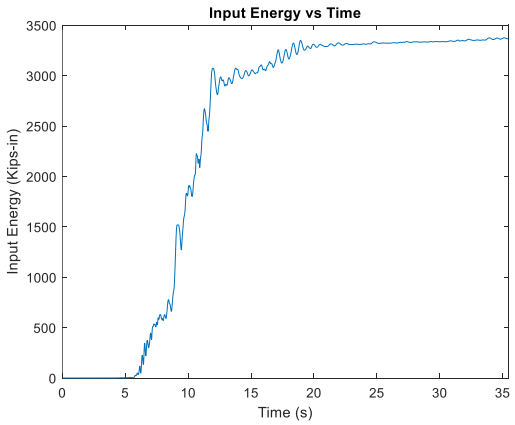

a. Input energy

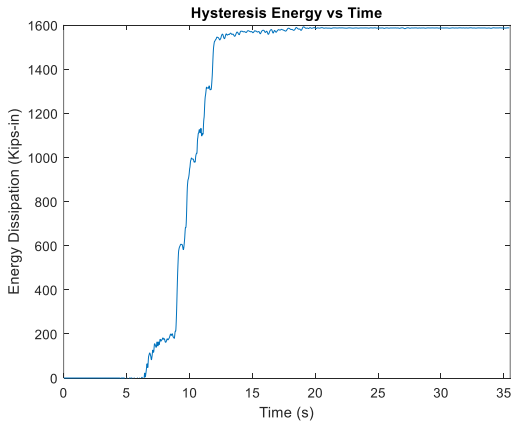

b. Hysteresis energy dissipation

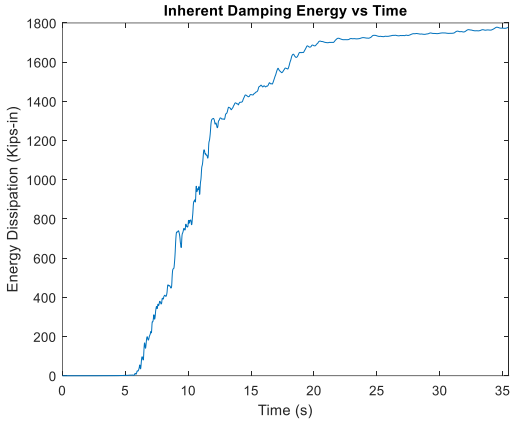

c. Inherent damping energy dissipation

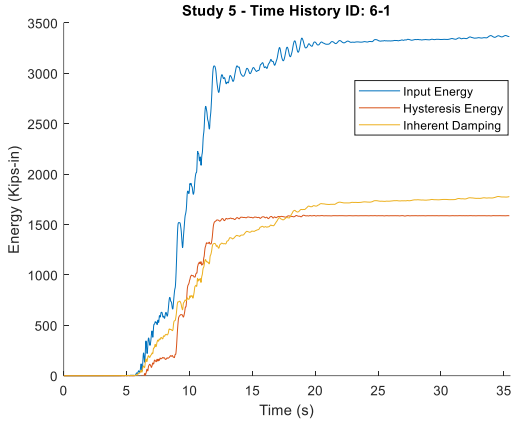

d. Input energy and energy dissipations

Figure C.4: The four-story MDOF system - Energy plots for the fifth method

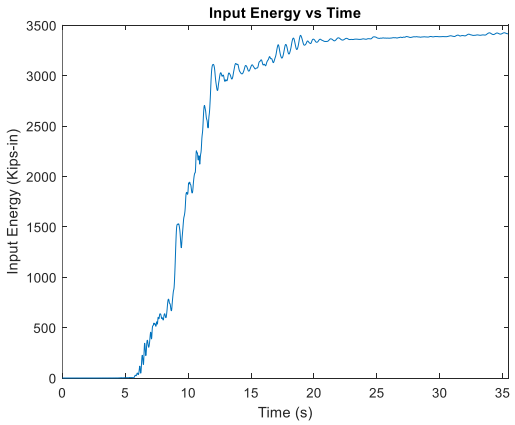

a. Input energy

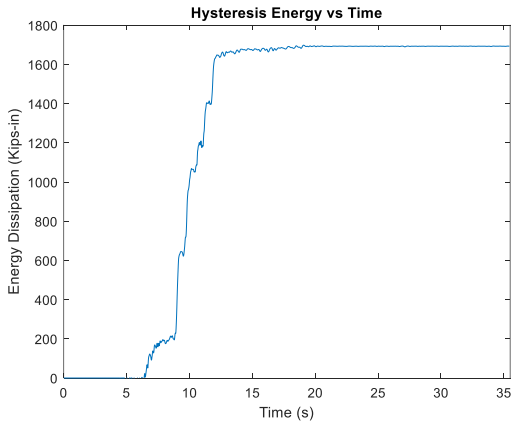

b. Hysteresis energy dissipation

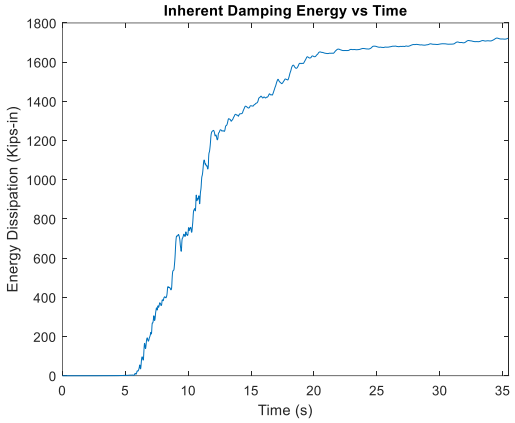

c. Inherent damping energy dissipation

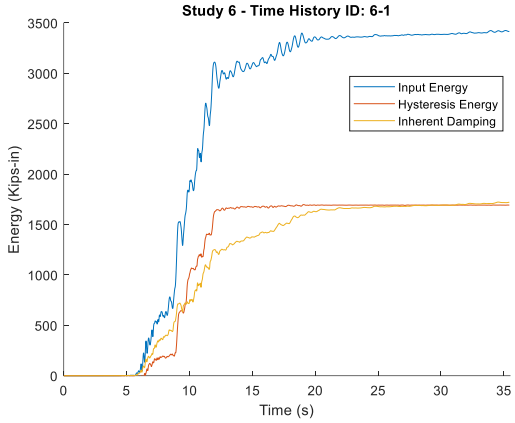

d. Input energy and energy dissipations

Figure C.5: The four-story MDOF system - Energy plots for the sixth method

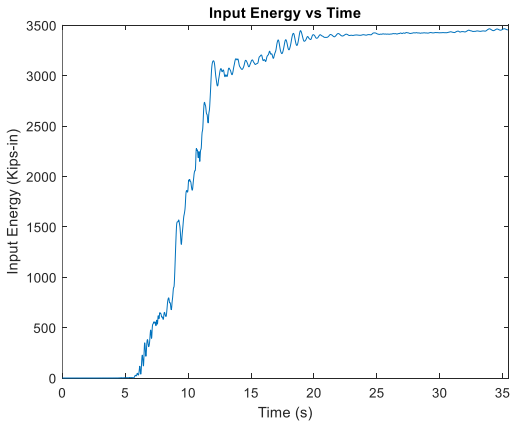

a. Input energy

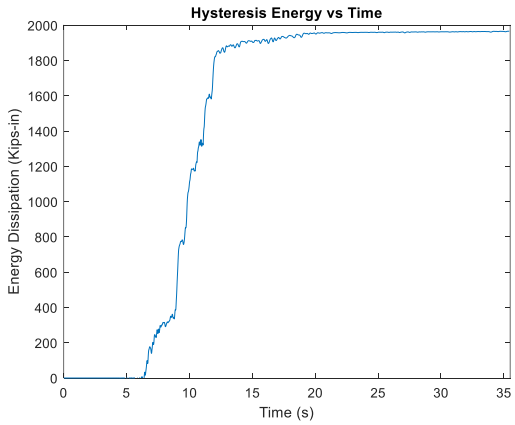

b. Hysteresis energy dissipation

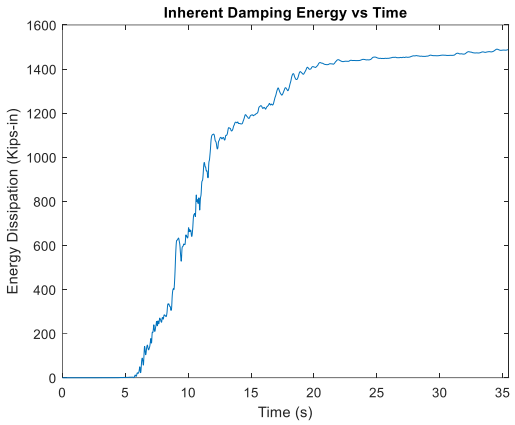

c. Inherent damping energy dissipation

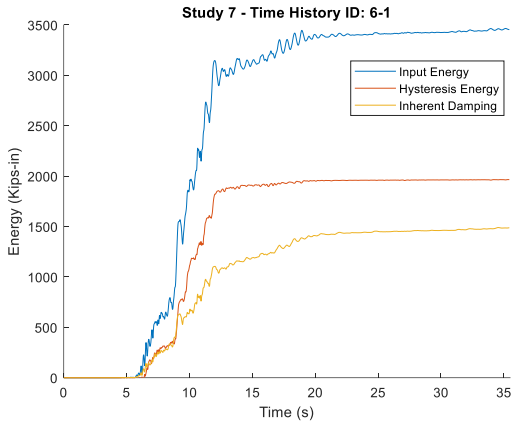

d. Input energy and energy dissipations

Figure C.6: The four-story MDOF system - Energy plots for the seventh method

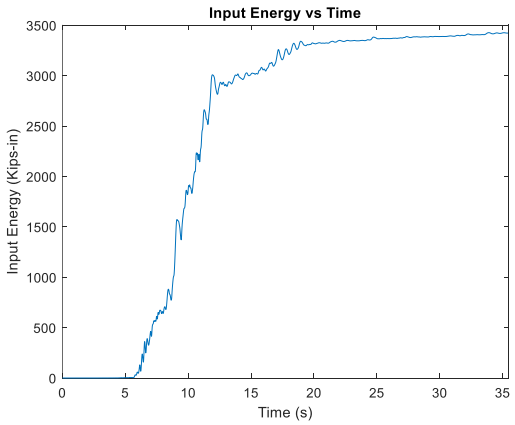

a. Input energy

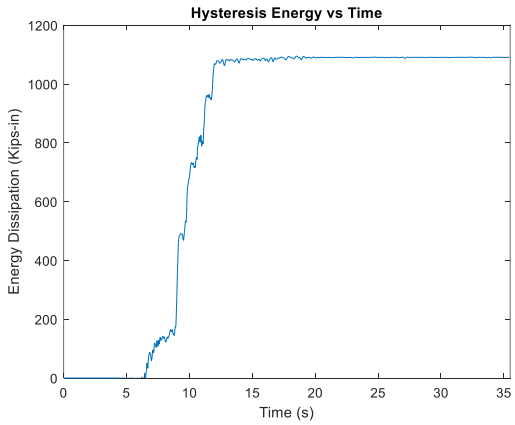

b. Hysteresis energy dissipation

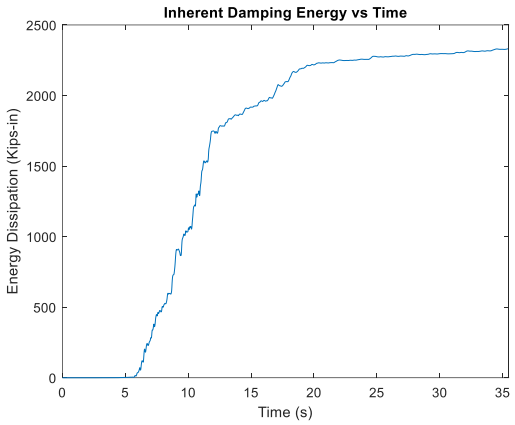

c. Inherent damping energy dissipation

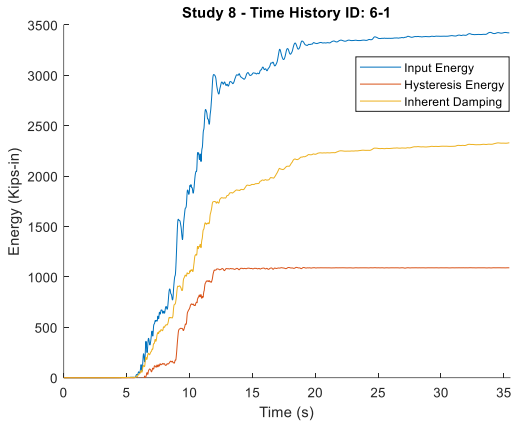

d. Input energy and energy dissipations

Figure C.7: The four-story MDOF system - Energy plots for the eighth method

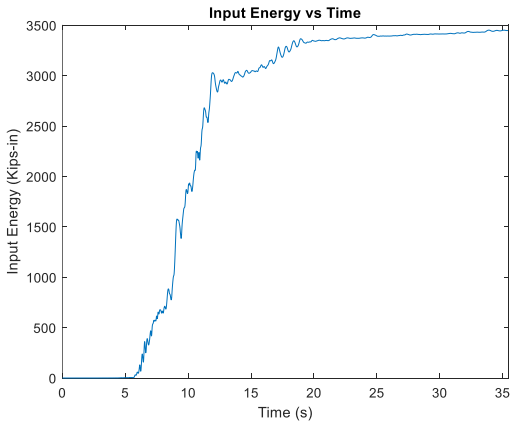

a. Input energy

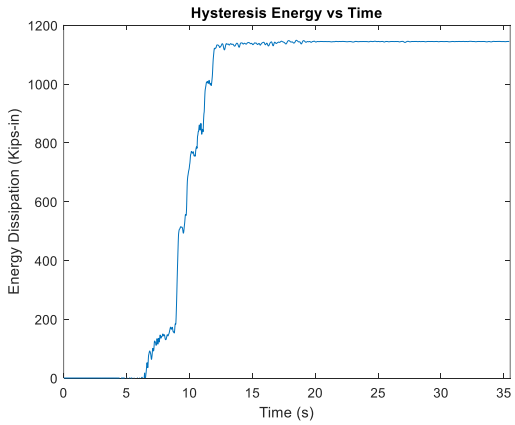

b. Hysteresis energy dissipation

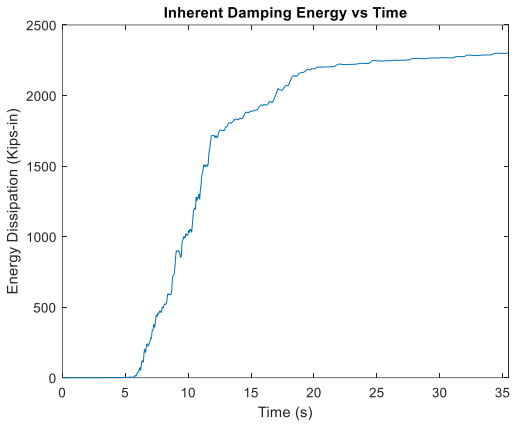

c. Inherent damping energy dissipation

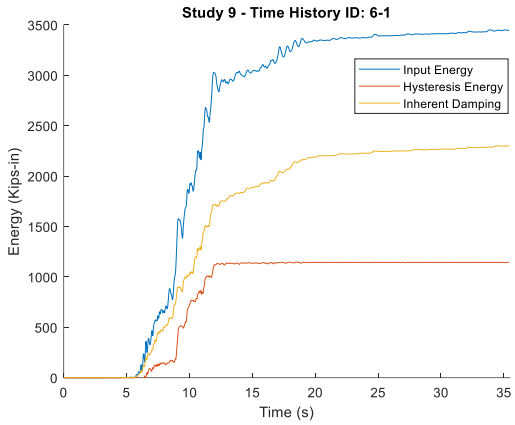

d. Input energy and energy dissipations

Figure C.8: The four-story MDOF system - Energy plots for the ninth method

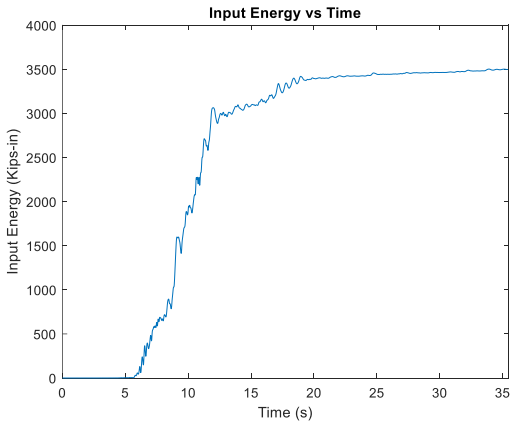

a. Input energy

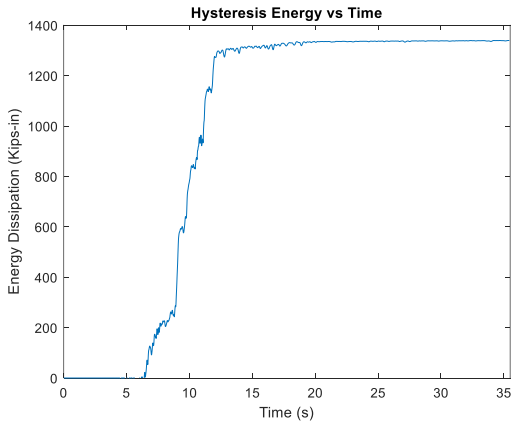

b. Hysteresis energy dissipation

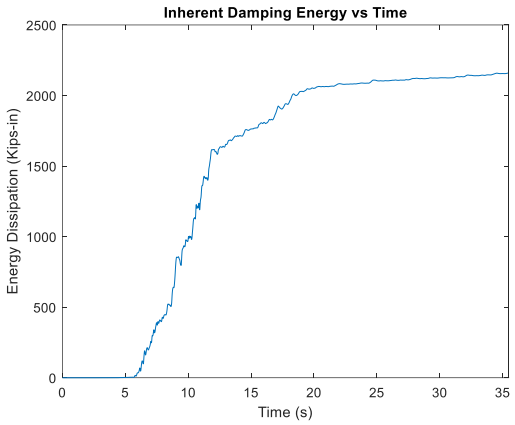

c. Inherent damping energy dissipation

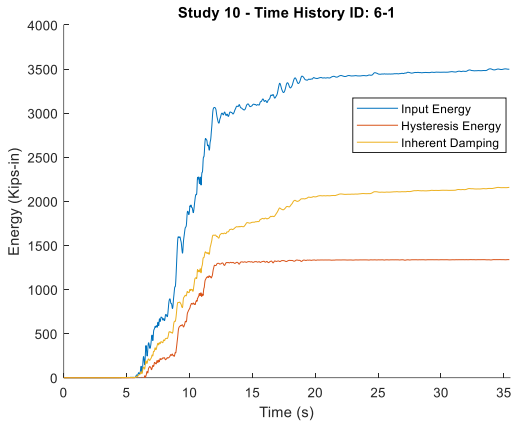

d. Input energy and energy dissipations

Figure C.9: The four-story MDOF system - Energy plots for the tenth method

C.2. Influence of Modeling Methods on IDA Results for the four-story MDOF system

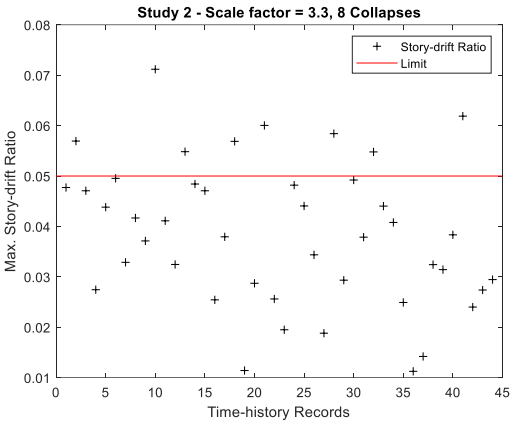

a. 8 Collapses occurred, scale factor = 3.3

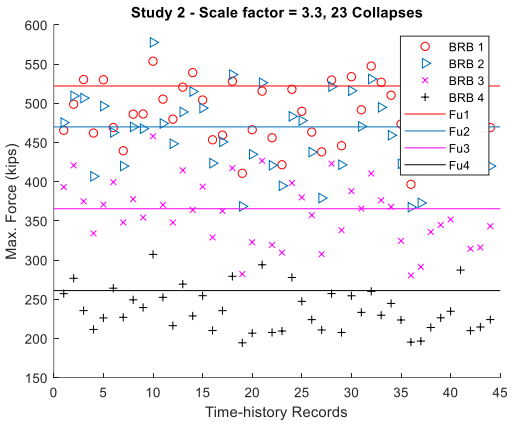

b. 23 Collapses occurred, scale factor = 3.3

Figure C.10: The four-story MDOF system - IDA results for the second method

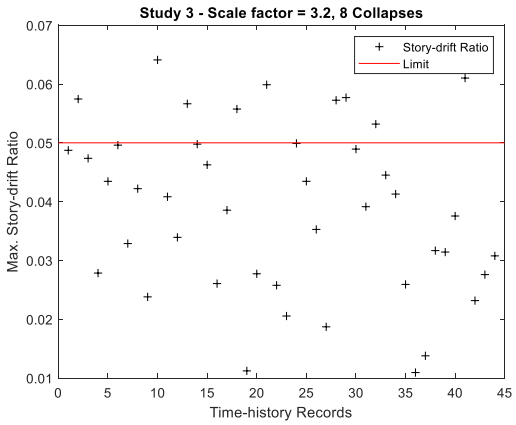

a. 8 Collapses occurred, scale factor = 3.2

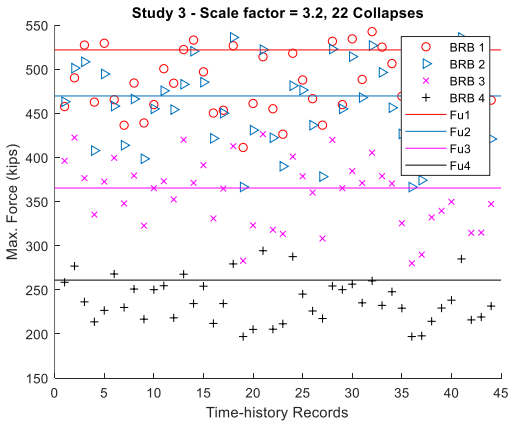

b. 22 Collapses occurred, scale factor = 3.2

Figure C.11: The four-story MDOF system - IDA results for the third method

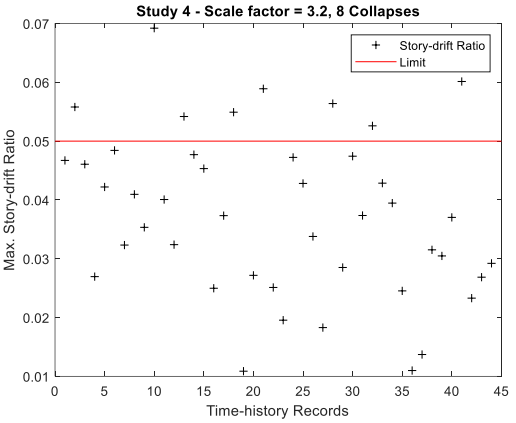

a. 8 Collapses occurred, scale factor = 3.2

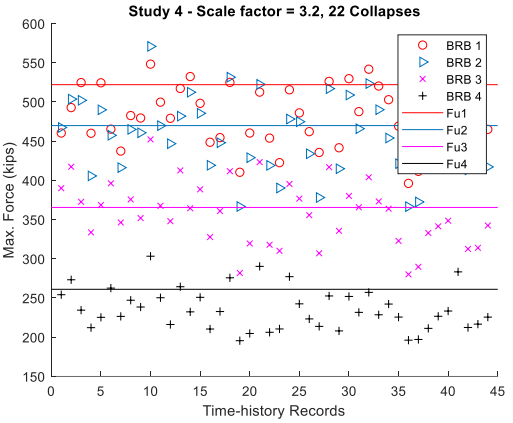

b. 22 Collapses occurred, scale factor = 3.2

Figure C.12: The four-story MDOF system - IDA results for the fourth method

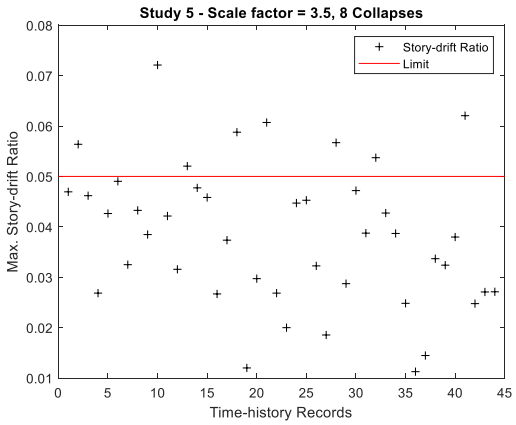

a. 8 Collapses occurred, scale factor = 3.5

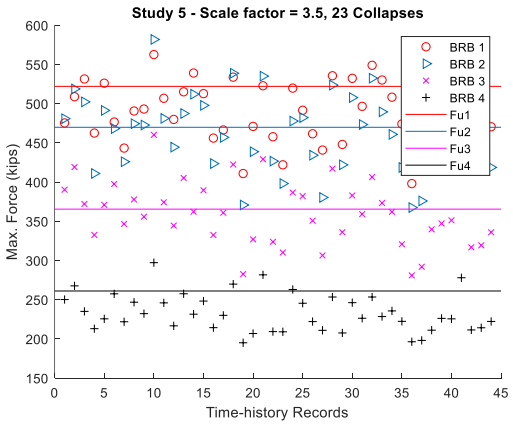

b. 23 Collapses occurred, scale factor = 3.5

Figure C.13: The four-story MDOF system - IDA results for the fifth method

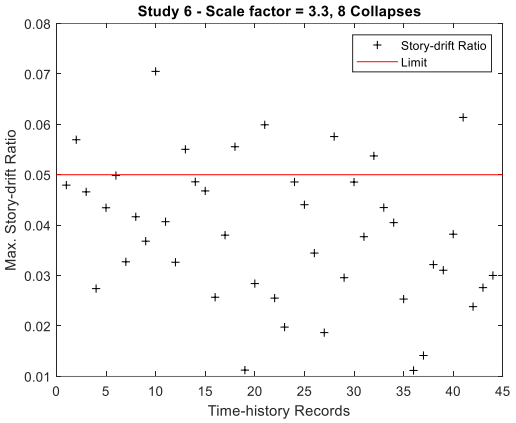

a. 8 Collapses occurred, scale factor = 3.3

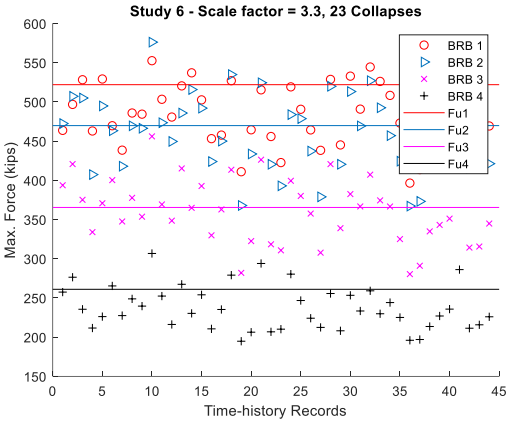

b. 23 Collapses occurred, scale factor = 3.3

Figure C.14: The four-story MDOF system - IDA results for the sixth method

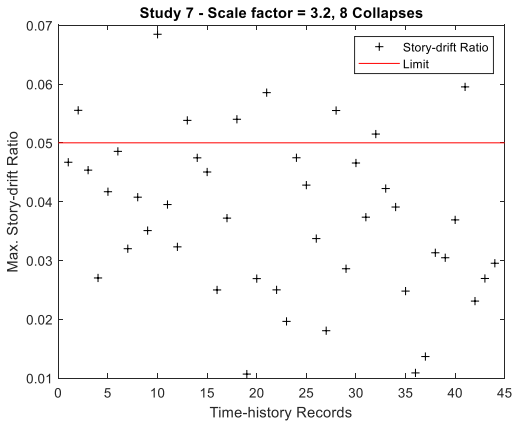

a. 8 Collapses occurred, scale factor = 3.2

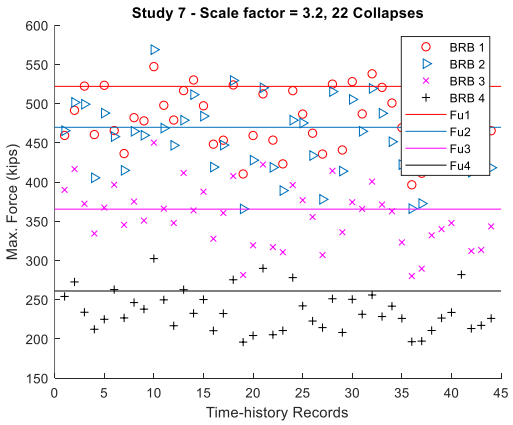

b. 22 Collapses occurred, scale factor = 3.2

Figure C.15: The four-story MDOF system - IDA results for the seventh method

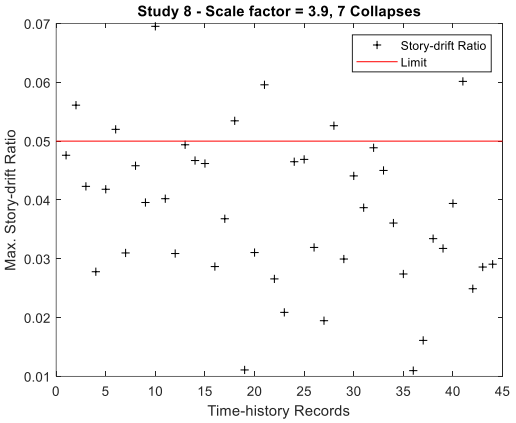

a. 7 Collapses occurred, scale factor = 3.9

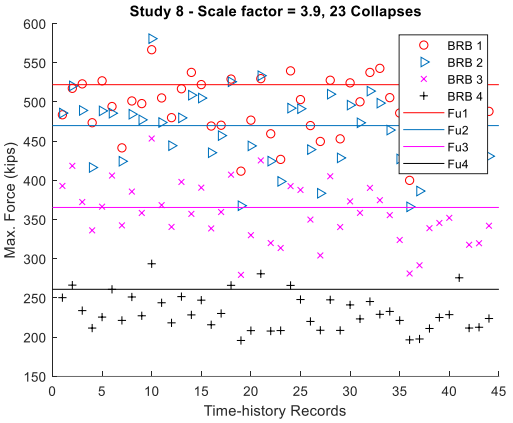

b. 23 Collapses occurred, scale factor = 3.9

Figure C.16: The four-story MDOF system - IDA results for the eighth method

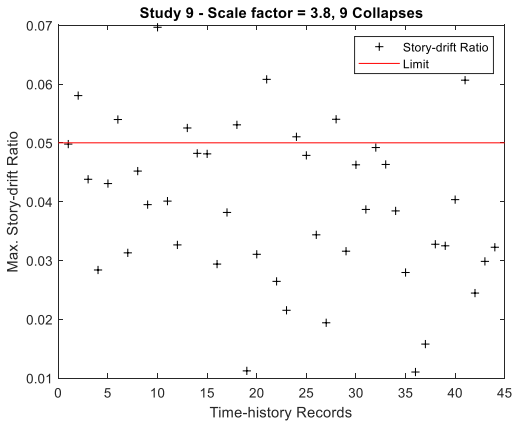

a. 9 Collapses occurred, scale factor = 3.8

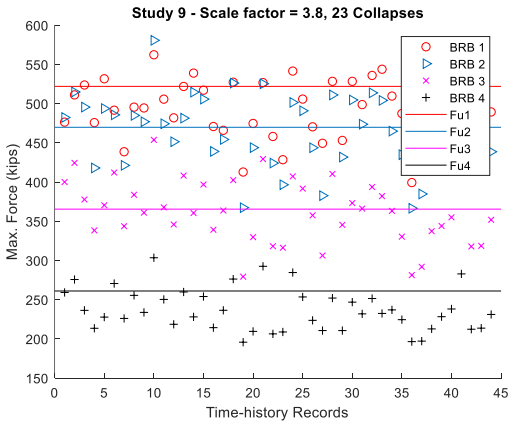

b. 23 Collapses occurred, scale factor = 3.8

Figure C.17: The four-story MDOF system - IDA results for the ninth method

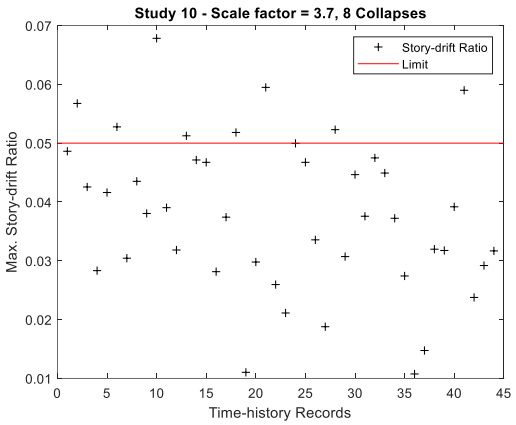

a. 8 Collapses occurred, scale factor = 3.7

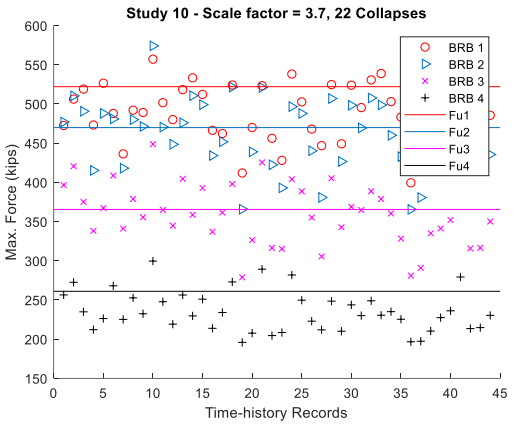

b. 22 Collapses occurred, scale factor = 3.7

Figure C.18: The four-story MDOF system - IDA results for the tenth method

C.3. Influence of Modeling Methods on IDA Results for the nine-story MDOF system

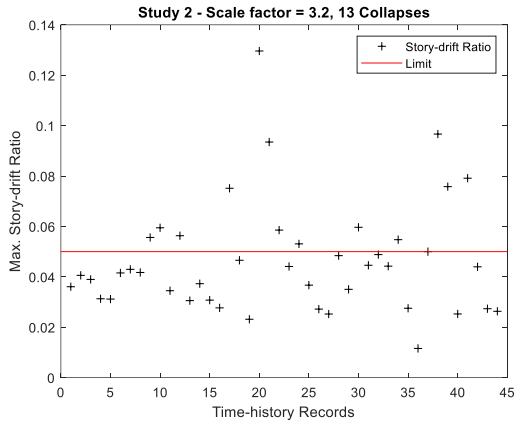

a. 13 Collapses occurred, scale factor = 3.2

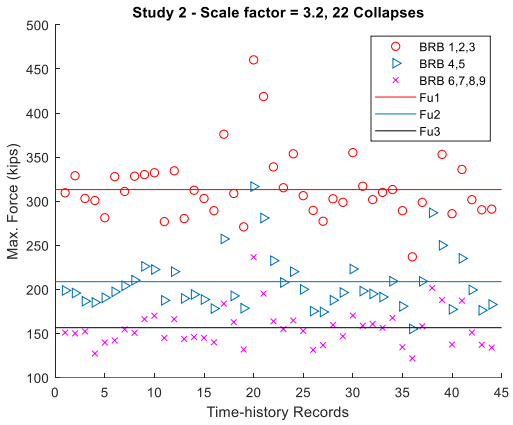

b. 22 Collapses occurred, scale factor = 3.2

Figure C.19: The nine-story MDOF system - IDA results for the second method

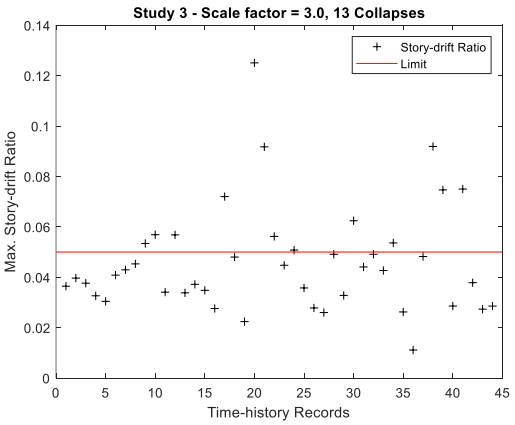

a. 13 Collapses occurred, scale factor = 3.0

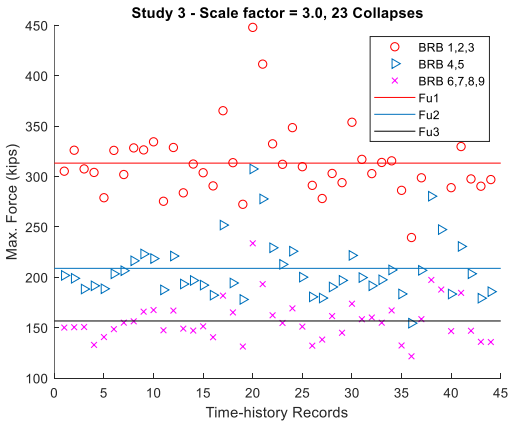

b. 23 Collapses occurred, scale factor = 3.0

Figure C.20: The nine-story MDOF system - IDA results for the third method

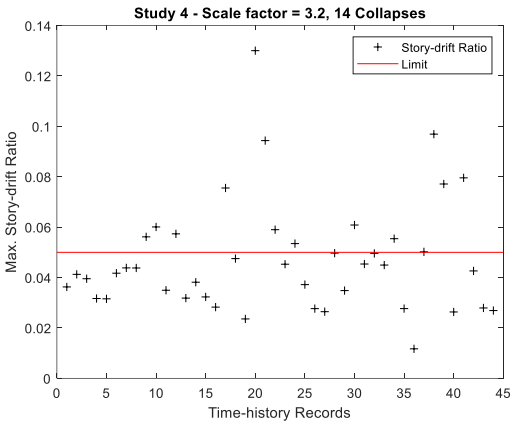

a. 14 Collapses occurred, scale factor = 3.2

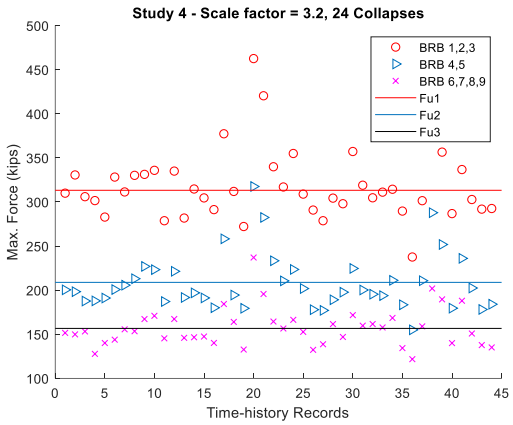

b. 24 Collapses occurred, scale factor = 3.2

Figure C.21: The nine-story MDOF system - IDA results for the fourth method

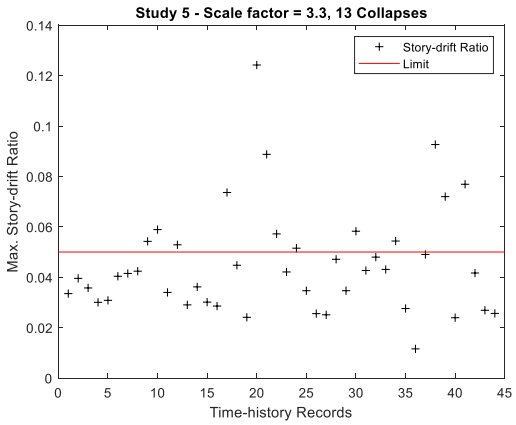

a. 13 Collapses occurred, scale factor = 3.3

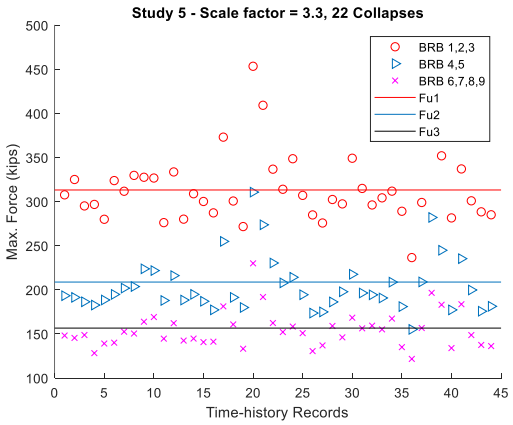

b. 22 Collapses occurred, scale factor = 3.3

Figure C.22: The nine-story MDOF system - IDA results for the fifth method

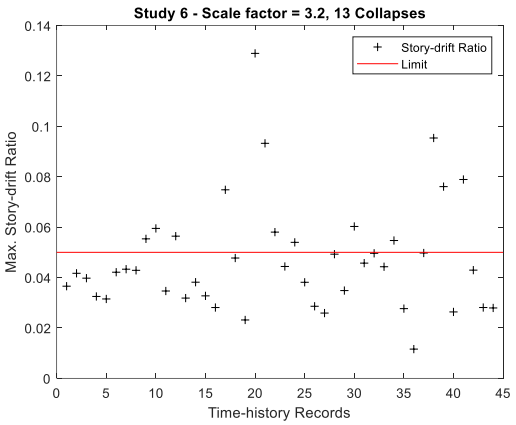

a. 13 Collapses occurred, scale factor = 3.2

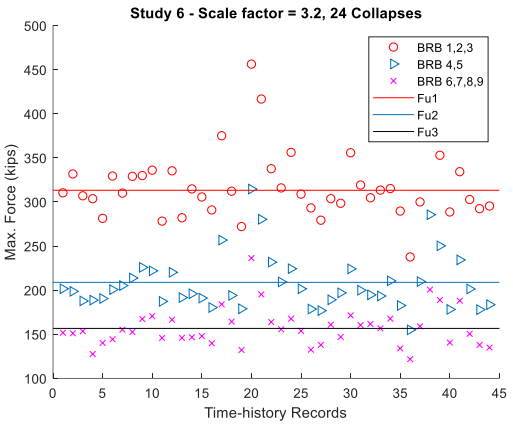

b. 24 Collapses occurred, scale factor = 3.2

Figure C.23: The nine-story MDOF system - IDA results for the sixth method

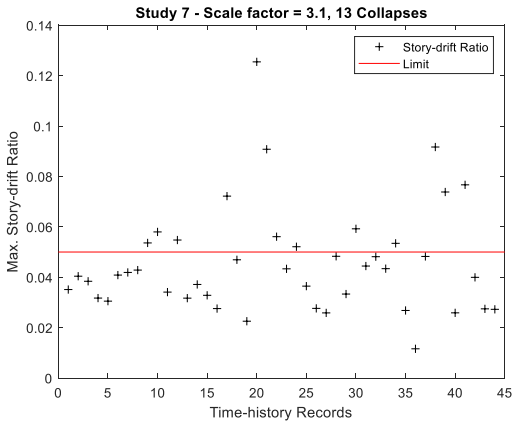

a. 13 Collapses occurred, scale factor = 3.1

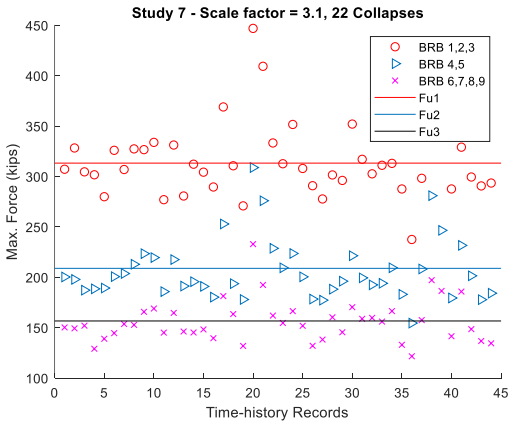

b. 22 Collapses occurred, scale factor = 3.1

Figure C.24: The nine-story MDOF system - IDA results for the seventh method

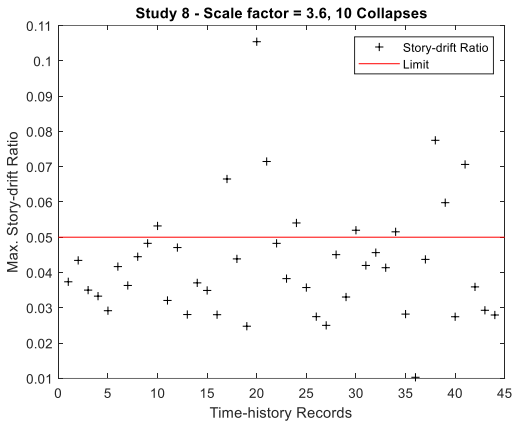

a. 10 Collapses occurred, scale factor = 3.6

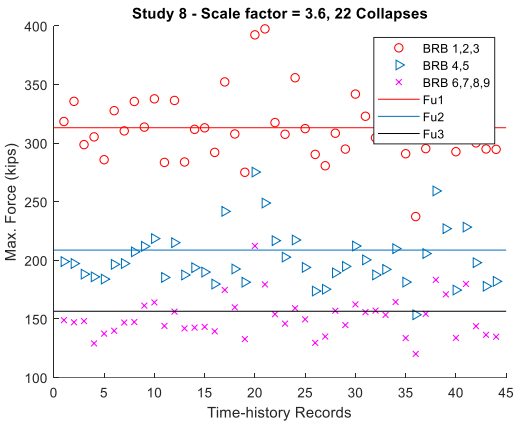

b. 22 Collapses occurred, scale factor = 3.6

Figure C.25: The nine-story MDOF system - IDA results for the eighth method

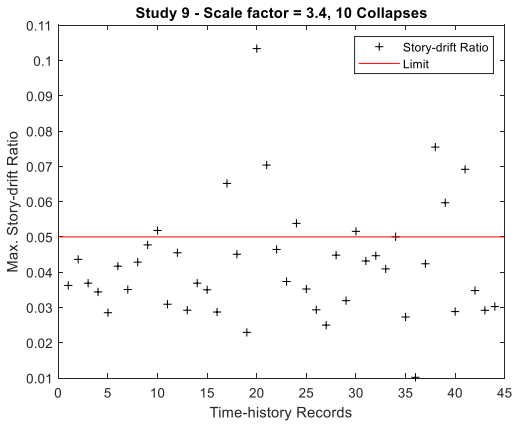

a. 10 Collapses occurred, scale factor = 3.4

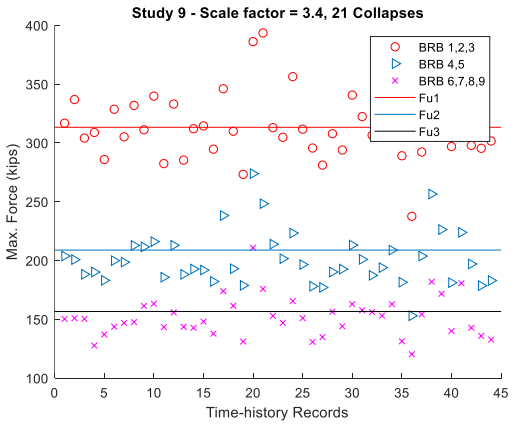

b. 21 Collapses occurred, scale factor = 3.4

Figure C.26: The nine-story MDOF system - IDA results for the ninth method

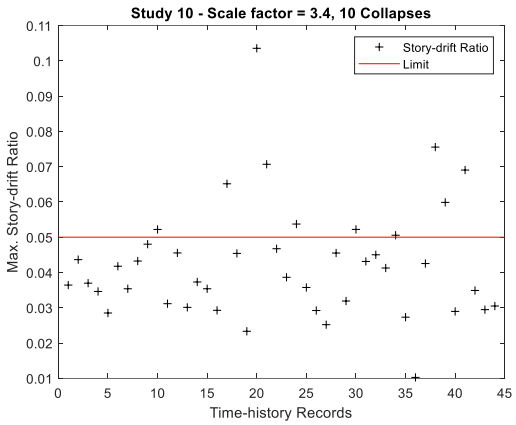

a. 10 Collapses occurred, scale factor = 3.4

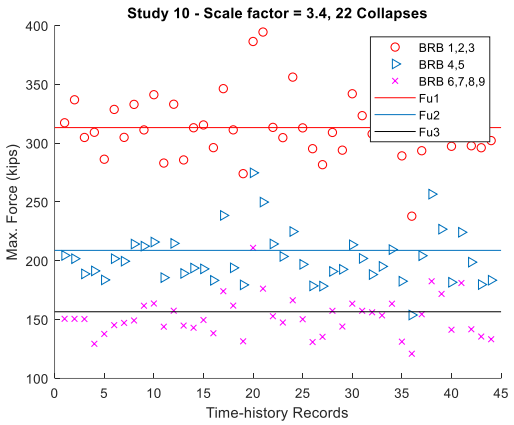

b. 22 Collapses occurred, scale factor = 3.4

Figure C.27: The nine-story MDOF system - IDA results for the tenth method

APPENDIX D: THE LIMITATION APPROACH

Here, under Section: incremental dynamic analysis (IDA) results,

- IDA results for the four-story MDOF system and
- IDA results for the nine-story MDOF system

are provided for each modified-method.

D.1. Incremental Dynamic Analysis (IDA) Results

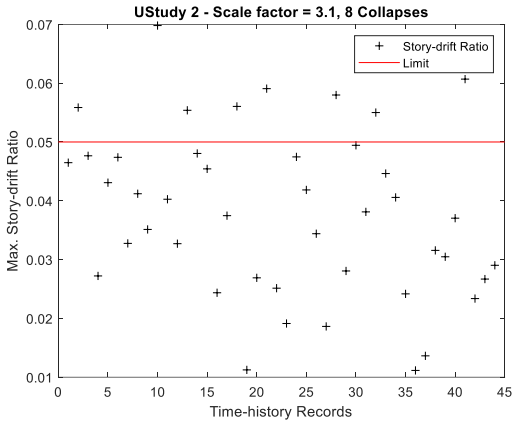

a. 8 Collapses occurred, scale factor = 3.1

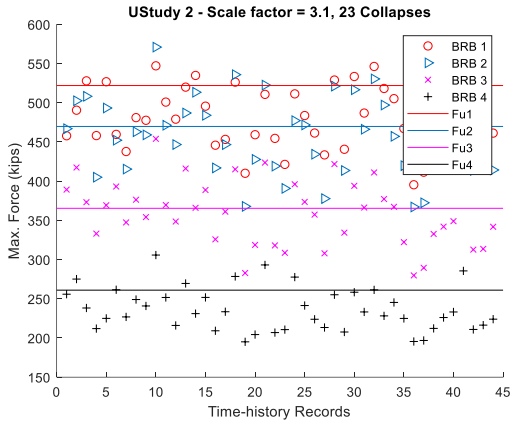

b. 23 Collapses occurred, scale factor = 3.1

Figure D.1: The four-story system - Updated IDA results for the second method

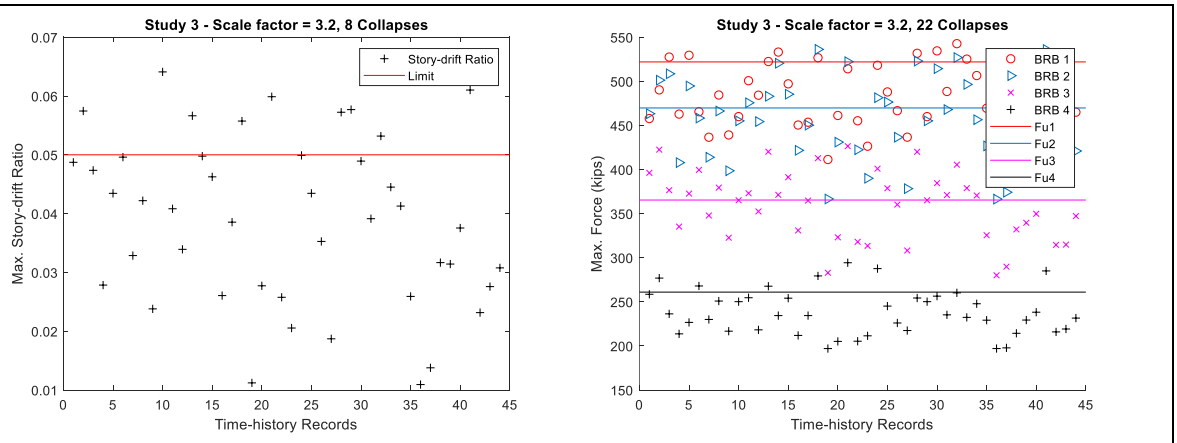

a. 8 Collapses occurred, scale factor = 3.2 b. 22 Collapses occurred, scale factor = 3.2

Figure D.2: The four-story system - Updated IDA results for the third method

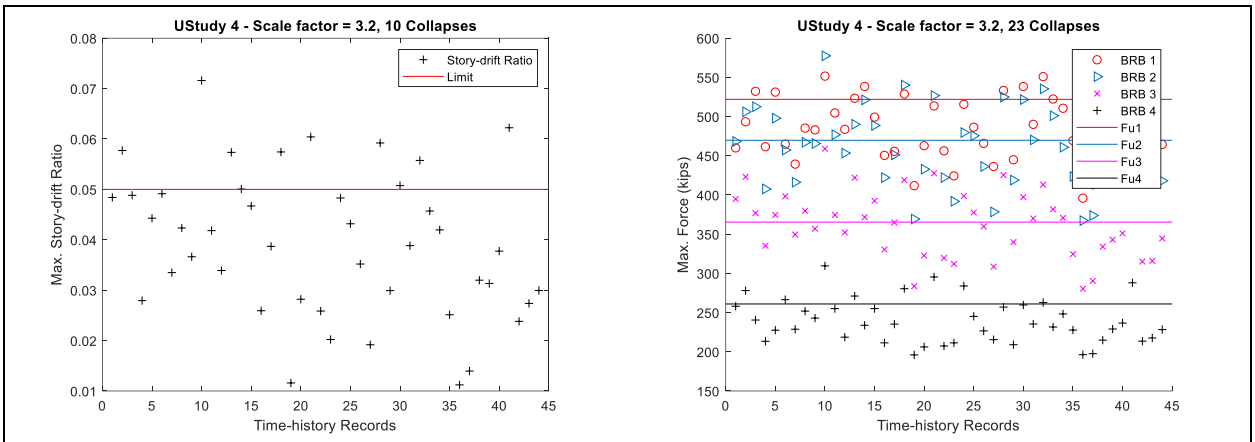

a. 10 Collapses occurred, scale factor = 3.2 b. 23 Collapses occurred, scale factor = 3.2

Figure D.3: The four-story system - Updated IDA results for the fourth method

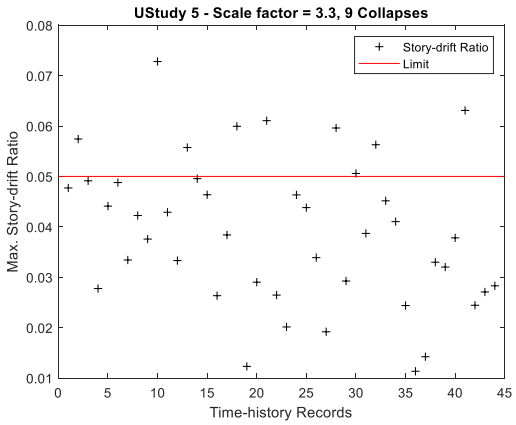

a. 9 Collapses occurred, scale factor = 3.3

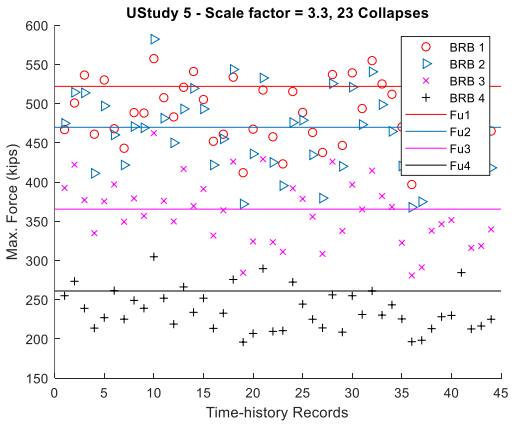

b. 23 Collapses occurred, scale factor = 3.3

Figure D.4: The four-story system - Updated IDA results for the fifth method

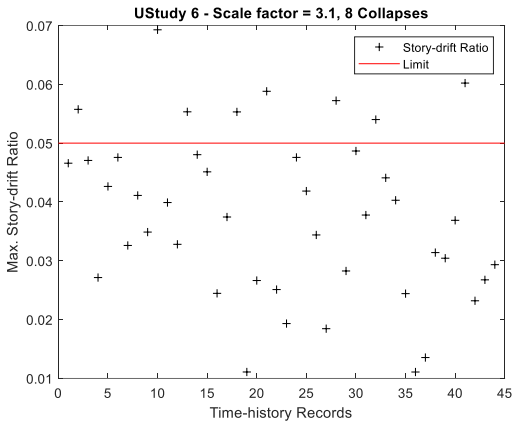

a. 8 Collapses occurred, scale factor = 3.1

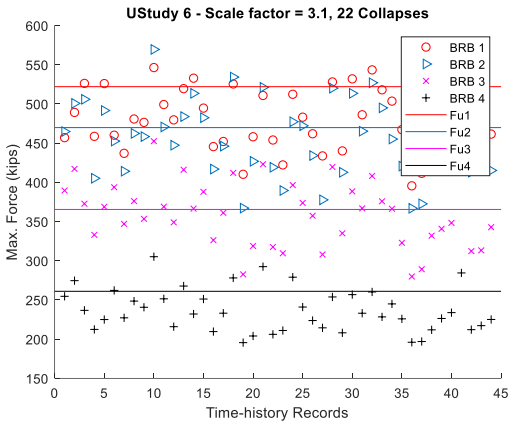

b. 22 Collapses occurred, scale factor = 3.1

Figure D.5: The four-story system - Updated IDA results for the sixth method

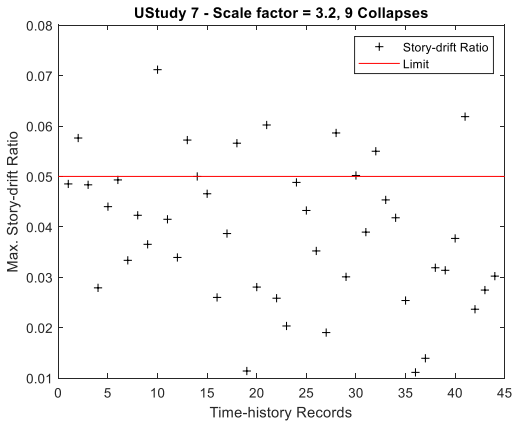

a. 9 Collapses occurred, scale factor = 3.2

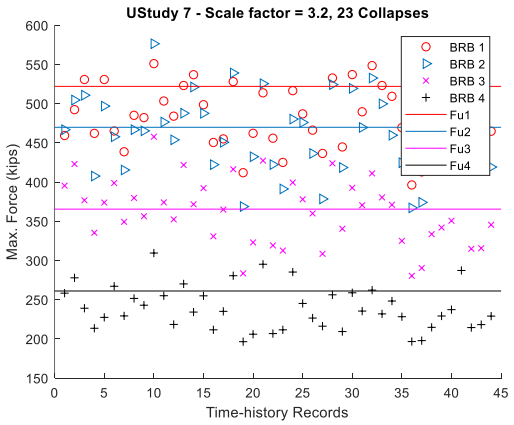

b. 23 Collapses occurred, scale factor = 3.2

Figure D.6: The four-story system - Updated IDA results for the seventh method

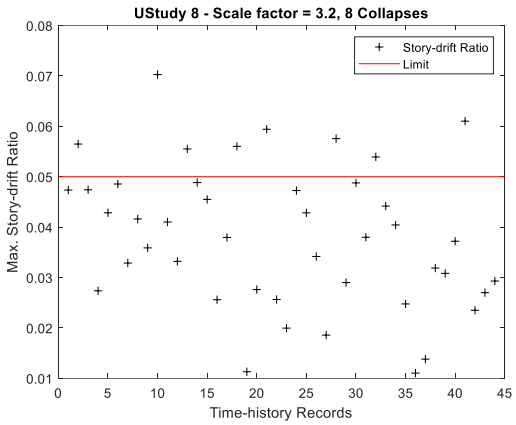

a. 8 Collapses occurred, scale factor = 3.2

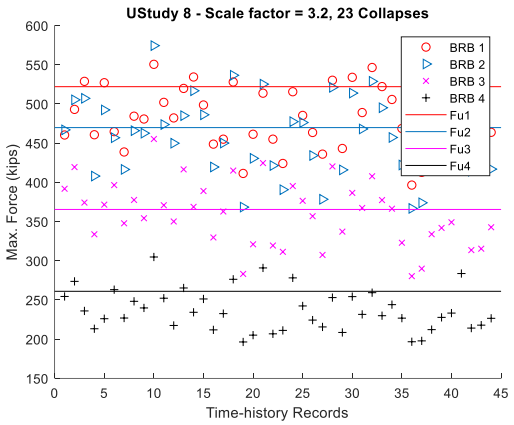

b. 23 Collapses occurred, scale factor = 3.2

Figure D.7: The four-story system - Updated IDA results for the eighth method

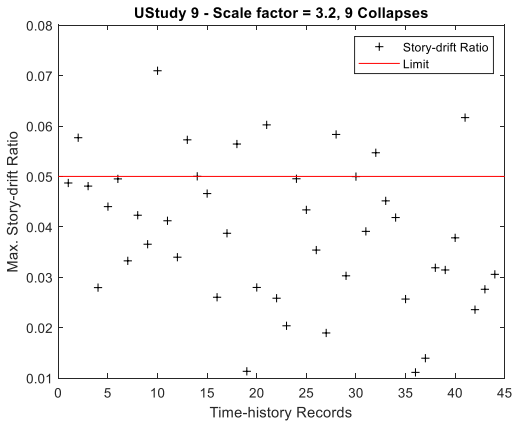

a. 9 Collapses occurred, scale factor = 3.2

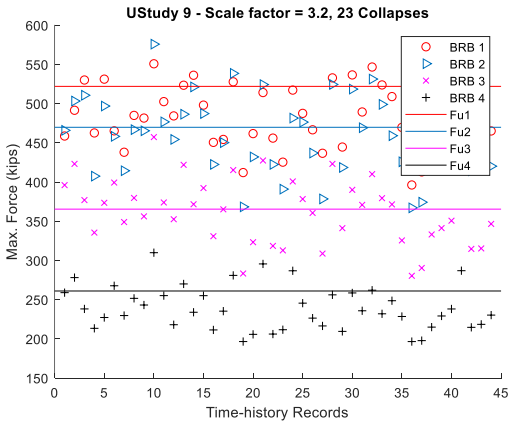

b. 23 Collapses occurred, scale factor = 3.2

Figure D.8: The four-story system - Updated IDA results for the ninth method

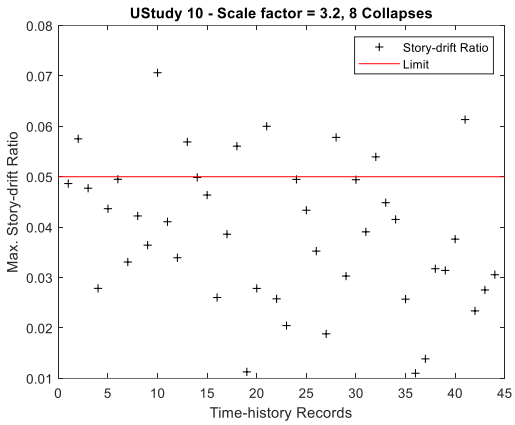

a. 8 Collapses occurred, scale factor = 3.2

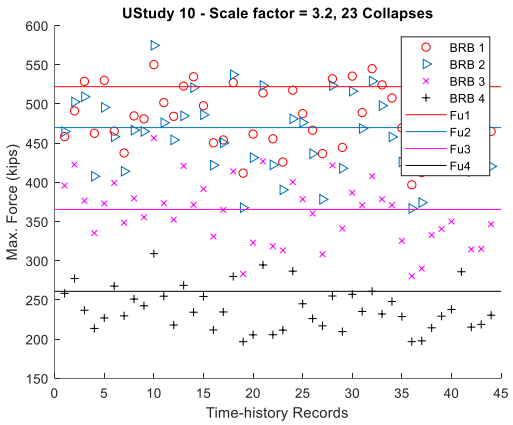

b. 23 Collapses occurred, scale factor = 3.2

Figure D.9: The four-story system - Updated IDA results for the tenth method

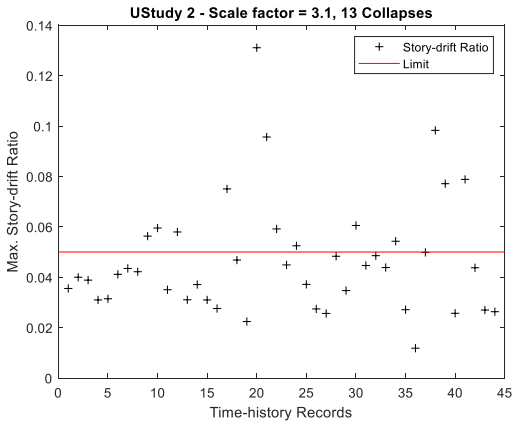

a. 13 Collapses occurred, scale factor = 3.1

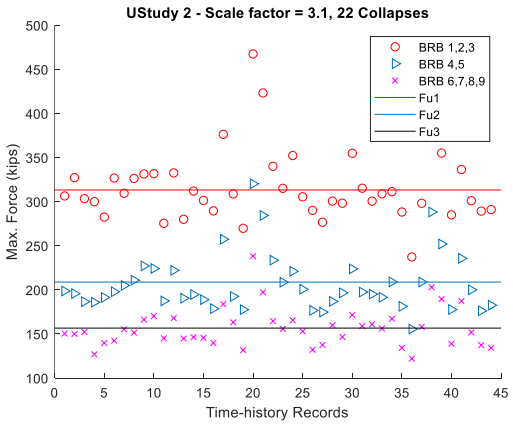

b. 22 Collapses occurred, scale factor = 3.1

Figure D.10: The nine-story system - Updated IDA results for the second method

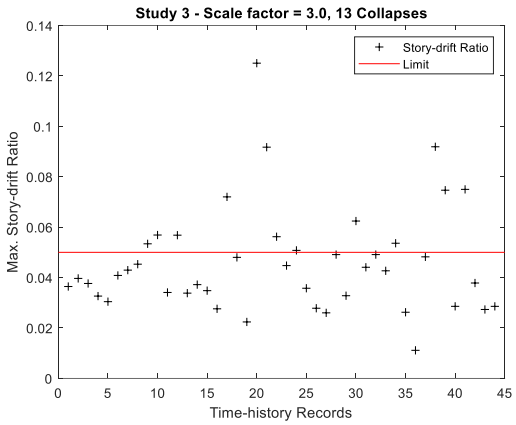

a. 13 Collapses occurred, scale factor = 3.0

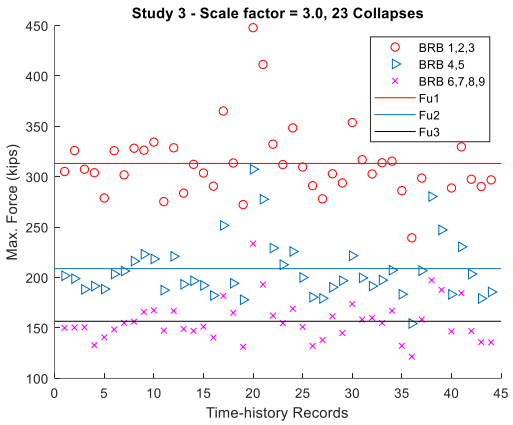

b. 23 Collapses occurred, scale factor = 3.0

Figure D.11: The nine-story system - Updated IDA results for the third method

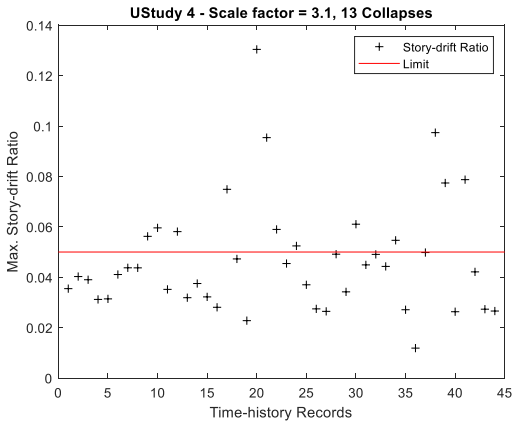

a. 13 Collapses occurred, scale factor = 3.1

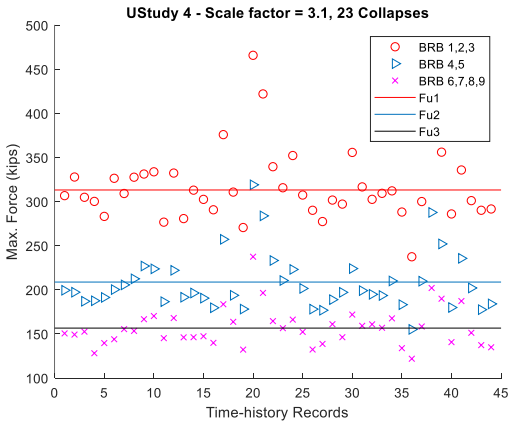

b. 23 Collapses occurred, scale factor = 3.1

Figure D.12: The nine-story system - Updated IDA results for the fourth method

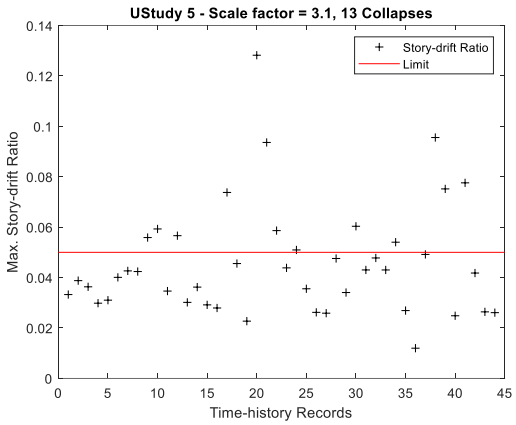

a. 13 Collapses occurred, scale factor = 3.1

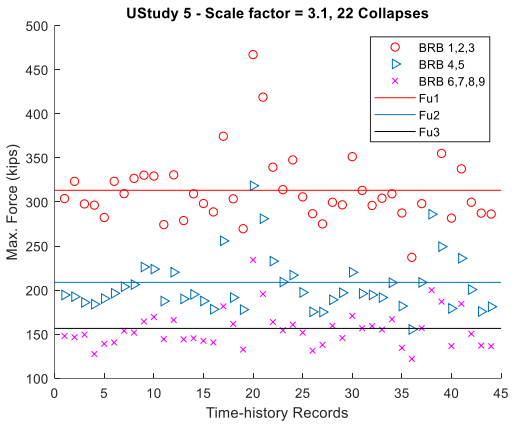

b. 22 Collapses occurred, scale factor = 3.1

Figure D.13: The nine-story system - Updated IDA results for the fifth method

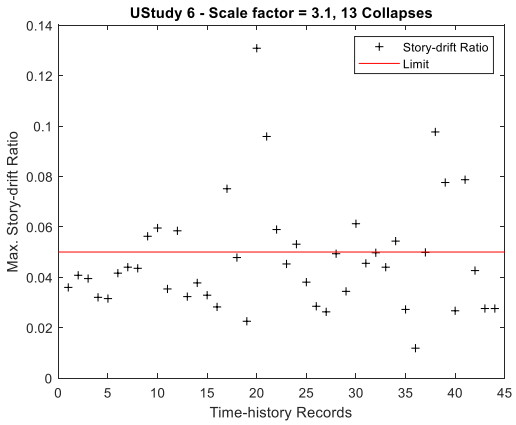

a. 13 Collapses occurred, scale factor = 3.1

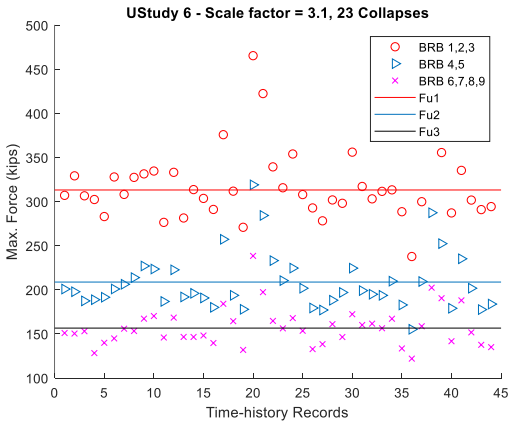

b. 23 Collapses occurred, scale factor = 3.1

Figure D.14: The nine-story system - Updated IDA results for the sixth method

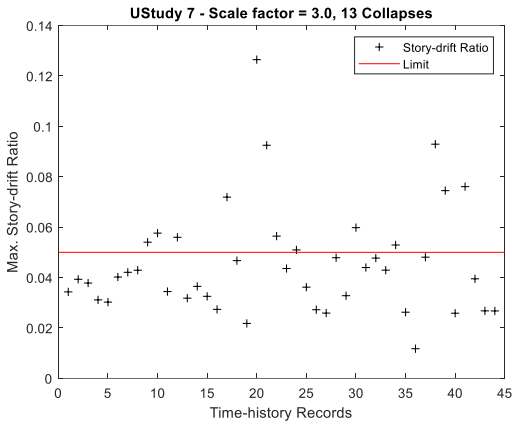

a. 13 Collapses occurred, scale factor = 3.0

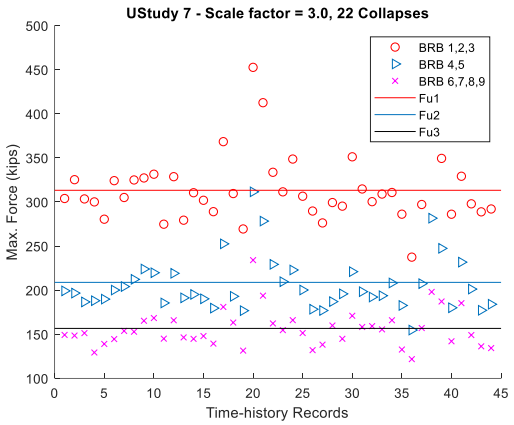

b. 22 Collapses occurred, scale factor = 3.0

Figure D.15: The nine-story system - Updated IDA results for the seventh method

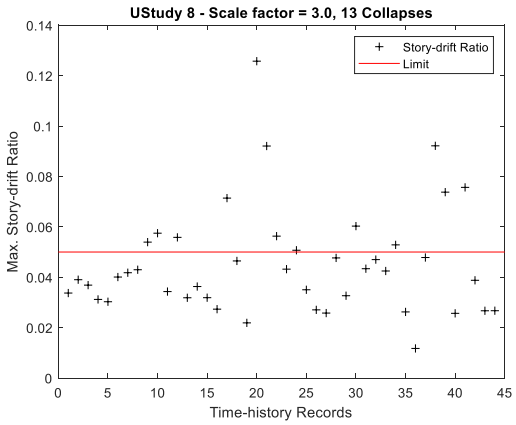

a. 13 Collapses occurred, scale factor = 3.0

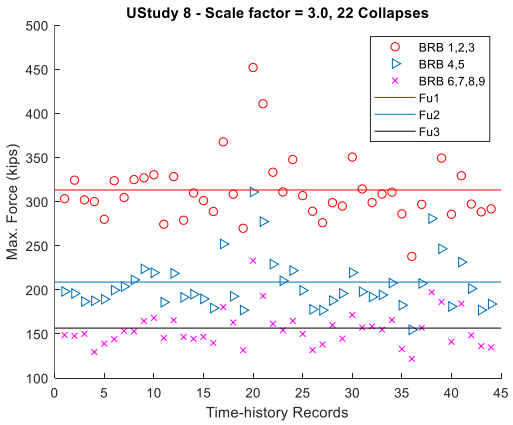

b. 22 Collapses occurred, scale factor = 3.0

Figure D.16: The nine-story system - Updated IDA results for the eighth method

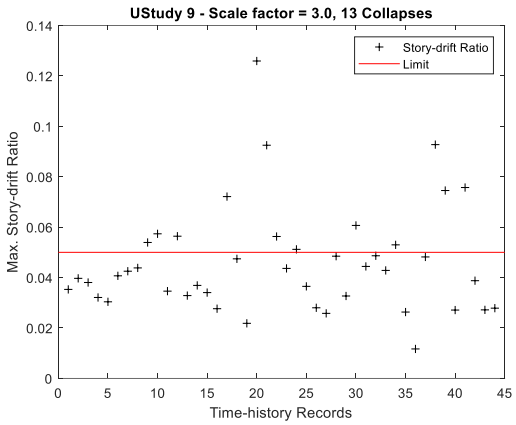

a. 13 Collapses occurred, scale factor = 3.0

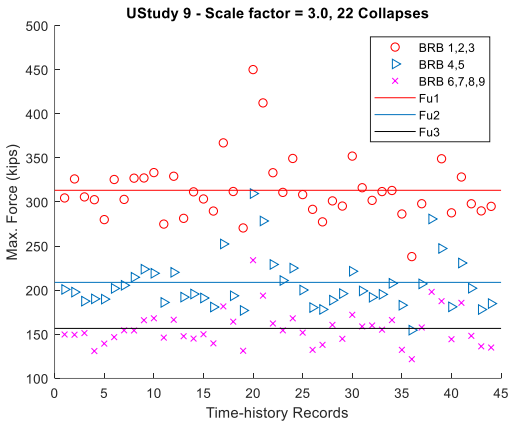

b. 22 Collapses occurred, scale factor = 3.0

Figure D.17: The nine-story system - Updated IDA results for the ninth method

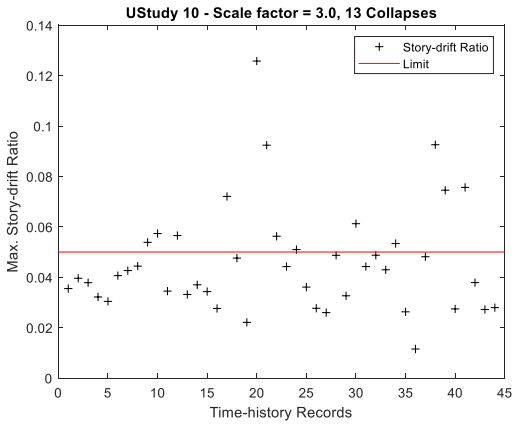

a. 13 Collapses occurred, scale factor = 3.0

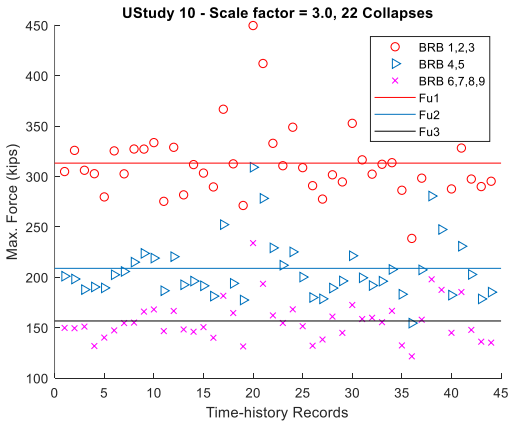

b. 22 Collapses occurred, scale factor = 3.0

Figure D.18: The nine-story system - Updated IDA results for the tenth method